

UNIVERSITY OF PORTSMOUTH

Deacetylation of GD3^A as a potential therapeutic strategy for paediatric medulloblastoma

Rebecca Louise Mather

2016

The thesis is submitted in partial fulfilment of the requirements for the award of the degree of Doctor of Philosophy of the University of Portsmouth

Declaration

Whilst registered as a candidate for the above degree, I have not been registered for any other research award. The results and conclusions embodied in this thesis are the work of the named candidate and have not been submitted for any other academic award

Word count: 55,642

Acknowledgements

Thank you to my supervisors Prof. Geoff Pilkington and Dr. Helen Fillmore, your guidance and expertise throughout this project have been invaluable. Thank you for making this experience so enjoyable. I am extremely grateful for the opportunities you have given me and the time you have spent helping me to achieve my dream.

Thank you to all of the neuro-oncology staff and students, it has been a joy to share this experience with you. Particular thanks go to Kathleen Keatley, for always making me laugh, even in the most stressful times. To Emily Pinkstone, for being such a great friend and for helping me through this process with encouragement and caffeinated cinnamon syrup. To Katie Loveson, for sharing the highs and lows of this project and for making it so enjoyable. Finally, to Mikaella Vouri and Samah Jassam for always being supportive.

Thank you to my brother Lee who has always supported my choices, believed in me and always been there to listen and advise me.

To my Godmother Una, although we lost you at the start of this project I know you would be encouraging me every day.

Thank you to Charlie's Challenge, Ali's Dream, Brain Tumour Research and Children with Cancer UK for the financial support that allowed this research to take place.

For my Nan, Olive.

Thank you for your invaluable support, guidance and reassurance. I could not have completed this process without your encouragement. I miss you every day.

For my Gamps, Wally.

Thank you for your love and support in everything I do, your kind and caring words of encouragement have helped me to complete this work.

For my Mum, Diane.

Thank you for always believing in me and for giving me the courage to pursue my dream.

For Jonathan Chamberlain,

Thank you for always having faith in me, for always understanding and for supporting me in everything I do.

Abstract

Medulloblastoma survivors frequently suffer from low quality of life as a result of aggressive treatment. New treatments are urgently needed to reduce down-stream sequelae. GD3, an oncofoetal ganglioside, has roles in embryonic brain development and is commonly modified to 9-*O*-acetyl GD3 (GD3^A). GD3^A plays a role in protecting cells from pro-apoptotic GD3 during brain development, after which GD3 accumulates above a threshold to collapse the mitochondrial membrane potentials of supernumary progenitor cells. GD3 and GD3^A then become minor ganglioside species of the postpartum brain. In medulloblastoma however, GD3 and GD3^A are re-expressed as shown here by the medulloblastoma cell lines RES256, UW402 and CHLA-01-Med where expression of GD3 is seen in 56.7%, 61.3% and 45.1% of the cell populations respectively. GD3^A is expressed by 84.5%, 74.4% and 79.4% of the populations respectively. By bioinformatic analysis we also show that the human endogenous deacetylation enzyme of GD3^A, Sialate-*O*-acetyl esterase (SIAE), is significantly down-regulated in medulloblastoma patient tissue ($p < 0.001$). This enzyme is thought to restore GD3 levels by cleaving the acetyl groups from GD3^A. In order to evaluate this pathway as a potential therapeutic target we used an inducible SIAE over-expression approach in RES256 cells, the highest intracellular GD3^A expresser. This transfection resulted in two SIAE wild-type expressing clones. Upon over-expression of SIAE (in clone 2) we show a significant increase in GD3 expression ($p < 0.05$), and in preliminary experiments a significant increase in depolarisation of the mitochondrial membrane potential was seen in SIAE expressing clone 1 ($p < 0.05$). These changes were not seen on induction of expression of a catalytic mutant SIAE-S127A or vector controls. We also demonstrate that wild-type SIAE expressing clones do not secrete the enzyme, however the catalytic mutant SIAE-S127A protein is secreted. We hypothesise that possible cleavage

of caspase 1 could be responsible for this secretion. The expression of SIAE and SIAE-S127A in cell lysates were confirmed by Western blot and demonstrated a possible cleavage product. We hypothesise that this possible cleavage may result in different abilities for these clones to secrete the enzyme. Furthermore, we show that induction of SIAE overexpression in combination with etoposide treatment resulted in a significant reduction in IC_{50} in SIAE overexpressing clones after 72 hours of treatment ($p < 0.001$; clone 2). Changes in IC_{50} for empty vector controls and SIAE-S127A were not significant.

Dissemination

Elements of this work have been presented at the following internal, national and international conferences:

- **July 2012** – British Neuro-oncology Society conference ‘Challenge’s and Controversies’ –Manchester, UK - Attended
- **March 2013**- Hammer Out patient conference – poster
- **April 2013** – International Summer School ‘Modern Approaches to Research and Treatment of Cancer’ – Piran, Slovenia – Attended
- **June 2013** – Institute of Biomedical and Biomolecular Sciences post-graduate research day – Portsmouth, UK – Attended
- **July 2013** - British Neuro-oncology Society conference ‘Art and Science’–Durham, UK – Attended
- **July 2013** – University of Portsmouth Faculty of Science poster day – Poster presentation – Portsmouth, UK
- **May 2014** – Institute of Biomedical and Biomolecular Sciences post-graduate research day – Portsmouth, UK – Poster presentation
- **October 2014** – International Institute of Anti-Cancer Research 9th international conference – Sithonia, Greece - Oral presentation
- **May 2015** - Institute of Biomedical and Biomolecular Sciences post-graduate research day – Portsmouth, UK – Oral presentation
- **June 2015** – Three minute thesis – Portsmouth, UK – Oral presentation
- **November 2015** – Society for Neuro-oncology 20th annual meeting – Texas, USA- Oral poster

- **January 2016** – Children with Cancer UK conference ‘drug delivery in childhood brain tumours’ – London, UK – Attended
- **June 2016** – International Symposium of Paediatric Neuro-oncology – Liverpool, UK – Accepted for oral poster presentation
- **October 2016** – European association of Neuro-oncology – Mannheim, Germany – Accepted for poster presentation

Table of contents

DECLARATION	2
ACKNOWLEDGEMENTS	3
ABSTRACT	5
DISSEMINATION	7
1 INTRODUCTION	25
1.1 PAEDIATRIC BRAIN TUMOURS	26
1.1.1 INCIDENCE	26
1.1.2 EPIDEMIOLOGY	27
1.1.3 LOCATION AND SYMPTOMS OF CHILDHOOD BRAIN TUMOURS	27
1.1.4 PROGNOSIS	29
1.2 MEDULLOBLASTOMA	29
1.2.1 ORIGINS OF MEDULLOBLASTOMA	30
1.3 DEVELOPMENT OF THE CEREBELLUM	31
1.4 BRAIN DEVELOPMENT AND MOLECULAR SUBGROUPS OF MEDULLOBLASTOMA	32
1.4.1 THE WNT SUBGROUP	33
1.4.2 INACTIVE WNT SIGNALLING	33
1.4.3 ACTIVE WNT SIGNALLING	34
1.4.4 WNT SIGNALLING IN MEDULLOBLASTOMA	34
1.4.5 SUBGROUP FEATURES	35
1.4.6 THE SHH SUBGROUP	39
1.4.7 INACTIVE SHH SIGNALLING	39
1.4.8 ACTIVE SHH SIGNALLING	40
1.4.9 SHH SIGNALLING IN MEDULLOBLASTOMA	40
1.4.10 GROUP 3 AND GROUP 4 MEDULLOBLASTOMAS	45
1.4.11 GROUP 3	45
1.4.12 GROUP 4	48
1.5 OTHER SIGNALLING PATHWAYS IMPLICATED IN MEDULLOBLASTOMA PATHOGENESIS	53
1.6 EMERGING MOLECULAR-SUBGROUP TARGETED THERAPIES	56
1.7 HISTOPATHOLOGICAL VARIANTS	57
1.7.1 CLASSIC VARIANT OF MEDULLOBLASTOMA	59
1.7.2 DESMOPLASTIC /NODULAR VARIANT OF MEDULLOBLASTOMA	59
1.7.3 LARGE CELL/ ANAPLASTIC VARIANT OF MEDULLOBLASTOMA (LCA)	59
1.7.4 MEDULLOBLASTOMA WITH EXTENSIVE NODULARITY (MBEN)	60
1.7.5 MYOGENIC DIFFERENTIATION	60
1.7.6 MELANOTIC DIFFERENTIATION	61
1.8 TREATMENT OF MEDULLOBLASTOMA	63
1.8.1 TREATMENT PROTOCOLS BASED ON DISEASE RISK	66
1.9 OPPORTUNITY FOR NEW THERAPY	68
1.10 GANGLIOSIDES	68

1.10.1	GANGLIOSIDE BIOSYNTHESIS	69
1.11	GD3 AND GD3 ^A IN THE DEVELOPING NON-NEOPLASTIC BRAIN	72
1.12	SIALIC ACIDS	76
1.13	GD3 ACETYLATION TO GD3 ^A	76
1.14	THE ROLES OF GD3 AND GD3 ^A IN PRIMARY BRAIN TUMOURS	81
1.14.1	CAS1	85
1.14.2	SIALIC ACID <i>O</i> -ACETYL ESTERASE	87
1.15	HYPOTHESIS	93
1.16	AIMS	94
1.17	OBJECTIVES	94
2	MATERIALS AND METHODS	95
2.1	CELL LINES	96
2.2	MAINTENANCE OF CELL LINES	98
2.3	FREEZING OF CELL LINES	101
2.4	HUMAN AUTHENTICATION OF CELL LINES	101
2.5	ROUTINE MYCOPLASMA TESTING	103
2.6	ANTIBODIES	104
2.7	SIAE ANTIBODY PRODUCTION	106
2.8	FLOW CYTOMETRY	106
2.9	IMMUNOCYTOCHEMISTRY	108
2.10	IMMUNOFLUORESCENT STAINING OF WILD-TYPE MOUSE BRAIN SECTIONS	109
2.11	CLONING	111
2.11.1	TRANSFORMATION AND PREPARATION OF PLASMID DNA	125
2.12	STABLE AND TRANSIENT TRANSFECTION WITH PCMV-N3-SIAE	128
2.13	STABLE TRANSFECTION – INDUCIBLE SYSTEM CONSTRUCTS	129
2.14	EGFP TRANSFECTION EFFICIENCY ASSAY	130
2.15	LUCIFERASE ASSAY	130
2.16	CLONE SELECTION	131
2.17	LYSIS OF CELLS	132
2.17.1	DETERMINATION OF PROTEIN CONTENT IN CELL LYSATES (BCA ASSAY)	133
2.18	WESTERN BLOT	135
2.19	MITOCHONDRIAL MEMBRANE POTENTIAL ASSAY (JC-1 ASSAY)	137
2.20	CHEMOTHERAPY EXPERIMENTS	140
2.21	MOLECULAR MODELLING	143
2.22	BIOINFORMATICS	143
2.23	STATISTICS	152
3	RESULTS	153
3.1	INTRODUCTION	154
3.2	BIOINFORMATIC CHARACTERISATION OF THE GD3 ACETYLATION PATHWAY	155
3.2.1	REGULATORS OF THE GD3 ACETYLATION PATHWAY ARE ATYPICALLY EXPRESSED IN MEDULLOBLASTOMA TISSUE AT THE MRNA LEVEL	157

3.2.1.1	EXPRESSION OF THE GD3 ACETYLATION PATHWAY REGULATORS VARIES ACCORDING TO MOLECULAR SUBGROUP	160
3.2.2	CHARACTERISATION OF GD3 ACETYLATION PATHWAY REGULATORS BY METASTATIC STAGE	167
3.2.3	SUMMARY	172
3.3	CHARACTERISATION OF GD3 AND GD3 ^A EXPRESSION IN MEDULLOBLASTOMA CELL LINES	174
3.3.1	INTRODUCTION	174
3.3.2	GD3 AND GD3 ^A ARE EXPRESSED BY MEDULLOBLASTOMA CELL LINES	174
3.3.3	CONCLUSION	183
3.4	SIAE OVEREXPRESSION STUDIES	185
3.5	THE TET-ON 3G INDUCIBLE SYSTEM	188
3.6	GENERATING AND SCREENING A TET-RESPONSIVE CELL LINE	191
3.6.1	THE EFFECT OF SIAE EXPRESSION ON MITOCHONDRIAL MEMBRANE POTENTIAL	210
3.6.2	SIAE OVEREXPRESSION IN CONJUNCTION WITH CURRENT CHEMOTHERAPEUTICS	212
3.6.3	CHANGES IN IC ₅₀ WITH CHEMOTHERAPY TREATMENTS	219
4	DISCUSSION	225
4.1	INTRODUCTION	226
4.2	THE GD3 ACETYLATION PATHWAY IN NEOPLASTIC DISEASE	227
4.3	SYNTHESIS AND TURNOVER OF GD3 AND GD3 ^A	229
4.4	GD3 SYNTHESIS ENZYMES ARE ATYPICALLY EXPRESSED IN MEDULLOBLASTOMA ACROSS SUBGROUPS AND METASTATIC STAGES	230
4.4.1	BIOINFORMATICS SUMMARY OF THE GD3 SYNTHESIS ENZYMES	232
4.5	GD3 AND GD3 ^A TURNOVER ENZYMES ARE ATYPICALLY EXPRESSED IN MEDULLOBLASTOMA ACROSS SUBGROUPS AND METASTATIC STAGES	233
4.5.1	BIOINFORMATICS SUMMARY OF THE GD3 AND GD3 ^A TURNOVER ENZYMES	236
4.6	GD3 AND GD3 ^A ARE RE-EXPRESSED BY MEDULLOBLASTOMA CELL LINES	236
4.7	OVER-EXPRESSION OF SIAE IN RES256 CELLS	239
4.8	AN INDUCIBLE SYSTEM APPROACH TO SIAE OVER-EXPRESSION REVEALS CHANGES IN GD3 EXPRESSION	240
4.9	SIAE OVEREXPRESSION COLLAPSES THE MITOCHONDRIAL MEMBRANE POTENTIAL IN RES256 CELLS	242
4.10	CHEMOTHERAPEUTIC RESPONSE WITH SIAE OVEREXPRESSION	244
4.11	CONCLUSIONS	249
4.12	FURTHER WORK	251
	REFERENCES	253
	APPENDICIES	275
	APPENDIX 1 – PLASMID MAPS AND SEQUENCE HOMOLOGY	276
	APPENDIX 2 – TRANSFECTION EFFICIENCY AND GD3/GD3 ^A CHANGES	282
	APPENDIX 3 – PLASMID MAPS AND SEQUENCE HOMOLOGY OF INDUCIBLE SYSTEM CONSTRUCTS	285
	APPENDIX 4 – INDUCTION TESTING OF PCMV-TetON3G CLONES	290
	APPENDIX 5 – RES256 ANTIBIOTIC CLONE SELECTION	293
	APPENDIX 6 – CELL LINE AUTHENTICATION AND CELL MORPHOLOGY	295
	APPENDIX 7- IC ₅₀ DATA AFTER TREATMENTS WITH CISPLATIN AND ETOPOSIDE	301
	APPENDIX 8- HIGH NG2 mRNA EXPRESSION IS ASSOCIATED WITH THE WNT SUBGROUP	303
	APPENDIX 9 – UPR16 FORM AND ETHICAL APPROVAL LETTER	304

List of tables

TABLE 1.2 DISEASE FEATURES OF SHH MEDULLOBLASTOMA	44
TABLE 1.3 DISEASE FEATURES OF GROUP 3 MEDULLOBLASTOMA	47
TABLE 1.4. DISEASE FEATURES OF GROUP 4 MEDULLOBLASTOMA	50
TABLE 1.5 SUMMARY OF DISEASE FEATURES IN EACH OF THE MOLECULAR SUBGROUPS OF MEDULLOBLASTOMA	52
TABLE 1.7 M STAGES OF CHANG'S STAGING CLASSIFICATION OF MEDULLOBLASTOMA	65
TABLE 1.8 MODIFICATION SITES OF HUMAN SIAE PROTEIN, ISOFORM 1	90
TABLE 2.1 TABLE OF CELL LINES USED THROUGHOUT THIS PROJECT	97
TABLE 2.2 CELL LINES AND CULTURE CONDITIONS	100
TABLE 2.3 TABLE OF THE ANTIBODIES USED THROUGHOUT THE PROJECT	106
TABLE 2.4 COMPONENTS USED FOR LINEARIZATION OF PTRE3G-IRES BACKBONE VECTOR	114
TABLE 2.5 PRIMERS WITH INFUSION CLONING OVERHANGS FOR CLONING	116
TABLE 2.6 COMPONENTS OF PCR REACTIONS FOR AMPLIFICATION OF GENES	116
TABLE 2.7 THERMAL CYCLING CONDITIONS FOR CLONING	116
TABLE 2.8 INFUSION PLUS HD ECO DRY REACTIONS	118
TABLE 2.9 PRIMERS USED FOR THE AMPLIFICATION OF SIAE AND SIAE-S127A GENES	120
TABLE 2.10 COMPONENTS USED FOR LINEARIZATION TO CONFIRM GENE INSERTION	122
TABLE 2.11 DILUTIONS FOR THE BCA ASSAY PROTEIN STANDARDS	134
TABLE 3.1 CHANG'S M STAGE CLASSIFICATION OF MEDULLOBLASTOMA PATIENTS	168

List of figures

FIGURE 1.1 THE WNT SIGNALLING PATHWAY FUNCTIONS IN CEREBELLAR DEVELOPMENT AND MEDULLOBLASTOMA	37
FIGURE 1.2 THE SHH PATHWAY IN CEREBELLAR DEVELOPMENT	43
FIGURE 1.3 ERBB SIGNALLING IN MEDULLOBLASTOMA	55
FIGURE 1.4 HISTOLOGICAL SUBGROUPS OF MEDULLOBLASTOMA	62
FIGURE 1.5 THE GANGLIOSIDE BIOSYNTHESIS PATHWAY	71
FIGURE 1.6 THE PROPOSED MECHANISM OF ACETYLATION OF GD3 TO 9-O-ACETYL GD3 BY CAS1	78
FIGURE 1.7 THE PRIMARY SEQUENCE OF SIAE ISOFORMS 1 AND 2	91
FIGURE 1.7 SIAE MODIFICATIONS SITES SHOWN AS PART OF THE HOMOLOGOUS AND HYPOTHESISED STRUCTURE OF THE SIAE PROTEIN	92
FIGURE 2.1 THERMAL CYCLING CONDITIONS FOR HUMAN AUTHENTICATION OF CELL LINES	102
FIGURE 2.2 AN OVERVIEW OF THE LIGASE-INDEPENDENT INFUSION PLUS HD CLONING PROTOCOL	112
FIGURE 2.3 PTRE3G-IRES CONSTRUCT IS LINEARISED BY RESTRICTION ENDONUCLEASE DIGESTION	114
FIGURE 2.4 EGFP INCORPORATION INTO THE PTRE3G-IRES CONSTRUCTS IS CONFIRMED	119
FIGURE 2.5 LINEARISATION OF THE PTRE3G-IRES-EGFP-SIAE CONSTRUCT DEMONSTRATES INTEGRATION OF THE GENE	123
FIGURE 2.6 CONFIRMATION OF SIAE AND SIAE-S127A INSERTION	125
FIGURE 2.7 THE JC-1 ASSAY	139
FIGURE 2.8 MECHANISM OF ACTION OF ETOPOSIDE	141
FIGURE 2.9 MECHANISM OF ACTION OF CISPLATIN	142
FIGURE 2.10 STEP-BY-STEP METHOD FOR DATA ACQUISITION FROM THE R2 DATABASE	151
FIGURE 3.1 THE MAJOR COMPONENTS OF THE GD3 ACETYLATION PATHWAY	156
FIGURE 3.2 EXPRESSION OF GD3 PATHWAY COMPONENTS AT THE MRNA LEVEL AS DETERMINED USING A BIOINFORMATICS APPROACH	159
FIGURE 3.3 THE CONCEPT OF GANGLIOSIDE BIOSYNTHESIS	162
FIGURE 3.4 ST8SIA1 AND ST8SIA5 EXPRESSION VARIES WITH MOLECULAR SUBGROUP OF MEDULLOBLASTOMA	163
FIGURE 3.5 MRNA EXPRESSION OF THE ACETYLATION AND DEACETYLATION REGULATING ENZYMES OF GD3 IN MEDULLOBLASTOMA TISSUE	164
FIGURE 3.6 A SUMMARY OF THE MRNA EXPRESSION OF THE REGULATING ENZYMES OF THE GD3 ACETYLATION PATHWAY BY MOLECULAR SUBGROUP	165
FIGURE 3.7 MRNA LEVELS OF ST8SIA1 AND ST8SIA5 ACCORDING TO METASTATIC STAGE	170
FIGURE 3.8 MRNA EXPRESSION OF CAS1 AND SIAE ACCORDING TO METASTATIC STAGE	171
FIGURE 3.9 EXPRESSION OF GD3 AND GD3 ^A WAS CONFIRMED BY FLOW CYTOMETRY	177
FIGURE 3.10 EXPRESSION OF GD3 AND GD3 ^A IS CONFIRMED BY IMMUNOCYTOCHEMISTRY	180
FIGURE 3.11 EXPRESSION OF GD3 AND GD3 ^A IN THE POST-NATAL DAY 5 AND DAY 60 WILD-TYPE MOUSE CEREBELLUM	182
FIGURE 3.12 HYPOTHESIS	184
FIGURE 3.13 SANGER SEQUENCING DEMONSTRATES THAT SIAE AND SIAE-S127A GENES WERE SUCCESSFULLY CLONED INTO THE PTRE3G-IRES-EGFP PLASMIDS	187
FIGURE 3.14 THE TET-ON 3G INDUCIBLE EXPRESSION SYSTEM	189
FIGURE 3.15 TWO PROTEINS ARE EXPRESSED FROM ONE MRNA TRANSCRIPT USING AN INTERNAL RIBOSOMAL ENTRY SITE	190
FIGURE 3.16 EGFP GENE EXPRESSION IS INDUCED IN THE PRESENCE OF DOXYCYCLINE	193
FIGURE 3.17 SIAE EXPRESSION IS INDUCED BY RES256 CLONES IN THE PRESENCE OF DOXYCYCLINE	195

FIGURE 3.18 SIAE AS A SECRETED ENZYME	197
FIGURE 3.19 CLEAVAGE SITES OF SIAE	199
FIGURE 3.20 A SUMMARY OF CASPASE 1 PATHWAYS	202
FIGURE 3.21 A HOMOLOGOUS SIAE STRUCTURAL MODEL PREDICTS THE CASPASE 1 CLEAVAGE SEQUENCE IS ACCESSIBLE TO CASPASE 1	204
FIGURE 3.22 GD3 EXPRESSION IS INCREASED WITH SIAE OVER-EXPRESSION	209
FIGURE 3.23 THE MITOCHONDRIAL MEMBRANE POTENTIAL IS DEPOLARISED BY SIAE OVER-EXPRESSION	211
FIGURE 3.24 RES256 CLONES ARE TREATED WITH CISPLATIN	215
FIGURE 3.25 RES256 CLONES ARE TREATED WITH ETOPOSIDE	217
FIGURE 3.26 DOSE-RESPONSE OF INDUCIBLE RES256 CLONES TO CISPLATIN TREATMENT	222
FIGURE 3.27 DOSE-RESPONSE OF INDUCIBLE RES256 CLONES TO ETOPOSIDE TREATMENT	224

List of abbreviations

[i(17q)] – isochromosome 17q

ADP – adenosine diphosphate

AIF – apoptosis inducing factor

AKT – protein kinase

ALL – acute lymphoblastic leukaemia

ANOVA – analysis of variance

APC – adenomatous polyposis coli

ATCC – American tissue culture collection

ATP – adenosine triphosphate

BCA – bicinchoninic acid

Bcl-2 – B-cell lymphoma 2

BCR – breakpoint cluster region

BET – bromodomain and extraterminal domain

Bid – BH3 interacting-domain death agonist

BrdU – 5-bromo-2'-deoxyuridine

BSA – bovine serum albumin

C-Myc – V-Myc avian myelocytomatosis viral oncogene homolog

Cas1 – cas1 domain containing 1 protein

CASD1 – gene encoding cas1 domain containing 1

CD95 – cluster of differentiation 95

cDNA – complementary deoxyribonucleic acid

CHO – Chinese hamster ovary

CK1 α – casein kinase 1 α

CMV – cytomegalovirus

CNS – central nervous system

CO₂ – carbon dioxide

CSF – cerebral spinal fluid

CT – computer aided tomography

CTNNB1 – gene encoding β -catenin

Cu – copper

CWC – column wash solution (commercial, Clontech)

DAPI – 4',6-diamidino-2-phenylindole

DKK1 – dickkopf-related protein 1

DKK4 – dickkopf-related protein 4

DMEM – Dulbecco's modified Eagle's medium

DMSO – dimethyl sulfoxide

DNA – deoxyribonucleic acid

Dox – doxycycline

DSH – dishevelled

E.coli – *Escherichia coli*

ECM – extracellular matrix

EDTA – ethylenediaminetetraacetic acid

EGF-2 – epidermal growth factor 2

EGFP – enhanced green fluorescent protein

EGFPF – enhanced green fluorescent protein forward primer

EGFPR – enhanced green fluorescent protein reverse primer

EGL – external granule layer

EMEM – minimum essential medium Eagle

ER – endoplasmic reticulum

ERB – endotoxin removal wash (commercial, Promega)

ERBB – Erb-B2 receptor tyrosine kinase

ERBB (1/2/3/4) – Erb-B2 receptor tyrosine kinase (1/2/3/4)

FACS – fluorescence-activated cell sorting

FBS – foetal bovine serum

FGF – fibroblast growth factor

FZDs – frizzleds

G-418 – geneticin

GAB1 – GRB2-associated-binding protein 1

GBM – glioblastoma multiforme

GCP – granule cell precursor

GD3 – ganglioside disialo 3

GD3^A – 9-O-acetyl GD3

gDNA – genomic deoxyribonucleic acid

GFAP – glial fibrillary acidic protein

GFP – green fluorescent protein

GLI (1/2/3) – glioma associated homologue (1/2/3)

GluCer – glucosylceramide

Golgi – Golgi apparatus

GSK3 – glycogen synthase kinase 3

GSLs – glycosphingolipids

GTML – mouse model of group 3 disease, the Glt1-tTA/TRE-MYCN-Luc mouse driven by the MYCN oncogene

Gy – gray (of radiation)

HBSS – Hank's balance salt solution

HE – haemagglutinin esterase

HiFi – high fidelity

HSK TK – herpes simplex virus thymidine kinase

IC₅₀ – inhibitory concentration eliciting a 50% response

ICE – interleukin 1 β converting enzyme

Ig(G/M) – immunoglobulin G/M

NHS – national health service

IGL – internal granule layer

JC-1 – 5,5',6,6'-tetrachloro-1,1',3,3'-tetraethylbenzimidazolylcarbocyanine iodide

IRES – internal ribosomal entry site

KCNA1 – potassium channel, voltage gated shaker related subfamily A, member 1

KDM6A – lysine (K)-specific demethylase 6A

LacCer – lactosylceramide

LARII – commercial buffer (Promega)

LCA – large cell anaplastic

LEF/TCF – T-cell factor/lymphoid enhancer factor

LP – lumbar puncture

M stage – metastatic stage

M-PER – mammalian protein extract reagent (commercial, Thermo Scientific)

MAPK – mitogen-activated protein kinase

MB – medulloblastoma

MBEN – medulloblastoma with extensive nodularity

MCS – multiple cloning site

MRI – magnetic resonance imaging

mRNA – messenger ribonucleic acid

MTA – material transfer agreement

MTS – [3-(4,5-dimethylthiazol-2-yl)-5-(3-carboxymethoxyphenyl)-2-(4-sulfophenyl)-2H-tetrazolium, inner salt]

MUSCLE – multiple sequence comparison by log-expectation

MYC – see C-Myc

MYCN – V-Myc avian myelocytomatosis viral oncogene neuroblastoma derived homolog

NE – proprietary buffer contained in Nucleospin kit (Clontech)

Neu – the rodent orthologue of ERBB2

NEU3 – sialidase 3

Neu5Ac – *N*-acetylneuraminic acid

NF- κ B – nuclear factor of kappa light polypeptide gene enhancer

NG2 – neuron-glia 2

NGS – normal goat serum

NPR3 – atrionatriuretic peptide receptor C

NRES – national research ethics service

NRL – neural retina leucine zipper

NT3 – proprietary buffer contained in Nucleospin kit (Clontech)

NTI – proprietary buffer contained in Nucleospin kit (Clontech)

OTX2 – orthodenticle homeobox 2

p – plasmid

PBS – phosphate buffered saline

PCR – polymerase chain reaction

PDB – protein data bank

PDGFR – platelet-derived growth factor receptor

PDT – population doubling time

PFA – paraformaldehyde

PI – propidium iodide

PKA – protein kinase A

PL – Purkinje cell layer

PNET – primitive neuroectodermal tumour

PTC1 – patched receptor 1

PTC2 – patched receptor 2

PTCH1 – patched 1 gene

PTPC – mitochondrial permeability transition pore complex

pUC – plasmid University of California

PVDF – polyvinylidene fluoride

qRT-PCR – quantitative real time polymerase chain reaction

RAS – protein first discovered in rat sarcoma

RLT – commercial buffer (Qiagen)

RNA – ribonucleic acid

RPE – commercial buffer (Qiagen)

RT – reverse transcriptase

RT-PCR – real time polymerase chain reaction

RW1 – commercial buffer (Qiagen)

SDS-PAGE – sodium dodecyl sulphate polyacrylamide gel electrophoresis

SFRP1 – secreted frizzled-related protein 1

SGNH – serine-glycine-asparagine-histidine domain

SHH – sonic hedgehog

SIAE – sialic acid *O*-acetyl esterase

SIAEF – sialic acid *O*-acetyl esterase forward primer

SIAER – sialic acid *O*-acetyl esterase reverse primer

siRNA – short interfering ribonucleic acid

SJMB'96 – A study by St. Jude's Children's hospital

SKK2 – mitogen-activated protein kinase kinase 3

SMO – smoothened

SNCAIP – gene encoding the α -synuclein-interacting protein

SOAT – sialic acid acetyl transferase

SOC – super optimal broth with catabolite repression

LB – lysogeny broth

ST8Sia1 – ST8 alpha-*N*-acetyl-neuraminide alpha-2,8-sialyltransferase 1 (GD3 synthase)

ST8Sia5 – ST8 alpha-*N*-acetyl-neuraminide alpha-2,8-sialyltransferase 5 (GT3/GD2 synthase)

STAT – signal transducer and activator of transcription

STR – short tandem repeat

SUFU – suppressor of fused

SV40 – simian virus 40

TAE – Tris-acetic acid ethylenediaminetetraacetic acid

TAG1 – transient Axonal Glycoprotein 1

TBS – Tris(hydroxymethyl)aminomethane hydrochloride buffered saline

TBST – Tris(hydroxymethyl)aminomethane hydrochloride buffered saline with tween 20

Tet – tetracycline

Tn5 – neomycin/kanamycin resistance gene

TP53 – the gene encoding p53

Tris-HCl – Tris(hydroxymethyl)aminomethane hydrochloride

TRKC – tropomyosin receptor kinase C

UK – United Kingdom

US – United States

UTR – untranslated region

VEGF – vascular endothelial growth factor

WHO – World Health Organisation

WNT – wingless

Wnt-1 – component of the wingless pathway

Wnt-7a – component of the wingless pathway

WR – working reagent

XIAP – X-linked inhibitor of apoptosis

$\Delta\Psi_m$ – change in the mitochondrial membrane potential

1 Introduction

1.1 Paediatric Brain tumours

1.1.1 Incidence

Brain tumours are the most common solid form of cancer in children and the second most common paediatric cancer, affecting 3.3 per 100,000 children (Gilbertson 2004). In England brain tumours have accounted for approximately 18% of all newly diagnosed cancers of childhood when averaged between 2008 and 2013. In England in 2010 there were 217 new cases of paediatric brain cancer and 76 resulting deaths, meaning over a third of these patients succumbed to their disease (35%) (Office for National Statistics 2013). These statistics have been generated from data obtained from patients under the age of 15, making this a likely under-estimation of true incidence. Today, brain tumours are the leading cause of childhood cancer related deaths (Brain Tumour Research 2015).

There are several embryonic brain tumours that can occur in the central nervous system (CNS). These have recently undergone re-classification by the World Health Organisation (WHO) (Louis et al. 2016). The currently recognised embryonal tumours are medulloblastoma (genetically or histologically defined; or not otherwise specified); embryonal tumour with multilayer rosettes (C19MC-altered or not otherwise specified); CNS neuroblastoma; CNS ganglioneuroblastoma; medulloepithelioma; atypical teratoid/rhabdoid tumour; CNS embryonal tumour with rhabdoid features; and finally, CNS embryonal tumour not otherwise specified (Louis et al. 2016; National cancer institute 2015).

1.1.2 Epidemiology

There are very few known risk factors associated with brain tumour development. The only well-established environmental risk factor is radiation exposure (American Cancer Society 2014). Most radiation-induced brain tumours however are caused by the treatment of other cancers, such as leukaemia. These secondary tumours usually develop 10 to 15 years after radiotherapy to the head, so tend not to affect children (Cancer Research UK 2015).

Other causes of childhood brain tumours include, in rare instances (< 5% of cases), inherited genetic mutations, which can increase the risk of some brain tumours. In other cases, the mutations are somatic. Known conditions which can increase the risk of childhood brain tumours, include neurofibromatosis type 1, the most common syndrome linked to brain and spinal cord tumours; neurofibromatosis type 2, tuberous sclerosis, Von Hippel-Lindau disease, Li-Fraumeni syndrome, Gorlin syndrome, Turcot syndrome, Cowden syndrome, hereditary retinoblastoma and Rubinstein-Taybi syndrome (American Cancer Society 2014). Some of these syndromes have helped to understand some of the underlying biology of their associated tumours, such as Gorlin syndrome, in which patients have mutations in the patched 1 gene *PTCH1*, which predisposes them to certain cancers including medulloblastoma (Fujii & Miyashita 2014).

1.1.3 Location and Symptoms of childhood brain tumours

The symptoms of brain tumours are general. Tumours in any part of the brain can raise intracranial pressure due to the location and/or size of the tumour in the confined space of the skull (American Cancer Society 2014). General symptoms that may indicate raised intracranial pressure include headaches, nausea, vomiting, crossing of the eyes or blurred

vision, balance problems, behavioural changes, seizures, drowsiness or coma (HeadSmart 2011). Headaches that worsen over time are a symptom of brain tumours, but importantly not all brain tumours cause headaches (American Cancer Society 2014). Patients may present with symptoms that gradually worsen over time, or their symptoms may present suddenly (Macmillan 2014).

In the first few years of life, symptoms of brain tumours can also include irritability, loss of appetite, developmental delay, and a drop in intellectual and physical ability (Macmillan 2014). In very young children a parent may also notice an increased head circumference that can be accompanied by bulging of the fontanelles as the tumour pushes outward against the unfused bone plates (American Cancer Society 2014). This diverse range of symptoms make brain tumours particularly devastating as they are often difficult to diagnose (Brain Tumour Research 2015).

Symptoms of brain tumours are often a result of their location, with the space-occupying lesions impacting on the function of surrounding tissue. Childhood brain tumours are most commonly infratentorial, meaning they occur at the lower portion of the back of the head (below the tentorium) (Patel et al. 2011). The structures that reside in this area include the cerebellum, brainstem and spinal cord. Most of the childhood tumours occur in these regions due to rapid proliferation of cells in this area during development of the brain, including the granule neuron precursors of the cerebellum which can give rise to medulloblastoma when faults occur (Gibson et al. 2010). Medulloblastoma is an embryonal cancer which most commonly arises from the neuronal precursor cells. This cellular origin differs from adult brain tumours which are most commonly glial in origin and are most often located supratentorially (Swartling et al. 2013).

1.1.4 Prognosis

Brain tumours are generally associated with a worse prognosis than many other paediatric cancers, such as leukaemia, and as a group they account for more than a quarter of childhood deaths from cancer (Gilbertson 2004). Survivors of childhood brain tumours commonly have life-long treatment-induced side effects that are exemplified in patients with medulloblastoma, the leading cause of childhood related mortality and the focus of this study (Hooper et al. 2014).

1.2 Medulloblastoma

Medulloblastoma is a malignancy of the cerebellum and is the most common malignant paediatric brain tumour, accounting for around 20% of cases (Millard & De Braganca 2015). Most cases of this disease are diagnosed in children under ten, with a peak incidence between the ages of three and eight (Millard & De Braganca 2015). The WHO defines medulloblastoma as a grade IV disease. Grade IV is the highest grade of malignancy that the WHO assigns. This classification means that this tumour is cytologically malignant, mitotically active, prone to necrosis and is associated with rapid pre- and post-operative disease evolution. Medulloblastoma also meets grade IV criteria as the disease features widespread infiltration of surrounding brain tissue and tendency for cranial-spinal dissemination (World Health Organisation 2007).

Symptoms of medulloblastoma encompass the general symptoms of brain tumours described in section 1.1.3, but due to their location patients also show symptoms associated with cerebellar dysfunction and blockage of cerebral spinal fluid (CSF) flow. Symptoms of medulloblastoma include vomiting, particularly in the morning. The time of day a patient vomits is important because the increased intracranial pressure from the

tumour blocking the flow of CSF through the fourth ventricle is affected by movement from the prone position to standing. Patients may also show 'sunset sign', a phenomenon where the eyes appear like a setting sun (the sclera of the eye is visible above the iris which is partly covered by the lower eyelid, as if the eyes are being forced downwards); this is a sign of raised intracranial pressure. Other symptoms of medulloblastoma also include a loss of fine motor movement, and rarely vision problems.

1.2.1 Origins of medulloblastoma

Medulloblastoma is a developmental tumour of the cerebellum so named by Harvey Cushing and Percival Bailey in 1925. The name medulloblastoma was given as they hypothesised the cell of origin as the 'medulloblast' (Millard & De Braganca 2015). We now know that the medulloblast, or cell of origin is actually several cells of origin, described later (Marshall et al. 2014) but its name has been retained. It is also known that some signalling pathways which have roles in the patterning and development of the cerebellum have cross-overs with medulloblastoma tumorigenesis (Wechsler-Reya & Scott 2001b). Patients who have Turcot and Gorlin syndrome have helped in the understanding of some of the underlying tumour biology as these patients are predisposed to medulloblastoma (Millard & De Braganca 2015). It is important to understand how these oncogenic signalling pathways contribute to medulloblastoma as this will help to improve clinical management of the disease. With these discoveries there will be more accurate predictors of disease risk and refinement of appropriate therapeutic strategies. Pharmacological intervention of these pathways will become more targeted and could lead to the development of new and effective treatments for this disease. In order to understand the tumorigenesis of this tumour, we must consider the development of the cerebellum.

1.3 Development of the cerebellum

The cerebellum (or 'little brain') is located at the back of the skull and is an important structure of the brain that controls, among others, learning and motor co-ordination. The cerebellar cortex contains intricate connections and five varieties of neuron (the granule neuron, Golgi cells, Purkinje cells, basket cells and stellate cells) (Bihannic & Ayrault 2016). The granule neuron in particular is implicated in the pathogenesis of medulloblastoma (Butts et al. 2014).

The granule neuron is by far the most numerous cell type of the cerebellum and actually outnumbers the rest of the neurons in the brain (Butts et al. 2014). The role of the granule neuron is to regulate the output and activity of the Purkinje cells, which means that they ultimately control the output of the cerebellum to the rest of the brain. Patients who have congenital granule cell degeneration have severe deficits in motor co-ordination, language and cognitive function which indicates their importance in these processes (Wechsler-Reya & Scott 2001a).

Neurogenesis of the granule cell has unique features; most neurons arise around the ventricles and migrate outwards towards the cortex. Granule cells however are generated outside of the cerebellum and migrate inwards, using the Bergmann glial tracts (reviewed by Butts et al. 2014). This process involves the dorsal hindbrain structure the rhombic lip, where granule neurons arise and migrate across the surface of the early cerebellum to form the external granule layer (EGL) (Alcántara et al. 2000; Wingate 2001; Alder et al. 1996). In rodents, a single layer of undifferentiated cells proliferates rapidly and generates a large pool of granule cell precursors (GCPs) at birth (Wechsler-Reya & Scott 2001a). As the GCPs are generated, the older cells begin to differentiate and migrate inwards, by extending

across the axons of Bergmann glia which are in contact with Purkinje cell dendrites (Wechsler-Reya 2003). The GPC cell bodies then migrate past the Purkinje cell bodies. The granule cells are then at their final destination, the internal granule layer (IGL) (Butts et al. 2014). The proliferation and differentiation of GCPs continues until about 3 weeks of age when the EGL depletes and the GCPs all mature into granule neurons (Wechsler-Reya 2003). It is thought that if faults arise during this process, medulloblastoma occurs (Wechsler-Reya & Scott 2001b). Medulloblastoma cells are not completely like any non-neoplastic cerebellar cell, but they are most similar to the granule neuron precursors, leading investigators to believe that the GCPs are the cell of origin for medulloblastoma (Wechsler-Reya & Scott 2001a).

1.4 Brain development and molecular subgroups of medulloblastoma

Patients with Turcot syndrome and Gorlin syndrome have a higher incidence of medulloblastoma and have shed some light on the origins of this disease (Cancer Research UK 2015). These patients have germline mutations in proteins involved in wingless (WNT) signalling and sonic hedgehog (SHH) signalling respectively, leading investigators to explore and confirm the roles of these developmental pathways in medulloblastoma pathogenesis (de Bont et al. 2008; Fujii & Miyashita 2014). The discovery of these pathways has allowed the stratification of patients into molecular subgroups of disease.

In 2012, the consensus on the molecular classification of medulloblastoma was published by Taylor et al. (2012). These molecular subgroups are defined by genetic and transcriptional signatures, which include mutations in the WNT and the SHH signalling pathways. Generic names are given to subgroups 3 and 4 as there is much less known about the underlying biology of these subgroups, importantly the subgroups are also clinically

distinct. These molecular subgroups will ultimately lead to the identification of new treatments and improvements in the way existing therapies are utilised.

1.4.1 The WNT Subgroup

The WNT signalling pathway controls a diverse range of developmental processes including the proliferation and fate of neural progenitor cells and also functions in cerebellar growth, patterning, and differentiation (Kalderon 2002). WNT proteins are a family of secreted molecules. Wnt-1, the first WNT protein to be identified, is known to be required in early embryogenesis for midbrain/hindbrain boundary (isthmus) formation from which the cerebellum arises (Buckles et al. 2004). When Wnt-1 mutations have been studied in mice they have serious defects of their midbrain and little to no cerebellum formation, indicating the importance of this pathway (Buckles et al. 2004). Another WNT protein, Wnt-7a, has been implicated in axon branching and synapse formation in granule cells and mossy fibres of the cerebellum (Ciani & Salinas 2005).

The WNT pathway regulates expression of proteins such as V-Myc Avian Myelocytomatosis Viral Oncogene Homolog (C-Myc) and cyclin D1, proteins which have roles in development, but are also known oncogenes (Gilbertson 2004). This pathway works through the controlled degradation of β -catenin and is summarised in figure 1.1.

1.4.2 Inactive WNT signalling

In the absence of WNT protein β -catenin concentrations are kept low through degradation (Ciani & Salinas 2005). This degradation is achieved through a protein complex that includes glycogen synthase kinase 3 (GSK3), the scaffolding protein axin, casein kinase 1 α (CK1 α) and adenomatous polyposis coli (APC). In the absence of ligand, casein kinase 1 α

phosphorylates β -catenin for further phosphorylation by GSK3 on residues 33, 37 and 41 (Gilbertson 2004). These phosphorylated residues provide binding sites for a protein, which promotes the polyubiquitination and complete proteolysis of β -catenin. Another complex that is known to degrade β -catenin has been described that includes presenilin 1 and shown in figure 1.1 (Kang et al. 2002).

1.4.3 Active WNT signalling

WNT proteins bind to their receptors, frizzleds (FZDs). With WNT protein bound, the protein dishevelled (DSH) is phosphorylated. This phosphorylation leads to GSK3 inactivation and results in the reduced phosphorylation and degradation of β -catenin (Ciani & Salinas 2005). The β -catenin can then be released from the protein complex containing APC, Axin, GSK3 and CK1 α or the complex containing protein kinase A (PKA), Presenilin-1 and GSK3 (Kang et al. 2002). β -catenin then accumulates and translocates to the nucleus where it interacts with transcription factors such as T-cell factor/lymphoid enhancer factor (LEF/TCF). LEF/TCF transcription factors can initiate transcription of C-Myc and cyclin D1, known oncogenes (Ciani & Salinas 2005).

1.4.4 WNT Signalling in Medulloblastoma

Mutations in APC were first implicated in medulloblastoma pathogenesis in Turcot syndrome patients (Hatten & Roussel 2011). Mutations in APC have only been found in 4% of sporadic medulloblastomas (Huang et al. 2000). Activating somatic mutations in *CTNNB1*, the gene encoding β -catenin have been found in between 8 and 15% of sporadic cases (Eberhart et al. 2000; Dahmen et al. 2001; Zurawel et al. 1998; Huang et al. 2000). Most of the reported activating β -catenin mutations in sporadic medulloblastomas target

residues S33 and S37 (Gilbertson 2004). These mutations prevent the phosphorylation-dependent degradation of β -catenin by GSK3. These mutations cause β -catenin to accumulate, driving oncogenic gene transcription (Gilbertson 2004). This occurs in the hypothesised cell of origin for this subgroup, the neural stem cell (Gajjar & Robinson 2014), the location and characteristics of which are described in table 1.1.

1.4.5 Subgroup features

Patients with WNT subgroup tumours have a very good long-term prognosis and five-year survival rates are around 95% (Gajjar & Robinson 2014). This subgroup is the rarest in incidence, accounting for 10% of cases (Goschzik et al. 2015). Of these only 5% of cases present with metastatic disease (Gajjar & Robinson 2014). Generally, patients who die from this subgroup of medulloblastoma die from complications of treatment or secondary neoplasm rather than the primary disease Taylor *et al.* 2012. Treatment of this subgroup is justifiably considered too aggressive given the high survival rates. Some patients are therefore given reduced-dose craniospinal radiotherapy and reduced intensity chemotherapy because of this, but they must not have metastatic disease and must be enrolled in clinical trial (Gilbertson 2004). The reason for better outcome for WNT patients remains unknown (Phoenix et al. 2016). However it has been suggested that it may be because these cells exhibit increased radio-sensitivity or that they have reduced invasive capacity (Salaroli et al. 2015). Others have suggested a disrupted blood brain barrier only seen in WNT disease which allows for a higher concentration of drug to reach the tumour (Phoenix et al. 2016).

The location of this subgroup of tumour is distinct, it occurs in the cerebellar midline, occupying the fourth ventricle where it can infiltrate the brain stem (Gilbertson 2004;

Raybaud et al. 2015). In the WNT mouse model of medulloblastoma the cell of origin is in the lower rhombic lip. When the cells gain oncogenic mutations of the WNT pathway, the cells fail to migrate and tumour forms (Eberhart 2012).

Overall this subgroup has an incidence of 1:1 male: female, differing from the general medulloblastoma ratio of incidence being 2:1 male: female. This subgroup of disease can occur at all ages but is less common in infants (0-3 years of age) (Gajjar & Robinson 2014).

Histologically WNT subgroup tumours demonstrate positive nuclear staining for β -catenin which guides diagnosis (Gajjar & Robinson 2014). Monosomy 6 also occurs in this subgroup but does not occur in every patient. Other than monosomy 6 there are very few other genetic amplifications or deletions in the genome of this subgroup (Gajjar & Robinson 2014).

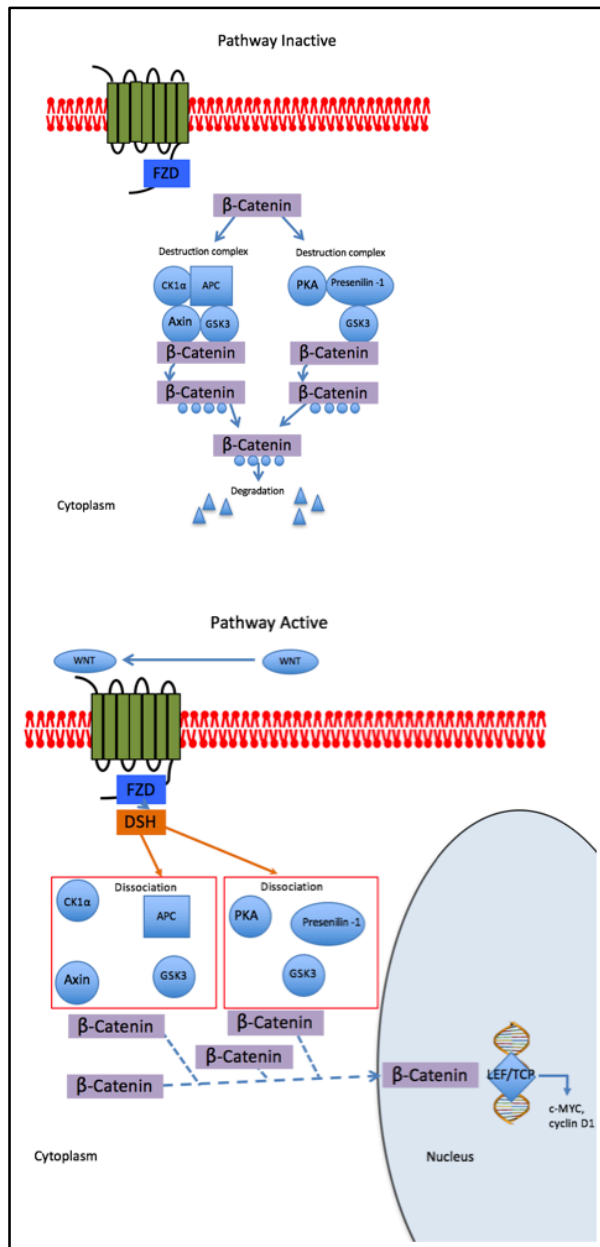


Figure 1.1 The WNT signalling pathway functions in cerebellar development and medulloblastoma. When the WNT pathway is inactive no ligand is bound to the frizzled receptor (FZD) and β -catenin is bound to the destruction complexes containing Casein kinase 1 α (CK1 α), adenomatous polyposis coli (APC), Axin and glycogen synthase kinase 3 (GSK3) or protein kinase A (PKA), presenilin-1 and GSK3). The bound β -catenin is then phosphorylated (blue circles) and allows the protein to be ubiquitinated and degraded in the cytoplasm. When the WNT pathway is active, WNT ligand is bound to FZD and the protein dishevelled (DSH) is phosphorylated, this inactivates GSK3 meaning β -catenin is not phosphorylated and the destruction complex dissociates. β -catenin then accumulates and translocates to the nucleus where it binds to the transcription factor T-cell factor/lymphoid enhancer factor (LEF/TCF) and initiates the transcription of known oncogenes such as *c-myc* and cyclin D1. In Medulloblastoma, WNT signalling can be activated without WNT ligand binding due to mutations in the β -catenin protein sequence that prevent its phosphorylation. These mutations mean β -catenin is not degraded as it cannot be ubiquitinated. Adapted from Gilbertson 2004.

Table 1.1 Disease features of WNT medulloblastoma. The proposed cell of origin and developmental stage are thought to be when aberrant WNT signalling drives tumorigenesis adapted from Gajjar & Robinson (2014).

Disease Feature	WNT Subgroup
Proposed cell of origin	Neural Stem cell <6 weeks post-embryonic
Origin	Possibly the sub-ventricular zone or fourth ventricle
Location of disease	Dorsal stem
Neoplastic event	WNT deregulation (among others?)
Candidate genes	WNT pathway, Dickkopf-related protein 1 (DKK1), Mitogen-Activated Protein Kinase Kinase 3 (SKK2), Dickkopf-related protein 4 (DKK4)
Underlying mechanism	Over-activation of stem cell maintenance

1.4.6 The SHH subgroup

PTCH1 is an example of a gene that controls cell fate and growth in the developing cerebellum (Tichy et al. 2015). If PTC1 function is reduced, for example by mutation, then this growth can become unregulated and contribute to pathogenesis of medulloblastoma (Northcott et al. 2015). The discovery of PTC1 in medulloblastoma pathology led to the identification of the PTC1 ligand SHH as a mitogen for cerebellar granule neuron precursors (Wallace 1999; Wechsler-Reya & Scott 1999; Tanaka et al. 2009; Dahmane & Ruiz i Altaba 1999).

In embryonic brain development SHH, a glycoprotein, is secreted by the Purkinje cells and maintains granule-neuron precursor cells in the undifferentiated, proliferating state (Tichy et al. 2015). Components of the signalling pathway, PTC1, PTC2, SMO, GLI1 and GLI2 are produced by the GCPs in the EGL (Wechsler-Reya & Scott 2001a). When Purkinje cells are absent GCP proliferation fails suggesting that SHH from the Purkinje cells plays a major role, or may be required for, the proliferation of GCPs (Smeyne et al. 1995).

1.4.7 Inactive SHH signalling

The SHH receptor patched 1 (PTC1) suppresses the activity of smoothed protein which is closely related to the frizzled family of WNT receptors (Taipale et al. 2002). PTC1 may suppress smoothed (SMO) indirectly, by acting as a transmembrane transporter for a small intermediary molecule (Gilbertson 2004). In the absence of SMO activity, the glioma-associated oncogene homologue (GLI) transcription factors, which are the effectors of the SHH pathway, are tethered to microtubules in the cytoplasm by a multi-protein complex that includes fused and suppressor-of-fused (SUFU) (Rubin & de Sauvage 2006). GLI1 is

sequestered into this complex, preventing the activation of gene transcription. GLI2 and GLI3 are cleaved to produce transcriptional repressors (Ruiz i Altaba 1997; Gilbertson 2004).

1.4.8 Active SHH signalling

The binding of the SHH ligand to PTC1 removes the suppression of smoothened (Gupta et al. 2010). Active smoothened can disrupt the multi-protein complexes which contain fused and SUFU (Gilbertson 2004). The binding of SHH to PTC1 removes the suppression of smoothened (Taipale et al. 2002). When smoothened is active the multi-protein complex, which contains fused and suppressor-of-fused, is disrupted (Gilbertson 2004). Subsequently, GLI1 is released and activates gene expression (Rubin & de Sauvage 2006). Cleavage of GLI1 and GLI3 is blocked. Although full length GLI2 and GLI3 can enter the nucleus, how they can affect gene transcription is currently unknown (Ruiz i Altaba 1997). A summary of this pathway is shown in figure 1.2.

1.4.9 SHH signalling in medulloblastoma

In the hereditary disease, Gorlin's syndrome, patients were found to have a predisposition for neoplasms, including medulloblastoma (Smith et al. 2014). The patients were found to have germline mutations in *PTCH1* (Smith et al. 2014).

Other mutations have also been identified in this subgroup, suggesting that heritable forms of the disease can result from several mutations in the SHH pathway Taylor et al. 2012.

Murine models of medulloblastoma exist and of these 14% of mice with a heterozygous loss of *PTCH* develop medulloblastoma. This low incidence may indicate that second-hits of the genome are required for tumourigenesis. Note that these mice do not exhibit loss of

p53, however tumours are more rapidly and frequently seen in heterozygous *PTCH* mice that have a deletion in *TP53*. Gilbertson (2004) has suggested that tumours occur in *PTCH* heterozygous *TP53* wild-type mice not due to disruption of the P53 pathway, but rather this deletion destabilises the genome (Gilbertson 2004). Finally, there is also evidence to suggest that overexpression of SHH in granule-neuron precursor cells can induce medulloblastoma in mouse models even in the absence of *GLI1* (H. L. Weiner et al. 2002).

1.4.10 Subgroup Features

This subgroup of medulloblastoma accounts for 30% of cases, with 15 – 20% of patients presenting with metastatic disease (Gajjar & Robinson 2014). Five-year survival for patients with this subgroup is in excess of 80% (Northcott et al. 2015), however a subset of patients with mutations in *TP53* have extremely poor prognosis, similar to that of group 3 patients (Zhukova et al. 2013). This subgroup has a distinct location compared to WNT tumours, suggesting a different origin (Gibson et al. 2010). SHH tumours tend to occur in the cerebellar hemispheres, and rarely in the midline (Raybaud et al. 2015; Gajjar & Robinson 2014).

The SHH subgroup of medulloblastoma occurs largely in infants (0-3 years) and adults (<16 years) but is much less frequent in the ages between (Taylor et al. 2012). There is an incidence of 1 : 1 male : female for this subgroup (Gajjar & Robinson 2014). SHH subgroup medulloblastomas are mostly identified by transcriptional profiling (Taylor et al. 2012; Northcott et al. 2015). Other approaches to identifying this subgroup have been via immunohistochemical staining for Secreted Frizzled-Related Protein 1 (SFRP1) and GRB2-associated-binding protein 1 (GAB1) (Taylor et al. 2012). Other characteristics for this subgroup include loss of chromosome 9q (where the *PTCH* gene is located) (Ellison et al.

2011). Because PTC1 is a negative regulator of the SHH pathway, deletion of *PTCH1* in granule-neuron precursor cells may result in malignant transformation (Gilbertson 2004). In fact, most SHH medulloblastomas are thought to arise from the transformed granule-neuron precursor cells, the location and characteristics of this subgroup are summarised in table 1.2. Mutations of *PTCH* have also been identified in 10-20 % of sporadic cases (Wechsler-Reya & Scott 2001a; Northcott et al. 2015).

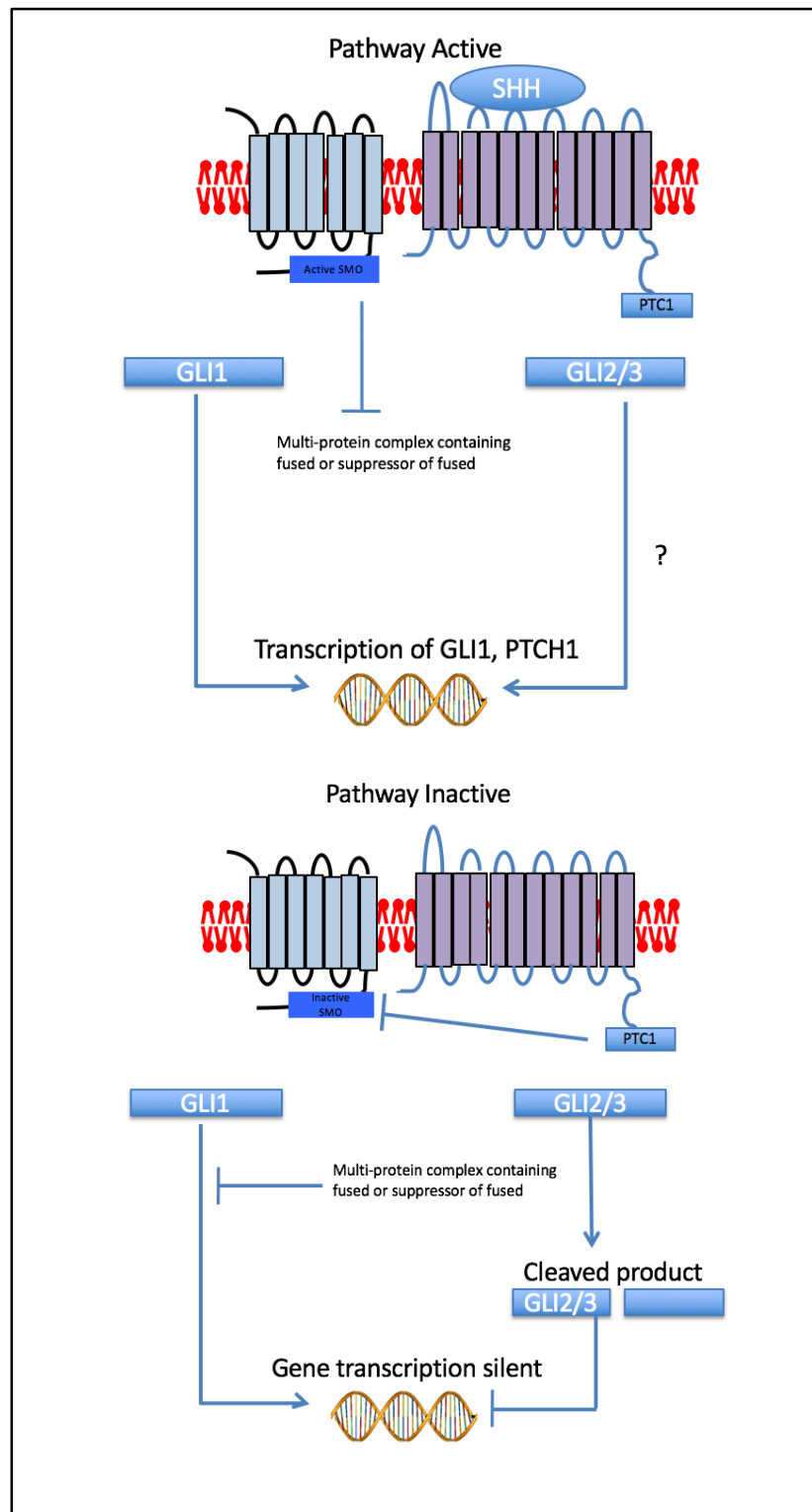


Figure 1.2 The SHH pathway in cerebellar development. In SHH is a secreted ligand which binds to the receptor Patched 1 (PTC1), this removes the inhibition on the receptor smoothened (SMO) and inhibits a multi-protein complex containing fused or suppressor of fused allowing glioma-associated homologue 1 (GLI1) and GLI2/3 to drive transcription. When the pathway is inactive gene transcription is silent due to inhibition of SMO. In SHH medulloblastomas there are mutations in this pathway, such as mutations of SMO and PTC1, which drive expression of the oncogenes. Adapted from (Gilbertson 2004)

Table 1.2 Disease features of SHH medulloblastoma. The proposed cell of origin and developmental stage are thought to be when aberrant SHH signalling drives tumorigenesis. Adapted from Gajjar & Robinson 2014.

Disease Feature	SHH Subgroup
Proposed cell of origin	Neural Stem cell or granule precursor cell <10 weeks embryonic
Origin	External granule layer of the cerebellum
Location of disease	External granule layer
Neoplastic event	SHH deregulation in the granule precursor cell
Candidate genes	SHH pathway PTCH1, GLI1, V-Myc Avian Myelocytomatosis Viral Oncogene Neuroblastoma Derived Homolog (MYCN)
Underlying mechanism	Over-activation of stem cell maintenance

1.4.11 Group 3 and Group 4 medulloblastomas

There is much less known about the signalling pathways involved in the pathogenesis of group 3 and group 4 medulloblastoma, and they are so named as currently there is no known consistent signalling pathway involvement for either (Taylor et al. 2012).

1.4.12 Group 3

25% of medulloblastoma patients have group 3 disease (Gajjar & Robinson 2014). Group 3 carries the worst prognosis of the medulloblastoma subgroups (Taylor et al. 2012). 5 year-survival is currently around 50% (Gajjar & Robinson 2014). Patients who have this subgroup of tumour very frequently present with metastatic disease (40-45 % cases) (Gajjar & Robinson 2014). This subgroup is more common in infants and children but is almost never seen in adults, it is also more common in males than females (Taylor et al. 2012). No germline mutations have been found (Schroeder & Gururangan 2014). The location of the group 3 tumours is generally in the fourth ventricular midline (Gajjar & Robinson 2014).

Group 3 tumours overexpress a number of genes that were initially discovered for their roles in retinal development (de Haas et al. 2006). It is currently not known what role these genes play in the pathogenesis of this subgroup (Northcott et al. 2015). This subgroup also expresses high levels of MYC (but not MYCN) which lead some investigators to suggest this group should be remained the MYC subgroup (Taylor et al. 2012). Over-expression of MYC however is not strictly limited to this subgroup (Roussel & Robinson 2013). For example, some patients with favourable prognosis WNT tumours may exhibit overexpression of MYC, although this almost never occurs (Roussel & Robinson 2013). Despite this, the favourable outcome of the WNT subgroup is retained in these patients (Staal et al. 2015). Another

suggested marker of this subgroup is immunohistochemical positivity for atrionatriuretic peptide receptor C (NPR3) (Taylor et al. 2012). Despite these suggestions group 3 is currently stratified by a similar molecular signature to other group 3 tumours, and a different signature from the other subgroups (Northcott et al. 2011) .

Group 3 share some of the characteristics of group 4 tumours, such as amplification of the patterning gene Orthodenticle Homeobox 2 (*OTX2*), which represses differentiation and can up-regulate MYC (Marshall et al. 2014).

Genetic characteristics of this subgroup are also shared with group 4, however gain of chromosome 1q and/or loss of chromosomes 5q and 10q are much more likely to be seen in group 3 tumours than group 4 (Taylor et al. 2012; Gilbertson 2004). Genetic abnormalities seen in this subgroup are gains in 1q and 7 and losses in 10q and 16q (Taylor et al. 2012; Packer et al. 1994). This subgroup can also exhibit isochromosome 17q, seen in 26 % of patients, this is also seen in group 4 patients, but not in WNT or SHH tumours (Gajjar & Robinson 2014). The characteristics of this subgroup are summarised in table 1.3.

One mouse model of group 3 is currently available, the GTML (Glt1-tTA/TRE-MYCN-Luc) mouse driven by the MYCN oncogene (Ahmad et al. 2015; Gendoo et al. 2015). Despite MYC amplification being more common in this subgroup, these mice exhibit similar histology to group 3 tumours in humans (Pöschl et al. 2014).

Table 1.3 Disease features of group 3 medulloblastoma. Adapted from Gajjar & Robinson 2014.

Disease Feature	Group 3
Proposed cell of origin	Granule neuron precursor cell 10-20 weeks early foetal
Origin	Immature pineal or retinal region
Location of disease	External granule layer
Neoplastic event	Granule neuron precursor lineage switch to rod precursor
Candidate genes	MYC, neural retina leucine zipper (NRL), rod proliferation
Underlying mechanism	Decoupling of differentiation/proliferation

1.4.13 Group 4

Group 4 is the most common subgroup of medulloblastoma, encompassing approximately one third of patients (Gajjar & Robinson 2014). Currently, group 4 medulloblastoma patients are identified through a transcriptional profile that clusters them with other group 4 patients (Northcott et al. 2011). This subgroup has a higher incidence in males with a 3:1 male : female incidence (Taylor et al. 2012; Gajjar & Robinson 2014). This subgroup carries an intermediate prognosis similar to that of the SHH subgroup. 35-40 % of patients present with metastatic disease (Gajjar & Robinson 2014).

Group 4 tumours have been shown to overexpress neuronal differentiation markers which may help to define this subgroup (Taylor et al. 2012). It has also been suggested that positive immunohistochemical staining of the protein Potassium Channel, Voltage Gated Shaker Related Subfamily A, Member 1 (KCNA1), a potassium channel, could define this subgroup (Taylor et al. 2012). Both of these markers requires further validation as expression may not be exclusive to group 4 tumour and the clinical relevance of these markers are not yet apparent (Taylor et al. 2012). The most frequent mutation seen in this subgroup is in Lysine (K)-Specific Demethylase 6A (KDM6A), a demethylase gene that regulates trimethylation status of lysine 27 of histone 3 (H3K27) in stem cells (Robinson et al. 2012; Northcott, Jones, et al. 2012; Jones et al. 2012; Pugh et al. 2012). The KDM6A gene is located on the X chromosome and there is a homologue located on the Y chromosome, however this mutation is more commonly seen in males than females (Robinson et al. 2012). In addition 10% of patients also have a single copy gain of 5q23.2, where the α -synuclein-interacting protein (*SNCAIP*) gene is located (Gajjar & Robinson 2014). In Parkinson's disease patients the encoded synphillin-1 binds to α -synuclein to promote the

formation of Lewy bodies. The role of synphilin-1 in medulloblastoma is however currently unknown (Northcott, Jones, et al. 2012; Northcott, Shih, et al. 2012). This subgroup does not overexpress MYC like the group 3 tumours, the expression of MYCN is also generally low apart from a few cases which have MYCN amplification (Roussel & Robinson 2013).

Although isochromosome 17q is seen in group 3 tumours, it is much more common in group 4 tumours, seen in 66 % of patients, and is the most common genetic change (Gajjar & Robinson 2014). The only other genetic change in group 4 tumours that is commonly seen is the loss of the X chromosome in female patients that occurs in 80 % of cases (Gajjar & Robinson 2014). No mouse model of this subgroup currently exists (Eberhart 2012; Gajjar & Robinson 2014). The characteristics of this subgroup are summarised in table 1.4.

Table 1.4. Disease features of group 4 medulloblastoma. Adapted from Gajjar & Robinson 2014.

Disease Feature	Group 4
Proposed cell of origin	Granule neuron precursor cell >20 weeks late foetal
Origin	Premature glutamatergic neuronal networks
Location of disease	External granule layer/ internal granule layer
Neoplastic event	Deregulation during synaptic pruning
Candidate genes	α -Synuclein-Interacting Protein (SNCAIP), α -synuclein/semaphorin apoptosis
Underlying mechanism	Imbalance of apoptosis, survival and proliferation

In summary the four molecular subgroups of medulloblastoma that have currently been identified share some disease features and have distinct defining features. These are summarised in table 1.5.

Table 1.5 Summary of disease features in each of the molecular subgroups of medulloblastoma demonstrating similarities and differences within each of the subgroups. Adapted from Gajjar & Robinson, 2014.

Disease Feature	WNT	SHH	Group 3	Group 4
Proposed cell of origin	Neural Stem cell <6 weeks post-embryonic	Neural Stem cell or granule precursor cell <10 weeks embryonic	Granule neuron precursor cell 10-20 weeks early foetal	Granule neuron precursor cell >20 weeks late foetal
Origin	Possibly the sub-ventricular zone or fourth ventricle	External granule layer of the cerebellum	Immature pineal or retinal region	Premature glutamatergic neuronal networks
Location of disease	Dorsal stem	External granule layer	External granule layer	External granule layer/ internal granule layer
Neoplastic event	WNT deregulation (among others?)	SHH deregulation in the granule precursor cell	Granule neuron precursor lineage switch to rod precursor	Deregulation during synaptic pruning
Candidate genes	WNT pathway, Dickkopf-related protein 1 (DKK1), Mitogen-Activated Protein Kinase Kinase 3 (SKK2), Dickkopf-related protein 4 (DKK4)	SHH pathway PTCH1, GLI1, V-Myc Avian Myelocytomatosis Viral Oncogene Neuroblastoma Derived Homolog (MYCN)	MYC, neural retina leucine zipper (NRL), rod proliferation	α -Synuclein-Interacting Protein (SNCAIP), α -synuclein/ semaphorin apoptosis
Underlying mechanism	Over-activation of stem cell maintenance	Over-activation of stem cell maintenance	Decoupling of differentiation/ proliferation	Imbalance of apoptosis, survival and proliferation

1.5 Other signalling pathways implicated in medulloblastoma pathogenesis

The WNT and SHH pathways are unlikely to be the only cell-signalling systems that are deregulated during medulloblastoma formation. For example, the amplification of MYC occurs quite commonly in large-cell anaplastic medulloblastomas, described later, and is thought to be associated with poor clinical outcome (Roussel & Robinson 2013). In contrast, tumour cell expression of the neurotrophic receptor Tropomyosin receptor kinase C (TRKC) has been associated with favourable outcome in medulloblastoma patients (Segal et al. 1994). Studies have also identified platelet-derived growth factor receptor (PDGFR) and RAS MAPK pathway activation as potential mediators for dissemination of medulloblastoma (Gilbertson & Clifford 2003; MacDonald et al. 2001).

There is also evidence that the aberrant expression of Erb-B2 Receptor Tyrosine Kinase 2 (ERBB2) in granule-neuron precursor cells of the cerebellum may have a role in medulloblastoma formation (Gilbertson et al. 1997; Gilbertson et al. 2001; Gajjar et al. 2004). In studies of more than 150 paediatric medulloblastoma patients ERBB2 protein expression was shown in 80 % of the tumour samples (Gilbertson et al. 1997; Gilbertson et al. 2001; Gajjar et al. 2004). The finding contrasts from non-neoplastic cerebellum where ERBB2 is not expressed at any stage during normal development (Gilbertson et al. 1998). ERBB2 has been associated with poor clinical outcome in these patients (Gilbertson et al. 1997; Gilbertson et al. 2001; Gajjar et al. 2004).

ERBB1, ERBB2, ERBB3 and ERBB4 are members of the receptor tyrosine kinase I family. A summary of this pathway is shown in figure 1.3. These receptors interact through a complex network of hetero- and homodimerisations (Muthuswamy et al. 1999). ERBB dimers activate the cell signalling pathways of mitogen-activated protein kinase (MAPK), AKT and

signal transducer and activator of transcription (STAT), which allows them to regulate several key cell processes such as proliferation, apoptosis, migration and differentiation (Zomerman et al. 2015).

When aberrant up-regulation of ERBB2 occurs cell transform can also occur (Yarden & Sliwkowski 2001; Segatto et al. 1988). In rodents, a point mutation (V664E) results in a significant increase in homodimerisation of the transmembrane domain of *Neu* (the rodent orthologue of ERBB2) (Weiner et al. 1989; Padhy et al. 1982) inducing tumour formation in the CNS. Although an equivalent mutation in human ERBB2 transforms cells, this mutation has not been identified in sporadic human tumours (Segatto et al. 1988; Gilbertson 2004) .

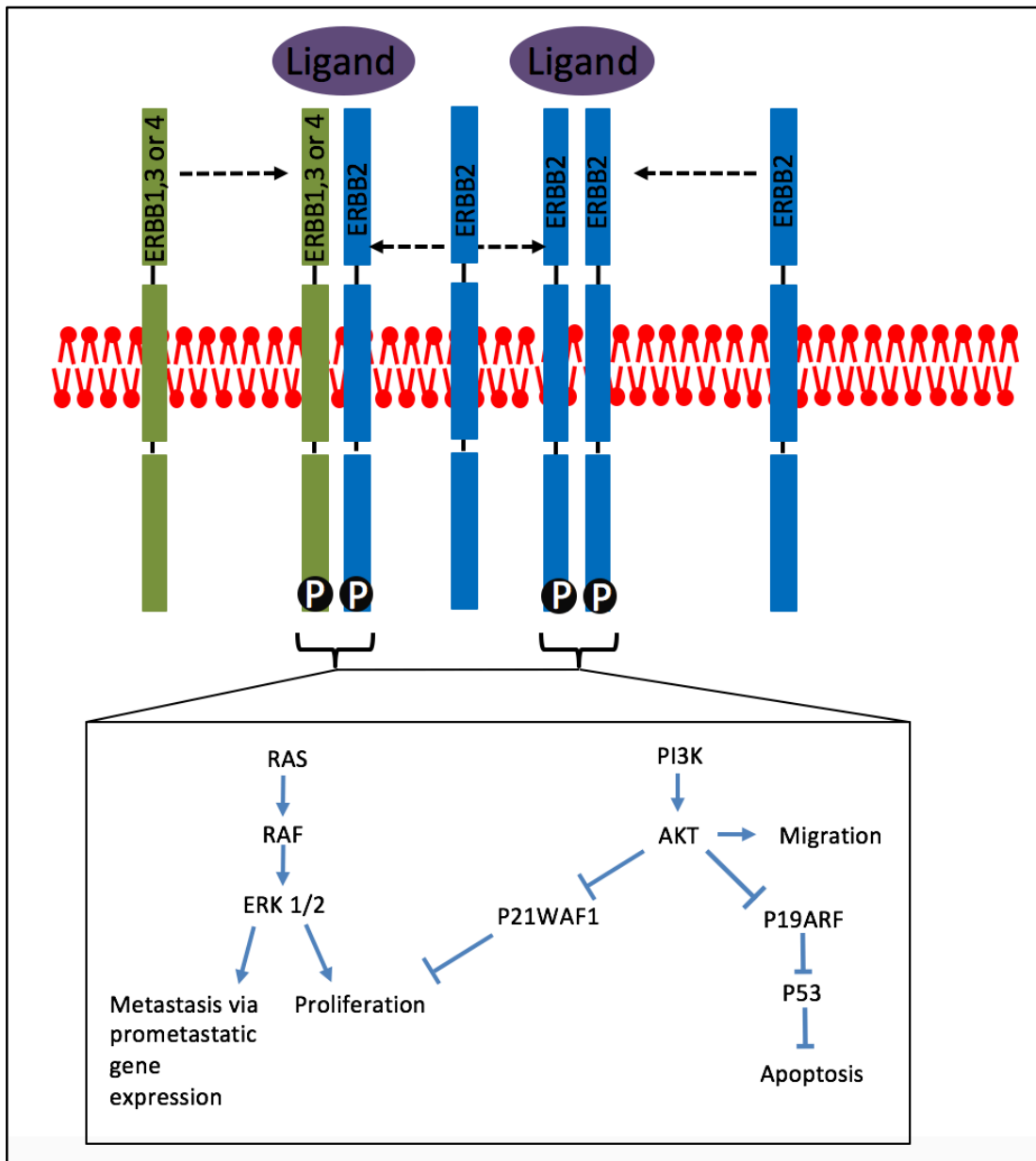


Figure 1.3 ERBB signalling in medulloblastoma. ERBB1, 3 or 4 can heterodimerise with ERBB2, and when overexpressed ERBB2 can homodimerise. Upon dimerization autophosphorylation occurs (P) and activates downstream signalling via RAS and PI3K leading to increased proliferation, metastasis and inhibition of apoptosis. Adapted from (Gilbertson 2004)

1.6 Emerging molecular-subgroup targeted therapies

Survival of patients with medulloblastoma varies according to molecular subgroup (Taylor et al. 2012). In order to address this problem more targeted therapeutics are beginning to emerge. These therapeutics target cell-signalling pathways that function abnormally in medulloblastoma.

Cyclopamine is a plant-derived teratogen that inhibits the SHH pathway (Samkari et al. 2015). The mechanism of action of this drug is to bind to and thus inactivate smoothened (Samkari et al. 2015). This drug is only suitable for patients with recurrent disease and either PTC1 mutations or some SMO mutations, leaving around 50% of SHH patients predicted to respond (Gilbertson 2004). Cyclopamine specifically targets the SHH pathway in medulloblastoma cells, causing the inhibition of GLI-mediated gene expression, cell cycle arrest and therefore has antineoplastic activity (Gilbertson 2004; Samkari et al. 2015). Other smoothened antagonists are in preclinical development and are expected to enter early clinical trials for medulloblastoma within the next few years. Recently, resistance to SHH pathway inhibitors have been reported (Gilbertson 2004). The mechanism of resistance is reported to be mutations in SMO which occur with prolonged exposure, these mutations prevent drug binding and therefore a reduction in efficacy (Samkari et al. 2015; Gilbertson 2004).

Small-molecular inhibitors of receptor tyrosine kinases are a second class of potential molecular-targeted therapies for medulloblastoma (Hernan et al. 2003). A diverse range of agents that inhibit ERBB2 expression and function are currently being developed. These inhibitors include the non-selective ERBB1 and ERBB2 antagonist erlotinib (Hernan et al. 2003). Erlotinib treatment selectively blocks the expression of several ERBB2-dependent

pro-metastatic genes and reduces the invasive capacity of medulloblastoma cells (Gilbertson 2004). This drug is currently under phase I and II trials for medulloblastoma in the Children's Oncology Group and through the US Paediatric Brain Tumour Consortium and has shown good tolerance and efficacy in phase I trials (Jakacki et al. 2008; Gilbertson 2004).

Other treatments that may prove useful for subgroup directed therapy for group 3 tumours are gemcitabine and pemetrexed, these drugs have been shown to have some efficacy against MYC amplification (Morfouace et al. 2014). Bromodomain and extraterminal domain (BET) antagonists, which interfere with MYC-associated transcription have also shown some efficacy against these tumours in mice and some xenografted cell lines (Bandopadhyay et al. 2014; Henssen et al. 2013).

1.7 Histopathological variants

Molecular subtyping has not yet found a place within most UK clinical settings and therefore patients are stratified based on their histological subgrouping (Packer et al. 2003; Ramaswamy et al. 2015). Overlap of histological and molecular subgroups is shown in table 1.6.

Table 1.6 Overlap of molecular subgroup and histology. Adapted from Taylor *et al.* 2012.

Molecular Subgroup	Histology
WNT	Classic, rarely large cell/anaplastic
SHH	Classic, desmoplastic/nodular (predominantly), large cell/anaplastic, MBEN (nearly all MBENs are SHH)
Group 3	Classic, large cell/anaplastic (40% of all large cell/anaplastic tumours are group 3)
Group 4	Classic, rarely large cell/anaplastic

Histological variants of medulloblastoma have been recognised by the WHO and so named classic, desmoplastic/nodular, large cell/anaplastic, and medulloblastoma with extensive nodularity (MBEN) subgroups may also exhibit myogenic or melanotic features, (World Health Organisation 2007; Gajjar & Robinson 2014).

1.7.1 Classic Variant of medulloblastoma

The classic variant of medulloblastoma is defined as having sheets of cells with small round nuclei, a high ratio of nuclei to cytoplasm and mild nuclear polymorphism. These cells occasionally show features of neuroblastic differentiation, demonstrated by the presence of neuroblastic rosettes figure 1.4A (World Health Organisation 2007; Gajjar & Robinson 2014).

1.7.2 Desmoplastic /nodular variant of medulloblastoma

This histological subgroup is defined by nodules of differentiated neurocytic cells that express neuronal proteins. There are also internodular regions which are characterised by undifferentiated embryonal cells and reticulin-rich strands of collagen figure 1.4B (World Health Organisation 2007; Gajjar & Robinson 2014).

1.7.3 Large Cell/ Anaplastic variant of medulloblastoma (LCA)

Large cell and anaplastic variants of medulloblastoma have considerable cytological overlap and are therefore grouped together as the large cell/anaplastic variant.

Histologically classified as having marked nuclear pleomorphism, nuclear moulding, cell-cell wrapping and high mitotic activity, often with atypical forms and abundant apoptotic bodies. To be defined as an anaplastic tumour there must be extensive regions of this

phenotype. The large cell variant has spherical cells with round nuclei, open chromatin and prominent central nucleoli (figure 1.4C). All medulloblastomas show some degree of atypia, these changes however are particularly pronounced in the anaplastic variant. In some patients, when biopsies are taken, a transition between classic and large/anaplastic histology can be seen (World Health Organisation 2007; Gajjar et al. 1999) .

1.7.4 Medulloblastoma with extensive nodularity (MBEN)

This variant is closely related to desmoplastic/nodular disease but differs as it exhibits an expanded lobular architecture. Expansion of these areas are due to reticulin-free zones which become usually large and rich in neuropil-like tissue. Reticulin-free zones contain a population of cells which resemble those of a neurocytoma and exhibit a streaming pattern. Between nodules the areas are rich in reticulin (figure 1.4D), it is this histology that is prevalent in the desmoplastic/nodular variant which is much reduced in this subgroup. This subgroup carries a more favourable prognosis than the classic subgroup medulloblastomas (World Health Organisation 2007; Gajjar & Robinson 2014).

1.7.5 Myogenic differentiation

Medulloblastoma with myogenic differentiation was referred to as medullomyoblastoma but is no longer considered a distinct subgroup, but rather a feature of any subgroup. To define myogenic differentiation, the tumour must contain rhabdomyoblastic elements and stain positive for desmin, myoglobin, fast myocin, but not smooth muscle α -actin alone. An example of this feature is shown in figure 1.4E.

1.7.6 Melanotic differentiation

This was previously termed melanocytic medulloblastoma, but much like medulloblastoma, this is no longer a distinct subtype but rather a feature of any other subgroup. An example of this histology is shown in figure 1.4F Cells with melanotic features may appear to be undifferentiated, or epithelial, with tubule or papillae formation, they also usually express S-100 protein (World Health Organisation 2007; Gajjar et al. 1999).

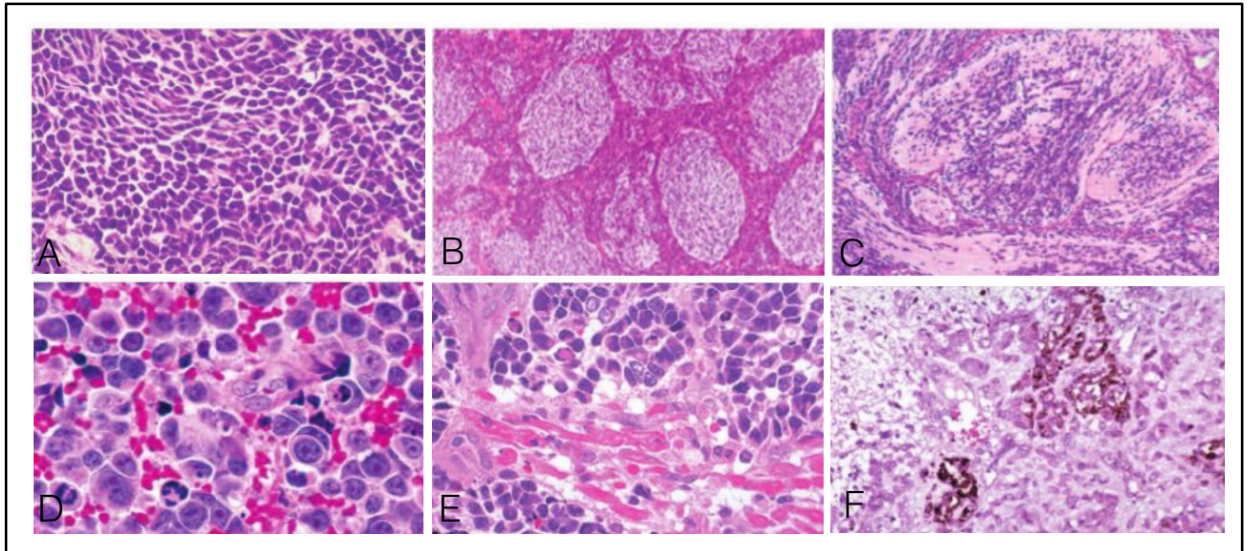


Figure 1.4 Histological subgroups of medulloblastoma. (A) Classic medulloblastoma showing a typical arrangement of sheets of undifferentiated cells. (B) Desmoplastic/nodular medulloblastoma showing pale nodular areas surrounded by densely packed hyperchromatic cells. (C) Large cell/anaplastic medulloblastoma showing enlarged vesicular nuclei, prominent nucleoli and moderate cytoplasm. (D) Medulloblastoma with extensive nodularity has a lobular architecture with large elongated reticulin-free zones. These zones contain small round neurocytic cells in the fibrillary background. (E) Medulloblastoma with myogenic differentiation showing striated muscle fibres with brisk mitotic activity. (F) Medulloblastoma with melanotic differentiation showing typical tubular-like features. Images from the World Health Organisation classification of central nervous system tumours (2007)

1.8 Treatment of medulloblastoma

Current treatment for medulloblastoma includes maximal safe surgical resection, radiotherapy if the patient is over 3 years of age, and high-dose chemotherapy (Schuler et al. 2014). Survivors of this disease often suffer significant treatment-related sequelae including endocrine disorders and neurocognitive deficits (Michiels et al. 1996). These problems occur as the nature of treatment is aggressive and damaging to the developing brain tissue (Gajjar et al. 1999).

Multimodality treatments have substantially improved survival for patients with medulloblastoma, however approximately one third of cases remain incurable (Gilbertson 2004). Medulloblastoma in children younger than three years is twice as likely to progress within five years of diagnosis than medulloblastoma occurring in older children (Gilbertson 2004). One explanation for age-dependent disease behaviour is the restriction that age imposes on treatment. Children under three do not have radiotherapy as it would inflict severe damage to their developing brains that is deemed unacceptable (Polkinghorn & Tarbell 2007). Others have speculated that young children have more aggressive tumours (Packer et al. 2003). Initial treatment for patients less than three years of age is generally restricted to surgical resection and chemotherapy (Michiels et al. 1996). This approach is associated with a median time to progression of less than nine months (Gilbertson 2004).

Poor clinical outcome is seen when surgical resection leaves more than 1.5 cm² on post-operative MRI and if there is presence of secondary tumours (Ramaswamy et al. 2015). Medulloblastoma has the ability to migrate and form secondary tumour masses through leptomeningeal dissemination or possibly via vascular metastasis (Garzia et al. 2015). Around a third of patients present with CNS dissemination at time of diagnosis (World

Health Organisation 2007). A small but important group of patients also develop extra-neural metastasis to the bone, bone marrow, lymph nodes, liver or lung. This type of medulloblastoma is staged according to Chang's criteria (metastatic or M stage; table 1.7) and these secondary tumours remain one of the most important prognostic markers of medulloblastoma (Dufour et al. 2012; Gilbertson 2004).

Table 1.7 M stages of Chang's staging classification of medulloblastoma adapted from (Dufour et al. 2012)

M stage

M0	No gross subarachnoid or haematogenous metastasis.
M1	Tumour cells found in cerebral spinal fluid on microscopic analysis.
M2	Gross nodular seeding in the cerebellum, cerebral subarachnoid space, or in third or fourth ventricles.
M3	Gross nodular seeding in spinal arachnoid space.
M4	Extra-neural metastasis.

Accurate predictions of disease-risk are necessary with medulloblastoma patients in order to reduce the risk of tumour recurrence, which is frequently fatal (Ramaswamy et al. 2013), and to avoid overtreatment of patients who would be likely to survive with less intense therapeutic intervention (Schuler et al. 2014).

Currently children with medulloblastoma are characterised into two risk groups. Patients with average-risk disease are those diagnosed over the age of three, with no secondary tumour masses and $<1.5 \text{ cm}^2$ residual disease on post-operative MRI and no presence of anaplasia on histological examination (Borowska & Józwiak 2016). Patients who do not meet these criteria are classified as high-risk (Tarbell et al. 2013). In Europe, the patient's age and m stage ($\leq M1$ vs $\geq M2$) alone are used to assign disease risk (Gilbertson 2004). This method of assessment is not precise; it does not identify the 20-30% of patients with average-risk disease. Nor does this method identify the unknown number of average-risk patients who are over-treated with current protocols which leads to increased toxicity and downstream sequelae for these children (de Bont et al. 2008).

1.8.1 Treatment protocols based on disease risk

Average-risk medulloblastoma is treated with maximal safe surgical resection, followed by chemotherapy and whole neuraxis radiotherapy (Kortmann et al. 2000; Taylor et al. 2003; Packer et al. 1999; Strother et al. 2001). As radiotherapy is so damaging to the non-neoplastic brain, in the US, standard radiation to the neuraxis for average-risk medulloblastoma has been reduced from 35 Gy to 23.4 Gy (Packer et al. 1999; Strother et al. 2001; Thomas et al. 2000). The concurrent introduction of adjuvant therapy has enabled this reduction in radiation dose without affecting the survival rate. A radiation dose of 23.4 Gy is however still associated with neurological deficits, especially in patients who are less

than 8 years of age (Ris et al. 2001). Because of this a phase III study by the Children's Oncology Group (ACNS0331) was carried out that tests the safety of further reductions in radiation dose down to 18.0 Gy for average-risk patients aged between three and eight years. The aim of this study is to ensure that if reductions of radiation dose reduced disease morbidity, they did not do so at the expense of under treating the pathology. This study is still in its recruitment stage (Children's Oncology Group 2013). Post-operative chemotherapy and radiation are also used to treat average-risk patients in Europe, although the neuraxis dose has not yet been reduced from 35.0 Gy (Gilbertson 2004).

There have been several chemotherapeutic regimens that have been investigated for the treatment of average-risk medulloblastoma. These include pre-radiation (sandwich) regimens and post-radiation chemotherapy (Taylor et al. 2003; Packer et al. 1999; Strother et al. 2001). These studies have shown that a combination of post-operative chemotherapy and radiotherapy is more effective at treating average-risk medulloblastoma than surgery and radiotherapy alone. However, which of the adjuvant chemotherapy regimens carries the greatest survival advantage is currently unclear as the 5-year survival rates for many tested protocols are reported to be around 75% (Kortmann et al. 2000; Taylor et al. 2003; Packer et al. 1999; Thomas et al. 2000).

Progression-free survival in children with high-risk medulloblastoma has been typically less than 50% (Ellison et al. 2003). Some combination chemotherapy and radiotherapy treatments have yielded more promising results. A study by St. Jude's Children's hospital (SJMB'96) has used radiotherapy followed by high-dose chemotherapy and autologous stem-cell rescue and has proven to be tolerated well and overall-survival was reported to

be 85% for average-risk; and 70% for high-risk patients (Gajjar et al. 2006). This treatment however is still associated with endocrine disorder risk (Laughton et al. 2008).

Patients whose disease recurs after the combined-modality therapy have very poor survival (Ramaswamy et al. 2013). Although several studies have shown the efficacy of high-dose chemotherapy for these patients, only children with isolated local relapse, chemo-sensitive disease and minimal residual disease at the time of high-dose chemotherapy benefit from such an approach (Ellison et al. 2003).

1.9 Opportunity for new therapy

Clearly refined risk analysis and new treatments will come hand-in-hand. New treatments are urgently needed to reduce the risk of adverse side-effects and improve quality of life for survivors while also improving survival rates for those with high-risk disease.

One such approach involves a ganglioside acetylation pathway known to function abnormally in high-grade gliomas (Birks et al. 2011). This pathway has been shown to influence cell survival and have roles in embryonic brain development (Svennerholm et al. 1989). As medulloblastoma is a brain tumour of development, we hypothesised that this pathway may have a role in the pathology of this tumour.

1.10 Gangliosides

Gangliosides were first discovered by Ernst Klenk in 1942 while he was analysing the lipids found in the post-mortem brains of patients with a fatal infantile condition known as Tay-Sachs disease (Svennerholm 1963). Gangliosides are glycosphingolipids (GSLs) ubiquitously expressed throughout the body but are most abundant in the grey matter of the brain (Schengrund 2015). There are currently 188 known gangliosides which differ in their

structure (Yu et al. 2004). Gangliosides have diverse structures (Krengel & Bousquet 2014) which allows their diverse roles in processes such as cell-signalling, adhesion and survival among others (Regina Todeschini & Hakomori 2008). Gangliosides are co-localised in the microdomain structures of the lipid rafts, often with signalling and adhesion molecules (Sorice et al. 2012). In addition to being localised on the cell surface, gangliosides are also found within cells and associate with organelles such as nuclear membranes, the Golgi apparatus and the endoplasmic reticulum (ER) (Schwarz & Futerman 1997).

Gangliosides are also components of the neuronal plasma membrane and they can affect neuronal function (Schengrund 2015). Their expression patterns are tightly regulated by their biosynthetic and catabolic steps as well as their intracellular trafficking (Yu et al. 2004; Sandhoff & Harzer 2013). Ganglioside metabolism is highly regulated by their constitutive degradation in endosomes and lysosomes (Sandhoff & Harzer 2013). Defects in the degradation process can result in massive accumulation of gangliosides in the lysosomal compartment and other organelles (Ryan et al. 2013).

The nomenclature of the gangliosides is according to Lars Svennerholm, who initially based their names on the migration order of the gangliosides when separated by chromatography (Svennerholm 1963).

1.10.1 Ganglioside Biosynthesis

Gangliosides are synthesised from ceramide which is translocated to the Golgi. Here, the addition of carbohydrate residues which make up the ganglioside backbone are added by a series of glycosyltransferases (Yu et al. 2004). Only GM4 differs in synthesis, every other ganglioside is derived from glucosylceramide (GluCer) or lactosylceramide (LacCer) (Yu et

al. 2004). The addition of the sialic acid residues which define the ganglioside are added by a series of sialyltransferases onto their LacCer or GluCer backbones shown in figure 1.5. GM3, the simplest ganglioside, is generated by the addition of sialic acid to its LacCer backbone by GM3 synthase (Proia 2004). Further sialic acid residues are then added to this GM3 structure by other specific sialyltransferases, for example GD3 synthase (ST8Sia1) forming GD3 (Yu et al. 2004). When GM3, GD3 and GT3 lack *N*-acetylgalactosamine, they serve as precursors for the more complex gangliosides which are generated through addition of sialic acids through more promiscuous sialyltransferases along specific pathways (Yu et al. 2004). The start of the ganglioside biosynthesis pathway is shown in figure 1.5. The expression levels and patterning of the gangliosides undergo dramatic changes throughout brain development and disease states such as cancer (Schengrund 2015). For example, in the human embryonic brain, the major gangliosides are simple, GM3, GD3 and 9-*O*-acetyl GD3 (GD3^A) (Ryan et al. 2013). As the brain develops, the expression of these simple gangliosides is replaced with the more complex gangliosides such as GM1, GD1a and GT1b (Yu et al. 2012). This change is tightly regulated at the transcriptional and post-translational levels by multiple systems and epigenetic modifications (Yu et al. 2004).

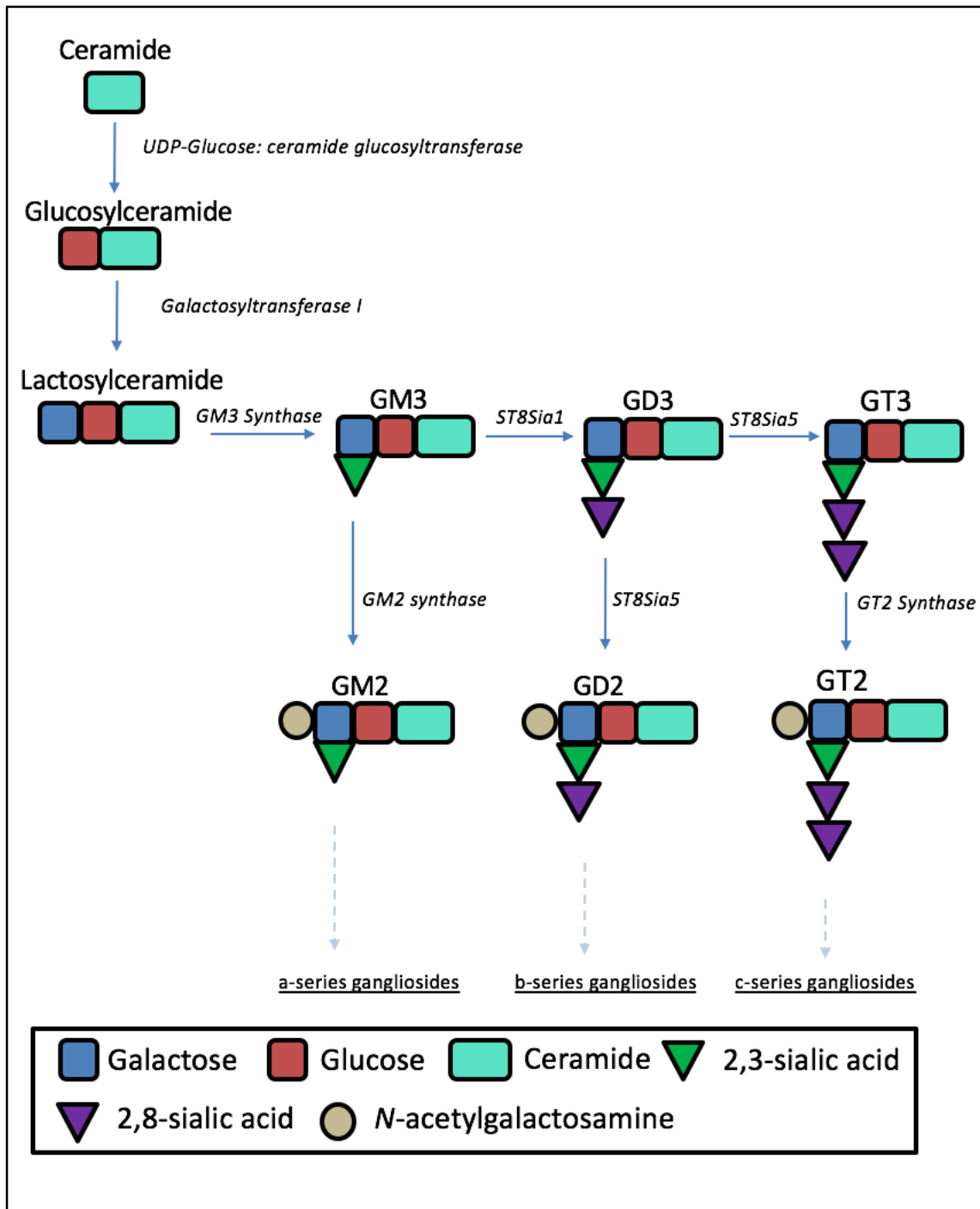


Figure 1.5 The ganglioside biosynthesis pathway. Ceramide has glucose and galactose residues added to it by glucosyl- and galactosyl-transferases respectively. The resulting lactosylceramide then has sialic acids added to it by a series of sialyltransferases generating the gangliosides. Biosynthesis of the individual gangliosides runs in parallel pathways forming the a- b- and c- series gangliosides. The synthesis of the gangliosides is regulated by control of the activity and expression of the sialyltransferases and modifications of the sugar-ceramide backbone. Adapted from Yu et al. 2004.

1.11 GD3 and GD3^A in the developing non-neoplastic brain

Gangliosides have important roles in embryonic and foetal brain development (Yu et al. 2004; Ngamukote et al. 2007; Schengrund 2015; Ryan et al. 2013; Svennerholm et al. 1989; Basu et al. 2012). During brain development there is a high abundance of gangliosides such as GD3 and GD3^A (Miyakoshi et al. 2001; Kotani et al. 1995). The expression of gangliosides in the brain changes significantly throughout neural development according to the specific function of each of the cell types (Yu et al. 2004). For example, during proliferation and migration, which occurs between 8 and 25 weeks of gestation, neuronal and glial precursor cells predominantly express GD3 and GM3 (Ryan et al. 2013). However, later in life, for example after birth, the expression of these gangliosides is significantly reduced (Molander et al. 2000; Yu et al. 2004) .

GD3 is an example of a ganglioside that has very restricted expression in non-neoplastic tissue but enhanced expression in some malignancies (Birklé et al. 2003). GD3 is a minor ganglioside in most non-neoplastic tissues after birth, except the thymus (Dyatlovitskaya & Bergelson 1987), placenta (Dyatlovitskaya & Bergelson 1987) and a small number of T-cells in the blood (Welte et al. 1987). GD3 expression may also be increased in non-neoplastic cells such as activated microglia (Wolswijk 1995) and reactive astrocytes (K. Kawai et al. 1994) which has been shown in rat brain.

In the 1980s several groups discovered that GD3 expression in the external granule layer (EGL) of the developing cerebellum was high (Goldman & Reynolds 1996). These cell types were both of neuronal and glial lineage and were described as neuroectodermal cells. Later the amoeboid microglia of the subventricular zone were also identified as GD3 expressing cells in the developing CNS (Goldman & Reynolds 1996). The dendrites of the Purkinje cells

also express GD3 in their cell membranes, this is first seen at post-natal day 7, and increases in intensity when the dendritic tree increases in complexity (Goldman & Reynolds 1996; Reynolds & Wilkin 1988).

In the developing cerebellum the immature GD3 positive granule neurons of the EGL retain the ganglioside until they begin to migrate through the molecular layer (Goldman & Reynolds 1996). The role of GD3 in development has linked the ganglioside to cell proliferation and activation which is thought to be due to its interaction with extracellular matrix (ECM) and integrin receptors (Cheresh et al. 1986; Ohkawa et al. 2010; Ohkawa et al. 2008) particularly the integrin β 1 receptor.

GD3 has been shown to have roles in differentiation and neurite sprouting (Sato et al. 2002), in a cell type dependent manner (Malisan & Testi 2002a). For example, in ST8Sia1 (GD3 synthase) overexpression experiments using mouse neuroblastoma cells demonstrated that cell differentiation and neurite sprouting was induced (Sato et al. 2002). However, GD3 was not essential as shown by Kawai in 1998 where mouse embryonic stem cells which overexpressed ST8Sia1 had a normal neuronal differentiation pattern (Kawai et al. 1998). In a rat model of pheochromocytoma, proliferation was also enhanced (Fukumoto et al. 2000). In this model, surface GD3 was shown to be associated with src-family kinases and the neuronal adhesion molecule Transient Axonal Glycoprotein 1 (TAG1) in cerebellar granule cells (Kasahara et al. 1997; Kasahara et al. 2000; Prinetti et al. 2001). In HeLa and CHO cells (Shi et al. 1996) (Malisan & Testi 2002a), GD3 expression was not reported to influence cell growth and differentiation (Malisan & Testi 2002a).

GD3 levels decline after birth, in order to do this GD3 is rapidly up-regulated and translocated to the mitochondria resulting in mitochondrially-mediated apoptosis of the

supernumary cells (Birks et al. 2011).

The mechanism by which GD3 causes apoptosis has been subject to some debate. For example, GD3 is known to rapidly accumulate upon signalling from cluster of differentiation 95 (CD95) which releases ceramide (Giussani et al. 2014). Ceramide promotes apoptosis through its rapid conversion to GD3 (Malisan & Testi 2002a). GD3 accumulation requires ceramides liberated from plasma membranes by acidic sphingomyelinase (De Maria et al. 1998). Further evidence for GD3-mediated apoptosis comes from experiments of ST8Sia1 over-expression, demonstrating that GD3 expression is sufficient to cause apoptosis (Malisan & Testi 2002a).

In other studies, the collapse of the mitochondrial membrane potential is the mechanism by which GD3 leads to cell death (Birks et al. 2011). This is the most well-accepted mechanism of action for GD3-mediated apoptosis (Malisan & Testi 2002a). The collapse of the mitochondrial membrane potential is a method of determining the health of the mitochondria (Perry et al. 2011). The collapse is thought to occur via the opening of the mitochondrial permeability transition pore complex (PTPC) the components of which are subject to much debate. The PTPC is located at contact sites between the inner and outer mitochondrial membranes (Zamzami & Kroemer 2001) and is under the control of B-cell lymphoma 2 (bcl-2) (Rippo et al. 2000). When the PTPC is opened, there is an outward movement of molecules under 1.5 kDa, a loss in the proton gradient between the membranes and inactivation of the oxidative phosphorylation system (Zamzami & Kroemer 2001). Once the mitochondria have swelled as a result of these events, there is the release of apoptogenic factors such as cytochrome c. From this the cell is committed to apoptosis and the activation of the caspase cascade is initiated via caspase 9. Apoptosis inducing

factor (AIF) is also released by the mitochondria (Susin et al. 1999), this can drive nuclear apoptosis (Ferri & Kroemer 2000).

In a study by Colell GD3 was shown to suppress the activation of the pro-survival transcription factor nuclear factor of kappa light polypeptide gene enhancer (NF- κ B) by preventing its nuclear translocation (Colell et al. 2001).

Another mechanism of GD3-induced cell death that has been described is autophagy (Garcia-Ruiz et al. 2015). Recent findings have revealed a previously undetermined role for GD3 in autophagy. GD3 has been shown in a study by Matarrese to regulate the autophagosome formation (Matarrese et al. 2014). Cells were amino acid deprived and ganglioside GD3 was shown to contribute to the biogenesis and maturation of autophagic vacuoles. Knock down studies of ST8Sia1 showed impaired autophagy while exogenous GD3 administration was shown to resume autophagy, providing supporting evidence of GD3's involvement in this process (Matarrese et al. 2014). In addition to these effects, gangliosides have been shown to induce autophagic cell death in astrocytes by a mechanism dependent on the generation of reactive oxygen species. GD3-induced cell death was abolished by knock down of beclin-1/Atg-6 or Atg-7 gene expression or by 3-methyladenine, a known autophagy inhibitor (Hwang et al. 2010). These results suggest that GD3 is capable of inducing autophagy, and that it can do so in several ways.

The apoptotic role of GD3 can be modified through acetylation to 9-*O*-acetyl GD3 (GD3^A) (Malisan et al. 2002; Kniep et al. 2006). The acetyl group responsible for this modification of properties is located at carbon 9 of sialic acid found in GD3 (Kniep et al. 2006).

1.12 Sialic acids

Sialic acids are a family of acidic nine-carbon amino acid sugars found in gangliosides and are commonly modified by the addition of functional groups (Schauer 2004; Li & X. Chen 2012). The most common sialic acid in vertebrates, and the sialic acid found in human gangliosides is *N*-acetylneuraminic acid (Neu5Ac) (Li & X. Chen 2012). The most commonly studied modification of Neu5Ac found in GD3 is *O*-acetylation (Baumann et al. 2015) which, as described above, affects its properties.

1.13 GD3 acetylation to GD3^A

The *O*-acetylation of GD3 requires both an active acetyl CoA transporter (acetyl CoA is thought to be the donor of the acetyl group), and an active *O*-acetyltransferase (Baumann et al. 2015). The acetylation of GD3 to GD3^A is thought to be via the carbon at position 7 (Baumann et al. 2015). GD3^A's acetyl group is actually found on carbon 9 of the terminal Neu5Ac however, this is thought to be from the spontaneous migration of the group from carbon 7 to carbon 9, although some have suggested that this requires an enzymatic step (Vandamme-Feldhaus & Schauer 1998). The structures of GD3 and GD3^A are shown in figure 1.6 as well as the possible mechanism of acetylation by cas1 and deacetylation by SIAE.

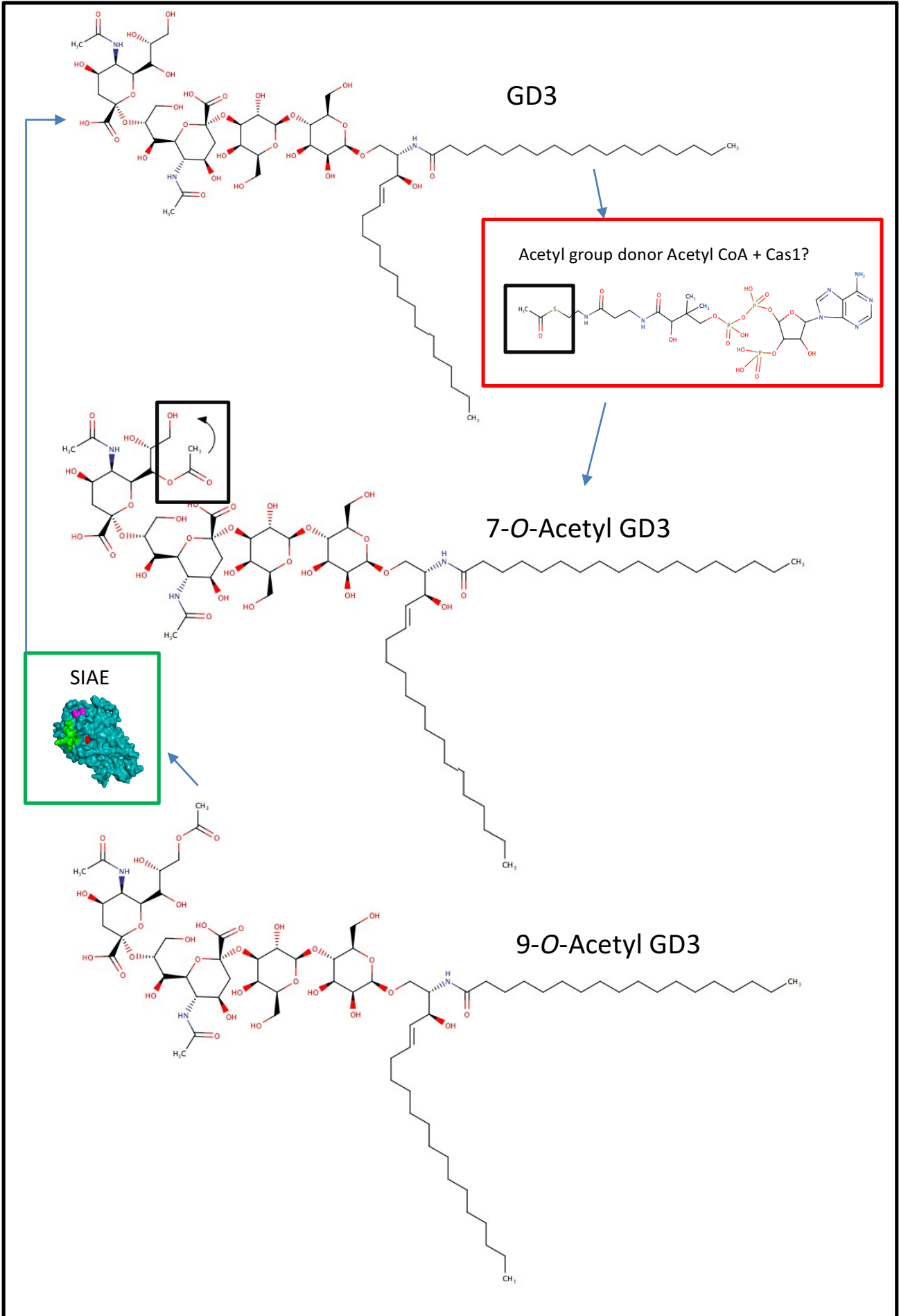


Figure 1.6 The proposed mechanism of acetylation of GD3 to 9-*O*-acetyl GD3 by Cas1. The chemical structures of the gangliosides show the site of acetylation on the terminal sialic acid. The acetyl group is thought to be donated by acetyl CoA and transferred to the 7-*O*-position of GD3 (red box). Then the acetyl group is either catalytically transferred to the 9-*O*-position or it spontaneously migrates there. SIAE is shown as the deacetylation enzyme, cleaving the acetyl group from 9-*O*-acetyl GD3 only (green box). Images drawn on Marvin Sketch (ChemAxon).

The balance between acetylated and non-acetylated sialic acids (and therefore between GD3 and GD3^A) is dependent on the activities of sialic *O*-acetyl transferases and sialic acid *O*-acetyl esterases which add and cleave acetyl groups from sialic acids (Mandal et al. 2012). In some neoplastic diseases, such as acute lymphoblastic leukaemia, this balance has been shown to be in favour of acetyltransferases, and in this case, GD3^A (Mandal et al. 2012).

The enzyme responsible for the transfer of acetyl groups from acetyl-CoA has remained elusive in cell-systems (Baumann et al. 2015). Candidate proteins for acetyl transferases include Cas1 (Arming et al. 2011). The enzyme responsible for the cleavage of acetyl groups from the 9 carbons position of Neu5Ac is the human endogenous acetyl esterase enzyme sialic acid *O*-acetyl esterase (SIAE) (Mandal et al. 2012).

In mice GD3^A is expressed in a stacked pattern in the EGL at post-natal week 1. The intensity of staining was shown by Santiago et al. 2001 to be different between various folia and suggested that the expression differences may reflect different stages of maturation. (Santiago et al. 2001). In co-labelling experiments with GD3^A antibodies and antibodies directed against glial acidic fibrillary protein (GFAP), staining was seen in cells of both glial and neuronal lineages (Santiago et al. 2001).

GD3^A has distinct roles in neuronal development and has been shown, in mice, to be co-localised in the contact sites between migrating granule cells and radial glial in the EGL and molecular layer of the developing cerebellum (Santiago et al. 2004). In a melanoma cell line abc-1 knock-down experiments using a viral *O*-acetyl esterase that cleaves acetyl groups from GD3^A, differentiation and proliferation were promoted, indicating that GD3^A may have roles in maintaining an undifferentiated state (Santiago et al. 2001).

In work done by the same group, (Santiago et al. 2004), early post-natal rats received intraventricular injections of an antibody specific to GD3^A. In these animals the migration of the granule neuron precursors was arrested in the EGL (Santiago et al. 2004). In control animals, the proliferating neuroblasts in the EGL of the cerebellum were also labelled via intraperitoneal injections of 5-bromo-2'-deoxyuridine (BrdU), allowing the directional movement of the granule cell precursors to be evaluated. Immunolabelled cells showed that GD3^A expression was restricted in the brain in regions such as the subventricular zone and the cerebellum (Santiago et al. 2004). The staining pattern GD3^A in the cerebellum of a post-natal day 9 rat showed that the EGL and the molecular layer have the highest degree of staining. Cells that are migrating from the EGL that express GD3^A do so in the cell bodies and also their processes. In addition, very few cells stain positively for GD3^A in the IGL (Santiago et al. 2001). These results were similar to those found by (Santiago et al. 2001) and (Mendez-Otero et al. 1988) and further implicates GD3^A in the migration of the granule neuron precursors to the IGL.

Unlike GD3, GD3^A is unable to induce apoptosis and has been shown to counteract the pro-apoptotic effects of GD3 (Kniep et al. 2006). In this study Jurkat cells were treated with micromolar concentrations of GD3^A and then apoptosis inducing agents such as *N*-acetyl sphingosine as well as daunorubicin. The cells became resistant to apoptosis inducing agents and had an increased viability. When cells were pre-treated with GD3, cells also became resistant and was shown to be correlated with increased GD3^A production (Kniep et al. 2006). In this study the group suggest that GD3^A formation may be a mechanism for how tumour cells evade apoptosis (Kniep et al. 2006). One of the reasons why pre-treatment of cells may become resistant to apoptosis is suggested by (Chen et al. 2006)

who suggested that GD3 can include its own acetylation machinery. This group used exogenously added GD3 to determine if the expression of GD3^A increased with treatment. Their results show that when exogenous GD3 was added to CHO cells, the cells incorporated the molecule and within 6 hours GD3^A expression was induced (Chen et al. 2006).

1.14 The roles of GD3 and GD3^A in primary brain tumours

Changes in ganglioside expression in brain tumours was first reported in 1966 (Brezicka 2015). Since then it has been established that changes in ganglioside expression levels are associated with many tumour types, but of particular note are those of neuroectodermal origin, including medulloblastoma. Gangliosides are present throughout the tissues of the body are particularly abundant in the nervous system (Maidment et al. 1996). On the cell surface, gangliosides occur in clusters or aggregates or micelles are found close to proteins embedded in the lipid bilayer (Merzak et al. 1994). Gangliosides are thought to have functional control over proteins on the cell surface (Merzak et al. 1994). Gangliosides also localised intracellularly, in association with the Golgi apparatus and the rough endoplasmic reticulum where they are synthesised and metabolised, and also in the lysosomes where they are degraded (Pilkington 1992).

Ganglioside expression may be altered in neoplastic disease and this alteration may refer to over-expression of gangliosides which are present also in the non-neoplastic tissue, and over-expression of gangliosides usually seen in different stages of development. The idea that tumour progression occurs in a ganglioside dependent manner has been shown in conjunction with clinicopathological studies which demonstrate that there are some ganglioside species with relatively simple structures, GD3 is an example of such a

ganglioside (Pukel et al. 1982), that shows very restricted expression in non-neoplastic tissues and markedly increased expression in some malignancies (Birklé et al. 2003). A number of functional roles for gangliosides have been proposed, many of which are important in neoplasia and also in the developing and non-neoplastic nervous tissue (Pilkington et al. 1993).

The ganglioside GD3 is the most widely studied in neoplastic disease as it is commonly expressed in tumour tissues such as malignant melanoma and glioma (Hersey 1991; Koochekpour & Pilkington 1996). GD3 and GD3^A are known to be expressed in brain development by the neural stem cells from which brain tissue arises (Svennerholm et al. 1989; Yanagisawa et al. 2011). These neural stem cells are common ancestors for every glial and neuronal cell type in the brain (Kennea & Mehmet 2002; Knott et al. 1990). As there is a common ancestor, the neural stem cell, the expression of the gangliosides GD3 and GD3^A has been studied in primary brain tumours (Parker & Pilkington 2005; Koochekpour & Pilkington 1996; Gratsa et al. 1997; Birks et al. 2011). GD3 has many known roles in neoplastic disease, for example in cell growth, invasion and evasion of the immune response (Birklé et al. 2003). GD3^A also has roles in neoplasia and has been shown to influence cell survival in several cancers such as acute lymphoblastic leukaemia (Mukherjee et al. 2008) and glioblastoma multiforme (Birks et al. 2011).

Human glioma-associated GD3 has been shown to be highly expressed by high grade tumour cells (anaplastic astrocytoma and glioblastoma multiforme) but not expressed by lower grade glial tumours (Koochekpour & Pilkington 1996). It has also been shown that expression of GD3 is maintained in culture even with prolonged passage (Knott et al. 1990). The role of GD3 is well established in neural development of the brain where it guides the

migration of neuronal progenitor cells as well as causing the apoptosis of supernumary progenitors (Ogiso et al. 1991). Expression of GD3 is tightly regulated depending on developmental stage and GD3 is also involved in cancers of development. GD3 is highly expressed by the brain tissue and several studies have investigated expression in primary brain tumours, particularly in glioma (Pilkington 1992; Pilkington et al. 1993; Merzak, Koochekpour & Pilkington 1995; Merzak et al. 1994; Merzak et al. 1995).

The expression of GD3 and its acetylated form, GD3^A have been shown to be altered in medulloblastoma (Gottfries et al. 1990). Expression of GD3 is known to be increased in the CSF of patients, but its role is thus far unknown in this setting (Malisan & Testi 2002a). There are few studies on GD3 and GD3^A expression on medulloblastoma but there have been other studies on the role of these gangliosides in other cancers.

In melanoma it has been shown that GD3 expression correlates with metastatic potential (Cheresh et al. 1986) and in glioma it has been shown that GD3 is pro-angiogenic as GD3 is a potent activator of vascular endothelial growth factor (VEGF) (Koochekpour & Pilkington 1996; Seyfried & Mukherjee 2010). The role of GD3 on VEGF has also been supported in neuroblastoma by the use of anti-GD3 antibodies which have been shown to reduce angiogenesis in a rat model (Zeng et al. 2000).

Studies have shown that GD3 is involved in the attachment of human melanoma and neuroblastoma cells to various extracellular matrix proteins, including laminin, fibronectin, collagen, and vitronectin (Cheresh et al. 1986). In glioma it has been shown that exogenously added gangliosides stimulate cell invasion *in vitro* and in addition this has been shown that gangliosides enhance the adhesion of glioma cell lines to fibronectin, laminin, vitronectin and collagen I (Merzak et al. 1994; Koochekpour et al. 1995). In a study by

Merzak *et al.* (1995) invasion in glioma cells was found to involve gangliosides and this was thought to be mediated by adhesion-promoting action to the basement membrane proteins (Merzak *et al.* 1995). It was also shown that secretion of matrix metalloproteinases 2 and 9 was affected by ganglioside expression, but this was not correlated with histological type of glioma (Maidment *et al.* 1996). In IPNN-8 medulloblastoma cells of low passage, cells adhered to fibronectin, collagen I and vitronectin (Merzak, Koochekpour & Pilkington 1995). GD3 however has been identified as a ganglioside which inhibits the binding of cells to fibronectin so perhaps GD3 expression is low in IPNN-8 cells. The mechanism for this was described by Wang *et al.* and was shown to be due to GD3 binding to integrin $\alpha_5\beta_1$ (Wang *et al.* 2001). It is this blockage of the integrin via carbohydrate-carbohydrate interactions between the ganglioside and the α_5 subunit of integrin $\alpha_5\beta_1$ which inhibits binding to fibronectin. This study demonstrated GD3 as a 'co-factor' in the complexes that form with ECM proteins and receptors (Cheresh *et al.* 1987). It is therefore no surprise that GD3 has roles in invasion and mobility of primary brain tumour cell lines which has been confirmed with the use of anti-GD3 antibodies (Hedberg *et al.* 2000; Gratsa *et al.* 1997).

GD3 is also known to have roles in apoptosis where acetylation of the ganglioside, commonly seen in glial tumours, helps to evade apoptosis (Malisan & Testi 2002a; Malisan & Testi 2002b; Birks *et al.* 2011; Colell *et al.* 2001) (further discussed in section 1.11).

Interactions between tumour cells and the cells of the immune system appear to be critical for tumour growth (Birklé *et al.* 2003). The hypothesis that gangliosides may be involved in the suppression of the anti-tumour immune response is supported by studies demonstrating that tumour cells synthesise and shed gangliosides into their microenvironments (Potapenko *et al.* 2007). GD3 can be actively shed from the tumour

cells to the microenvironment where it can bind and interact with a wide variety of proteins, including extracellular matrix (ECM) modulating proteins such as integrins (Kong et al. 1998; Dolo et al. 2000; Ohkawa et al. 2008). Shed GD3 can also be incorporated into the membrane of neighbouring cells, which helps to modulate tumour–host cell interactions (Olshefski & Ladisch 1996). This process is important as this is one of the mechanisms by which evasion of the immune response is thought to occur in glioma (Potapenko et al. 2007). Many studies have shown that exogenous or tumour-derived gangliosides inhibit multiple steps in the cellular immune response *in vitro*. For example, tumour-derived gangliosides inhibit the activity of several immune cells, including helper T cells (Offner et al. 1987) and natural killer cell cytotoxicity (Grayson & Ladisch 1992) among others.

1.14.1 Cas1

The search for the enzyme that catalyses the transfer of acetyl groups to GD3 began in the 1970s, since then many attempts to identify the gene by expression and cloning have failed (Arming et al. 2011). Arming however used a bioinformatics approach to identify the gene. Genetic evidence suggested one gene was responsible for the transfer of acetyl group (Arming et al. 2011; Campbell et al. 1994). The human genome database was screened for proteins with unknown functions which were predicted to encode acetyl transferases (Arming et al. 2011). Candidates were also chosen based on their localization to the Golgi membranes where acetylation was shown to occur (Arming et al. 2011).

From Arming's bioinformatics approach the human *CASD1* gene was identified. This gene consists of 18 exons and is located on chromosome 7q21.3 (Arming et al. 2011). The transcript length is 3942 nucleotides which encodes a protein of 797 amino acids (Baumann

et al. 2015). Analysis of the full length transcript revealed a signal sequence which is usually found in proteins that translocate to the ER, Golgi or plasma membrane. The protein consists of a serine-glycine-asparagine-histidine (SGNH) hydrolase domain and a C-terminal transmembrane domain (Arming et al. 2011). The protein also shares some sequence homology to the viral *O*-acetyl esterases, especially around the active site residues (Arming et al. 2011). In fact, the amino acid sequence of *CASD1* was originally identified as a homologue of *O*-acetyl esterase from the influenza C virus (Vlasak et al. 1987). Additional features of the enzyme include an ER export signal (D-X-E) and several *trans*-Golgi network (TGN)-endosome export signals (Y-xx-hydrophobic amino acid or D/E-xxx-L/I) (Baumann et al. 2015).

Arming *et. al* (2011) tested whether Cas1 protein was involved in the *O*-acetylation of GD3 by expressing ST8Sia1 and Cas1 proteins in COS cells. Interestingly, GD3 synthase expression alone was sufficient to increase both GD3 expression and 7-*O*-acetyl GD3 expression (Arming et al. 2011). This indicates that there may be an intrinsic *O*-acetyltransferase present in these cells. GD3 has also been shown to be capable of inducing its own acetylation (Chen et al. 2006). There was however a significantly higher expression of 7-*O*-acetyl GD3 when cells were co-transfected with ST8Sia1 and Cas1. In both experiments there was no significant change in the expression of 9-*O*-acetyl GD3 (GD3^A) indicating that Cas1 protein may catalyse only transfer of acetyl groups to the 7 carbon position of sialic acid. Knock-down studies of Cas1 using specific short interfering ribonucleic acid (siRNA) did however significantly reduce the expression of 9-*O*-acetyl GD3 after 24 hours, but the reduction was recovered after 96 hours (Chen et al. 2006).

There is some controversy as to the involvement of Cas1 in the acetylation forming 9-*O*-acetyl GD3. In another study by Baumann, Cas1 expression was shown to increase the expression of 9-*O*-acetyl GD3 in HEK293T, LM-TK⁻ and HAP cells. This group suggests that the effect of Cas1 on 9-*O*-acetylation of GD3 may be cell-type specific (Baumann et al. 2015).

Due to these results it is likely that either Cas1 protein is not the only enzyme involved in the acetylation of GD3 to 9-*O*-acetyl GD3, Arming *et. al* (2011) suggest that Cas1 stimulates the expression of intrinsic acetyl transferases (Arming et al. 2011). Another possibility is that the 7-*O*-acetyl group migrates to carbon 9 of sialic acid, most likely via a 'migrase' due to the distinct function of GD3^A during apoptosis (Wipfler et al. 2011).

In previous work, it was hypothesized that *O*-acetyltransferase activity may be associated within a membrane-bound complex made up of an acetyl-CoA transporter, sialyltransferase (such as ST8Sia1) and acetyltransferase and potentially an acetylated intermediate (Diaz et al. 1989; Lrhorfi et al. 2007). As well as this (Srinivasan & Schauer 2009) suggested that a soluble co-factor may also be required for activity.

1.14.2 Sialic acid *O*-acetyl esterase

Sialic acid *O*-acetyl esterase (SIAE) removes acetyl groups from the hydroxyl groups in position 9 and 4 of sialic acid such as those found in 9-*O*-acetyl GD3 (Mandal et al. 2012; Mahajan & Pillai 2016). Human SIAE is located on chromosome 11 at 11q24.2 (Zhu et al. 2004). Studies have reported that the SIAE gene encodes two transcript isoforms (Varki et al. 1986; Higa et al. 1987). The lysosomal variant is the longer of the two proteins but has the shortest transcript, which spans 10 exons. The cytosolic variant spans 12 exons and

differs in the 5' untranslated region (UTR), and its first coding exon corresponds to the second of the lysosomal variant (Orizio et al. 2015). In the study by Orizio, RNASeq data was analysed from the Illumina Human body map 2.0 project. The data indicated that in 15 of the 16 human tissues analysed, exon-exon boundaries correspond to the lysosomal variant, while there is no transcript model supporting cytosolic SIAE (Orizio et al. 2015). Adult human tissue expression studies of SIAE transcripts also suggest that expression is almost exclusively limited to the lysosomal SIAE isoform. It has been suggested that the cytosolic variant of SIAE arises from cleavage of the lysosomal variant (Takematsu et al. 1999), but there is little *in vitro* evidence of this. Despite its name, the lysosomal isoform of SIAE was not found in the lysosomal compartments in experiments done by Orizio in CHO cells (Orizio et al. 2015). Other studies did indeed find SIAE localised within the lysosomes, but its relevance remains unclear (Mandal et al. 2012) and the localisation of SIAE therefore could be cell-type dependent. As SIAE has been found to be associated with the ER and Golgi the secretion and glycosylation of SIAE may have important roles (Surolia et al. 2010; Chellappa et al. 2013).

In 2013, catalytically defective variants of SIAE were described and linked to autoimmunity which suggests this enzyme may also be involved in the immune response (Surolia et al. 2010), the primary structure of the SIAE protein is shown in figure 1.7 and includes mutation sites and cleavage sites. Studies on this enzyme have however resulted in contradictions and therefore the role of SIAE in physiology is not well defined (Chellappa et al. 2013).

The active site of SIAE was identified by multiple sequence comparison by log-expectation (MUSCLE) analysis (Orizio et al. 2015). The MUSCLE analysis was used to generate a multiple

sequence alignment with sequences from 32 protein orthologues of human SIAE and identified conserved motifs and regions. The conserved regions were identified as possible candidates for catalytic sites (Orizio et al. 2015). As a result of this work, eleven highly conserved sequence blocks were identified and the two essential residues for catalysis were determined as S127 and H377. These residues were confirmed to be required for the catalytic triad, along with T132 by site directed mutagenesis experiments and molecular docking (Orizio et al. 2015).

Following on from localisation studies by Mandal, (Mandal et al. 2012), this study also investigated the presence of *N*- and *O*- glycosylation sites and phosphorylation sites. 6 *N*-glycosylation, 10 *O*-glycosylation, and 24 phosphorylation sites were identified (Orizio et al. 2015). The identified sites are shown in table 1.8 and shown as part of the primary and tertiary structures in in figures 1.7 and 1.8.

Table 1.8 modification sites of human SIAE protein, isoform 1, adapted from (Orizio et al. 2015).

Modification	Predicted sites
N-glycosylation	N107, N138, N267, N290, N401, N422
O-glycosylation	S177, S231, S242, T511
Phosphorylation	S30, Y31, T52, S74, S79, S144, S156, S158, S217,T221, S227, S228, S247, S255, T303, S308, T312, S328, S331, S332, Y349, S371, T461, S470

10 20 30 40 50
 MVAPGLVLGL VLPLILWADR SAGIGFRFAS YINNDMVLQK EPAGAVIWF
 60 70 80 90 100
 GTPGATVTVT IROGQETIMK KVT^RSVKAHS^D TWMVLDPMK^V PGGPFEVMAQ
 110 120 130 140 150
 QTLEKINFTL RVHDVLFQDV WLCSGQSNMQ MTVLQIF^NAT RELSNTAAYQ
 160 170 180 190 200
 SVRILSV^SPI K^RQAEQELEDLV AVDLQWSKPT SENLGHGYFK YMSAVC^FWLFQ
 210 220 230 240 250
 RHL^RYDTLQYP IGLIAS^SWGG TPIEAW^SSGR^W SLKACGVPKQ GSIPYDSVTG
 260 270 280 290 300
 PSKH^SVLWNA MIHPLC^GNMTL KGVVWYQGES NINYN^TTDLY^N CTFPALIEDW
 310 320 330 340 350
 RE^TFHRGS^PQG C^TER^MFFPFG^HL VQLSSDLSK^K SSDDGFPQIR WHQTADFG^CYV
 360 370 380 390 400
 PNPKMPNTFM AVAMDLC^RDRD SPFGSIHPRD KQTVAYRLHL GARALAYGE^HK^N
 410 420 430 440 450
 NLTIFEGPLPE KIELLAHKGL LNLTYYQQIQ VQKKDNKIFE ISCCSDHR^RCK
 460 470 480 490 500
 WLPAS^IMNTVS T^RQSLTLA^VIDS CHGTVVALR^CY AWTTPWCEYK QCPLYHPSSA
 510 520
 LPAPPFIAFI TDQGPQH^SSN VAK

Figure 1.7 The primary sequence of SIAE isoforms 1 and 2. Isoform 2 lacks the 35 amino acids shown in teal. Naturally occurring mutations are shown in boxes, mutations in purple boxes give rise to normally secreted and catalytically normal variants of SIAE. Mutations in blue boxes give rise to mutations with unknown effects on the SIAE protein. Mutations in yellow boxes give rise to SIAE protein that is associated with a pathological condition (M89V and T312M are associated with autoimmunity and K400N with Crohn's disease). Mutations in pink boxes are associated with defective secretion and catalytic activity. All post-translational modification sites are also shown, N-glycosylation sites are highlighted in red, O-glycosylation sites in blue and phosphorylation sites in orange. Adapted from Serolia (2010).

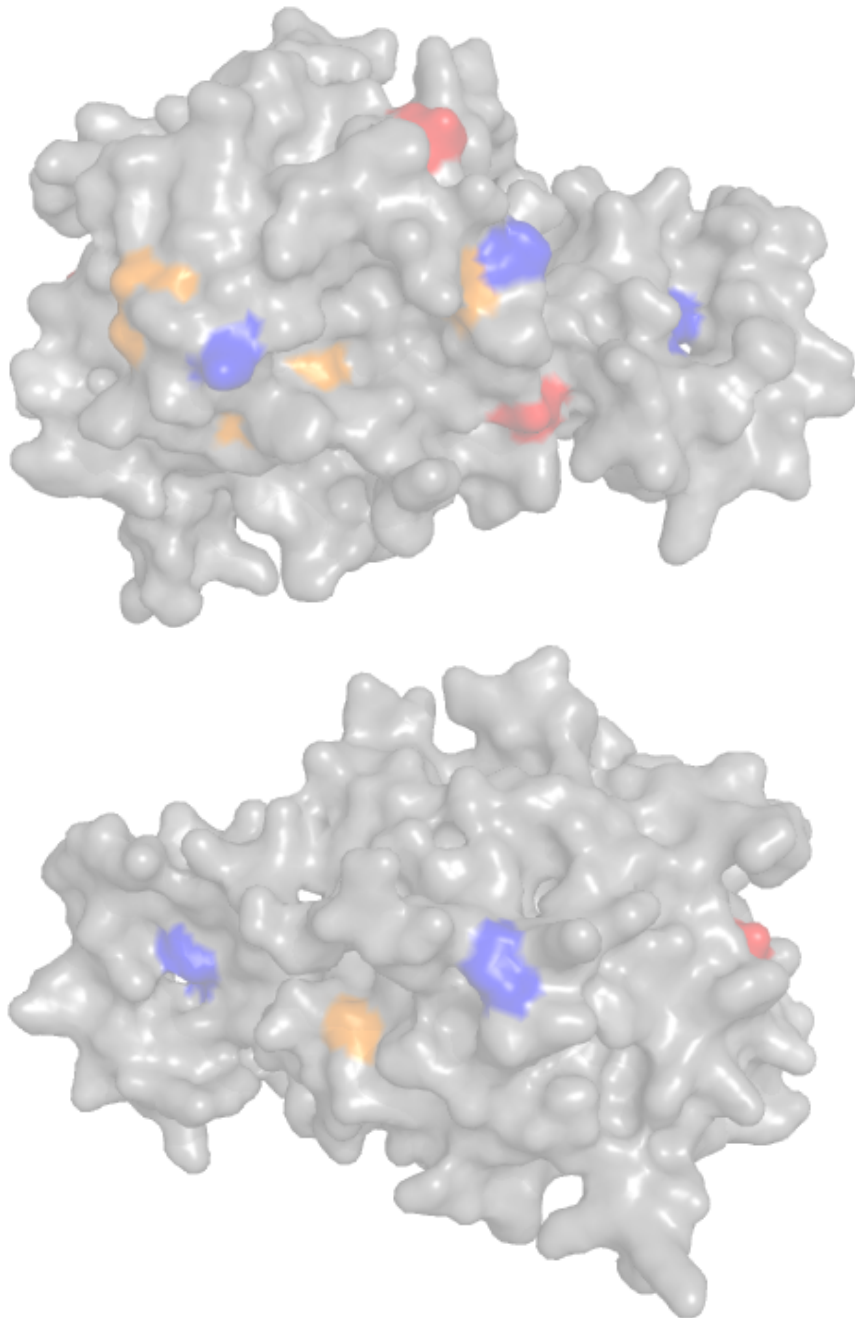


Figure 1.8 SIAE modifications sites shown as part of the homologous and hypothesised structure of the SIAE protein. *N*-glycosylation sites are shown in red, *O*-glycosylation sites in blue and phosphorylation sites in orange. Structure obtained from the protein data bank (PDB) and visualised on Mac PyMol.

Further to this Orizio *et. al* published *in silico* predictions of the SIAE protein. This group demonstrated presence of an *N*-terminal signal peptide that corresponds to amino acids M1-A18. Further to this this study used Secretome 2.0 prediction, the human SIAE protein had a high score, which implicates SIAE as a secreted protein (Orizio et al. 2015). In *in vitro* studies, Western blot analysis revealed that SIAE was found in both cell extracts and conditioned media (Surolia et al. 2010; Orizio et al. 2015). In these cases, the SIAE protein had a higher than expected molecular weight of 62 kDa. This was thought to be due to glycosylation so cells were treated with tunicamycin and this form of SIAE was no longer seen, confirming glycosylation was responsible for this molecular weight (Orizio et al. 2015).

It was then explored whether glycosylation was required for activity of SIAE, and if it was required for extracellular trafficking. In cell lysates and conditioned media experiments SIAE activity was determined to correlate with the intensity of the bands associated with the glycosylated form. These data suggest that SIAE glycosylation is required for secretion and also influences the activity of the enzyme (or indeed its stability) (Orizio et al. 2015; Surolia et al. 2010).

1.15 Hypothesis

We hypothesise that GD3 and GD3^A are expressed by medulloblastoma cells. By overexpressing SIAE in medulloblastoma cell lines GD3^A levels will decrease leading to an increase in GD3. Due to the increase in GD3 cells will undergo mitochondrially-mediated apoptosis or be sensitised to treatment with chemotherapeutics in a cell-cycle dependent or cell-cycle independent manner.

1.16 Aims

1. To assess the expression of the regulators of the GD3 acetylation pathway in medulloblastoma patient tissue samples.
2. To confirm the expression of GD3 and GD3^A in medulloblastoma cell lines.
3. To determine the effects of SIAE overexpression on the expression of GD3 and GD3^A in medulloblastoma cell lines.
4. To assess the effects of SIAE overexpression on medulloblastoma cell viability.
5. To determine the effects of SIAE overexpression on medulloblastoma cell response to cell-cycle dependent and cell-cycle independent chemotherapeutics currently used to treat medulloblastoma.

1.17 Objectives

1. Using bioinformatics the expression of the regulators of the GD3 acetylation pathway in medulloblastoma patient tissue samples will be assessed.
2. The expression of GD3 and GD3^A in medulloblastoma cell lines will be explored using flow cytometry and immunocytochemistry.
3. The effects of SIAE overexpression on the expression of GD3 and GD3^A in medulloblastoma cell lines will be assessed using flow cytometry.
4. The effects of SIAE overexpression on medulloblastoma cell viability will be assessed using JC-1 assays to assess the mitochondrial membrane potential.
5. The effects of SIAE overexpression on medulloblastoma cell response to chemotherapeutics will be determined using MTS viability assays.

2 Materials and Methods

2.1 Cell Lines

RES256 and UW402 cells were obtained under the ethics study number 13773 at The University of Washington, Seattle, headed by Dr John Silber. Under this study number informed consent for each of the patient's biopsy material or cell lines was obtained. The use of these cells at the University of Portsmouth is possible through an arranged Material Transfer Agreement (MTA).

For all other cell lines, the brain tumour research centre at the University of Portsmouth was given a favourable ethical opinion by the national research ethics service (NRES) committee South Central- Hampshire A (REC reference number 11/SC/0048) for a study titled 'The Cellular and Molecular Biology of Brain Tumours: Migration, apoptosis, malignancy and therapeutic applications' which can be found in appendix 8.

The cell lines used in this project are briefly described in table 2.1

Table 2.1 Table of cell lines used throughout this project including histology, source and where cells were derived from.

Cell line	Source	Patient age and Sex	Histology	Site
RES256	University of Washington, Seattle	16 years Male	Paediatric Medulloblastoma	Cerebellum
CHLA-01-MED	ATCC	8 years Male	Paediatric Medulloblastoma	Cerebellum
UW402	University of Washington, Seattle	Unknown Unknown	Paediatric Medulloblastoma	Cerebellum
MeWo	ATCC	78 years Male	Melanoma	Metastatic site lymph node
LNCaP	ATCC	50 years Male	Prostate Carcinoma	Metastatic site supraclavicular lymph node

2.2 Maintenance of Cell Lines

Cell culture was carried out in a class II Nuare biological safety laminar flow hood. All cell lines were maintained at 37°C in a 5 % CO₂ humidified atmosphere within a Hereaus Hera Cell incubator.

Throughout this project the growth and morphology of each cell line was monitored using an Olympus IX71 inverted phase contrast microscope. Images were captured using Analysis software (Soft imaging systems).

All cell lines were maintained in the media described in table 2.2

Table 2.2 Table of cell lines used throughout this project including base media and supplements

Cell line	Base media	Supplements
RES256	Dulbecco's modified Eagle Media (DMEM)	10% Foetal Bovine Serum (FBS)
CHLA-01MED	DMEM F-12 modification	20 ng/mL Fibroblast Growth factor (FGF); Epidermal Growth Factor-1 (EGF-2) and 2% (v/v) B27
UW402	DMEM	10% FBS
MeWo	Eagle's minimum essential media (EMEM)	10% FBS

Adherent cultures were maintained by removing media and washing cells with Hank's balanced salt solution (HBSS; Gibco) to remove any FBS, which inhibits the trypsin enzyme found in TrypLE Express. Next, TrypLE Express (Gibco), a dissociation reagent, was added and incubated on the cells for up to 5 minutes to dissociate the cells from the plastic surface. TrypLE Express was then neutralised with growth media supplemented with serum. The solution was aspirated from the flask and centrifuged for 5 minutes at 300 g using a Boeco C-28A centrifuge. The supernatant was removed from the pelleted cells and the cells resuspended in 1 mL of the appropriate media. The cell suspension was then appropriately diluted and added to tissue culture flasks or plates. All cell lines were cultured in monolayers at 37°C in a 5 % CO₂ environment.

Cells were counted and viability was determined via a trypan blue exclusion assay using a Countess II cell counter (Life Technologies). Cells were harvested as previously described and the pellet resuspended in 1 mL of appropriate complete media. To plate cells for experimental purposes 10 µL of cell suspension was mixed with 10 µL Trypan Blue (Life Technologies) and loaded into a chamber of a countess II cell counting slide (Life Technologies). Cell viability and cell count was determined using the automatic focusing setting on the Countess II machine. Appropriate dilutions were made for experiments by using the following formula.

$$\frac{\text{Volume cells diluted in } x \text{ required seeding density}}{\text{Number of viable cells}} = \quad \mu\text{L of cell suspension to use}$$

CHLA-01-Med suspension cultures were passaged by centrifuging at 300 g using a Boeco C-28A centrifuge, cells were diluted for subsequent cultures in 75 % fresh media, 25 % conditioned media in suspension culture vessels (Greiner).

2.3 Freezing of Cell Lines

Cells to be frozen down for long-term storage were harvested as above. The pelleted cells however were re-suspended in 1 mL recovery cell culture freezing medium containing the cryoprotectant dimethyl sulfoxide (DMSO, Gibco) and aliquotted into cryovials (Nunc). The cryovials were placed into a Mr. Frosty container (Thermo) and placed into -80°C overnight. This allows vials to be cooled slowly (1°C per minute). Cryovials were then transferred and added to the vapour phase of liquid nitrogen (-196°C).

When cells are resurrected from liquid nitrogen storage they are thawed quickly at 37°C in a water bath. Cells are then added drop-wise to 9 mL fresh complete media and centrifuged for 5 minutes at 300 g using a Boeco C-28A centrifuge. The supernatant was removed to remove residual cytotoxic DMSO and the cells were added drop-wise to T-25 flasks containing 5 mL complete media appropriate to the cell line. All cell lines were cultured in monolayers at 37°C in a 5 % CO_2 environment.

2.4 Human Authentication of Cell Lines

Deoxyribonucleic acid (DNA) fingerprint analysis was carried out on each cell line to ensure its authenticity as published by (An et al. 2014). Total genomic DNA (gDNA) was extracted from cultured cells using QIAamp DNA mini kit (Qiagen). Short tandem repeat-based multiplex polymerase chain reaction (PCR) was then carried out using 2 ng template gDNA by a MyCycler thermal cycler (Bio-Rad). The PCR program was run as shown in figure 2.1

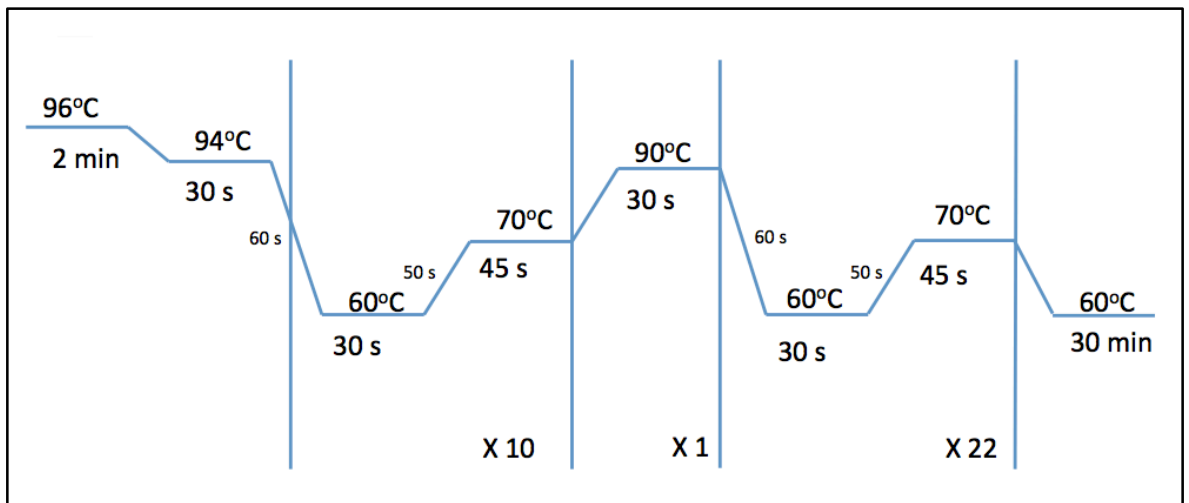


Figure 2.1 Thermal cycling conditions for human authentication of cell lines. The PCR program above allows sufficient amplification of each STR fragment unique to each cell line. The amplified products are then compared using an Agilent 2100 bioanalyser and unique genotypes for each cell line identified. Adapted from An *et. al*, 2014

Primers used were from the StemElite ID system kit and used to amplify 9 human short-tandem repeat (STR) loci, including D21S11, TH01, TPOX, vWA, CSF1PO, D16S539, D7S820, D13S317, and D5S818, as well as amelogenin for gender identification. These markers are selected from the set of core STR loci that has been approved for human identity testing. A no template negative control PCR reaction was included in each run to ensure specific amplification. Amplified alleles from the short-tandem repeat PCR and a DNA ladder were resolved using a 2100 Bioanalyser (Agilent) using the DNA 1000 kit (Agilent). Data were analysed using Agilent 2100 expert software. All samples were run in triplicate.

2.5 Routine Mycoplasma Testing

Mycoplasmas are a species of bacteria that are resistant to many classes of antibiotics commonly used in laboratories, and undetectable by phase contrast microscopy. *Mycoplasmas* affect cell behaviour on many levels, including gene expression, growth and metabolism so it is critical for cultures to remain uncontaminated. Contamination of cell lines with mycoplasma is difficult to detect and they cannot be removed through sterile filtering.

Cell cultures were routinely tested for *Mycoplasma* infections every two weeks using MycoAlert PLUS *Mycoplasma* Detection Kit (Lonza). The *Mycoplasma* assay exploits the activity of enzymes found in all six of the most prevalent *Mycoplasma* species and are not found in eukaryotic cells. Viable *Mycoplasma* is detected, if present, in the conditioned media of cell cultures. The *Mycoplasmas*, if present, are lysed and react with the MycoAlert substrate in which the conversion of ADP to ATP is catalysed. The ATP converted into a light signal using the luciferase enzyme in the MycoAlert reagent. By measuring the level of ATP

in the sample both before and after the addition of the MycoAlert substrate, a ratio can be obtained which indicates the of presence or absence of infection.

The *Mycoplasma* assay procedure required 1.5 mL of conditioned media in which the cells were incubated for a minimum of 24 hours. The media was then centrifuged at 200 g for 5 minutes at room temperature using an Eppendorf 5415r microcentrifuge. A 100 µL aliquot of cell suspension was added to a white flat-bottomed 96 well plate (Gibco). A positive control, MycoAlert assay control set (Lonza), was added to a control well, this consisted of 50 µL assay buffer (Lonza) and 50 µL of positive control (Lonza). A negative control of 100 µL assay buffer was also added to well of the plate. 100 µL MycoAlert reagent was added to each well and incubated for 5 minutes at room temperature. Read A was then taken before 100 µL of MycoAlert Substrate was then added to every well and incubated for 10 minutes at room temperature. Reading B was then taken. Readings were taken on a BMG labtech POLARstar Optima plate reader. A ratio taken of $\frac{\text{Reading B}}{\text{Reading A}}$ yields a ratio, which indicated presence or absence of infection, a ratio of greater than 1 indicated infection (i.e. active mycoplasma enzymes). No mycoplasma infections were detected using this method in the cells used throughout this project.

2.6 Antibodies

The antibodies used throughout this project are shown in table 2.3.

Table 2.3 Antibodies used throughout this project, concentrations and diluents are listed in materials and methods as per technique.

Antigen	Species and isotype	Company sourced from
GD3	Mouse anti-human IgG	Millipore (MAB2053)
GD3 ^A	Mouse anti-human IgM	Thermo Fisher (MA1-34707)
SIAE	Sheep anti-human IgG	Custom made (see section 2.7)
Beta Actin	Mouse anti-human IgG	Sigma (A4700)
Alexafluor 488	Goat anti-mouse IgG and IgM	Life Technologies (A-11029 and A-21042)
Alexafluor 568	Goat anti-mouse IgG and IgM	Life Technologies (A-11031 and A-21043)
Infrared 700/800 CW	Goat anti-mouse and Donkey anti-goat IgG	Licor (926-32214 and 926-68071)

2.7 SIAE Antibody Production

Several commercial SIAE antibodies that had been raised against the whole SIAE peptide or an 84 amino acid section that included alpha helices and beta sheets were tested without success. We decided to design and produce a custom polyclonal SIAE antibody to overcome this problem. Specialist technician Mrs Katie Loveson designed an immunogenic candidate SIAE peptide using well-established software (NHLBI-AbDesigner). With help from Alta Bioscience Ltd potential peptides were reviewed. A 17 amino acid peptide sequence (SSDLSKKSSDDGFPQIR) was selected for optimal immunogenicity and minimal cross-reactivity. The SIAE peptide was used to produce antibodies in sheep by National health service (NHS) Scotland, sheep were bled and the antibody was purified for use in this project. This antibody was validated by Western blot analysis, carried out by Mrs. Katie Loveson.

2.8 Flow Cytometry

The quantitative expression of several antigens was determined using flow cytometry. Antigens were either intra- or extracellular and are distinguishable through a permeabilisation step described below. Methodology remained the same regardless or previous treatment of the cells. Expression was determined for each antigen three times in triplicate, in parallel to controls.

Cells were cultured in 1.5 mL media and treated as per experiment, cells were seeded at 250,000 cells per well. Cells were harvested using a cell scraper; the 1.5 mL cell suspension was centrifuged for 5 minutes at 300 rcf in an Eppendorf 5145R centrifuge at 4°C to pellet the cells. The supernatant was aspirated and cells resuspended in 1 mL ice-cold phosphate

buffered saline (PBS; Sigma) supplemented with 5 % normal goat serum (NGS; Biosera) to wash the cells and prevent internalisation of extracellular antigens. Cells were once again pelleted and the supernatant was removed using the same conditions previously described. For intracellular antigens the cells were permeabilised by resuspending in 250 μ L of cold cytofix/cytoperm solution (BD Biosciences) and incubating at 4°C for 20 minutes. The cytofix/cytoperm solution disrupts cell membranes in a reversible manner so for intracellular antigen analysis the cells were then kept in the presence of 0.1 % saponin (Sigma). Cells were pelleted to remove cytofix/cytoperm solution by centrifuging as previously described. Cells were then washed in 500 μ L of cold PBS supplemented with 5 % NGS and 0.1 % saponin, cells were pelleted by centrifuging as described previously, the supernatant was aspirated. For extracellular antigen analysis permeabilisation steps were omitted and cells were not incubated with saponin for any of the subsequent steps. Cells were resuspended in appropriate, optimised, concentrations of primary antibody in cold PBS supplemented with 1 % NGS and 0.1 % saponin at 4°C for 30 minutes. Dilutions for flow cytometry were anti-GD3 1:50 (20 μ g/mL) and anti-9-*O*-acetyl GD3 1:10 (10 μ g/mL). Autofluorescent, no primary antibody and isotype controls were included at this stage. Cells were pelleted to remove primary antibody solutions by centrifuging as previously described. Cells were then washed with 500 μ L of cold PBS supplemented with 5 % NGS and 0.1 % saponin was added to each sample and cells were pelleted by centrifuging as described previously, the supernatant was aspirated. Cell pellets were then resuspended in appropriate isotype and species alexafluor-conjugated secondary antibody (diluted 1:500) and incubated for 15 minutes at 4°C. Cells were pelleted to remove secondary antibody solutions by centrifuging as previously described. 500 μ L of cold PBS supplemented with 5 % NGS was added to each sample and cells were pelleted by centrifuging as described

previously, the supernatant was aspirated. Cells were then resuspended in 300 μ L cold PBS supplemented with 2 % NGS and 0.01 % sodium azide (Sigma), 500 μ L for controls and filtered using 20 μ m nylon mesh filter (Millipore). A 5 μ L volume of propidium iodide (PI; Sigma) was added to each extracellular antigen sample. PI binds to the DNA of non-viable cells, allowing their exclusion in the gating procedure. This step was omitted for intracellular antigen samples. Samples were analysed on a multi-parameter fluorescence-activated cell sorting (FACS) Calibur flow cytometer. Acquisition and analysis of data was carried out using CellQuest Pro Software.

2.9 Immunocytochemistry

To qualitatively analyse the expression of antigens within the cell and on the cell-surface immunocytochemistry was used. Each experiment was performed three times in triplicate and included isotype controls and no primary antibody controls.

Cells were seeded at 200,000 cells per well onto sterile glass coverslips in 6 well plates (Greiner) and were allowed to adhere for 24 hours at 37°C in a 5 % CO₂ humidified atmosphere. Cells were washed with PBS and fixed using 4 % paraformaldehyde (PFA; Sigma) in PBS (Sigma). Cells were then washed and permeabilised using 0.01 % Triton X-100 (Sigma) in PBS for intracellular antigens and incubated for 10 minutes at 4°C, for extracellular antigens this was omitted. Cells were then washed three times in PBS. Non-specific binding was blocked for 1 hour at room temperature using 500 μ L NGS in PBS. After this block buffer was aspirated and each sample was incubated with 500 μ L of the appropriate primary antibody (anti-GD3 1:50 (20 μ g/mL and anti-9-*O*-acetyl GD3 1:100 (1 μ g/mL) diluted in PBS containing 1 % NGS for 1 hour at room temperature. Cells were washed three times with PBS. Alexafluor conjugated secondary antibodies (diluted 1:500)

were then added to each sample using the appropriate species and isotype. A 500 µL aliquot of secondary antibody in PBS containing 1 % NGS was added to each sample and incubated at 4°C for 30 minutes. Cells were then washed three times in PBS. To counterstain nuclei, 100 µL of 10 µg/mL hoechst blue (Sigma) was incubated with the cells for 10 seconds. Cells were washed three times in PBS. Cells were mounted onto slides using a drop of VectaShield mounting medium (Vector Labs). Cells were then imaged using the Zeiss Axioimager ZI epifluorescence microscope equipped with a Hamamatsu digital camera and Velocity image software (Improvision).

2.10 Immunofluorescent staining of wild-type mouse brain sections

P5 and P60 wild-type mouse brains were used for ganglioside staining of the post-partum brain (P5) in which migration of the granule neuron precursors (GPCs) was still taking place, and the P60 mature brain where the external granule layer was not present (and therefore the GPCs had ceased to migrate). The staining was carried out to determine where staining of the gangliosides occurred, and if this occurred in regions of the cerebellum where medulloblastoma is thought to occur.

The mouse-on-mouse immunodetection kit was used to stain mouse brain tissue with anti-ganglioside antibodies. This kit was designed by Vector Labs to localise mouse primary antibodies on mouse tissues and reduce the endogenous immunoglobulin staining of the tissue. High background staining of tissues is therefore reduced using this kit by using Vector Labs blocking agent.

Perfused and frozen P5 and P60 mouse brains were kindly harvested by cervical dislocation and provided by Dr James Hallet and Dr Andrea Rivera from the University of

Portsmouth. Frozen brain sections were mounted using cryo-M-bed (fisher) onto a cork board (fisher) in the correct orientation for cutting sagittal sections. The brain tissue was allowed to cool to -20 °C for cutting and 50 µm sections were cut using a Leica CM3050C cryostat. Slices were placed into a 24 well plate containing PBS + 0.5 % sodium azide for preservation prior to staining.

To determine ganglioside expression in the wild-type mouse frozen brain sections first sections were fixed with 4 % paraformaldehyde (sigma) for 30 minutes. Each subsequent step was carried out in wells of a 24 well tissue culture plate (Greiner). Sections were allowed to air dry after before being washed twice for two minutes each in PBS. Next sections were blocked for 1 hour in mouse-on-mouse blocking reagent (vector labs) and once again washed twice in PBS for two minutes each. Tissue sections were then incubated for 5 minutes in mouse-on-mouse diluent (vector labs) before the excess was removed and the primary antibody (optimized anti-GD3 (1:5 (0.2 µg/mL); Millipore) or anti-9-*O*-acetyl GD3 (1:50 (2 µg/mL); Thermo) were added and incubated on the sections for 1 hour along with diluent only, and no primary antibody controls. The sections were then washed twice for two minutes each in PBS and appropriate secondary antibodies (diluted 1:500) were added and incubated for 30 minutes. Sections were washed twice in PBS for two minutes each. Cell nuclei were counterstained using 100 µL of 10 µg/mL hoechst blue (Sigma). Sections were incubated with Hoechst blue for 10 seconds and were were washed twice in PBS for two minutes each. Brain sections were transferred onto glass slides using a paint brush and finally were mounted onto slides using a drop of VectaShield mounting medium (Vector Labs). Cells were then imaged using the Zeiss Axioimager ZI epifluorescence microscope equipped with a Hamamatsu digital camera and Velocity image software

(improvision).

2.11 Cloning

pCMV-N3, pCMV-N3-SIAE and pCMV-N3-SIAEHis cloning vectors were kindly provided by Professor Reinhard Vlasak, University of Salzburg, Austria. Vector maps and sequence homology for these constructs can be found in Appendix 1.

For inducible system transfections, constructs were purchased from Clontech Takara. A tet-responsive bicistronic expression system was purchased (#631166) and cloned into using InFusion Plus HD Eco Dry (Clontech #638912). An overview of this process is outlined in figure 2.2. Plasmid maps can be found in Appendix 3.

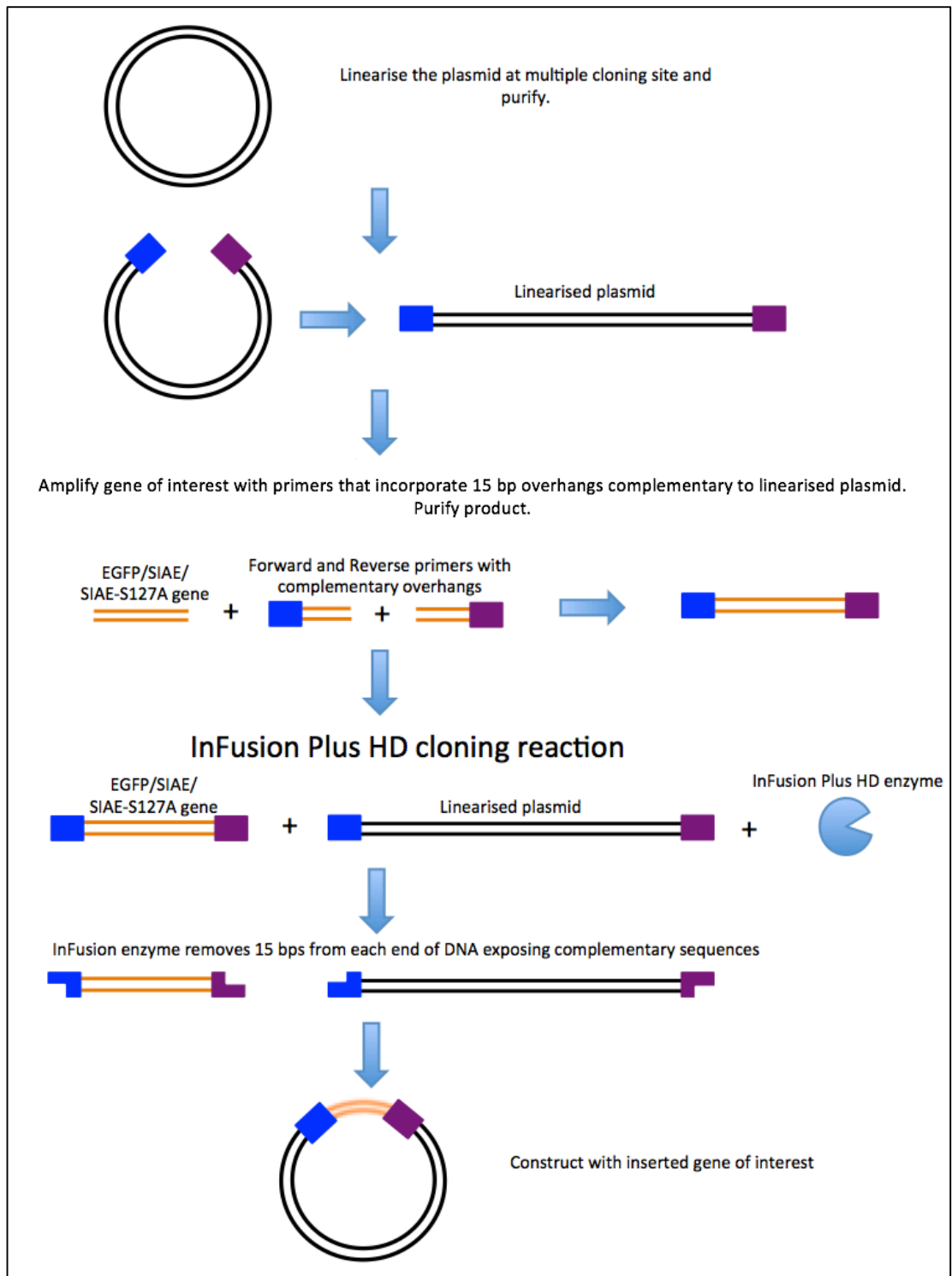


Figure 2.2 An overview of the ligase-independent InFusion Plus HD cloning protocol. To generate plasmids containing genes of interest the parent plasmid first linearised using restriction enzymes appropriate for the multiple cloning site. The resulting linearised plasmid is then gel-purified. Genes of interest are amplified using primers designed with 15 bp overhangs complementary to the multiple cloning sites used. The gene of interest and the linearised plasmid are then joined together using the InFusion HD enzyme. During the reaction sticky ends are generated by the InFusion enzyme which digests 15 bps from the ends of both the gene and the linearised plasmid. The DNA then re-joins through complementary base pairing in an enzyme-independent manner.

In order to clone into pTRE3G-TetOn3G, the backbone was first linearised using restriction endonucleases that had unique sites within the construct. For cloning of the enhanced green fluorescent protein (EGFP) gene into multiple cloning site 2 (MCS2) the restriction endonucleases MluI (New England Biolabs #R3198S) and BamHI (New England Biolabs #R3136S) were used.

To linearise the pTRE3G-IRES plasmid the following conditions were used at 37°C for three hours using a heat block, table 2.4 and run on a 1% TAE agarose gel for 90 mins at 80 V (figure 2.3).

Table 2.4 Components used for linearization of pTRE3G-IRES backbone vector for cloning.

Component	Amount (μL)
Restriction enzyme (BamHI/MluI)	1 each
DNA	1 μg
10 X NEB cut smart buffer	5
Total Reaction volume	50 (made up to 50 μL in ddH ₂ O)

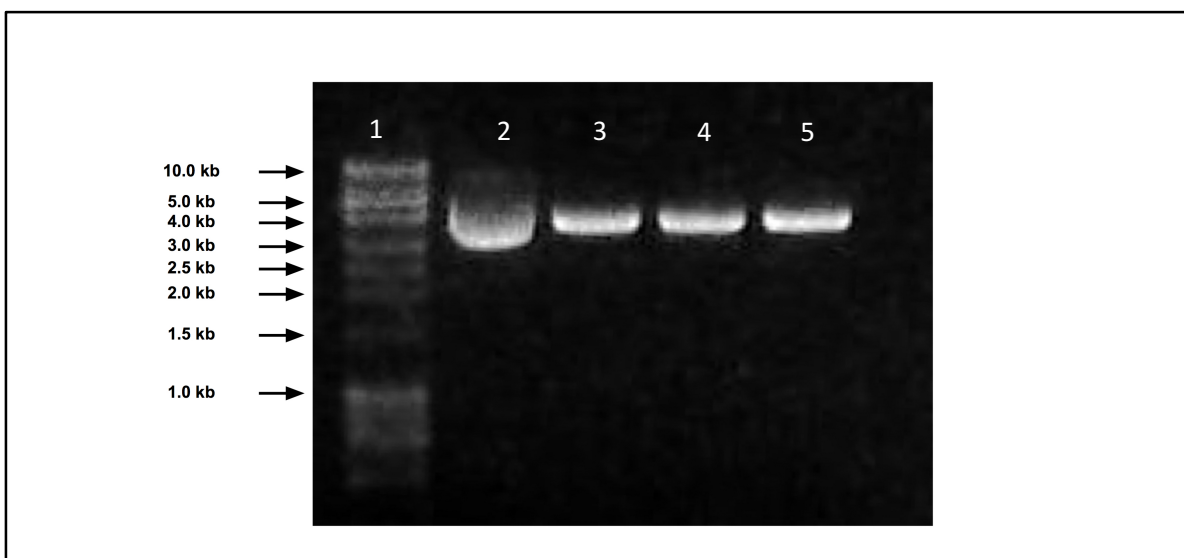


Figure 2.3 pTRE3G-IRES construct is linearised by restriction endonuclease digestion run on 1% TAE agarose and run at 80 V for 90 mins. 20 μL of sample was added to each lane (1) DNA molecular marker (2) Undigested supercoiled plasmid pTRE3G-IRES runs more quickly than linearised plasmid due to the compact size generated by supercoiling (this however means it cannot be accurately sized) (3-5) Linearised pTRE3G-IRES is confirmed by electrophoresis and is the correct size for purification (4002 bp).

The bands were excised from the agarose gel using a scalpel and spin-column purified using Nucleospin Gel and PCR clean up kit (Clontech). The weight of the gel slice was determined and for each 100 mg of agarose gel 200 μ L Buffer NT1 (Clontech) was added. The samples were then incubated for 10 minutes at 50°C on a heat block with vortexing every 2 minutes to ensure the agarose gel had dissolved. A 700 μ L aliquot of dissolved product was then loaded onto a Nucleospin column and centrifuged at 11000 g for 30 seconds, this step was repeated until all of the sample had been loaded onto the column. The membrane was then washed using 700 μ L of buffer NT3 (Clontech) and centrifuged for 30 seconds at 11000 g. The wash step was repeated to ensure chaotropic salt carry over. The column was then centrifuged for 1 minute to ensure complete removal of ethanol. The DNA was then eluted using 20 μ L of buffer NE (Clontech) by incubating at 70°C for 5 minutes. The sample was centrifuged at 40 g for 1 minute and then 11000 g for 1 minute to elute DNA.

Once the plasmid backbone was linearised and purified the EGFP gene was amplified out of the parental vector using infusion primers. These primers were designed to have 15 bp overhangs that are complementary to the plasmid backbone for ligase independent cloning the following primers for EGFP (Eurofins genomics) are shown in table 2.5.

To amplify out the gene the following PCR master mix was prepared on ice, components are shown in table 2.6. The contents of the tube were mixed by flicking and briefly centrifuged to bring the contents to the bottom of the tube. The sample was placed in a BioRad thermal cycler, conditions shown in table 2.7.

Table 2.5 Primers with InFusion cloning overhangs for cloning. 15 base pair overhang regions allow ligase independent incorporation of genes into the linearised plasmid.

Primer	Sequence
MluI/BamHI_EGFPF	GCC GGA TAT CAC GCG TAT GGT GAG CAA GGG CGA GGA GCT G
MluI/BamHI_EGFPR	CAG TTA CAT TGG ATC CTT ACT TGT ACA GCT CGT CCA TGC C

Table 2.6 Components of PCR reactions for amplification of genes from parent vector constructs.

Component	Amount
CloneAmp HiFi PCR premix	12.5 μ L
Forward Primer	10 pmol
Reverse primer	10 pmol
Template	1 μ g
Nuclease-free water	To 25 μ L

Table 2.7 Thermal cycling conditions for amplifying genes from parent constructs

Temperature / °C	Time / seconds
98	10
55	15
72	8 (5 sec / kb)

The PCR product was then run on a 1% agarose TAE gel which was run at 80 V for 90 minutes and visualised using safe view stain and visualised using a Syngene G box (Syngene). Finally, the product was spin column purified as previously described. To join the gene and the linearised backbone together an Infusion Plus HD Eco Dry cloning kit was used (Clontech). The following reaction was set up in the provided InFusion lyophilised reaction tubes as shown in table 2.8.

The PCR reactions were incubated for 15 minutes at 37°C, followed by 15 minutes at 50°C using a Biorad Thermal Cycler, and placed on ice. The resulting DNA was then transformed and plasmid DNA purified as described below.

To ensure the EGFP gene had been incorporated, the resulting DNA was digested once again with MluI and BamHI and the insert sized on an agarose gel as shown in figure 2.4.

The resulting construct was pTRE3G-IRES-EGFP and was further cloned into to generate pTRE3G-IRES-EGFP-SIAE and pTRE3G-IRES-EGFP-SIAE_S127A by digestion with EagI and Sall enzymes unique to multiple cloning site 1 (MCS1).

The Primers used to amplify the SIAE and S127A genes from their parent plasmids are shown in table 2.9.

Table 2.8 InFusion Plus HD Eco Dry reactions for both pTRE3G-IRES-EGFP and pTRE3G-IRES-EGFP-SIAE and pTRE3G-IRES-EGFP-SIAE-S127A reactions.

Reaction	Cloning Reaction		Negative	Positive control reaction
Component			control reaction	
Purified fragment	PCR	100 ng	0 ng	2 µL of control insert (Clontech)
Linearised vector		50 ng	1 µL	1 uL of control pU19 vector (Clontech)
Deionised water		To 10 µL	To 10 µL	To 10 µL

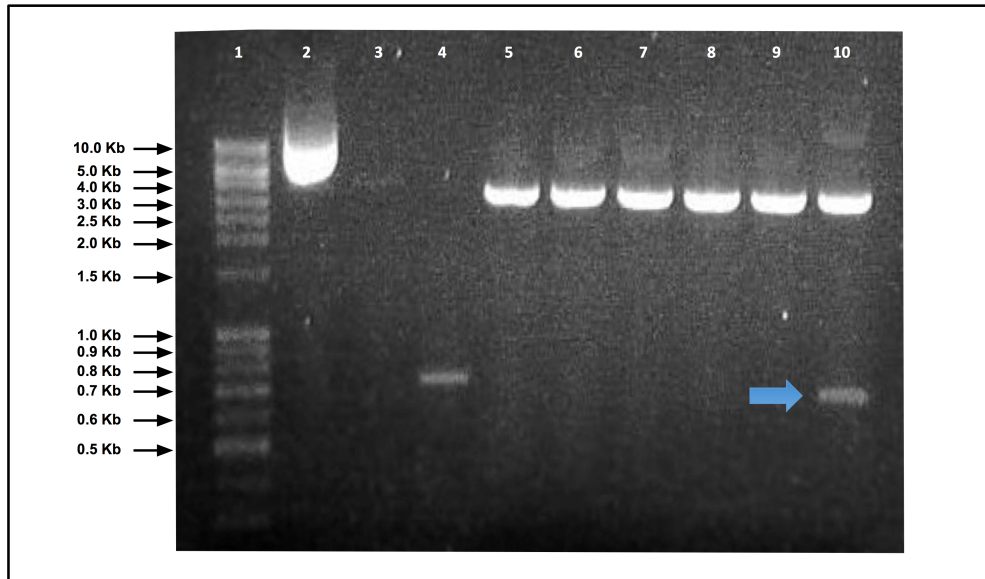


Figure 2.4 EGFP incorporation into the pTRE3G-IRES constructs is confirmed with digestion of plasmid DNA with MluI and BamHI. The products of the digest were run on a 1% TAE agarose gel at 80 V for 90 minutes. (1) DNA molecular marker (2) undigested supercoiled plasmid DNA was run as a control for the linearization reaction (3) Empty lane (4) Purified EGFP DNA (750 bp) (5-9) Unsuccessful incorporation of the EGFP gene shown by no presence of EGFP at 750 bp despite digestion with MluI and BamHI. (10) Successful incorporation of the EGFP gene as shown by presence of a digest product at 750bp (blue arrow).

Table 2.9 Primers used for the amplification of SIAE and SIAE-S127A genes including 15 bp overhang regions complementary to linearised pTRE3G-IRES-EGFP to allow ligase-independent cloning.

Primer	Sequence
Sall/EgII_SIAEF	CCC TCG TAA AGT CGA CAT GGT CGC GCC GGG GCT TGT ACT C
Sall/EgII_SIAER	GGA GAG GGG CCG GCC GTC ATT TAG CAA CAT TGC TCT GAT G

The cloning process was repeated as for EGFP, using SIAE and S127A purified genes. To ensure the insertion of the gene into the construct, KpnI digests were carried out as the KpnI site is unique within the construct and linearises the backbone through the SIAE gene insert as shown in figure 2.5. Digest conditions are shown in table 2.10. If insert was present, the product could be sized appropriately for insertion of the gene when run on a 1% TAE agarose gel for 90 minutes at 80 V (figure 2.6).

The constructs were then sequenced by Eurofins genomics using Eurofins genomics primers to confirm insertion of the gene resulted in the correct sequence, confirmed in appendix 3.

Table 2.10 Components used for linearization of pTRE3G-IRES-EGFP-SIAE and SIAE-S127A vectors to confirm successful integration of the genes.

Component	Amount (μL)
Restriction enzyme (KpnI)	1
DNA	1 μg
10 X NEB cut smart buffer	5
Total Reaction volume	50 (made up to 50 μL in ddH ₂ O)

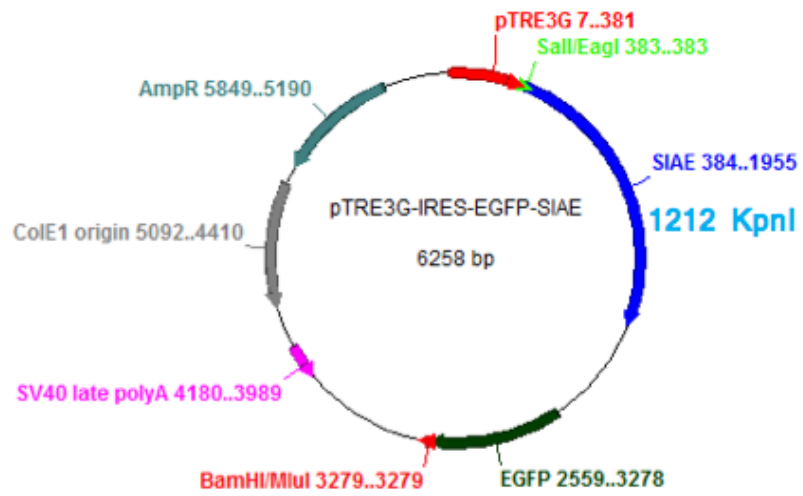


Figure 2.5 Linearisation of the pTRE3G-IRES-EGFP-SIAE construct demonstrates integration of the gene as the restriction site only occurs within the SIAE gene itself.

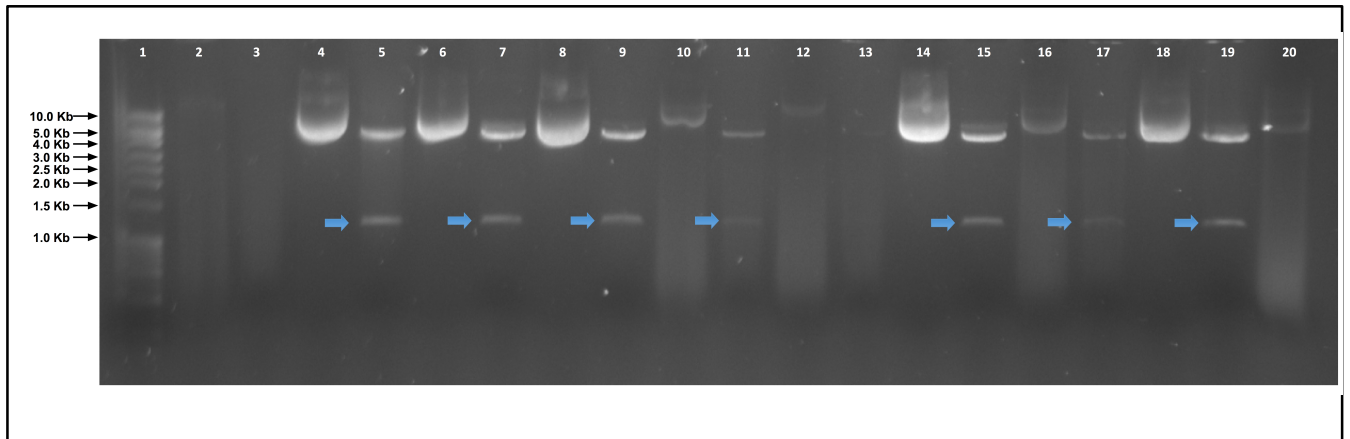


Figure 2.6 Confirmation of the insertion of the SIAE gene into pTRE3G-IRES-EGFP vector. (1) DNA molecular marker, (2-3) Empty lanes. (Even lanes) Supercoiled plasmid DNA to confirm linearity. (Odd lanes) KpnI digested plasmid DNA. Arrows show products of restriction digest by KpnI (present only in the SIAE sequence, confirming presence of inserted gene with a band at 1193 bp; blue arrows).

2.11.1 Transformation and Preparation of Plasmid DNA

To transform Stellar competent *E.coli* (Clontech) 50 ng of plasmid DNA was required. Each plasmid was diluted to the appropriate concentration in nuclease-free water. A 1 μ L aliquot was added to 50 μ L of defrosted stellar cells on ice. The cells were incubated with plasmid on ice for 30 mins. The cells were then placed on a heat block for 50 seconds at 42°C (heat shock). For recovery cells were incubated for 5 minutes on ice. A 425 μ L aliquot of SOC media was then added to each tube and they were placed into the shaking incubator for 1 hour at 37°C. After the recovery incubation the whole aliquot of cells were plated in aseptic conditions onto the appropriate selection antibiotic on Luria-Bertani (LB)-agarose plates. All plasmids were plated on 50 μ g/mL ampicillin. The plates were incubated at 37°C overnight to allow colonies to form. The next day plates were sealed with parafilm and stored at 4°C until colony selection.

A 5 mL volume of sterile LB broth was added to universal tubes (one per construct). A concentration of 50 μ g of ampicillin was added to the LB broth in appropriate tubes. Single colonies were then selected using sterile pipette tips and placed into the media (in aseptic conditions). The tubes were then taped loosely shut to allow gas exchange and incubated for 16 hours at 37°C in a rocking incubator.

When transformation was complete and an overnight culture had been grown, glycerol stocks were prepared. A total volume of 1.125 mL of bacteria culture was added to duplicate sterile screw top eppendorf tubes. A volume of 375 μ L of sterile 60 % glycerol (Sigma) was added. The tubes were vortexed and snap-frozen in liquid nitrogen for 10 minutes before being stored at -80°C.

Plasmid DNA was then isolated from the *E.coli* using a plasmid PureYield Minicolumn kit (Promega). A volume of 1.5 mL of bacterial culture was centrifuged for 30 seconds at maximum speed (16900 g) in an Eppendorf 5415r microcentrifuge. The supernatant was discarded before an additional 1.5ml of bacterial culture was added to the same tube and centrifuged again for 30 seconds at maximum speed. A 600 µL aliquot of nuclease-free water was added cell pellet, and the cells re-suspended. The cells were then lysed using lysis buffer (Promega) for 3 minutes at room temperature with 5 inversions to mix. The lysis buffer was then neutralised using 350 µL cold neutralisation solution (Promega) and the supernatant transferred to a PureYield™ Minicolumn without disturbing the cell debris pellet. The minicolumn was then placed into a Collection Tube, and centrifuged at maximum speed for 15 seconds. The flow-through, was discarded and 200µl of Endotoxin Removal Wash (ERB; Promega) was added to the minicolumn to wash the DNA. This was then centrifuged at maximum speed for 15 seconds. 400µl of Column Wash Solution (CWC; Promega) was then added to the minicolumn and centrifuged at maximum speed in a microcentrifuge for 30 seconds to ensure the complete removal of ethanol which can interfere with transfection. The minicolumn was then transferred to a 1.5ml microcentrifuge tube and DNA was eluted using 30 µL of nuclease-free water, this was incubated at at room temperature for one minute before centrifugation for 15 seconds at full speed to elute the plasmid DNA. Plasmid DNA was stored at –20°C.

Cells were seeded in a single well of a 6-well plate at a density sufficient to reach near confluence at 48 h after transfection (200,000 cells). Then pCMV-Tet3G was transefected into cells using Xfect transfection reagent.

After 48 h, the confluent well was divided into 4 x 10 cm dishes. After an additional 48 h, G-418 was added at the selection concentration that was determined from kill curves (appendix 5). The medium was replaced every four days to ensure presence of G-418 remained constant. Cells that have not integrated the plasmid begin to die after 3–5 days. After 2 weeks, G418-resistant colonies begin to appear. When the colonies were large enough to transfer, colonies were picked and transferred into separate wells of a 24-well plate. When confluent, the clones from each well were split into three wells of a 6-well plate for testing and maintenance.

For each clone to be tested, two wells of the six well plates were used for induction tests by seeding at 200,000 cells/well again. The remaining well of each clone was used as a 'stock plate' for propagation if needed after testing. The wells that were seeded were then transfected with 5 µg of pTRE3G-Luc using Xfect transfection reagent as previously described. After 4 h, the culture medium was replaced with fresh medium containing 1 µg/mL doxycycline to one of the duplicate wells, while leaving the second well doxycycline-free. After 24 h, an assay for luciferase activity was carried out (described below) and the fold-induction calculated to determine the best clones.

Clones with the highest fold induction (ratio of maximal to basal gene expression) were used for propagation and further testing.

Stocks of each promising clone were made as soon as possible after expanding the culture as described in section 2.1.3.

The Tet3G-expressing cell line was once again plated at 200,000 cells per well in three wells of a 6-well plate. Using Xfect transfection reagent pTRE3G-IRES-EGFP, pTRE3G-IRES-EGFP-

SIAE and pTRE3G-IRES-EGFP-SIAE-S127A constructs were transfected at 2 µg each along with 100 ng of a linear puromycin selection marker.

After 48 h cells were divided 4 x 10 cm dishes. After an additional 48 h, puromycin was added at the selection concentration that was determined by kill curve analysis. Medium was replaced with fresh complete medium supplemented with puromycin every four days. Cells that have not integrated the plasmid should die after 3–5 days. After 2 weeks, drug-resistant colonies begin to appear. When the colonies were large enough to transfer they were moved into separate wells of a 24-well plate. When confluent, the cells were split into three wells of a 6-well plate for testing and maintenance as before and assayed for SIAE expression.

Stocks were then made of each promising clone as soon as possible after testing and expanding.

2.12 Stable and Transient Transfection with pCMV-N3-SIAE

To transfect cells with pCMV-N3, pCMV-N3-SIAE and pCMV-N3-SIAE-His constructs JetPrime reagent was used (Polyplus transfection). Plasmids were kindly provided by Prof. Reinhard Vlasak. Cells were seeded at 200,000 cells per well in 6 well plates (Greiner) in full media, 24 hours before being transfected using 2 µg plasmid DNA per well. DNA was first diluted in 200 µL per well of JetPrime buffer, vortexed and briefly centrifuged. A 4 µL aliquot of JetPrime reagent per well was then added to the tube which was then vortexed and briefly centrifuged before incubating for 10 minutes at room temperature. The DNA was then added in a drop-wise manner to appropriate wells with gentle swirling. The cells were

incubated at 37°C in a 5 % CO₂ environment for four hours before media was changed to prevent toxicity.

2.13 Stable Transfection – Inducible System Constructs

For transfection with pCMV-TetOn3G, pTRE3G-Luc, pTRE3G-IRES-EGFP, pTRE3G-IRES-EGFP-SIAE and pTRE3G-IRES-EGFP-SIAE-S127A constructs Xfect Transfection reagent (Clontech) was used.

Cells were plated for transfection 24 hours prior to addition of DNA complexes. Adherent cells were plated at 200,000 cells per well of a 6 well plate (Greiner) in 1 mL full media. Suspension cells were plated at 1×10^6 cells per well in 3 mL growth media in one well of a 6 well plate (Greiner). Xfect polymer was vortexed and briefly centrifuged to ensure no separation of components had occurred.

A volume containing 2 µg plasmid DNA (or 5 µg for pTRE3G-Luc) was diluted in 100 µL Xfect buffer per well. The solution was mixed by vortexing and briefly centrifuged and 0.3 µL per 1 µg DNA of Xfect Polymer was then added and the components mixed by vortexing, and then briefly centrifuged. The DNA mix was then incubated at room temperature for 10 minutes to allow nanoparticle complexes to form. A 100 µL aliquot of DNA complex mix was then added drop-wise to cells with gentle swirling. The cells were incubated at 37°C in a 5 % CO₂ environment for four hours before media was changed to prevent toxicity.

2.14 EGFP transfection efficiency assay

pEGFP-N3, pEGFP-N3-SIAE and pEGFP-N3-SIAE-His constructs each express an enhanced green fluorescent protein (EGFP) tag. This tag can be detected using the EGFP transfection efficiency assay protocol and analysed on the Nucleocounter 3000 (Chemometec).

Cells were transiently transfected with each construct as previously described and harvested using tryPLE express (Life technologies) as previously described. A volume of 96 μL of each cell sample was added to a microcentrifuge tube and 2 μL of 500 $\mu\text{g}/\text{mL}$ Hoechst 33342 was added and mixed by pipetting to counterstain nuclei. The cells were then incubated at 37°C for 15 minutes using a heat block. After the incubation period 2 μL of 500 $\mu\text{g}/\text{mL}$ propidium iodide was added and mixed by pipetting to determine the dead cell population. A 30 μL sample was loaded into a nucleocounter A2 chamber slide (Chemometec) and analysed using Nucleoview software (Chemometec).

2.15 Luciferase assay

Cells were transfected as previously described. The cells were then washed once in 2 mL PBS in the culture vessel, or if a suspension culture is being tested, centrifuged at 300 g for 5 minutes in an Eppendorf 5415r microcentrifuge, washed in 1 mL PBS and again centrifuged at 300 g for 5 minutes. 500 μL of passive lysis buffer (promega) was added to each well. The plate was then placed on a rocker at room temperature at a slow speed for 15 minutes. The lysate was then collected and stored in 1.5 mL eppendorf tubes at -80°C. A 20 μL aliquot of cell lysate was added in triplicate to wells of a white-walled flat bottom plate (Greiner). Then, 100 μL volume per well of buffer LARII (Promega) was added and luciferase activity measured on a BMG labtech POLARstar Optima plate reader using a program that

provides a 2-second pre-read delay, followed by a 10-second measurement period. The fold-induction was calculated as the fold-change between clones in the absence and presence of doxycycline.

2.16 Clone Selection

In order to select transfected clones from a heterogeneous population of transfected and not-transfected cells selective antibiotics are used. For pCMV-N3, pCMV-N3-SIAE, pCMV-N3-SIAE-His and pCMV-TetOn3G G-418 (BioChrom) was used. For pTRE3G-IRES-EGFP, pTRE3G-IRES-EGFP-SIAE and pTRE3G-IRES-EGFP-SIAE-S127A puromycin (Life Technologies) was used.

In order to determine the concentration of antibiotic required to kill cells that have not integrated plasmid kill curves were carried out.

The seeding density of cells was determined previously by seeding cells at various densities and conducting MTS assays and imaging cells to determine when a monolayer of cells was formed. This seeding density was then used for subsequent experiments and was cell line dependent.

To determine a concentration of antibiotic, various concentrations of G-418 or puromycin were incubated with cells that had not been transfected before MTS assays and cell imaging was carried out. For G-418, a concentration that kills more than 50 % of the cells within 5 days and all cells within 14 days was selected. For puromycin a concentration was selected that killed greater than 50 % of cells within 3 days and all cells within 5 days was selected. All media was changed every 4 days to ensure antibiotic was always present in the cell culture media.

To carry out an MTS assay media was changed to 100 μ L media without antibiotics. 20 μ L of CellTiter 96 AQ_{ueous} One solution reagent (Promega) was added to each well. Plates were incubated at 37°C for 3 hours. The absorbance was then read at 490 nm using the BMG labtech POLARstar Optima plate reader. Cells were imaged to verify MTS results. Data for clone selection for RES256 cells can be found in appendix 5.

2.17 Lysis of cells

Cells were cultured and treated as per experimental protocol. For total protein analysis cells were lysed using Mammalian Protein Extract Reagent (M-PER; Thermo).

For Western blot analysis, small volumes of lysate were required for SIAE detection. In this case, cells were harvested using cell scrapers and centrifuged at 300 g using a Boeco C-28A centrifuge. The cell pellet was washed in ice-cold PBS to remove phenol red, which interacts with the downstream protein assay (BCA Assay) and transferred to 1.5 mL Eppendorf tubes and centrifuged at 300 g for 5 minutes at 5°C using an Eppendorf 5415r microcentrifuge to pellet cells. Cells were lysed in M-PER reagent (750 μ L per T-75 culture flask) supplemented with 1 X protease and phosphatase inhibitor cocktail (Thermo) for 5 minutes on ice. The lysates were centrifuged at maximum speed (16,900 g) using an Eppendorf 5415r microcentrifuge for 10 minutes at 4°C to remove cell debris. The pellet and lysate supernatant were then separated; the lysate was aliquotted to avoid freeze-thaw cycles for down-stream assays and stored at -20°C.

2.17.1 Determination of Protein Content in Cell Lysates (BCA Assay)

The bicinchoninic acid (BCA) assay is a colorimetric detection and quantitation method for total protein. The assay combines two reactions, protein reduction of Cu^{2+} to Cu^{1+} and colourimetric detection of Cu^{1+} by bicinchoninic acid.

The first step of the assay is chelation of copper with protein in an alkaline solution to form a light-blue complex, the biuret reaction. Peptides containing three or more amino acid residues form a coloured chelate complex with copper (cupric) ions in an alkaline solution containing sodium potassium tartrate. The second step involves bicinchoninic acid (BCA) which reacts with the reduced copper ions formed in step 1. This forms a purple reaction product which results from the chelation of two molecules of BCA with one Cu^{1+} ion. The BCA/copper complex gives a strong linear absorbance at 562 nm that increases with increasing protein concentration.

This method is strongly influenced by the amino acid residues cysteine or cystine, tyrosine, and tryptophan in the amino acid sequence of the protein. However, unlike the Coomassie dye-binding method, the universal peptide backbone also contributes to colour formation, helping to minimize variability caused by the different compositions of proteins.

A protein standard curve was generated using 2 mg/mL stock bovine serum albumin (BSA) diluted to the appropriate concentrations using lysis buffer. The following dilutions were made using table 2.11

Table 2.11 Dilutions for the BCA assay protein standards. This table was used to generate a standard curve for BCA assays. The final concentration of BCA protein will be used to determine the total protein concentration in the samples.

Standard	Volume of lysis buffer (μL)	Volume and Source of BSA (μL)	Final BSA concentration ($\mu\text{g/mL}$)
A	0	300 of stock (2 mg/mL BSA)	2000
B	125	375 of stock	15000
C	325	325 of stock	1000
D	175	175 of vial B solution	750
E	325	325 of vial C dilution	500
F	325	325 of vial E dilution	250
G	325	325 of vial F dilution	125
H	400	100 of vial G dilution	25
I	400	0	0

The BCA working reagent (WR; 50 parts of bicinchoninic acid 1 part copper (II) sulphate) was prepared using the following formula.

$(\# \text{ standards} + \# \text{ samples to be tested}) \times (\# \text{ replicates}) \times (\text{volume of WR per sample (200 } \mu\text{L)}) = \text{total volume required}$

A volume of 10 μL of each unknown sample and standard was pipetted in triplicate into a clear flat-bottomed 96-well plate (Greiner). 200 μL of the WR was then added to each well and the plate covered and incubated at 37°C for 30 minutes.

The plate was then cooled to room temperature and absorbance measured at 562 nm on the Optima BMG labtech POLARstar plate reader.

The concentration of protein was then determined using a standard curve and linear regression.

2.18 Western Blot

Expression of antigens was confirmed at the protein level by Western blot analysis.

Cells were seeded in cell culture flasks and were incubated, and treated appropriately for any given experiment. Each experiment was performed in triplicate. After the required incubation period, cells were lysed and protein concentration determined as described above. If conditioned media was loaded onto the gel then cells were serum starved over 48 hours (as a step-down from 10% to 5 % for 6 hours, 2% overnight, 1% for 6 hours and then 0%). The media was then harvested and centrifuged at 1,000 rpm for 5 minutes to remove cells. This supernatant was used for conditioned media gels described below.

A 10% polyacrylamide sodium dodecyl sulphate (SDS) gel (Thermo) was placed into a

BioRad Miniprotean gel rig (BioRad), wells were washed with Tris-HCl running buffer (2.5 mM Trizma base; 19.2 mM Glycine; 0.1 % Sodium dodecyl Sulphate). Samples were diluted with lysis buffer (M-PER, Thermo) and 5 X Llameli buffer (Sigma) supplemented with lysis buffer and β -mercaptoethanol (Sigma) at an appropriate concentration and volume for sodium dodecyl sulphate polyacrylamide gel electrophoresis (SDS-PAGE). Samples were briefly vortexed and heated at 95°C for 5 minutes to break down disulphide bonds allowing the linear running of sample.

A volume of 5 μ L of Precision Plus Protein molecular weight standard (Bio-Rad) was loaded on to the gel followed by appropriate volume of sample. Where wells were unfilled, an appropriate volume of lysis buffer and loading buffer were loaded to ensure no curvature of bands in the gel. The gel was run for around 90 minutes at 100 V.

The gel was then removed from the rig and plates and allowed to equilibrate in transfer buffer (2.5 mM Trizma base; 19.2 mM glycine) for 15 minutes. PVDF membrane (Millipore) was hydrated for 15 seconds in methanol (Sigma) and placed into transfer buffer until needed. In order to transfer the protein from gel to PVDF membrane, the sandwich method was used. Mini-Blot filter paper (Bio-Rad) and 2 sponges were soaked in transfer buffer and assembled in the sandwich cassette. The assembly was carried with a sponge on the cathode side of the plate, then one page of blotting paper, the gel, then the membrane, followed by another blotting paper page and finally the sponge. This was added to the rig with an ice pack and a magnetic stirrer and transferred at 100 V for 90 minutes.

If conditioned media was loaded into the gel, the membrane was stained for 5 minutes with Ponceau S (Sigma) and washed with distilled water 3 times for five minutes each. If cell lysates were loaded onto the gel then this step was omitted. Then the following steps

were carried out.

Before the membrane could be probed with primary antibody it was necessary to first carry out a blocking step to reduce the amount of background and non-specific binding. Blocking buffer was added to the membrane and incubated for 1 hour at room temperature with gentle rocking. The blocking buffer was made up from 5 % non-fat milk (Marvel) dissolved in Tris-buffered saline (TBS; 0.2 mM Trizma base; 1.4 mM sodium chloride; pH 7.6). The membrane was then incubated overnight at 4°C on a platform shaker with the appropriate primary antibody and the loading control antibody. The membrane was then washed 5 times with Tris-buffered saline (0.2 mM Trizma base; 1.4 mM sodium chloride; pH 7.6) containing 0.1% Tween-20 (TBST) for five minutes each. The appropriate infrared conjugated secondary antibody was then incubated for 1 hour at room temperature. The membrane was then washed 5 times with TBST for five minutes each. The membrane was then imaged on the Licor Odyssey (Licor) using Image Studio 5.0 software.

2.19 Mitochondrial Membrane Potential Assay (JC-1 Assay)

Mitochondrial membrane potential ($\Delta\Psi_m$) is an important measure of mitochondrial function and is used to determine cell health.

The JC-1 assay measures monomers and aggregates of the lipophilic cationic JC-1 dye. The JC-1 dye changes its fluorescent properties based on the aggregation of the probe, shown as green and red fluorescence. In healthy cells, with polarised mitochondrial membrane potentials (high $\Delta\Psi_m$), JC-1 forms red aggregates within the mitochondria. In cells with depolarised mitochondrial membrane potentials (low $\Delta\Psi_m$) green monomers of dye are formed outside of the mitochondria (figure 2.7). A ratio of red to green fluorescence is used

to determine the degree of depolarisation of the sample. DAPI staining is included for dead cell staining. This assay was carried out in parallel to a positive and a negative control. Each experiment was carried out three times in triplicate with help from Mrs. Katie Loveson.

Cells were harvested by trypsinisation and resuspended in 1 ml PBS at 1×10^6 cells/mL. A volume of 12.5 μ L of 200 μ g/ml JC-1 (Satorius) giving a final concentration of 2.5 μ g/mL was added to each sample and incubated for 10 minutes at 37°C. Cells were centrifuged at 400 g for 5 minutes at room temperature using an Eppendorf 5415r microcentrifuge. The supernatant was discarded and the cell pellet washed by resuspending in 1 mL PBS and centrifuging at 400 g for 5 minutes at room temperature as before. This wash step was repeated. The cell pellet was then resuspended in 250 μ L of 1 μ g/mL of DAPI solution (Satorius). The cells were then added to an A2 nucleocounter slide (Satorius) and analysed on the Nucleocounter 3000 (Chemometec) using Nucleocounter 3000 software (Chemometec).

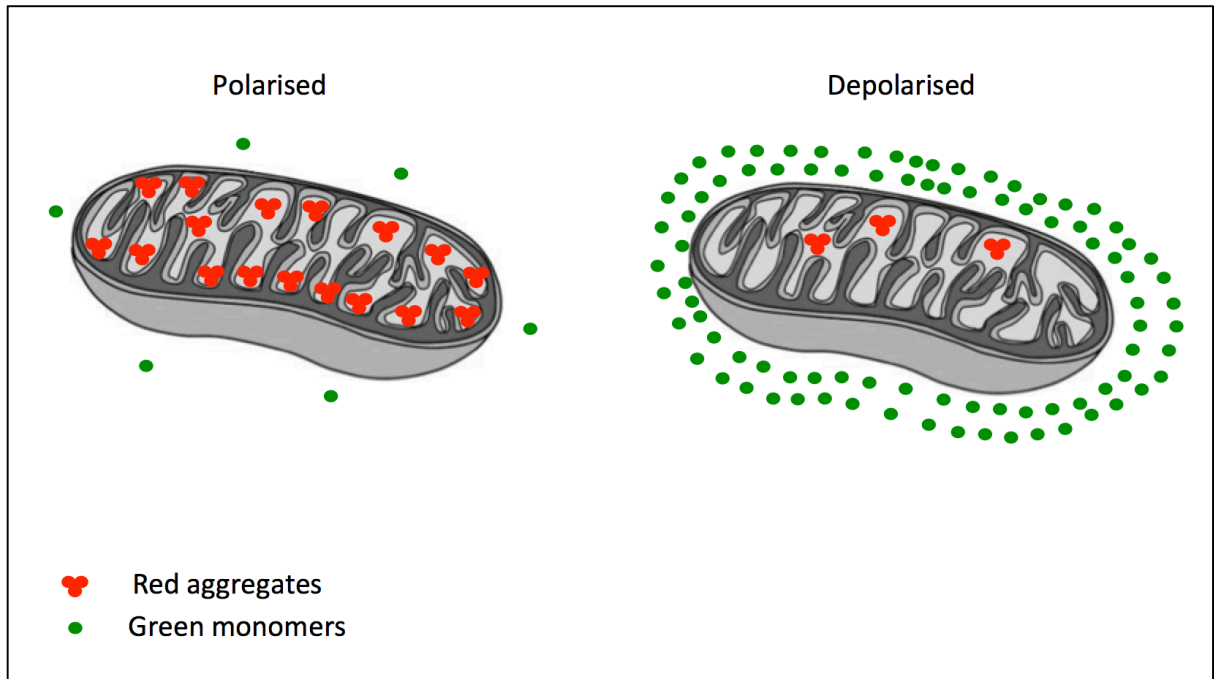


Figure 2.7 The JC-1 assay is used as a measure of the mitochondrial membrane potential. Aggregates of dye within the mitochondria emit red fluorescence and are indicative of functioning mitochondria. Monomers of dye outside of the mitochondrial membranes emit green fluorescence and are indicative of a collapsed membrane potential and early apoptosis. This is a transient event and therefore must be used in combination with other methods to determine apoptosis.

2.20 Chemotherapy Experiments

The agents chosen for chemotherapy experiments were cisplatin and etoposide, these were used as examples of cell-cycle non-specific (cisplatin) and cell-cycle specific (etoposide) agents currently in use for treatment of brain tumours in children. Etoposide was also chosen for its reported mechanism of action on the collapse mitochondrial membrane potential in isolated mitochondria (Robertson et al. 2000). As the mechanism by which GD3 causes apoptosis is most widely accepted to be via the collapse of the mitochondrial membrane potential it was thought that a synergistic or additive effect of etoposide with SIAE over-expression may be seen (Malisan & Testi 2002a).

Etoposide is a cell cycle-specific antineoplastic drug belonging to a family of topoisomerase II inhibitors (Jacob et al. 2011). The cell cycle is arrested at G₂/S phase. Etoposide stabilises the DNA/protein complex and the breaks inserted by topoisomerase II are therefore permanent. The inability for cells to transcribe or replicate DNA causes apoptosis as the DNA damage overwhelms the DNA repair machinery. The primary mechanism of action of Etoposide is described in figure 2.8.

Cisplatin is a cell-cycle non-specific DNA alkylating drug that causes DNA adducts between guanine residues, which causes apoptosis through direct DNA damage (Dasari & Tchounwou 2014). The primary mechanism of action of Cisplatin is described in figure 2.9.

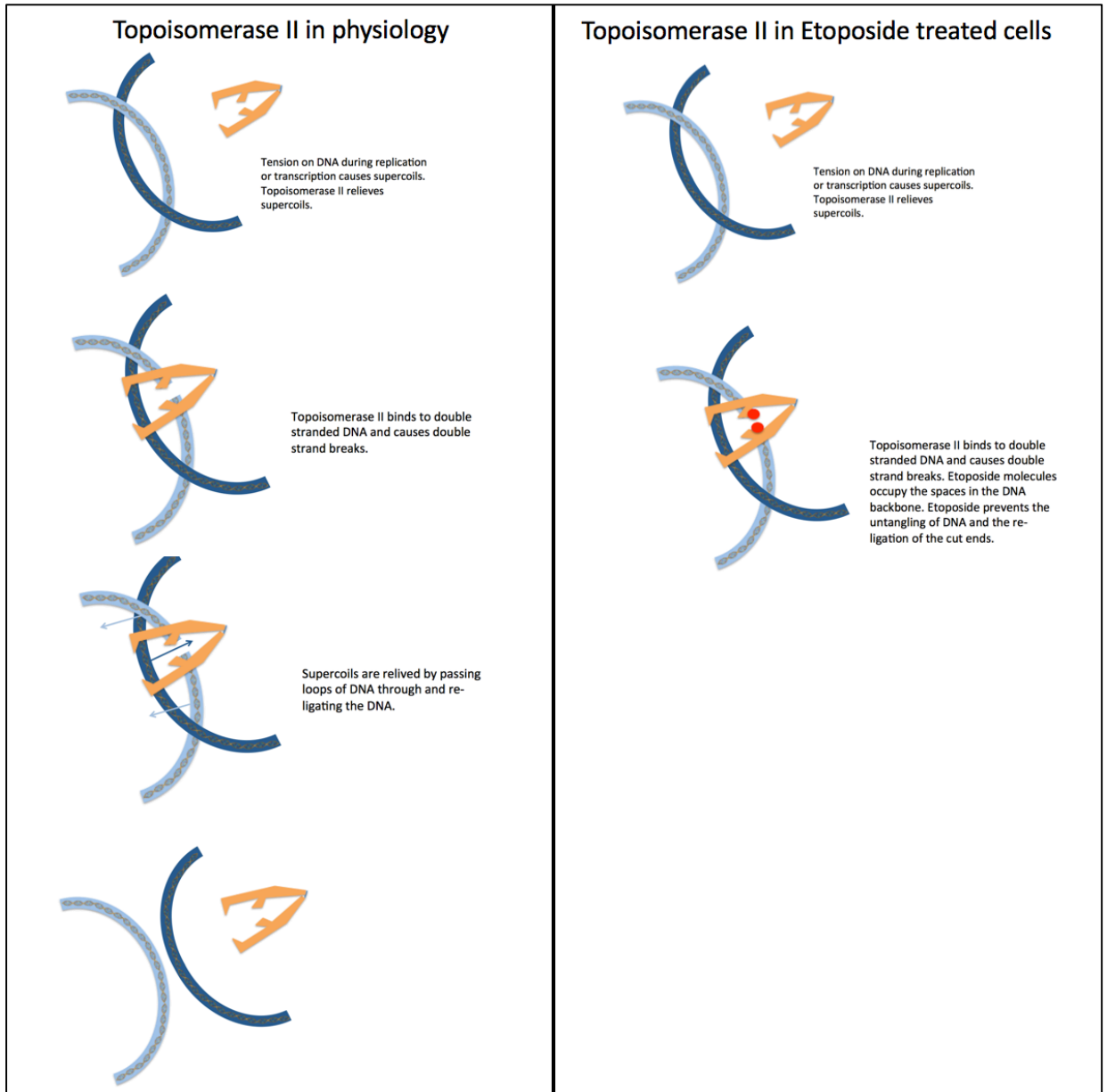


Figure 2.8 Mechanism of action of Etoposide. During transcription and replication of DNA, RNA and DNA polymerases cause tension on the DNA helix as extension takes place. Topoisomerase II releases tension on the DNA helix by creating transient double strand breaks thereby relieving supercoils. Topoisomerase II then joins the breaks back together. Etoposide is a topoisomerase II inhibitor that prevents this untangling of supercoiled DNA and stabilises the DNA breaks. When cells are treated with Etoposide, the apoptotic program can be initiated due to failure of the DNA damage repair machinery which cannot repair the breaks due to the presence of the drug. Adapted from Jacob (2011).

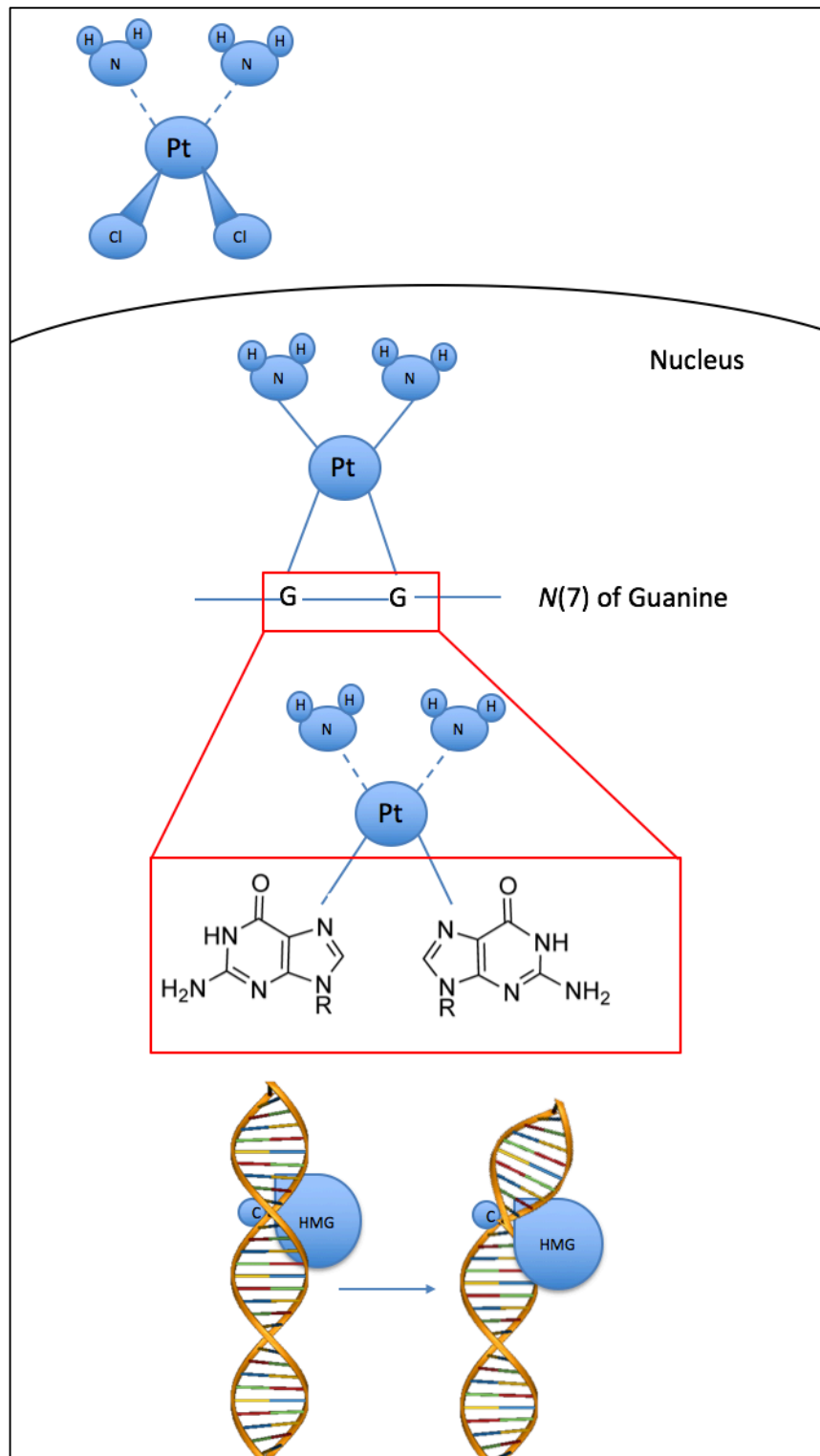


Figure 2.9 Mechanism of action of Cisplatin. The platinum (Pt) charge of cisplatin is stabilised by chloride (Cl) ions, but is more successfully stabilised by nitrogen (N) residues found at the *N7* position of Guanine (G). Binding of cisplatin to the *N7* residues forms adducts and recruits high motility group-containing proteins (HMGs), which causes the de-stacking of the nucleotide bases. This de-stacking cannot be repaired by the cell and damages the DNA such that the apoptotic program is initiated. Adapted from Dasari & Tchounwou, 2014.

Treatment of cells with chemotherapy was carried out by plating EGFP, SIAE and SIAE-S127A expressing clones at 2,500 cells per well in 100 μ L clear media in 96 well plates. Cells were plated in the presence and absence of doxycycline in order to determine if there was a difference in viability between clones expressing and not expressing genes. After 48 of doxycycline treatment, when SIAE expression was confirmed, cells were treated with Cisplatin (Sigma) made fresh in sterile PBS (Sigma) or Etoposide (Sigma) made in dimethylsulphoxide (DMSO; Sigma). Concentrations ranged from 1 μ M to 14 μ M at 1 μ M increases. Untreated cells and vehicle controls were included for each clone in order to determine any changes in viability seen were due to drug treatment. Cells were treated for 24, 48 and 72 hours post-chemotherapy addition. After each time course phase-contrast images were taken to confirm MTS assay results before MTS assays were carried out as previously described in section 2.16. These experiments were carried out three times in triplicate with help from Mrs. Katie Loveson.

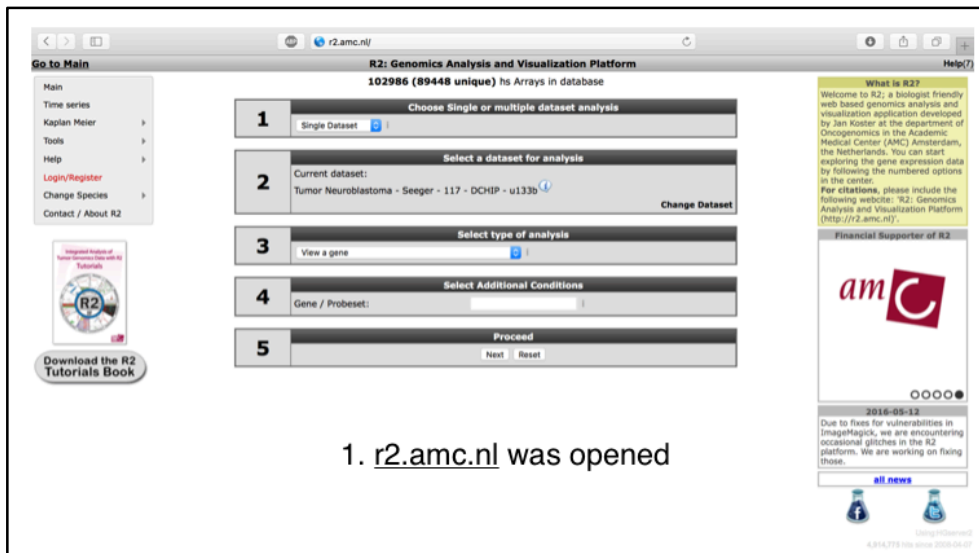
2.21 Molecular Modelling

Molecular modelling was carried out on the SIAE peptide sequence from the protein data bank (PDB; www.rcsb.org). PDB files were generated using homologous structures to the human SIAE peptide using Phyre2 (www.sbg.bio.ic.ac.uk/phyre2). The PDB file was uploaded to MacPyMol, where structural annotation and visualisation was carried out.

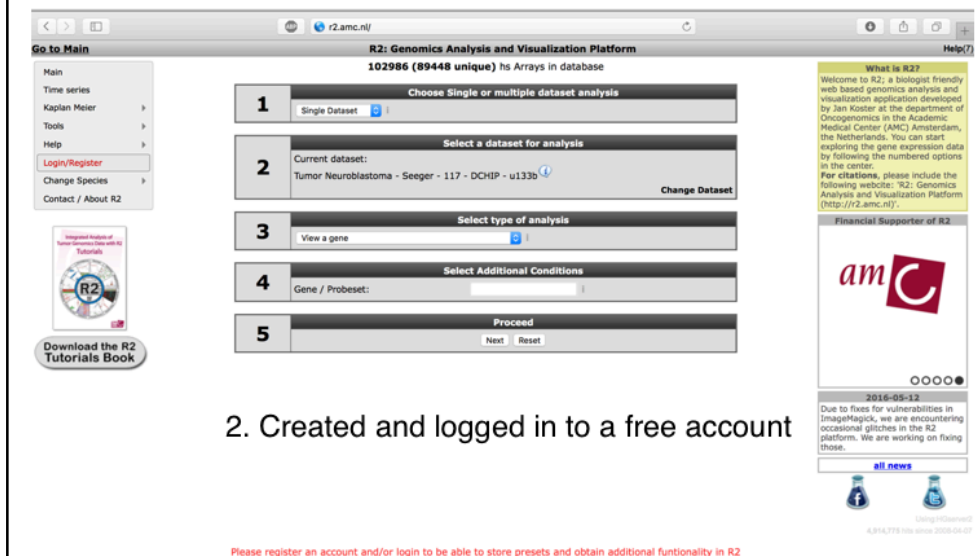
2.22 Bioinformatics

All Bioinformatic analysis was carried out using publically available data sets from the R2 database (r2.amc.nl). This dataset is a public domain for published datasets to be uploaded. It is hosted by the AMC cancer centre, Netherlands. Specific data sets used are annotated

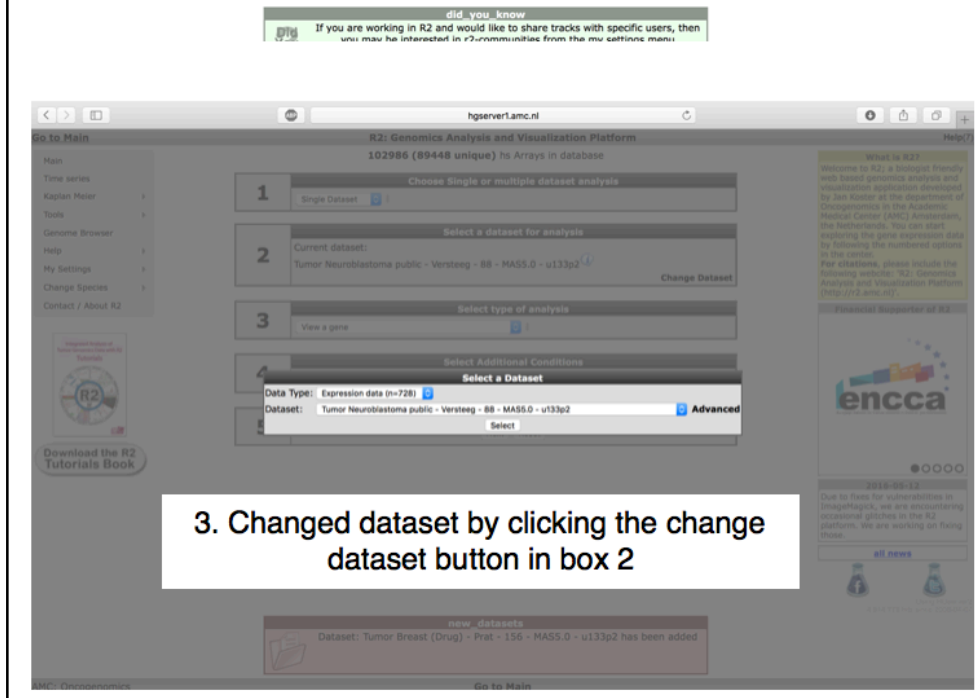
in figures shown in subsequent chapters. A step-by-step guide on how data was obtained from this database is shown in figure 2.10.



1. r2.amc.nl was opened



2. Created and logged in to a free account



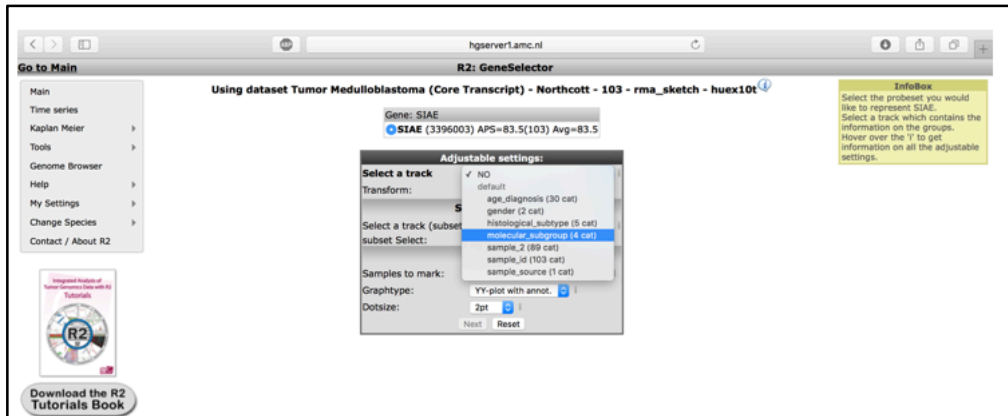
3. Changed dataset by clicking the change dataset button in box 2

The screenshot shows the R2 Genomics Analysis and Visualization Platform interface. A dropdown menu is open, listing various datasets. The selected dataset is 'Tumour medulloblastoma (core transcript- Northcott- 103- rma_sketch- huex10)'. Below the dropdown, a text box contains the text: '4. Selected dataset 'Tumour medulloblastoma (core transcript- Northcott- 103- rma_sketch- huex10)'. The main interface shows a progress bar with four steps. Step 1 is 'Choose Single or multiple dataset analysis'. Step 2 is 'Select a dataset for analysis', with the current dataset listed as 'Tumour Medulloblastoma (Core Transcript) - Northcott - 103 - rma_sketch - huex10'. Step 3 is 'Select type of analysis', with 'View a gene in groups' selected. Step 4 is 'Select Additional Conditions', with 'Gene / Probeset: SIAE' entered. Step 5 is 'Proceed'. A notification box at the bottom indicates 'Dataset: Mixed Ewing Sarcoma - Sevola - 117 - MASS.0 - u133p2 has been added'. The interface also includes a sidebar with navigation options, a 'Download the R2 Tutorials Book' button, and a 'What is R2?' section on the right.

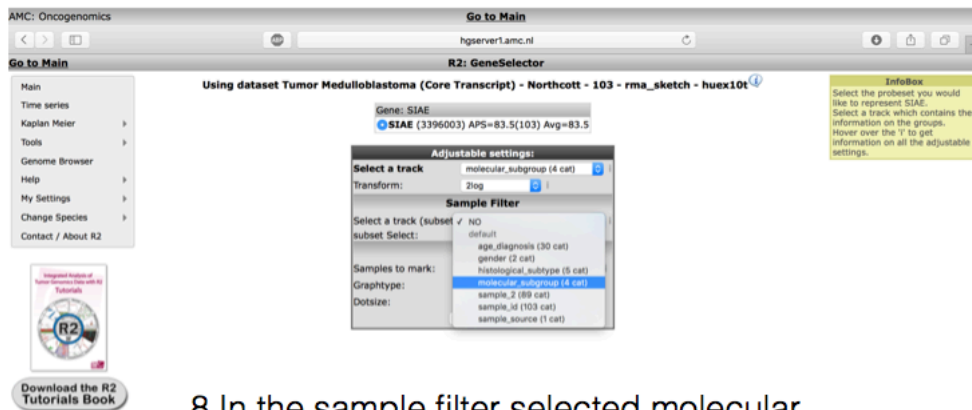
4. Selected dataset 'Tumour medulloblastoma (core transcript- Northcott- 103- rma_sketch- huex10)

5. In box 3 selected 'view a gene in groups' to compare tracks (e.g. molecular subgroups)

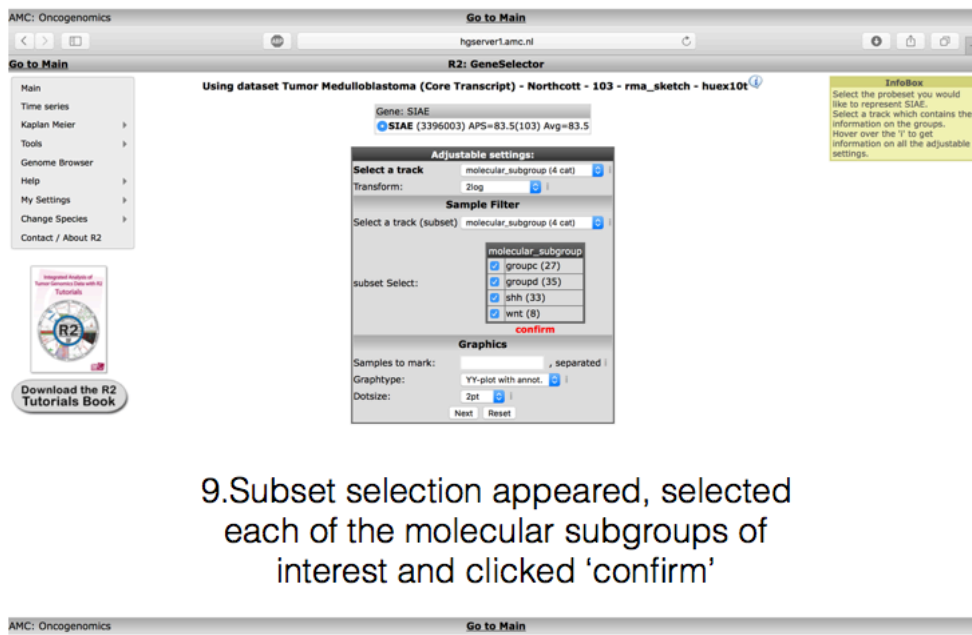
6. In box 4 entered the gene of interest (SIAE) and clicked next



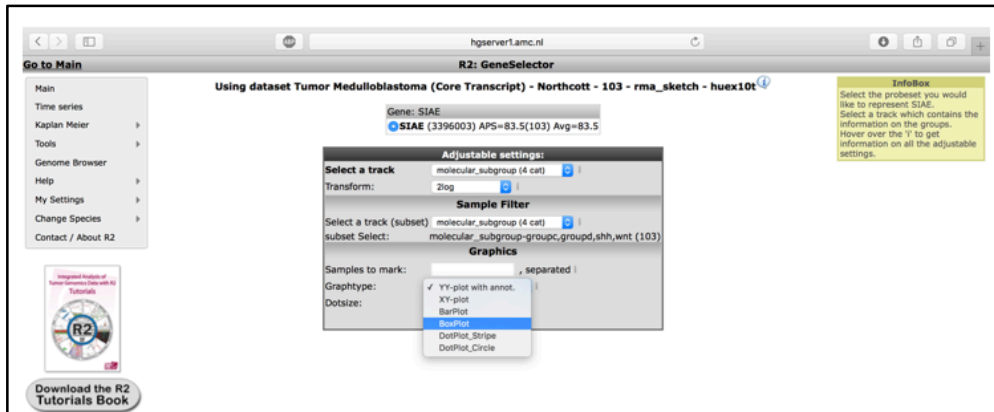
7. On the next screen selected track 'Molecular subgroups' to compare expression of SIAE in each category



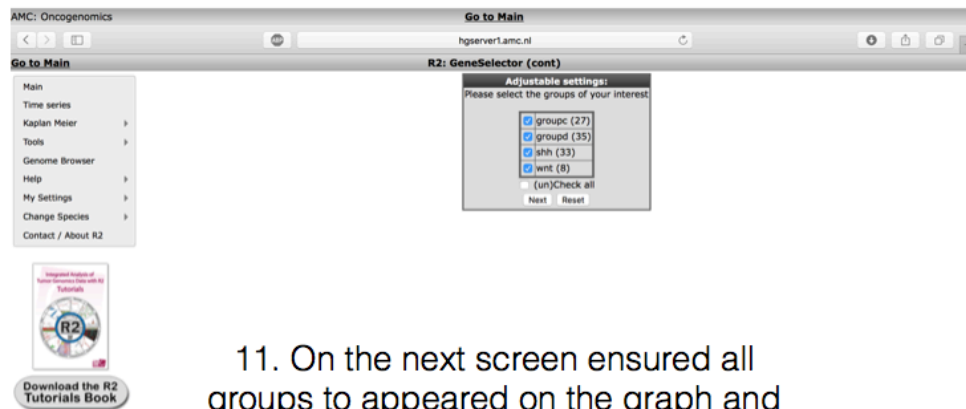
8. In the sample filter selected molecular subgroup



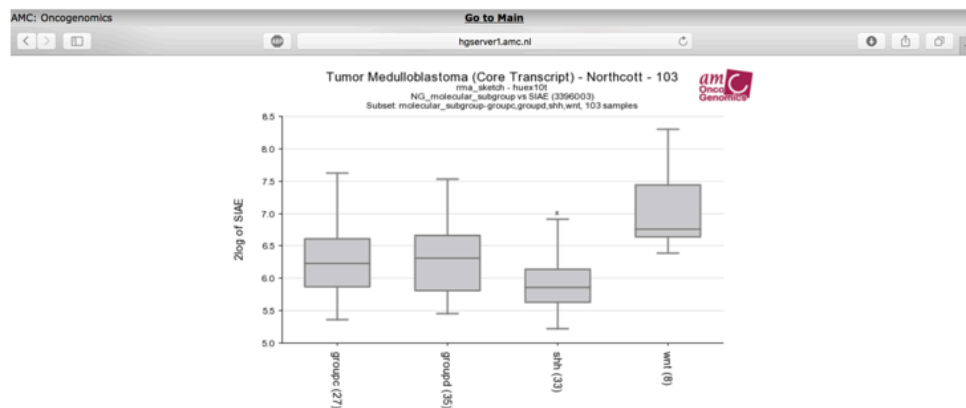
9. Subset selection appeared, selected each of the molecular subgroups of interest and clicked 'confirm'



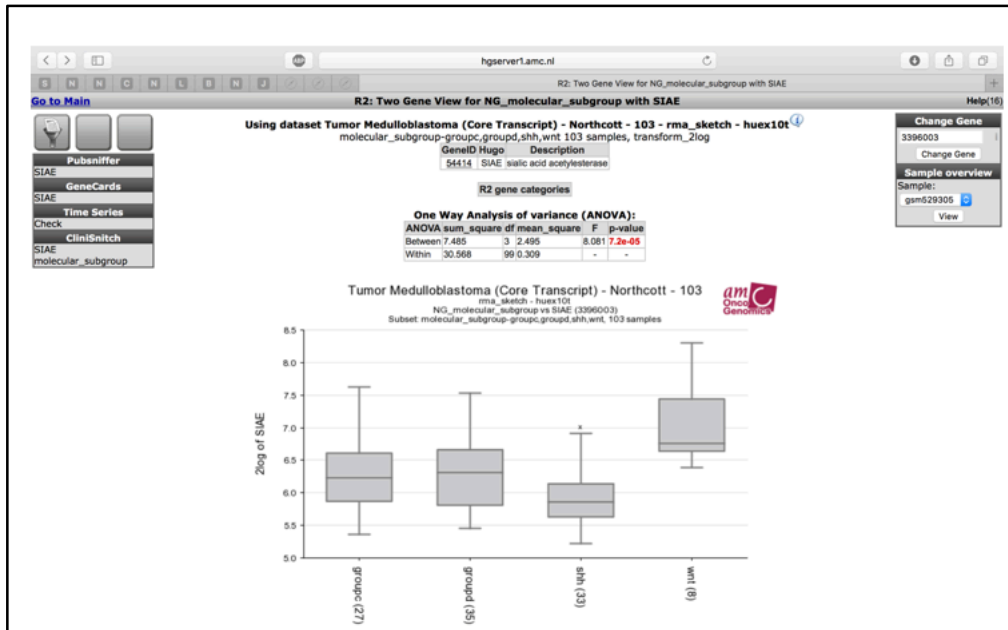
10. Selected the graphic type (box plot)



11. On the next screen ensured all groups to appeared on the graph and clicked next



12. Graphic view - samples were re-arranged and coloured appropriately on this screen



13. Downloaded data select by clicking 'Go to main' in the top left corner

R2: Genomics Analysis and Visualization Platform

102986 (89448 unique) hs Arrays in database

- 1 Choose Single or multiple dataset analysis
- 2 Select a dataset for analysis
- 3 Select type of analysis
- 4 Select Additional Conditions
- 5 Proceed

Download the R2 Tutorial Book

Financial Supporter of R2: Villa Joep!

14. Selected 'tools', 'data grabber'

R2: DataGrabber

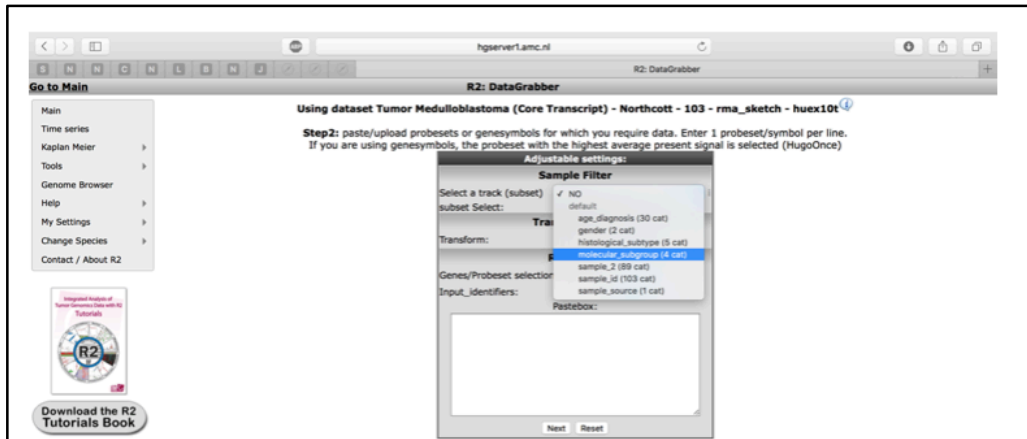
Step1: Select the dataset from which you want to grab data.

Data Type: Expression data (n=728)

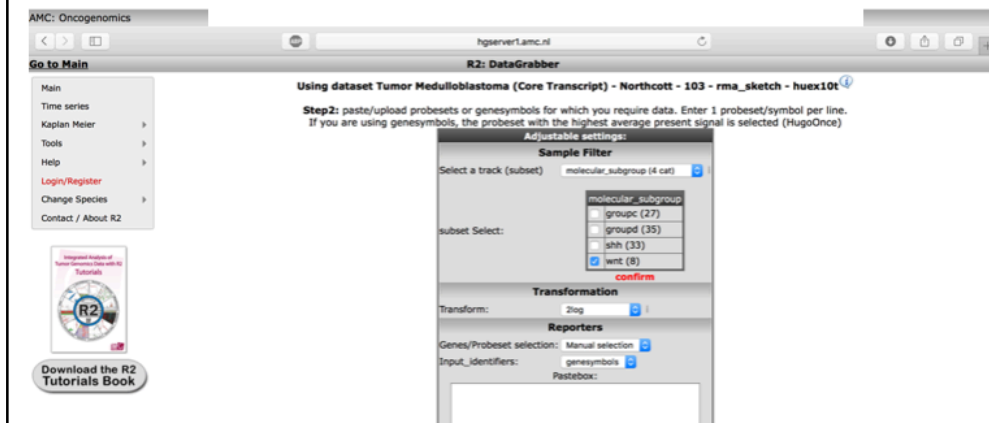
Dataset: Tumor Medulloblastoma (Core Transcript) - Northcott - 103 - rma_sketch - huex10t

Download the R2 Tutorial Book

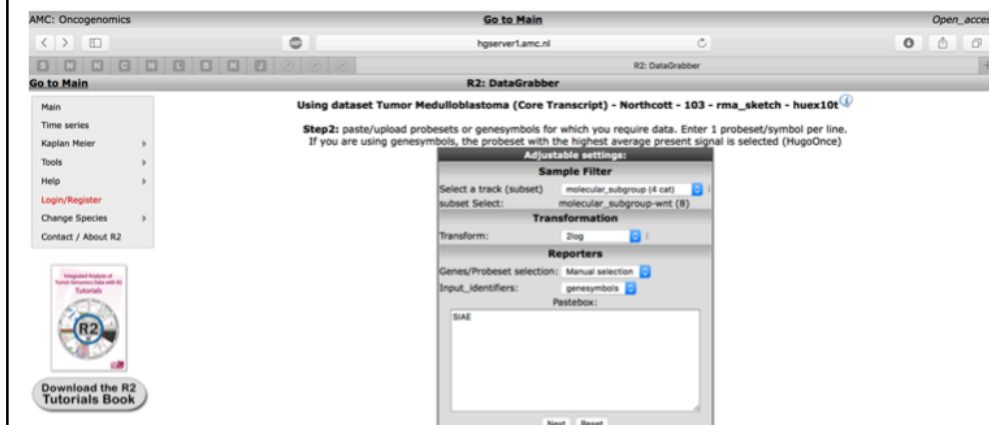
15. Selected dataset



16. Selected track 'molecular subgroup'



17. Selected each molecular subgroup separately in order see data separately for each group



18. Entered gene of interest into the box (SIAE)

The screenshot shows the R2 DataGrabber web interface. The top navigation bar includes 'Go to Main', 'R2: DataGrabber', and 'R2: DataGrabber'. A message states: 'Your data has been stored in the txt file below [datagrabber.txt](#)'. A yellow tooltip on the right says: 'Right click on the "table.txt" link and select "save target as" to store the txt file to your computer.' A sidebar on the left contains a 'Main' menu with options: 'Time series', 'Kaplan Meier', 'Tools', 'Help', 'Login/Register', 'Change Species', and 'Contact / About R2'. Below the menu is a 'Download the R2 Tutorials Book' button. The main content area contains the text: '19. Clicked on the link to open the data file'. At the bottom, a table of data is displayed with columns for probe IDs and SIAE values.

#	hugo	probeset	gsm529312	gsm529323	gsm529338	gsm529340	gsm529341	gsm529366	gsm529368	gsm529378
SIAE	3396003	6.68229237143083	6.39231742277876	6.59544398458948	8.30332412685951	6.83541884047548	6.98641093525204			
	6.69209237542757		7.88386515450979							

20. Log2 (normalised) expression data was shown for SIAE in each WNT subgroup sample after the name of the probe. This data was then analysed

Figure 2.10 Step-by-step method for data acquisition from the R2 database using SIAE expression from the Northcott database as an example. Steps 1-20 demonstrate data visualisation as a box-plot graphic and acquisition of log2 normalised data for statistical analysis.

2.23 Statistics

All statistical analyses were carried out using GraphPad Prism 6.0 software. Appropriate statistical tests are annotated in figures shown in subsequent chapters.

3 Results

3.1 Introduction

Medulloblastoma, the most common malignant childhood brain tumour, occurs predominantly in the cerebellum and is associated with poor quality of life in survivors due to the aggressive nature of treatment (Michiels et al. 1996). Four molecular subgroups of medulloblastoma have been identified and have different molecular and clinical features, including varying prognoses (Taylor et al. 2012). Patients who have lower-risk disease or fall into the better prognosis subgroups are considered as having been over-treated at the expense of their quality of life. Other patients who have high-risk disease or fall into the poorer prognosis subgroups may need more tailored therapy to improve their survival (Gilbertson 2004). The refining of treatments for each subgroup is just beginning to emerge as we learn more about this disease. Medulloblastoma is a tumour of development and therefore our work focuses on a pathway that functions in the development of the cerebellum (Wechsler-Reya & Scott 2001a; Svennerholm et al. 1991; Miyakoshi et al. 2001). The GD3 acetylation pathway is known to have roles in brain development (Liang et al. 2011; Yu et al. 2004) and in malignancies such as high grade gliomas (Birks et al. 2011). GD3, a simple ganglioside, is expressed by the granule neuron precursor cells of the developing cerebellum where it guides their migration (Goldman & Reynolds 1996). In rats it has been shown that upon maturation of the brain, GD3 rapidly accumulates within the supernumary cells where it causes their mitochondrially-mediated apoptosis (Birks et al. 2011; Higgins et al. 2015; Ogiso et al. 1991). After birth, the expression of GD3 is virtually absent (Yu et al. 2012; Yu et al. 2004). In some cancers of neural crest origin, such as high grade gliomas (Birks et al. 2011), melanomas (Ohkawa et al. 2008), and as we show here, in medulloblastomas, GD3 also becomes re-expressed. In acute lymphoblastic leukaemia

(ALL) high levels of GD3 have been shown to protect from a pro-apoptotic phenotype, due to acetylation of GD3 to GD3^A. GD3^A is thought to protect cells from GD3-mediated apoptosis and this balance of GD3 and GD3^A is thought to influence cell survival (Mandal et al. 2012; Mukherjee et al. 2008). In this study we analysed publically available data sets to conduct bioinformatic analysis of the enzymes involved in the GD3 acetylation pathway. We also investigated the expression of GD3 and GD3^A by three medulloblastoma cell lines. As a proof of principle we determined if the GD3 acetylation pathway could be a potential therapeutic target for paediatric medulloblastoma by over-expressing the human enzyme responsible for deacetylation of endogenous sialate-*O*-acetyl esterase enzyme (SIAE). As GD3^A expression plays a role in protecting cells from GD3-mediated apoptosis, we predicted that SIAE would be expressed in high levels in medulloblastoma subgroups with the poorest prognosis. SIAE cleaves acetyl groups from the carbon 9 position of SIAE, such as those found in GD3^A. We believe that by deacetylating GD3^A, medulloblastoma cells would be more susceptible to chemotherapeutics, thereby lessening the devastating side-effects as a result of toxicity.

3.2 Bioinformatic characterisation of the GD3 acetylation pathway

In order to determine if the GD3 acetylation pathway was abnormally expressed in medulloblastoma, the major components were characterised using a bioinformatics approach. The major components of the pathway are shown in figure 3.1.

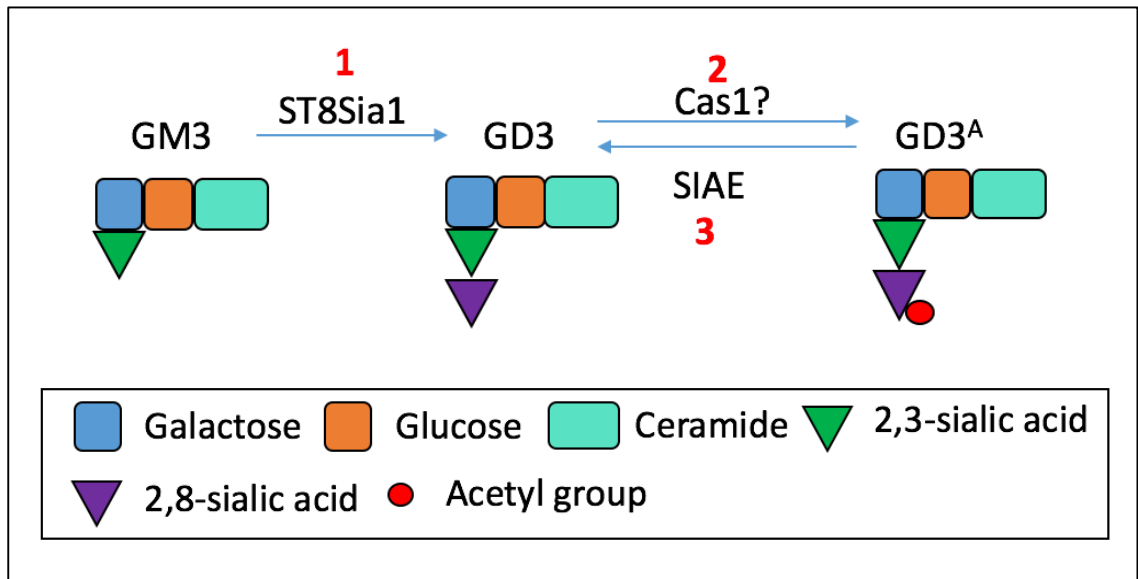


Figure 3.1 The major components of the GD3 acetylation pathway. GD3 is synthesised from its precursor ganglioside GM3 by the enzyme ST8Sia1. The ST8Sia1 enzyme adds a second sialic acid residue to GM3 via a 2,8-glycosidic bond, forming GD3 (reaction 1). GD3 can be acetylated to 9-*O*-acetyl GD3 (GD3^A), which is hypothesised to be due to the action of Cas1 (Cas1 domain containing 1). Cas1 transfers acetyl groups from the donor acetyl CoA to form 7-*O*-acetyl GD3. The 7-*O*-acetyl GD3 has been shown to be converted to 9-*O*-acetyl GD3 by non-enzymatic and enzymatic means (reaction 2). 9-*O*-acetyl GD3 can be converted back to GD3 by the human endogenous deacetylation enzyme SIAE (Sialic acid *O*-acetyl esterase). SIAE cleaves the acetyl group from GD3^A at this position restoring levels of GD3 in the cell (reaction 3). Adapted from Yu et al. 2004.

A publicly available genome-wide transcriptional analysis of 103 sub-grouped medulloblastoma patients that included non-neoplastic foetal and adult brain controls was analysed with help from Dr L. Donovan (Personal communication, March 2012).

The medulloblastoma samples used for the bioinformatics analysis were obtained from the R2 database (r2.amc.nl). Tissue samples were derived from patients whose ages ranged from 11 months to 39 years, which encompasses infant, child and adult patients. Patients who are infants are defined as 0-3 years of age; child patients as 3-16 years of age and adult patients as over the age of 16, as defined by Taylor et al. 2012. Using these criteria, the sample set was comprised of 15 infant patients, 73 children and 14 adults (and 1 case of unknown age at diagnosis). Of these patients, 35 had group 4 tumours, followed by 33 patients with SHH subgroup tumours, 27 patients with group 3 tumours and finally 8 patients with WNT subgroup tumours. The distribution of subgroups was similar to the incidence seen in the clinic (Northcott, Korshunov, et al. 2012).

3.2.1 Regulators of the GD3 acetylation pathway are atypically expressed in medulloblastoma tissue at the mRNA level

GD3 synthase, also known as ST8Sia1, is the enzyme responsible for synthesis of GD3 from its precursor GM3. ST8Sia1 mRNA was found to be significantly down-regulated in medulloblastoma tissue compared to non-neoplastic foetal and adult brain ($p < 0.0001$) (figure 3.2A).

Cas1 is the enzyme hypothesised to catalyse the acetylation of GD3 to GD3^A (reaction 2; figure 3.1). High levels of acetylation to GD3^A requires a high level of expression of the acetylation enzyme. The expression of Cas1 was shown to be significantly up-regulated in medulloblastoma samples compared to foetal and adult non-neoplastic brain ($p < 0.0001$)

(figure 3.2B) which may indicate that the balance of GD3 to GD3^A is in favour of GD3^A. This however must be taken into consideration along with the deacetylation enzyme SIAE (Mukherjee et al. 2008; Mandal et al. 2012), SIAE cleaves the acetyl groups from sialic acid residues at the carbon 4 and carbon 9 positions, such as those found in GD3^A (Orizio et al. 2015). SIAE catalyses reaction 3 (figure 3.1) and was predicted to be of low expression compared to adult non-neoplastic brain where GD3^A expression is known to be low. The expression of SIAE was significantly down-regulated compared to non-neoplastic foetal and adult brain samples ($p < 0.0001$) (figure 3.2C).

Taken together these data suggest that at the mRNA level the expression of GD3 may be low in these samples due to the lower than expected ST8Sia1 expression, but any GD3 that is produced is likely to be acetylated to GD3^A. The expression of these enzymes in relation to the GD3 acetylation pathway is shown in figure 3.2D.

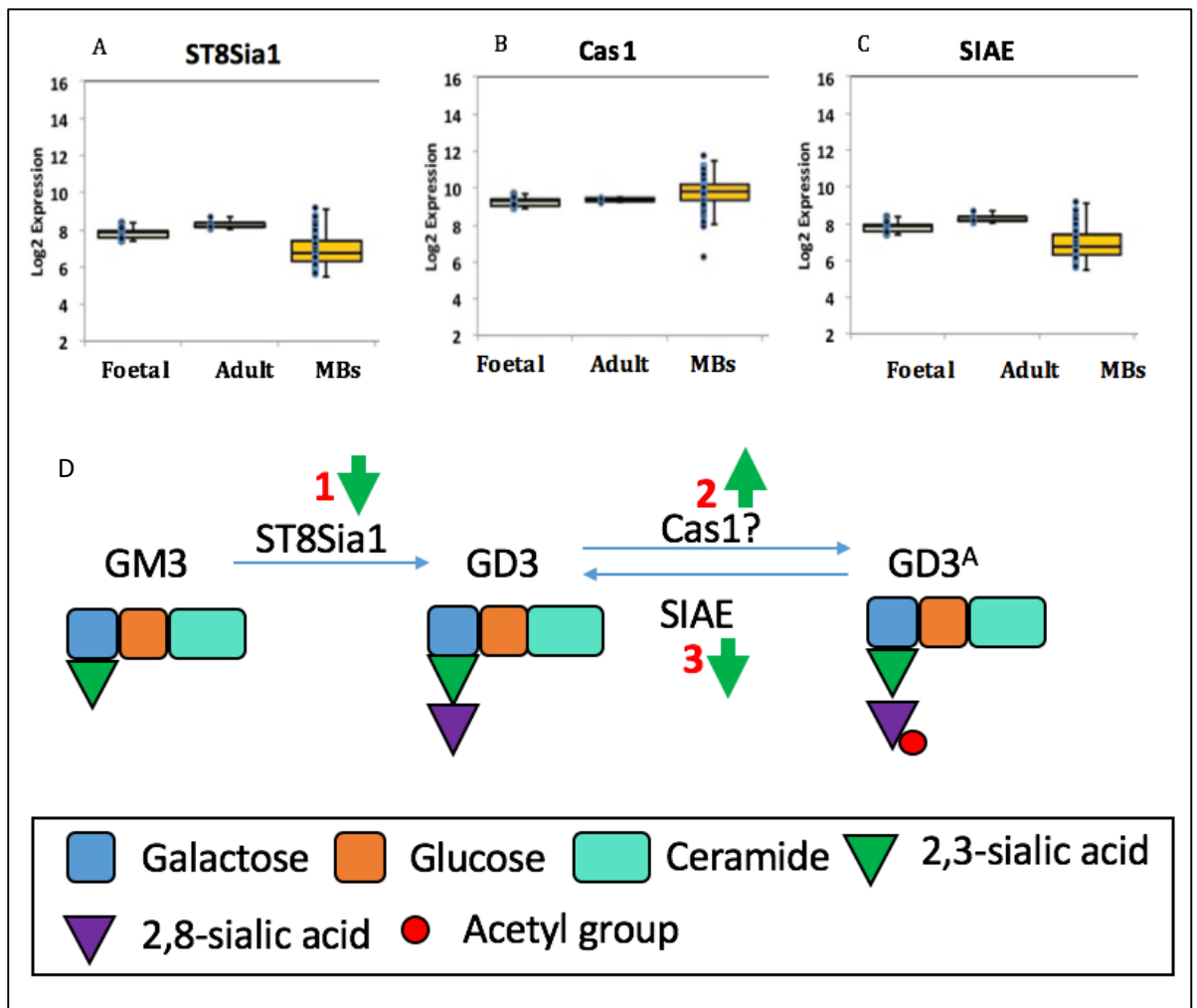


Figure 3.2 Expression of GD3 pathway components at the mRNA level as determined using a bioinformatics approach. (A) ST8Sia1 mRNA encoding the enzyme that converts GM3 to GD3, was found to be significantly down-regulated in medulloblastoma samples compared to non-neoplastic foetal and adult brain samples ($p < 0.0001$). (B) Cas1 mRNA encoding the hypothesised acetylation enzyme of GD3 was found to be significantly up-regulated in medulloblastoma samples compared to non-neoplastic foetal and adult brain samples ($p < 0.0001$). (C) SIAE mRNA encoding the acetyl esterase enzyme of GD3 was found to be significantly down-regulated compared to non-neoplastic foetal and adult brain samples ($p < 0.0001$). (D) **The major components of the GD3 acetylation pathway and their regulation as determined by bioinformatics analysis.** ST8Sia1 enzyme which adds a second sialic acid residue to GM3 via a 2,8-glycosidic bond, forming GD3 was found to be significantly down-regulated in medulloblastoma (reaction 1; green arrow). Cas1, the acetyl transferase hypothesised to acetylate GD3 to GD3^A was found to be significantly up-regulated in medulloblastoma (reaction 2; green arrow). SIAE (Sialic acid O-acetyl esterase) the enzyme which cleaves the acetyl group from GD3^A was found to be significantly down-regulated in medulloblastoma (reaction 3; green arrow). Data obtained from the R2 database using the Northcott (core Transcript) data set. The micro-array chip used for this data set was huex10t, and was normalised using the rma-sketch scheme. Data was analysed by one-way analysis of variance (ANOVA) followed by Tukey's multiple comparisons post hoc test using graph pad prism 6 software. $n = 103 \pm \text{SEM}$

3.2.1.1 Expression of the GD3 acetylation pathway regulators varies according to molecular subgroup

Further to the examination of medulloblastoma patient samples, the relevance to each of the molecular subgroups was then explored using a similar bioinformatics approach. Northcott (core transcript) data from the R2 database had been divided into subgroups using nano-string technology before uploading to the database. Data was mined from the database for this study. The medulloblastoma samples used were the same 103 as those described previously. Each gene of interest was selected from the database and the data used to determine if there were any statistically significant log-fold differences in mRNA expression of the regulators of the GD3 and GD3^A pathway between subgroups of medulloblastoma.

ST8Sia1 mRNA was lowest in the WNT subgroup compared to the highest level of expression seen in the SHH subgroup (figure 3.4A). The WNT subgroup expressed the lowest amount of ST8Sia1 mRNA, but this was not statistically different to groups 3 and 4 ($P > 0.05$; figure 3.4A). The SHH subgroup expressed the highest levels of ST8Sia1 mRNA in this sample set and was significantly higher than WNT, group 3 and group 4 expression ($p < 0.0001$; figure 3.4A). This data shows that the expression of ST8Sia1 in group 3 samples was similar to that of WNT tumours.

As we found expression of ST8Sia1 to be surprisingly down-regulated in our original analysis compared to non-neoplastic foetal and adult brain samples, we considered other enzymes that can affect the expression of GD3. As the expression of GD3 synthase does not define the expression level of GD3, the expression of the enzymes that use GD3 as a substrate were also considered. A publication by Yu in 2004 states that the expression of a ganglioside

is not only dependent on the expression of the synthesis enzyme, but also of the enzyme that uses the ganglioside as a substrate this concept is further explained in figure 3.3 (Yu et al. 2004). ST8Sia5, the enzyme that converts GD3 to GT3 and GD2 (reaction 4; figure 3.6) was therefore considered. This catalytic step is shown as part of the GD3 acetylation pathway in figure 3.3. ST8Sia5 is a more promiscuous enzyme and can convert GD3 into GT3 by the addition of a sialic acid residue, or it can convert GD3 to GD2 through the addition of *N*-acetylgalactosamine (reaction 4; figure 3.6). This process is also demonstrated in figure 1.5.

The mRNA expression of ST8Sia5 was found to be significantly higher in the WNT subgroup compared to group 3 ($p < 0.0001$) and group 4 ($p < 0.001$) (figure 3.4B). These data suggest that the expression of GD3 is more likely to be further converted to GT3 and GD2 in the WNT subgroup and GD3 is less likely to accumulate. This is because the enzyme which converts GD3 to GD2 and GT3 is expressed at a higher level allowing the ganglioside to be further modified into the more complex gangliosides. The SHH subgroup also expressed significantly more ST8Sia5 compared to group 3 and group 4 subgroups ($p < 0.0001$) also suggesting that in the SHH subgroup there may be further conversion of GD3 rather than accumulation of the ganglioside. Furthermore, there were no significant differences between ST8Sia5 mRNA expression in WNT and SHH subgroups ($p > 0.05$), nor were there any significant differences between expression in group 3 compared to group 4 ($p < 0.05$).

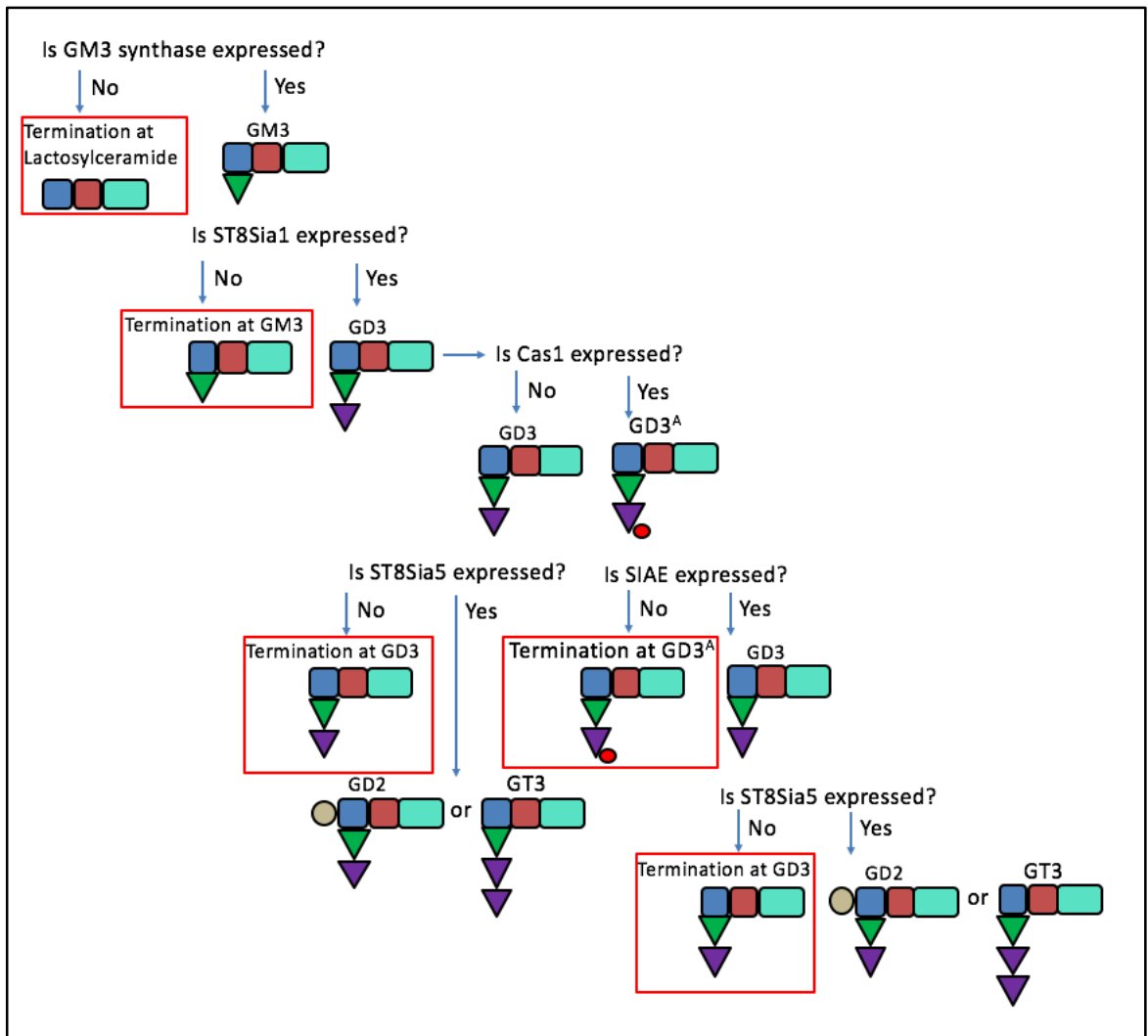


Figure 3.3 The concept of ganglioside biosynthesis as demonstrated by Yu in 2004. The gangliosides follow pathways of synthesis that are controlled by the expression (and activity) of the sialyltransferases. The termination of the biosynthesis pathway and the resulting ganglioside is shown in red boxes. Adapted from Yu et al. 2004.

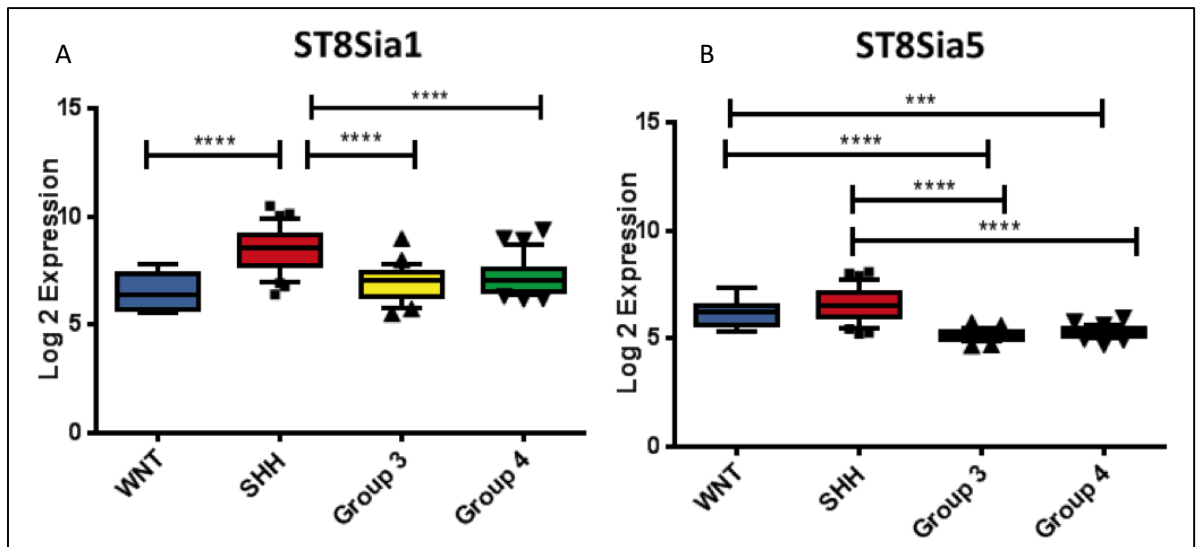


Figure 3.4 ST8Sia1 and ST8Sia5 expression varies with molecular subgroup of medulloblastoma. ST8Sia1 mRNA expression was analysed using the Northcott (core transcript) data set from the R2 database. In 103 subgrouped samples, the expression of the mRNA encoding ST8Sia1 showed highest expression in the SHH subgroup compared to WNT, group 3 and group 4 samples. (B) ST8Sia5 mRNA expression was also analysed using the same dataset and shows that there are significant differences in expression between the less aggressive subgroups WNT and SHH which demonstrated higher expression compared to the more aggressive subgroups group 3 and group 4 which demonstrates lower expression. Data analysed by one-way ANOVA using GraphPad Prism 6 software (** $p < 0.001$; **** $p < 0.0001$). Data obtained from the R2 database using the Northcott (core Transcript) data set. Data was analysed by one-way analysis of variance (ANOVA) followed by Tukey's multiple comparisons post hoc test using graph pad prism 6 software. $n = 103 \pm \text{SEM}$

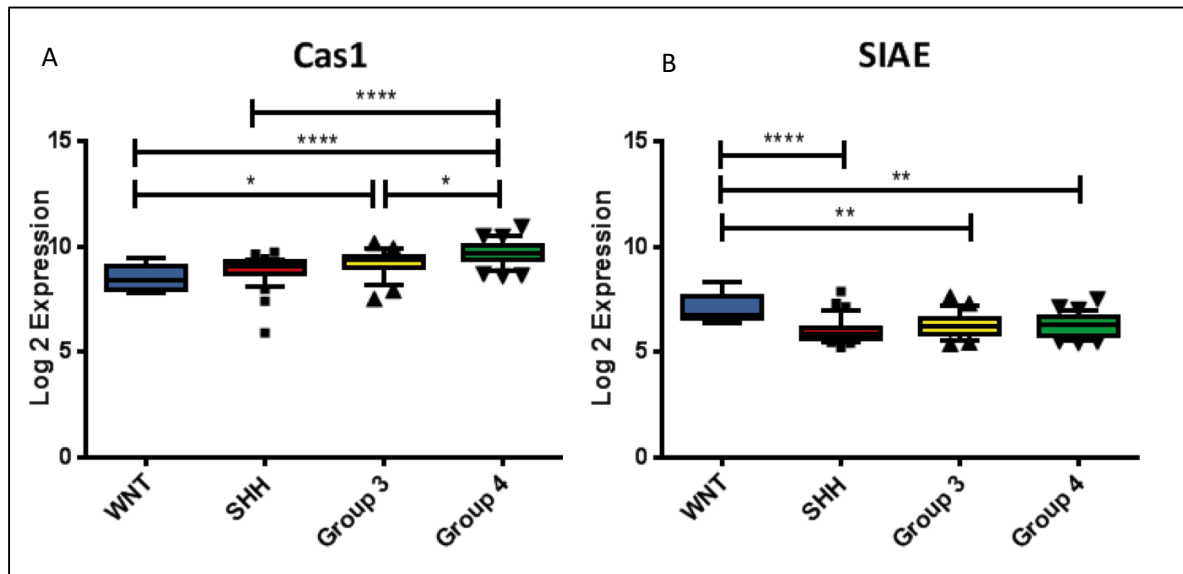


Figure 3.5 mRNA expression of the acetylation and deacetylation regulating enzymes of GD3 in medulloblastoma tissue. (A) Cas1 the hypothesised acetylation enzyme of GD3 was characterised in subgrouped samples and shows highest expression in group 4 disease and the lowest expression is seen in the WNT and SHH subgroup samples. (B) The level of SIAE mRNA (the human endogenous deacetylation enzyme of GD3^A) was also characterised in subgrouped medulloblastoma samples at the mRNA level. The expression of SIAE was highest in the WNT subgroup compared to all other subgroups. Data obtained from the R2 database using the Northcott (core Transcript) data set. Data was analysed by one-way analysis of variance (ANOVA) followed by Tukey's multiple comparisons post hoc test using graph pad prism 6 software. (* p<0.05; ** p<0.01; ** p<0.0001). n=103± SEM**

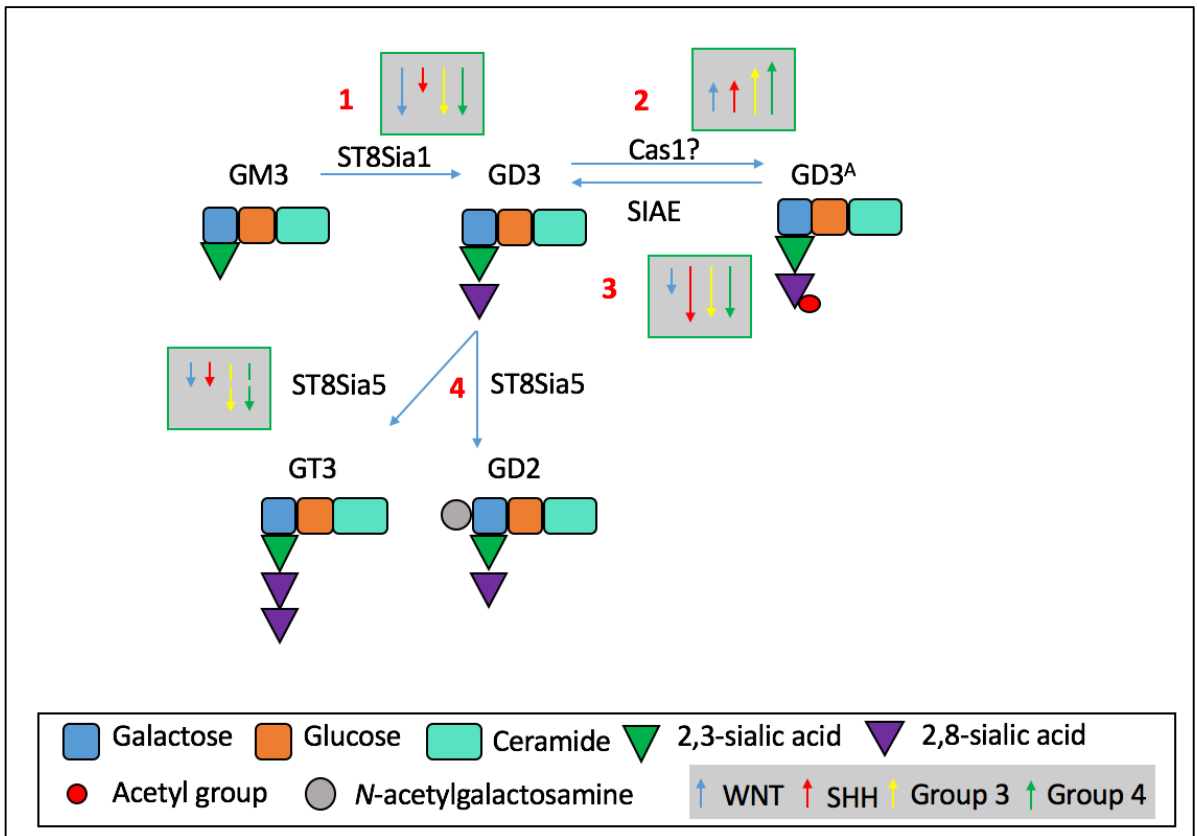


Figure 3.6 A summary of the mRNA expression of the regulating enzymes of the GD3 acetylation pathway by molecular subgroup. The expression of GD3 is determined by ST8Sia1, the enzyme which converts GM3 to GD3, and the enzyme that uses GD3 as a substrate, ST8Sia5 (reaction 4). ST8Sia1 expression was found to be low (green box; reaction 1) and we confirmed similar expression in each subgroup except SHH disease which expressed the highest level of ST8Sia1 mRNA. We also confirmed lowest expression of ST8Sia5 in groups 3 and 4, the more aggressive disease subgroups (green box, reaction 4). We could not however determine if the expression was up or down-regulated with respect to non-neoplastic brain tissue as this data was not available (dotted arrows represent unknown relationship to non-neoplastic brain controls) and we therefore cannot conclude that mRNA levels of ST8Sia5 are down-regulated in medulloblastoma samples. We also confirmed higher expression of Cas1, the hypothesised acetylation enzyme of GD3 in group 3 and group 4 disease compared to WNT and SHH samples, suggesting that there may be higher levels of GD3^A expression in these subgroups (green box; reaction 2). In agreement with this, the mRNA levels of SIAE (the deacetylation enzyme of GD3^A) show low levels of SIAE mRNA in group 3 and group 4 disease, and in this case in SHH disease as well, suggesting that GD3^A may be expressed in higher levels in these subgroups. Data obtained from the R2 database using the Northcott (core Transcript) data set.

In order to determine if the regulation of GD3 acetylation was atypically expressed we characterised the acetylation and deacetylation enzymes Cas1 and SIAE (figure 3.5). We found the mRNA expression of Cas1 to be significantly up-regulated in medulloblastoma compared to non-neoplastic foetal and adult brain controls we further explored this to see if this enzyme had a different expression level between medulloblastoma subgroups. Cas1 expression (if this is indeed the enzyme that is responsible for GD3 acetylation to GD3^A) should therefore correlate with GD3^A expression.

From this study the expression of Cas1 mRNA was shown to be lowest in WNT and SHH subgroups (figure 3.5A). Expression of Cas1 mRNA was significantly lower in the WNT subgroup compared to group 3 ($p < 0.05$) and group 4 ($p < 0.001$). SHH subgroup tumours expressed significantly less Cas1 mRNA than group 4 tumour samples ($p < 0.0001$) but not group 3 ($p > 0.05$), indicating a similar level of Cas1 mRNA expression in these subgroups. Group 4 subgrouped samples expressed the highest level of Cas1 mRNA, which was also significantly higher than group 3 ($p < 0.05$).

As the highest levels of expression of Cas1 were seen in groups 3 and 4, this suggests that there may be the highest levels of GD3^A in these subgroups, if Cas1 is the enzyme responsible for acetylation of GD3, supporting our hypothesis that the balance of GD3 to GD3^A in these cells is in favour of GD3^A.

In figure 3.2, our bioinformatics analysis showed that the mRNA expression of SIAE is up-regulated in medulloblastoma samples compared to non-neoplastic foetal and adult brain controls. We therefore further analysed the mRNA expression of SIAE by molecular subgroup in order to determine if the expression of SIAE (and therefore GD3) correlates with subgroup. In this data set the highest expression of SIAE mRNA was found in the WNT subgroup (figure 3.5B). The WNT subgroup which expressed SIAE mRNA significantly more than SHH ($p < 0.0001$), group 3 ($p < 0.02$) and group 4 subgroups ($p < 0.0001$). There were no significant differences found between any other subgroup demonstrating that the expression of SIAE mRNA was similar between SHH, group 3 and group 4.

3.2.2 Characterisation of GD3 acetylation pathway regulators by metastatic stage of medulloblastoma

At diagnosis, patients with medulloblastoma are typically grouped according to the Chang's staging system (Chang et al. 1969), in order for this classification to be applied to a patient magnetic resonance imaging (MRI) and a lumbar puncture (LP) are carried out (Phi et al. 2011). Using MRI scans tumour mass location can be determined. Using cerebral spinal fluid (CSF) obtained from LP, it can be determined if tumour cells are present. Using Chang's M staging system, the expression of each of the known GD3 acetylation pathway regulators was examined according to metastatic stage (Gilbertson 2004). Chang's M staging is outlined in table 3.1. We predicted, based on our hypothesis, that the most aggressive and metastatic medulloblastomas would have deregulated GD3 pathway enzymes which would be regulated in favour of GD3^A synthesis.

Table 3.1 Chang's M stage classification of medulloblastoma patients modified from Chang et al. 1969.

M stage	
M0	No gross subarachnoid or haematogenous metastasis.
M1	Tumour cells found in cerebral spinal fluid on microscopic analysis.
M2	Gross nodular seeding in the cerebellum, cerebral subarachnoid space, or in third or fourth ventricles.
M3	Gross nodular seeding in spinal arachnoid space.
M4	Extraneural metastasis.

For this study, publically available data was mined from the R2 database using the Heidelberg data set, this microarray was carried out on a custom chip set and normalised using the 4hm44k scheme. 64 patient samples were analysed. Age information was unfortunately not available for this data set. Of the patients analysed 45 were classified as having M₀ disease, 5 patients were classified as having M₁ disease, 4 patients were classified as having M₂ disease and the remaining 9 patients were classified as M₃. No patients in this cohort had extraneural metastasis (M₄ disease).

ST8Sia1 which synthesises GD3 from GM3 (reaction 1; figure 3.1). ST8Sia1 was down-regulated as shown by negative transformed log-fold values (figure 3.7A). The expression of ST8Sia1 appeared to be correlated with metastatic stage from M₁ to M₃, however the highest level of expression seen in M₀. There was however no significant difference between metastatic stages (figure 3.7A).

ST8Sia5, the enzyme that uses GD3 as a substrate for conversion to GT3 or GD2 was significantly higher in M₀ disease compared to M₃ ($p < 0.05$), showing that expression of this mRNA decreases with increasing M stage (figure 3.7B).

Cas1 is the enzyme that is hypothesised to acetylate GD3 to GD3^A. The expression of Cas1 at the mRNA level is shown to increase with increasing M stage (figure 3.8A). The expression of Cas1 is significantly higher in the M₃ stage compared to M₀ ($p < 0.05$). The expression of SIAE, the deacetylation enzyme of GD3^A, is decreased at the mRNA level with increasing M stage and is shown to be lowest in M₃ disease compared to M₀ and M₁ ($p < 0.05$; figure 3.8B). SIAE and Cas1 mRNA expression appear to inversely correlate, particularly in M₃ disease.

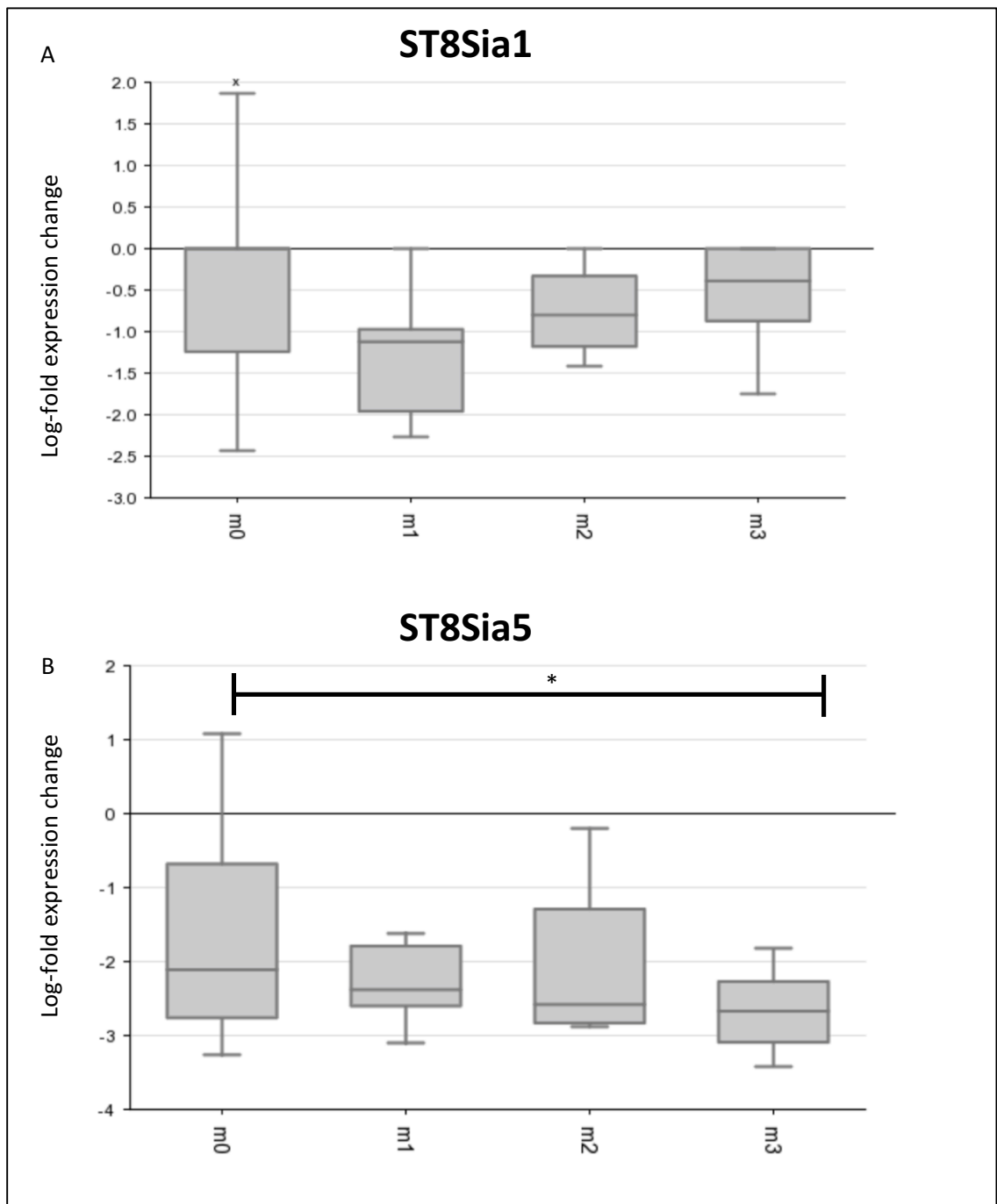


Figure 3.7 mRNA levels of ST8Sia1 and ST8Sia5 according to metastatic stage. Expression of ST8Sia1, the enzyme that synthesises GD3 from GM3, was similar between all metastatic stages as there was not significant difference in expression between any metastatic stage. (B) mRNA expression of ST8Sia5 appears to be correlated with metastatic stage of disease. There is a general trend that with increasing metastatic stage there is a lower expression of ST8Sia5 mRNA. There was statistically however only significantly less mRNA expressed in M₃ samples compared to M₀. Data obtained from the R2 database using the Heidelberg data set. Data was analysed by one-way analysis of variance (ANOVA) followed by Tukey's multiple comparisons post-hoc test using graph pad prism 6 software. (* p<0.05). n=64 ± SEM

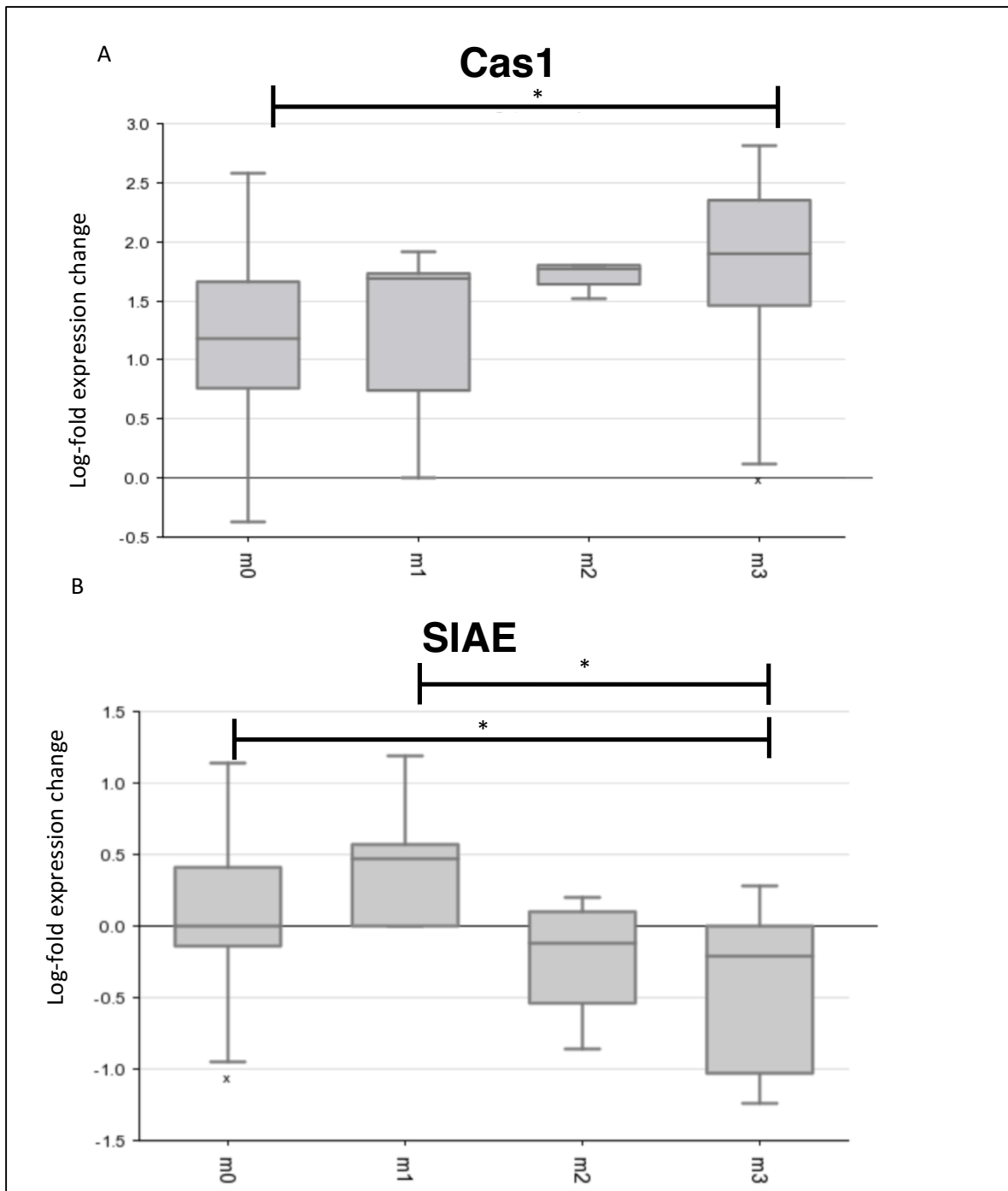


Figure 3.8 mRNA expression of Cas1 and SIAE according to Metastatic stage. (A) Analysis of Cas1 mRNA, the hypothesised acetylation enzyme of GD3^A, showed that expression correlated with metastatic stage as the higher the expression of Cas1 mRNA, the higher the metastatic stage. However, the only significantly different metastatic stages were M₀ and M₃ where M₃ expression was significantly higher than M₀. (B) mRNA expression of SIAE, the deacetylation enzyme of GD3^A, was highest in M₁ disease. The mRNA expression of SIAE was significantly lower in M₃ disease compared to M₁ and M₂. Data obtained from the R2 database using the Heidelberg data set. Data was analysed by one-way analysis of variance (ANOVA) followed by Tukey's multiple comparisons post hoc test using graph pad prism 6 software. (* p<0.05). n=64 ± SEM

3.2.3 Summary

Although the expression of the regulating enzymes of this pathway requires further investigation at the protein level, studies using publicly available mRNA expression data shed some light on the regulation of these enzymes in medulloblastoma.

The bioinformatics data supports the idea that the GD3 acetylation pathway is atypically expressed in medulloblastoma tissue.

The expression of ST8Sia1 is significantly down-regulated at the mRNA level in this study ($p < 0.001$), but is not the only enzyme involved in GD3 synthesis so may not correlate with the expression of GD3 when analysed alone. Cas1 is significantly up-regulated in the medulloblastoma samples in this dataset ($p < 0.001$) and inversely correlates with SIAE expression which may indicate that the balance of GD3 to GD3^A is in favour of GD3^A in these tumour samples.

When the medulloblastoma data set was analysed with respect to molecular subgroup the expression of ST8Sia1 was seen to be highest in the SHH subgroup which was significantly higher than WNT, group 3 and group 4 ($p < 0.0001$). This prompted us to explore the mRNA expression of ST8Sia5 to determine if GD3 was being used as a substrate to generate the more complex gangliosides in these cells. ST8Sia5 expression was found to be significantly higher in the WNT subgroup compared to group 3 ($p < 0.0001$) and group 4 ($p < 0.001$) suggesting that the more aggressive subgroups would be more likely to have higher levels of GD3. This was also the case for the SHH subgroup which expressed significantly more ST8Sia5 mRNA than group 3 and group 4 samples ($p < 0.0001$). Taken together, the concomitant low expression of ST8Sia1 and ST8Sia5 suggest that in the better prognosis

subgroups (WNT and SHH), the GD3 synthesised could be further converted to complex gangliosides than group 3 and group 4 tumours, however this would need further exploration to confirm this hypothesis.

In terms of medulloblastoma subgroups, data also show the highest level of Cas1 and lowest expression of SIAE are found in group 3 and group 4 medulloblastomas. This is supportive of the hypothesis that the balance of GD3 to GD3^A is in favour of GD3^A, particularly in the more aggressive subgroups of disease. When this data was examined in relation to metastatic stage the prediction that with increasing M stage GD3 and GD3^A expression would increase, in favour of GD3^A was also supported.

The bioinformatics data show that ST8Sia1 expression was generally correlated with increasing M stage (although highest in M₀ disease) but expression was not significantly different between the stages. ST8Sia5 expression was also examined and was decreased with increasing M stage, the expression of ST8Sia5 was found to be lowest in M₃ disease compared to M₀ (p<0.05). The expression of Cas1 and SIAE were found to be inversely correlated, particularly in M₃ disease. The data suggest that with increasing M stage of disease the expression of GD3 to GD3^A is likely to be in favour of GD3^A as the expression of Cas1 is up-regulated, the expression of SIAE is concomitantly down-regulated.

In summary, these findings support the idea that GD3 is likely to be re-expressed, particularly in the higher risk disease groups (groups 3 and 4, and high M stage) and is also likely to be acetylated to GD3^A in medulloblastoma. Therefore, we characterised the GD3 and GD3^A expression in medulloblastoma cell lines to compliment the bioinformatics-derived information. As a proof of principle study, we investigated the potential of

exploiting this pathway in order to determine if by increasing the deacetylation of GD3^A, render medulloblastoma cells are rendered more susceptible to chemotherapy.

3.3 Characterisation of GD3 and GD3^A expression in medulloblastoma cell lines

3.3.1 Introduction

The expression of GD3 and GD3^A has been shown to be in delicate balance in favour of GD3^A in cancers such as acute lymphoblastic leukaemia (Mukherjee et al. 2008) and glioblastoma multiforme (Birks et al. 2011). In this part of the study we aimed to characterise these gangliosides in three medulloblastoma cell lines (RES256, UW402 and CHLA-01-Med) in order to determine the relevance of this pathway in this tumour type. Based on bioinformatics data, the expression of GD3 and GD3^A may be expressed by medulloblastoma cells. There may also be a balance in favour of GD3^A in the medulloblastoma cell lines as suggested by information gathered from bioinformatic studies of SIAE, the deacetylation enzyme, and the up-regulation of Cas1, the acetylation enzyme of GD3.

3.3.2 GD3 and GD3^A are expressed by medulloblastoma cell lines

In order to test our hypotheses that GD3 and GD3^A are expressed by medulloblastoma cells, expression of GD3 and GD3^A in three cell lines was characterised using flow cytometry and immunocytochemistry.

Expression levels were determined by directly assaying GD3 and GD3^A to determine expression of the products, not the mRNA of the synthesis enzymes. Flow cytometry was used to determine quantitative expression of both antigens as a percentage of the cell

population, and was further confirmed with qualitative immunocytochemistry. A representative example of positive staining is shown in figure 3.9A.

The expression of cell surface-associated and intracellular GD3 and GD3^A were characterised and compared in medulloblastoma cell lines using flow cytometry. Three medulloblastoma cell lines RES256, UW402, and CHLA-01-Med were used and compared to that of a positive control cell line, MeWo, a metastatic melanoma cell line known to express both antigens (Kniep et al. 2006) (figure 3.9). Due to the fact that gangliosides are synthesised both within the cell and (to a lesser extent) on the cell surface, as well as and trafficked (Sorice et al. 2012) both the expression within the cell and on the cell surface was examined.

Analysis of intracellular GD3 and GD3^A showed that the population of cells expressing GD3 was similar for RES256, UW402 and CHLA-01-Med (56.7%, 61.3% and 45.1% respectively; figure 3.9B). The percentage of the cells expressing GD3^A was also found to be similar between the cell lines (85.4%, 74.4% and 79.4% respectively; figure 3.9B). When comparing GD3 to GD3^A by each individual cell line, the balance of the gangliosides is shown. The only cell line to have a higher population of GD3^A positive cells compared to GD3 positive cells was CHLA-01-Med (figure 3.9B; $p < 0.01$). This however may not be necessary for protection against high levels of GD3 as previous studies have shown that GD3^A can protect from GD3 mediated apoptosis at low levels (Kniep et al. 2006). Expression of both antigens in the positive control cell line MeWo was 49.0% GD3 and 79.5% GD3^A also demonstrating a balance in favour of GD3^A in this cell line, although the difference in expression was not significant.

When examined on the cell surface, expression of GD3 was found to be higher than that of GD3^A in the medulloblastoma cell lines. This was not found in the MeWo cell line whose expression of GD3 was 93.8% and expression of GD3^A was 91.7% (figure 3.9C). In both the UW402 and CHLA-01-Med cell line there is a significant difference in the balance of cell surface GD3 to GD3^A with UW402 (62.2% GD3 compared to 17.5% GD3^A) ($p < 0.01$), and the CHLA-01-Med cell line (77.1% GD3 compared to 0.6% GD3^A) ($P < 0.001$) (figure 3.9C). The expression of GD3 and GD3^A for RES256 cells was 55.0% and 36.0% respectively. These data are in agreement with published work showing that GD3 requires internalisation to become acetylated (Chen et al. 2006) and therefore the low levels of GD3^A on the cell surface are not surprising.

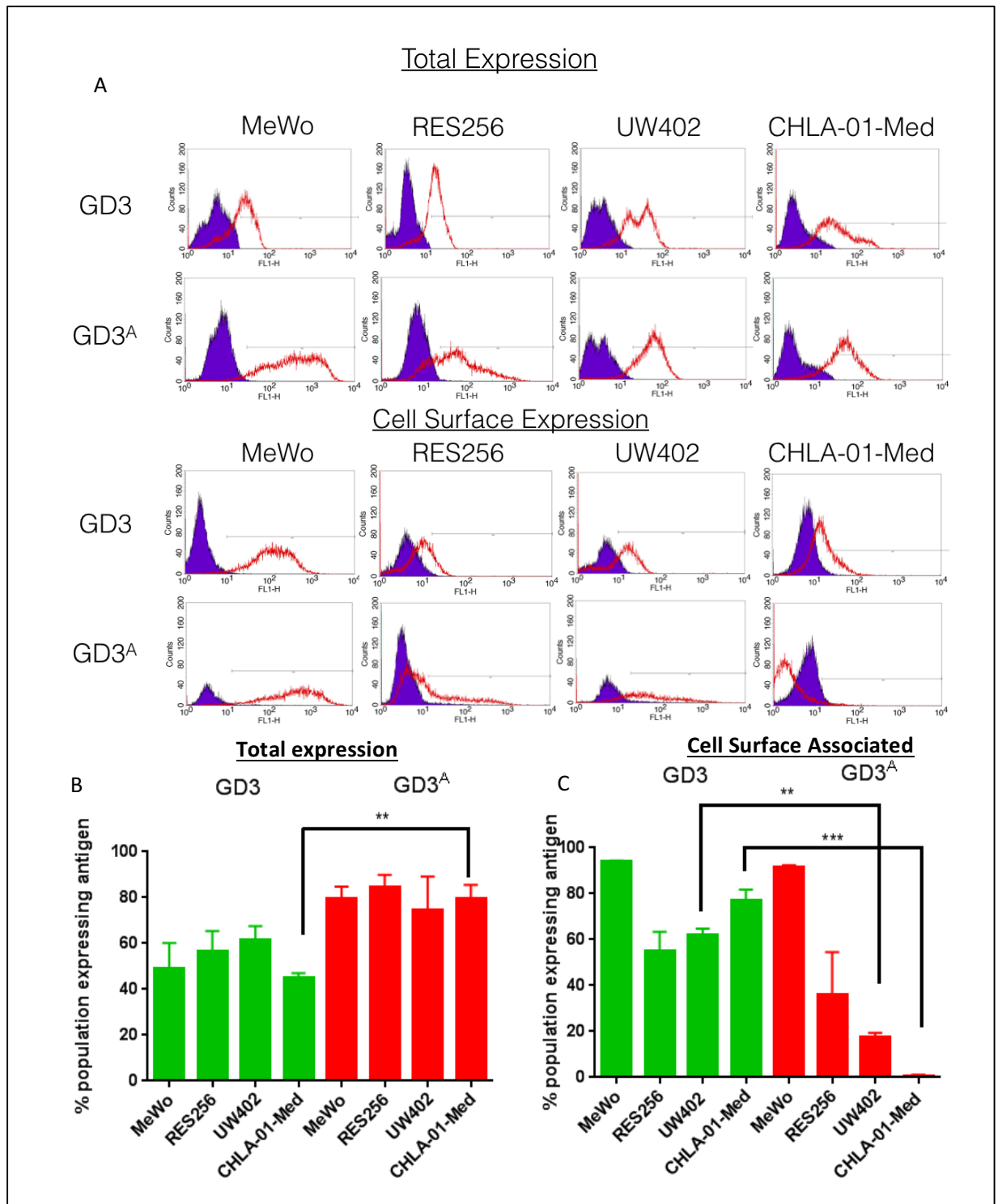


Figure 3.9 Expression of GD3 and GD3^A was confirmed by flow cytometry using a positive control cell line MeWo, known to express both antigens at high levels. (A) Examples of flow cytometry histograms demonstrating expression of GD3 and GD3^A. Purple filled peaks represent negative control samples from which gating was carried out, red peaks represent positive staining. Histograms represent one technical replicate from one experiment. (B) Intracellular expression of GD3 and GD3^A from three independent experiments demonstrates a higher level of GD3^A expression (red bars) compared to GD3 (green bars) in CHLA-01-Med, a group 4 cell line. (C) Cell surface expression of GD3 and GD3^A shows a higher expression of GD3 (green bars) compared to GD3^A expression (red bars) and shows a significantly higher level of GD3 expression in UW402 and CHLA-01-Med cells. Data analysed by unpaired two-tailed t-test using Graph Pad Prism 6 software (** p<0.01; *** p<0.001) n=3 ± SEM

To further confirm the expression of GD3 and GD3^A in medulloblastoma cell lines, immunocytochemistry was used (figure 3.10). This technique was used to qualitatively evaluate expression and validate flow cytometry data.

Immunocytochemistry revealed that intracellular expression of GD3^A (red) was higher than that of GD3 (green). There was some degree of co-localisation with these two antigens. Co-localisation studies cannot be conclusive in this manner however due to the influence of fixation methods on the localisation of the gangliosides (Schwarz & Futerman 1997). The expression of these antigens is confirmed by immunocytochemistry but not compared to flow cytometry data which reports the percentage of the population expressing antigen, not the expression of the antigens on a single cell basis. It is therefore not possible to conclude which of the cell lines expresses the highest levels of GD3^A in this way as the whole population of cells would be required.

Ganglioside expression was also examined in the wild-type mouse cerebellum. Two ages (P5 and P60) of mice were chosen to represent two stages of development. The P5 mouse brain is at a point in time where the GPCs are at their peak of migration, the expression of the gangliosides GD3 and GD3^A should therefore be at peak expression during these times. The P5 mouse brain represents a 32-36 week foetal brain. As we know that the expression of GD3 and GD3^A is present on medulloblastoma tumour cells, we stained the cerebellums of these mice to determine the location of ganglioside positive staining (figure 3.11). We then used this information to determine which of the subgroups of medulloblastoma could arise based on the location of GD3 and GD3^A staining and the age of the mouse. The P60 mouse was a control for a time when the brain should only express low levels of both GD3 and GD3^A, the P60 mouse represents a human brain over the age of 20 years.

Staining of the post-natal day 5 wild-type mouse cerebellum shows that high levels of GD3 expression are found in the internal granule layer (IGL) (figure 3.11A, green). Staining was shown to be cellular as there is localisation surrounding counterstained nuclei. The majority of the cells in the IGL express GD3 in this area of the cerebellum. Also in the P5 wild-type mouse cerebellum is a high level of GD3^A expression shown in red, staining is intense and present in a high percentage of the cell populations. Staining is also seen in projections in the EGL (figure 3.11A). Staining in the P60 cerebellum was diminished significantly (figure 3.11B). Little GD3 staining was present throughout the internal granule layer (IGL) and the PL in P60 samples. Only low intensity GD3 staining was seen in the molecular layer (figure 3.11B). GD3^A staining in the P60 wild-type mouse brain showed much the same pattern as the GD3 staining, with most being present at low intensity in the molecular layer (figure 3.11B), there was however some background fluorescence in this instance making the actual staining intensity of GD3^A difficult to determine.

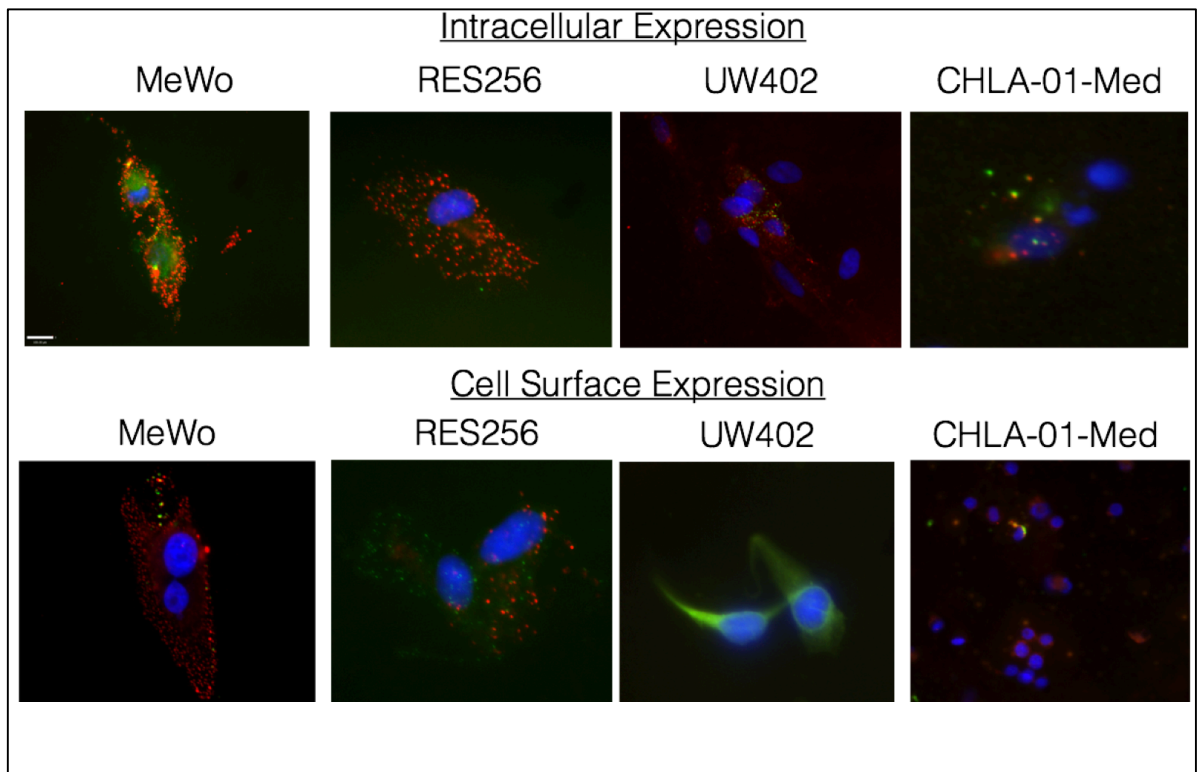


Figure 3.10 Expression of GD3 and GD3^A is confirmed by immunocytochemistry in fixed cell lines. MeWo, a positive control cell line confirms intracellular expression of GD3 (green) and GD3^A (red) with some co-localisation of the antigens (yellow). On the cell surface there is also expression of both antigens. Expression of GD3^A is seen throughout the cytoplasm of RES256 cells with faint GD3 staining also seen. On the cell surface the RES256 cell line shows a higher degree of GD3 staining compared to GD3^A. In UW402 cells there is a similar staining to RES256 cells, with more GD3^A expressed intracellularly compared to on the cell surface where GD3 is more highly expressed. In CHLA-01-Med cells GD3 and GD3^A are expressed in similar levels whereas GD3^A appears to be expressed more highly on the cell surface compared to GD3. Cell images taken using a Zeiss Axioimager ZI epifluorescence microscope equipped with a Hamamatsu digital camera and velocity imaging software. 40 X magnification, scale bar 100 μm . n=3

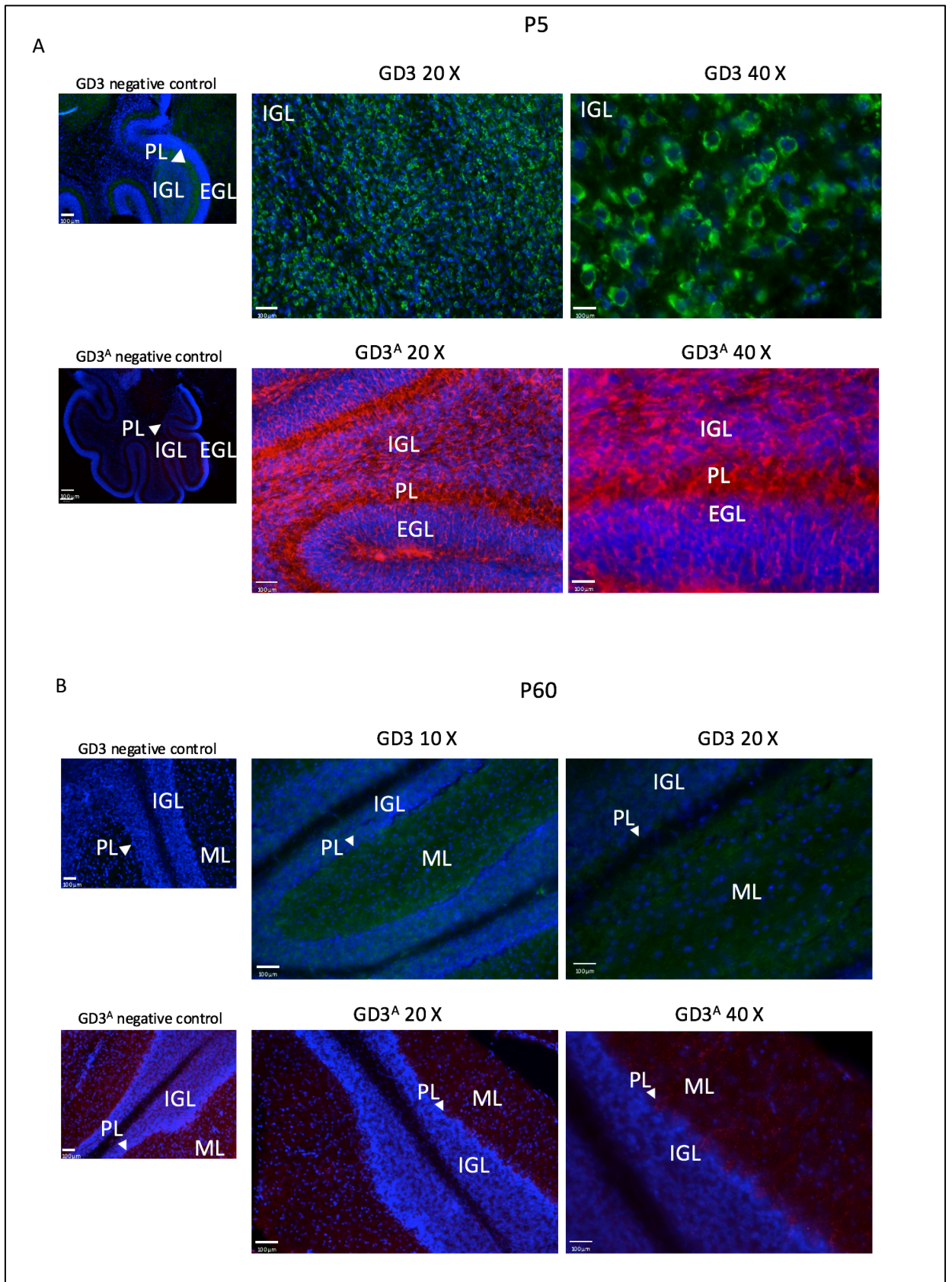


Figure 3.11 Expression of GD3 and GD3^A in the post-natal day 5 and day 60 wild-type mouse cerebellum. (A) The post-natal day 5 cerebellum shows a low level of background fluorescence when stained with secondary antibody only, the areas of the cerebellum are highlighted as the internal granule layer (IGL); the purkinje cell layer (PL; arrow head); and the external granule layer (EGL). High levels of GD3 expression (green) are seen in the internal granule layer (IGL). Staining is cellular as shown by localisation surrounding counterstained nuclei (blue). There is a large population of cells expressing GD3 in this area of the cerebellum demonstrated by the 20 X magnification image. Also in the P5 wild-type mouse cerebellum is a high level of GD3^A staining (red). There is also very little background fluorescence shown in the controls. Staining is intense throughout the cell bodies and the projections as seen in the EGL at 40 X magnification. (B) Staining in the P60 cerebellum is diminished significantly. Little GD3 staining is present throughout the internal granule layer (IGL) and the PL in P60 samples and is seen at low intensity in the molecular layer only. GD3^A staining shows much the same pattern as the GD3 staining with most being present at low intensity in the molecular layer, there is however background fluorescence in this instance making the actual staining intensity of GD3^A difficult to determine. taken using a Zeiss Axioimager ZI epifluorescence microscope equipped with a Hamamatsu digital camera and velocity imaging software. 40 X magnification, scale bar 100 μ m. n=3

3.3.3 Conclusion

The expression of GD3 and GD3^A was confirmed in each of the medulloblastoma cell lines we used. This data suggests that a balance between GD3 and GD3^A exists within these cells and that this balance is in favour of GD3^A within the cell and in favour of GD3 on the cell surface. The deacetylation of GD3^A has been shown in previous studies to influence cell survival (Birks et al. 2011). We therefore hypothesised that through overexpression of SIAE, the human endogenous deacetylation enzyme, that the balance of GD3^A to GD3 could be shifted in favour of GD3 and therefore apoptosis (figure 3.12).

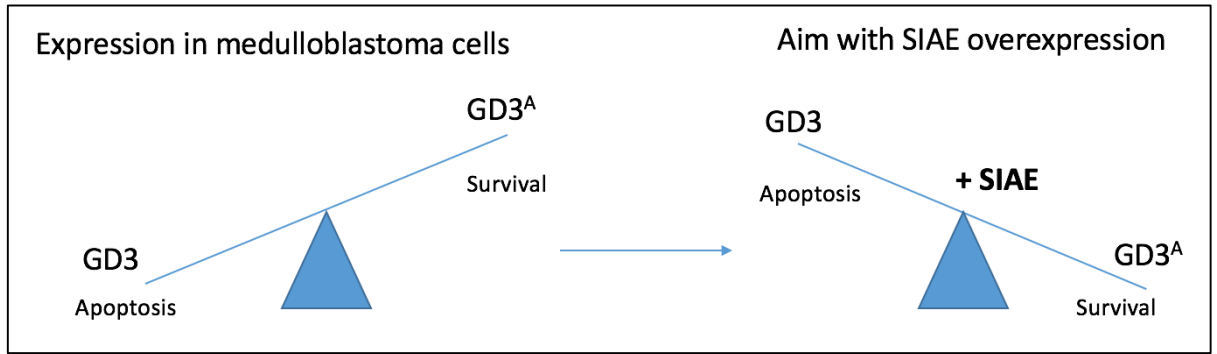


Figure 3.12 Our hypothesis, the balance of GD3 and GD3^A is in favour of GD3^A as shown in medulloblastoma cell cultures, and as suggested by bioinformatic analysis. Our aim is to, through SIAE over-expression, to shift the balance in favour of GD3. We hypothesise that by over-expression of SIAE, high levels of pro-apoptotic GD3 levels will be restored and that this may influence cell viability and sensitise cells to commonly used chemotherapeutics.

3.4 SIAE overexpression studies

After confirming GD3 and GD3^A expression in the three medulloblastoma cell lines, the highest expressing cell line of intracellular GD3^A (RES256) was selected for over-expression of SIAE. This cell line was also chosen for its rapid proliferation rate and relative ease of transfection compared to UW402 and CHLA-01-Med.

An inducible system was used to control SIAE transcript expression. These experiments were designed to test our hypothesis that over-expression of SIAE would result in an increase in GD3^A deacetylation. This GD3^A, when deacetylated, was hypothesised to increase the pool of GD3 which may then result in a collapse of the mitochondrial membrane potential and increase apoptosis. We also hypothesised that SIAE over-expression may make medulloblastoma cells more susceptible to apoptosis when treated with chemotherapeutics.

In standard stable over-expression experiments clones failed to expand (appendix 1). We also carried out transient transfections using these constructs (appendix 2) and although we cannot conclude from this data that SIAE overexpression was toxic to cells, we concluded that a well described inducible system approach would provide us with a model to directly test our hypothesis that SIAE overexpression leads to deacetylation of GD3^A. pCMV-TetOn3G and pTRE3G-IRES construct backbones were therefore purchased from Clontech and the SIAE gene (or the catalytic mutant SIAE-S127A) as well as an EGFP gene were cloned into them using InFusion HD Dry cloning (Clontech) described in chapter 2. Gene inserts were confirmed by size (by restriction digests, appendix) and by sequencing using SIAE primers (appendix 3).

The catalytic mutant SIAE-S127A has been described by several groups who, when investigating the possible sites for the catalytic triad of SIAE, conducted site-directed mutagenesis studies that demonstrated serine 127 (S127) as a conserved and critical residue for esterase activity (Surolia et al. 2010; Orizio et al. 2015). These studies also demonstrated that when the serine residue was mutated to an alanine (S127A), wildly changing the properties of the amino acid within the triad, catalytic activity was decreased significantly to almost negligible levels (Surolia et al. 2010). It is important to note that while this group describe many germline SIAE mutations and their activities, the S127A variant has not been found endogenously and was used as an artificial control for these studies.

When cloning the SIAE and SIAE-S127A genes into the pTRE3G-IRES-EGFP constructs, it was important to ensure the sequence was incorporated correctly (appendix 3). Of particular importance was the point mutation encoding the serine to alanine substitution in the SIAE-S127A plasmid (figure 3.13, black circle). The mutation from GAG to GGC encodes the serine to alanine mutation and is shown at positions 378-380 of the cDNA sequence (corresponding to amino acid 127).

The incorporation of the EGFP, SIAE and SIAE-S127A genes was successful as shown by sequencing (appendix 3), these plasmids were then used for down-stream transfection experiments.

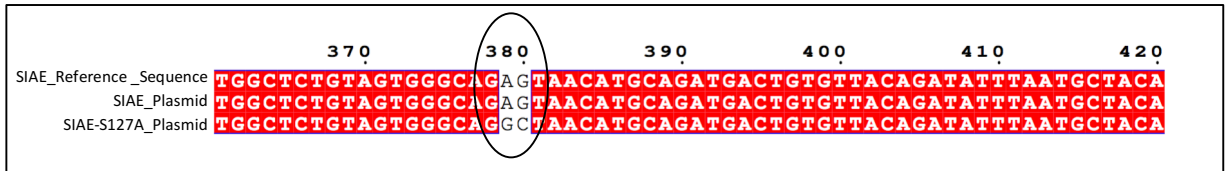


Figure 3.13 Sanger sequencing demonstrates that SIAE and SIAE-S127A genes were successfully cloned into the pTRE3G-IRES-EGFP plasmids. The mutation encoding S127A, a mutation of the catalytic triad of SIAE is shown in the black circle and corresponds to position 127 of the amino acid sequence.

3.5 The Tet-On 3G inducible system

The Tet-On 3G system is a well described inducible gene expression system for mammalian cells. There are two elements to the Tet-On3G system. The Tet-On 3G transactivator protein, which has a high sensitivity to doxycycline, and the P_{TRE3G} inducible promoter. The P_{TRE3G} promoter allows for very low basal expression and high expression of the genes of interest after induction. Within the tet-responsive construct pCMV-TetOn3G, there are 7 repeats of a 19 base pair *tet* operator sequence which is located upstream of a minimal CMV promoter. In the presence of doxycycline, Tet-On 3G protein undergoes a conformational change that allows binding to the P_{TRE3G} promoter (figure 3.14). The doxycycline concentration for induction of gene expression is far below cytotoxic concentrations for cell culture studies (1 $\mu\text{g}/\text{mL}$).

In these studies, cells are transfected with pCMV-TetOn3G and pTRE3G-IRES-EGFP-(SIAE or SIAE-S127A). The cells therefore express a Tet-On 3G transactivator protein and contain two genes of interest, EGFP and either SIAE (wild-type) or SIAE-S127A. Expression is under the control of the TRE3G promoter (P_{TRE3G}). The genes of interest are expressed only in the presence of doxycycline, and are not expressed as fusion proteins. This is achieved as the construct contains an internal ribosomal entry site (IRES), which allows the generation of two proteins from the same mRNA transcript shown in figure 3.15.

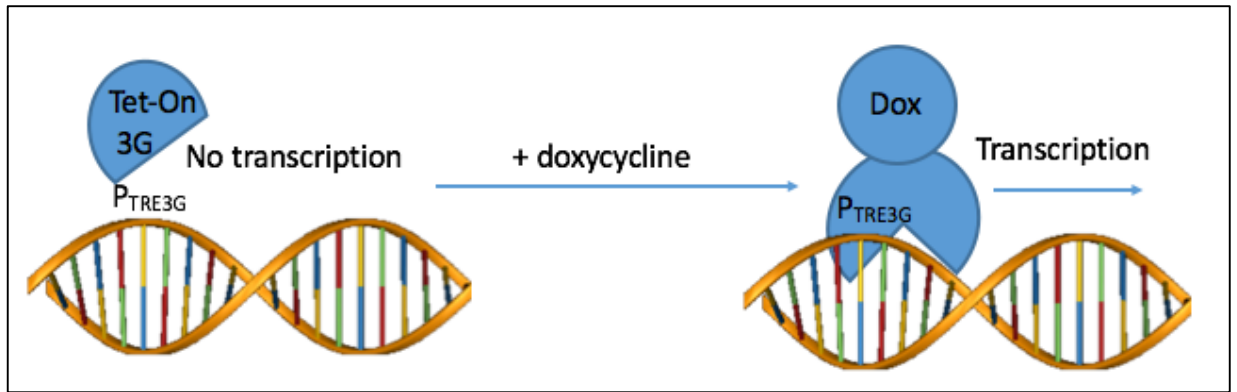


Figure 3.14 The Tet-On 3G inducible expression system. Cells are stably transfected with two constructs, pCMV-TetOn3G, which produces Tet-On 3G protein; and an inducible construct containing an internal ribosomal entry site (IRES) and cloned genes of interest. Tet-On 3G protein is then expressed by the Tet-On 3G transfected clone. When expressed, Tet-On 3G protein undergoes a conformational change in the presence of doxycycline- driving transcription. In the absence of doxycycline the Tet-On3G protein expressed by Tet-On stable cell lines is unable to bind to P_{TRE3G} and transcription does not take place. In the presence of doxycycline, the Tet-On 3G protein undergoes a conformational change that allows promoter binding of the pTRE3G-IRES tet-responsive construct and drives transcription of cloned genes of interest.

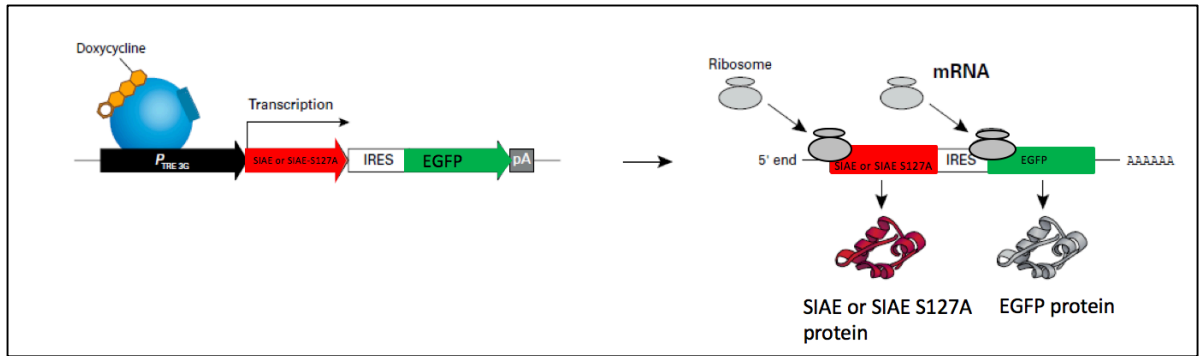


Figure 3.15 Two proteins are expressed from one mRNA transcript using an internal ribosomal entry site. The Tet-On 3G inducible system contains an internal ribosomal entry site (IRES) under the control of a tet-responsive promoter (P_{TRE3G}). Gene expression is only initiated in the presence of Tet-On 3G protein bound to doxycycline, allowing transcription. Two proteins are produced simultaneously from one mRNA transcript by the use of the IRES that is flanked by the two multiple cloning sites containing cloned genes (SIAE and EGFP or SIAE-S127A and EGFP). Translation initiation usually occurs at the 5' cap however the IRES allows ribosomes to bind at a second location allowing the proteins to be expressed separately. Adapted from Tet-On user guide (Clontech)

3.6 Generating and screening a Tet-responsive cell line

RES256 cells were first stably transfected with the pCMV-TetOn3G construct (map, appendix 3) as described in chapter 2. After clonal selection with selective antibiotic and picking of colonies, 24 clones were screened for expression. Cells were tested for induction of expression using transient expression with a Tet-responsive luciferase construct. This assay allows the functionality of the Tet-On 3G protein to be tested. The Tet-On 3G protein drives expression of a luciferase gene and the basal level of expression can be determined. To achieve this cells were transfected with pTRE3G-Luc (map, appendix 4) as described in chapter 2 and cultured in the presence and absence of doxycycline for 48 hours according to manufactures instructions. Cells were lysed using the lysis buffer provided with the Dual Luciferase kit (Promega). The assay was carried out and luminescence of the luciferase protein recorded. Fold-induction of expression was confirmed, and the clones which demonstrated the lowest basal expression and the highest induction of expression were propagated (appendix 4).

The clones with the highest fold-induction of luciferase gene expression were then transfected with pTRE3G-IRES-EGFP (empty vector control), pTRE3G-IRES-EGFP-SIAE (wild-type) or pTRE3G-IRES-EGFP-SIAE-S127A (catalytic mutant) plasmids. Following the transfection of SIAE genes, potential clones were screened for EGFP expression with and without doxycycline treatment (1 µg/mL) using ICC (figure 3.16). Expression of EGFP was confirmed and these clones were propagated. The next step was to ensure that SIAE (or SIAE-S127A) was expressed at the protein level.

To determine the level of SIAE protein expression, Western blot analysis was conducted. Cells were incubated in the presence and absence of doxycycline for 48 hours and lysed

using M-PER supplemented with protease and phosphatase inhibitors described in chapter 2. The protein content of the lysates was determined using the colorimetric bicinchoninic acid assay (BCA Assay; Thermo). Protein was separated using polyacrylamide gel electrophoresis and transferred to a PVDF membrane and prepared for Western blot analysis using an in-house anti-SIAE antibody (described in chapter 2). Two wild-type clones that expressed SIAE were analysed, along with empty vector control (EGFP) and the catalytic mutant cell line S127A (figure 3.16).

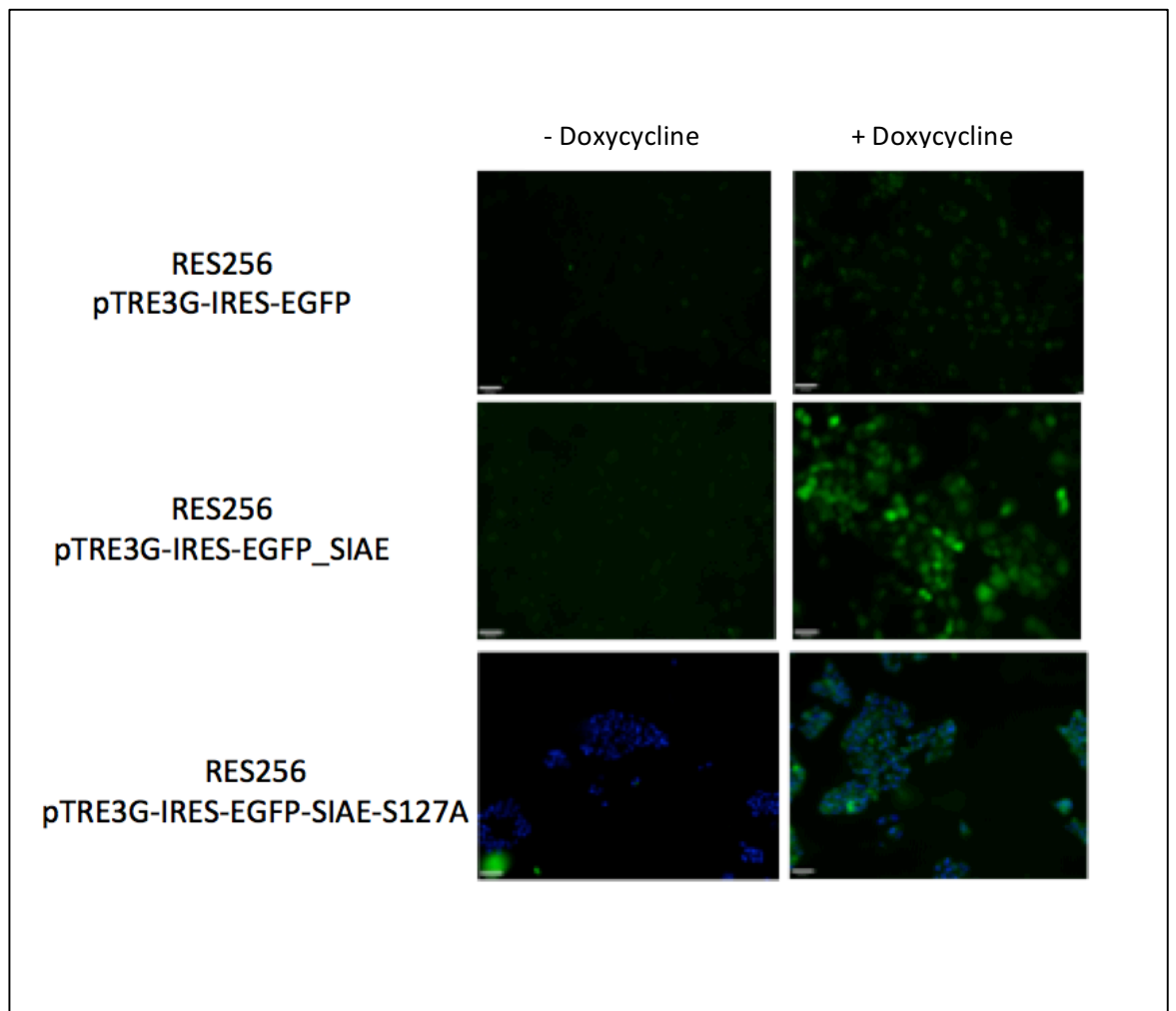


Figure 3.16 EGFP gene expression is induced in the presence of doxycycline. RES256 cells were screened for EGFP gene expression in the first instance to reduce clone numbers for SIAE expression screens. Clones expressing EGFP in the presence of doxycycline (green) that showed little expression in the absence of doxycycline were chosen for SIAE expression screening. (EGFP – green, nuclei - blue) 10 X objectives. SIAE clone 2 is shown as an example. Cell images taken using a Zeiss Axioimager Z1 epifluorescence microscope equipped with a Hamamatsu digital camera and velocity imaging software. 40 X magnification, scale bar 100 μ m. n=3

In RES256 cell lysates SIAE expression was confirmed by Western blot analysis and the expression appeared to be tightly controlled (as demonstrated by the absence of construct leakiness). This further confirmed the results from the luciferase assay that the conformational change of the TetOn 3G protein was under tight control (appendix 4.2). The predicted molecular weight of SIAE in its active form is a glycoprotein with a molecular weight of 62 kDa as described by Orizio *et. al.* Interestingly, the intensity of expression of the proteins expressed by SIAE and SIAE-S217A clones appears to be somewhat different (figure 3.17). Two immunoreactive bands for each clone are shown when gene expression is induced with doxycycline addition. The largest molecular weight band has a predicted size of 62 kDa as determined by ImageStudio software (Licor Biosciences), this is the same molecular weight reported by Orizio *et. al.* as active glycoprotein. The second molecular weight band, which is more intense in wild-type expressing clones, has a predicted molecular weight of 32 kDa. Initially we thought that the blot may be showing heavy and light chains of the antibody we used, however as we did not see these bands in our EGFP expressing cell lines, nor in lanes loaded with cells not treated with doxycycline, we disregarded this. Another explanation for the expression of a 32 kDa protein was that the processing of was somehow different. The protein loading of each clone is confirmed as equal between off and on using a beta-actin loading control (figure 3.17).

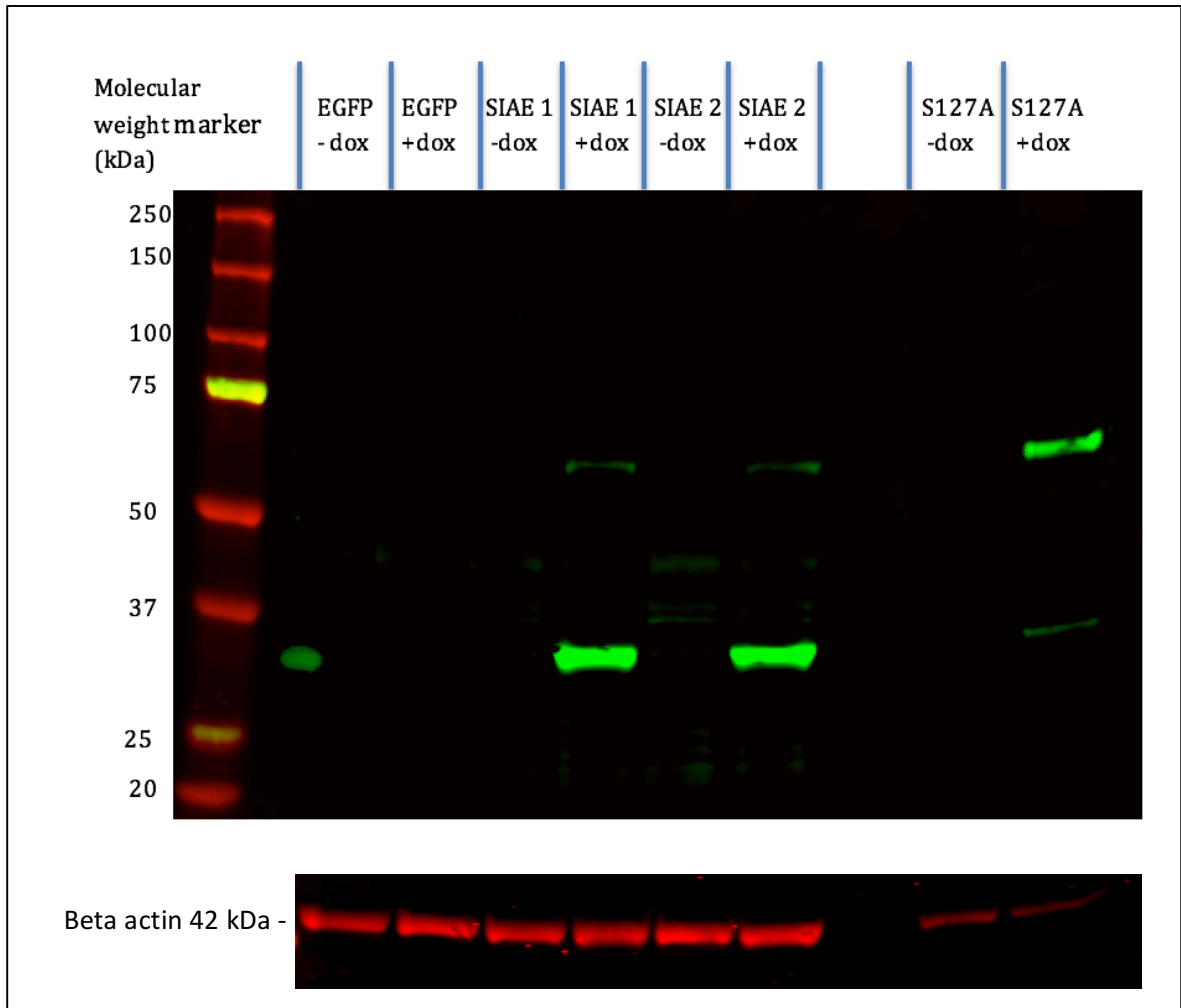


Figure 3.17 SIAE expression is induced by RES256 clones in the presence of doxycycline. Cells were cultured in the presence and absence of doxycycline for 48 hours and lysed using mammalian protein extraction reagent containing protease and phosphatase inhibitors. Protein was quantified using bicinchoninic acid assay (BCA assay) and was then loaded and resolved using sodium dodecyl sulphate polyacrylamide gel electrophoresis (SDS-PAGE). Resolved protein was then transferred onto a polyvinylidene fluoride (PVDF) membrane, blocked with 1 % non-fat milk and probed with an in-house anti-SIAE primary antibody and conjugated fluorescent secondary antibody. SIAE was expressed by two wild-type clones, SIAE 1 and SIAE 2, and by the catalytic mutant, S127A, importantly only when the cells were cultured with doxycycline for 48 hours. Two bands were present on each blot. The protein at approximately 62 kDa represents the glycosylated active form of SIAE. The second band at around 32 kDa is probably the result of cleavage. Equal protein loading between samples from each clone are confirmed with beta actin (red bands). Less protein was loaded in the S127A samples due to protein concentration of the lysate. Image acquired using the Licor Odyssey Clx equipped with ImageStudio 5 software. Image representative of n=3

We also considered whether the 62 kDa protein might be secreted. Orizio *et al.* demonstrated that the 62 kDa glycoprotein can be secreted in a cell-type dependent manner. This publication also demonstrated that the catalytic mutant secreted more enzyme than wild-type in their cell lines so we hypothesised that our mutant would do the same. In order to test this, we first serum-depleted the cells over 48 hours. We then treated with doxycycline for 48 hours as for previous experiments. Conditioned media was harvested and analysed by Western blot analysis (figure 3.18). Protein loading was adjusted and confirmed with Ponceau S staining (figure 3.18B). The conditioned media studies demonstrated that the SIAE-S127A mutant clone secreted enzyme (figure 3.18A). The molecular weight of the secreted protein was confirmed as 62 kDa, in line with Orizio *et al.* this protein was, therefore, confirmed as the fully glycosylated enzyme. As the wild-type SIAE expressing clones did not secrete enzyme at detectable levels, this may explain the difference in band intensities. In light of this we further explored the 32 kDa molecular weight band to elucidate what it could be.

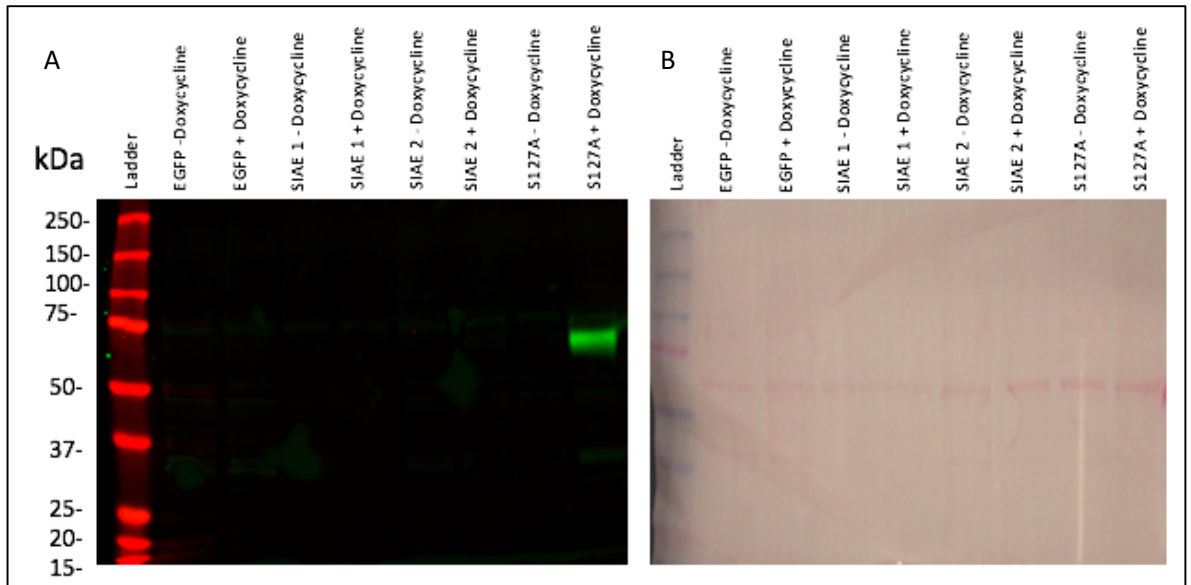


Figure 3.18 SIAE as a secreted enzyme. Cells were serum starved over a course of 48 hours, after which media was supplemented with (or without) doxycycline for 48 hours. Conditioned media was then loaded and resolved using sodium dodecyl sulphate polyacrylamide gel electrophoresis (SDS-PAGE). Resolved protein was then transferred onto a polyvinylidene fluoride (PVDF) and (B) stained with ponceau s to ensure equal loading. (A) The membrane was then blocked and probed with an in-house anti-SIAE primary antibody and conjugated fluorescent secondary antibody. SIAE was secreted only by the catalytic mutant, S127A, importantly only when the cells were cultured with doxycycline for 48 hours. The protein at approximately 62 kDa represents the glycosylated active form of SIAE. Image acquired using the Licor Odyssey Clx equipped with ImageStudio 5 software. n=3

Orizio *et. al* described a cleaved SIAE product with a molecular weight of 49 kDa, while our molecular weight was 32 kDa we considered cleavage products as an option for identifying this band. In further support of this analysis of the peptide sequence of SIAE by protparam (<http://web.expasy.org/protparam/>) suggests that SIAE is an unstable protein.

We first entered the SIAE sequence into peptide cutter software which recognises cleavage sites within the SIAE protein. When narrowing the searches of the protein sequence that gave rise to similar molecular weights shown in figure 3.17 and that also conserved the antibody recognition site, one candidate was identified, caspase 1 (figure 3.19). Peptide cutter software demonstrated that caspase 1 could cleave SIAE once to give rise to a 236 amino acid and a 287 amino acid product. The cleavage product containing the antibody recognition sequence was predicted to be 27 kDa in molecular weight. By Western blot analysis we showed the cleavage product to have a molecular weight of 32 kDa; this difference could be explained as the protein sequence contains 4 *N*-glycosylation, 2 *O*-glycosylation and 12 phosphorylation sites that are not considered by the software.

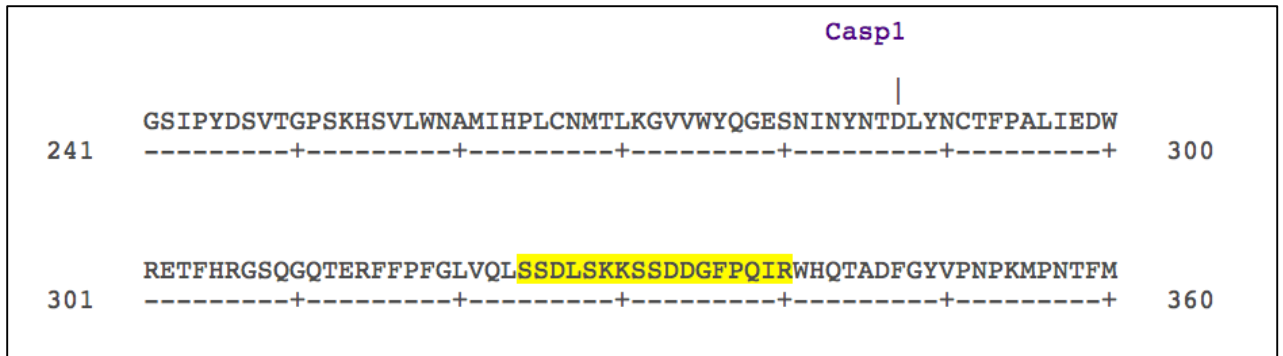


Figure 3.19 Cleavage sites of SIAE resulting in fragment sizes similar to 32 kDa. To determine if cleavage of SIAE protein could be a result of protein cleavage, giving rise to the 32 kDa band seen on western blot analysis of SIAE peptide cutter software was used. The full SIAE sequence was uploaded to peptide cutter software. This software demonstrates one potential cleavage site giving rise to a 27 kDa fragment containing the antibody recognition sequence (highlighted). Although a lower molecular weight to the 32 kDa band observed in figure 3.16, post-translational modification is not taken into consideration when sizing the fragment. The candidate enzyme peptide cutter software suggests that caspase 1 may be able to cleave the SIAE sequence in one place (shown above), resulting in this 27 kDa fragment. Caspase 1 cleaves towards the C-terminal side of the position marked above. Caspase 1 may be activated in SIAE wild-type expressing cells in the presence of doxycycline and will be the subject of further work beyond the scope of this project.

Caspase 1, also known as interleukin 1 β converting enzyme (ICE) is involved in the conversion of the interleukin to its active form (Denes et al. 2012). Interleukin 1 β (IL-1 β) is a key mediator of the inflammatory response, but has also been shown in rodents to have roles in neuronal cell apoptosis (via activation of caspase 3 and bid cleavage) however this link has yet to be confirmed in human brain. An outline of the roles of caspase 1 is shown in figure 3.20. We hypothesise that the wild-type SIAE enzyme is capable of activating caspase 1 and therefore the enzyme is being cleaved, we also hypothesise that this may not occur with the SIAE-S127A mutant as it may not have the ability to activate caspase 1. If this hypothesis was true it could explain the difference in intensity between 62 kDa and 32 kDa products detected by Western blot. Further work outside the scope of this project will be required to test this hypothesis.

In order to determine if the potential cleavage site for caspase 1 within the SIAE amino acid sequence is possibly accessible due to folding of the SIAE protein, molecular modelling was used. Using the Phyre 2 database, homologous sequences to the SIAE gene were used in order to generate a hypothesised structure (as a crystal structure for SIAE is not yet known). The database generated a structure of 74% of the SIAE sequence with >90% accuracy indicating a good quality in the prediction. The Phyre 2 software also generated a protein database file (PDB file) which was modelled using MacPyMol to visualise the hypothesised protein structure (figure 3.21). Using MacPyMol, the sequence of antibody recognition (figure 3.21, green), the active site residue mutated in in the S127A mutant (figure 3.21, red) and the potential caspase 1 cleavage site (figure 3.21, pink) were highlighted. The structural model (although not complete) provides good evidence that the caspase 1 cleavage site is assessable to caspase 1 as it is located on the surface of the protein and is

not buried in its structure. While the cleavage site is present in both the mutant and the native protein sequences, activation of the caspase 1 protein may be required in order for the protein to be cleaved.

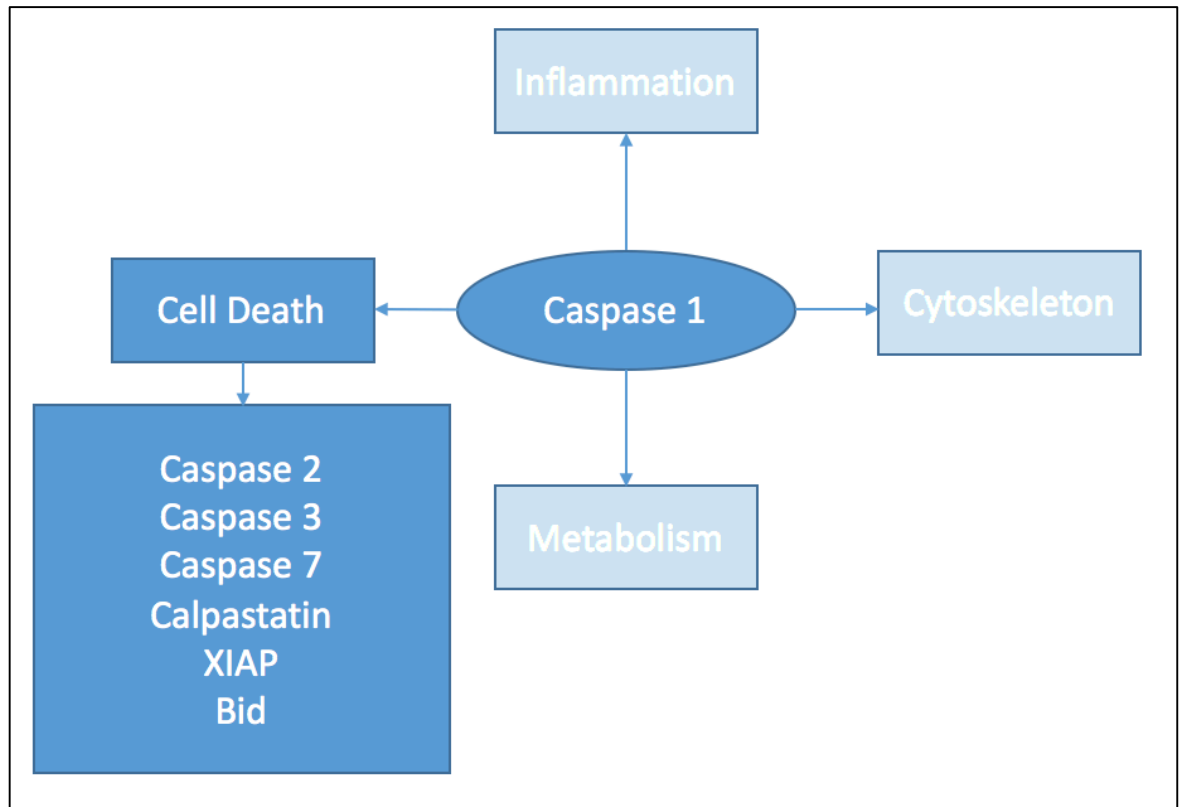
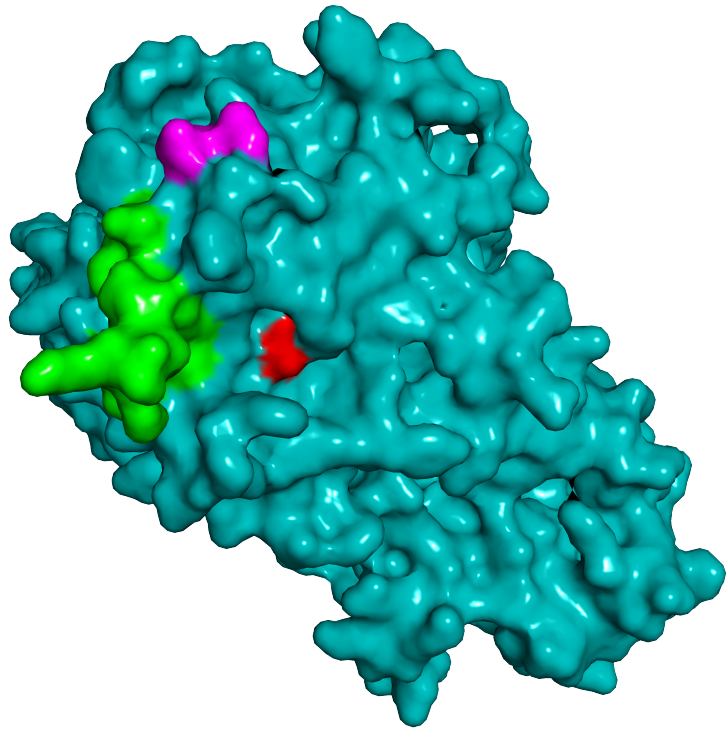


Figure 3.20 A summary of caspase 1 pathways. Caspase 1 has roles in inflammation, cytoskeletal modulation (via actin), metabolism (caspase 1 is a positive regulator of lipid metabolism) and, cell death. Neuronal cell death via caspase 1 has been shown in rodents but not in human central nervous system tissue. Caspase 1 can act via caspase 2, 3, 7, Calpastatin, X-linked inhibitor of apoptosis (XIAP) and BH3 interacting-domain death agonist (Bid). If caspase 1 has a role in neuronal cell death it may play a role in medulloblastoma as it is a tumour of the granule neuron precursor cells, this would however require further exploration. Adapted from Denes et al. 2012.

A



B

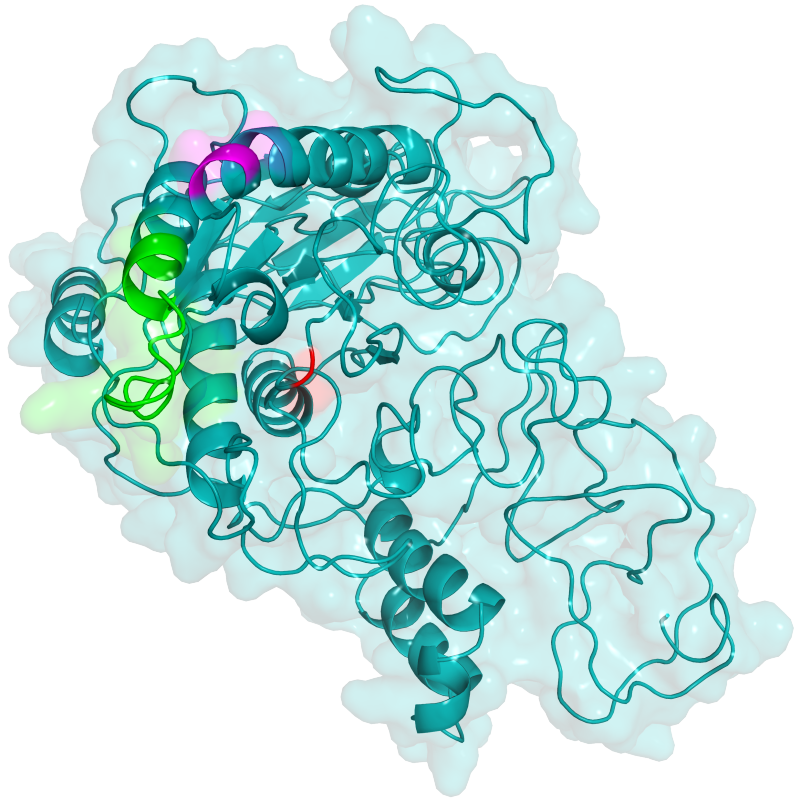


Figure 3.21 A homologous SIAE structural model predicts the caspase 1 cleavage sequence is accessible to caspase 1. (A-B) The predicted SIAE model is based on the amino acid sequence of human SIAE and is based on known structures with homologous sequences to SIAE generated by the protein fold-recognition server Phyre2. MacPyMol was used to generate the image of SIAE which is based on Phyre2 prediction. Phyre2 shows 74% of the protein was modelled with >90% confidence giving the structures above. With a confidence of >90% the program states that the overall fold of the protein (and the core of the protein) is modelled at high accuracy (2-4Å root-mean-square deviation of atomic positions (rmsd) from the native, true structure) however, surface unstructured loops may deviate from the actual structure. (A) Surface structure of SIAE as modelled by MacPyMol using a Phyre 2 generated sequence shows the active site serine residue (red), the in-house antibody recognition sequence (green) and the potential caspase 1 cleavage site (pink). (B) The hypothesised surface structure of SIAE is modelled with alpha helices shown, as the caspase 1 site is part of an alpha helix structure it is modelled with high confidence and while we cannot definitively say that the caspase 1 site is accessible to enzyme, its location within an alpha helix makes it is likely that this site will be accessible to the enzyme.

While preliminary and in need of further investigation, this data may help to explain data described below in which we tested the deacetylation of GD3^A and the role of SIAE in response to chemotherapeutic agents. The role of SIAE and its catalytic mutant will be discussed further in chapter 4.

Since we had confirmed SIAE expression and determined that our constructs did not leak expression of SIAE without doxycycline addition, the resulting cell lines were cultured in the presence of doxycycline for 48 hours according to the manufacturer's instructions to induce gene expression. These cell lines were then harvested for assays in order to determine changes in the GD3 and GD3^A expression as well as cell viability and response to chemotherapy.

In order to determine if SIAE overexpression results in a reduction of GD3^A (which potentially reflects the activity of the enzyme being expressed) flow cytometry was used.

Intracellular GD3 and GD3^A were analysed in order to determine if SIAE expression resulted in cleavage of the acetyl group from GD3^A and thereby increasing the pool of GD3. When analysed, GD3^A expression did not significantly reduce with expression of wild-type SIAE by either clone 1 or clone 2 ($p > 0.05$; figure 3.22A). The lack of significant changes in GD3^A status when SIAE protein expression was induced by the addition of doxycycline was not anticipated. We therefore considered possible explanations for this unexpected result. In a publication by Chen *et. al* GD3 was shown to be capable of inducing its own acetylation machinery (Chen et al. 2006). If this is indeed happening in this case, the deacetylation of GD3^A to GD3 may be recovered by induction of the acetylation machinery. This published phenomenon is reported to take place 6 hours after GD3's synthesis (in this case GD3 would be 'synthesised' by cleavage of the acetyl group from GD3^A). In further work this could be

explored with a time course experiment to determine when GD3^A cleavage was taking place, if at all.

Another possible explanation for this lack of significant changes in GD3^A expression is that the SIAE enzyme is being cleaved by the cells as shown in figure 3.17 or is failing to be processed to its fully glycosylated and active form sufficiently to significantly impact the expression of GD3^A. The trafficking of GD3 and GD3^A may also play a role in the observed changes in the ganglioside expression levels. These possibilities will need to be explored with further laboratory work.

The empty vector control however did express significantly less GD3^A upon induction of expression ($p < 0.05$; figure 3.22A) however this was not reflected by an increase in GD3 expression (figure 3.22B) suggesting that this may not be due to catalytic activity of an acetyl esterase and the reason for this is unknown.

When GD3 expression was analysed, there were some interesting differences. In the wild-type SIAE expressing clone 2 cultured in the presence of doxycycline there was a significant increase in the expression of GD3 compared to cells cultured in the absence of doxycycline ($p < 0.05$; figure 3.22B). This indicates that although there was no significant decrease in GD3^A expression there was an effect of SIAE overexpression on the cells in clone 2. Despite this, the increase in GD3 expression in SIAE expressing clone 1 failed to reach significance. Further to this the expression of GD3 followed an opposite trend in SIAE-S127A expressing cells with a lower (although not significantly lower) level of GD3 expression than cells cultured in the absence of doxycycline suggesting that SIAE-S127A may not only be catalytically different but also has a different role (figure 3.22B). An increase in GD3

expression did not occur with the empty vector control EGFP expressing cell line despite the changes in GD3^A expression ($p>0.05$; figure 3.22B).

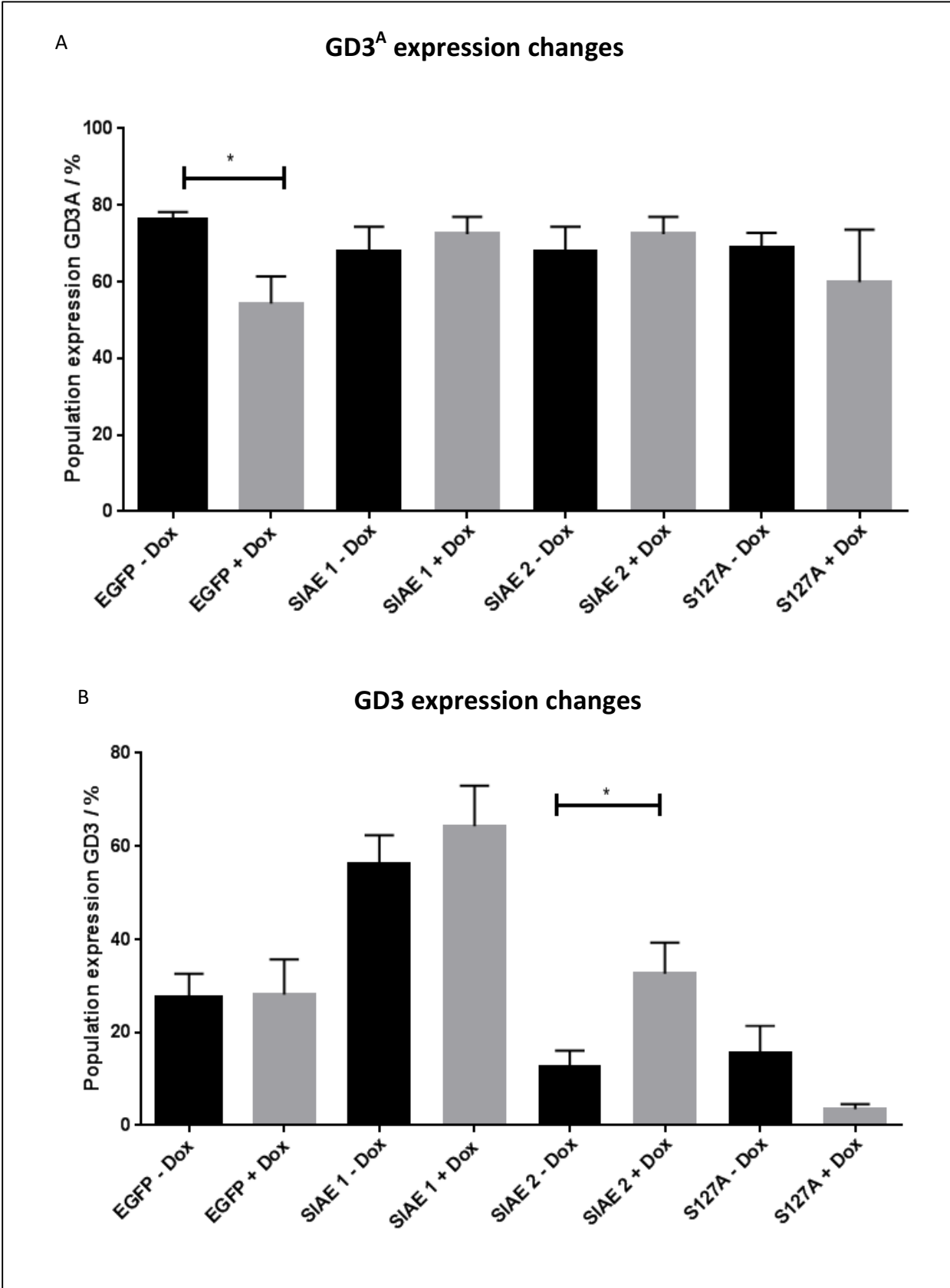


Figure 3.22 GD3 expression is increased with SIAE over-expression in RES256 cells. Intracellular changes in GD3 and GD3^A expression with induction of SIAE gene expression were examined by flow cytometry (A) The expression of GD3^A was not significantly lower with induction of SIAE in neither clone 1 nor clone 2 as hypothesised. In catalytic mutant SIAE-S127A expressing cells GD3^A was not decreased either, however, in empty vector EGFP expressing controls GD3^A was significantly decreased. In order to determine if GD3^A cleavage was occurring, the expression of GD3 was also examined. If cleavage of GD3^A did occur, an increase in GD3 would be expected as the pool of GD3 would be increased with the removal of acetyl groups from GD3^A. (B) GD3 expression was significantly increased in SIAE clone 2 in wild-type expressing RES256 cells compared to controls indicating that GD3^A cleavage may be occurring. This was not the case in clone 1, nor the catalytic mutant cell line SIAE-S127A which did not have an increase in GD3 expression which likely means that GD3^A cleavage was not occurring. The wild-type expressing cells expressed more GD3 than the catalytic mutant cell line in the presence of doxycycline. In EGFP expressing cells there was no increase in GD3 expression, which may indicate that the reduction in GD3^A expression may be due to something other than cleavage of the acetyl group. Samples were analysed using a multi-parameter fluorescence-activated cell sorting (FACS) Calibur flow cytometer and data was acquired using CellQuest Pro software. Data analysed by paired t-test using Graph Pad Prism 6 software (* p<0.05; ** p<0.01) n=3 data presented as mean ± SEM.

3.6.1 The effect of SIAE expression on mitochondrial membrane potential

The expression of GD3 is known to be associated with collapse of the mitochondrial membrane potential (Malisan & Testi 2002a). Depolarisation of mitochondrial membrane potential is a marker for early apoptosis, and is known to occur after a threshold of GD3^{A/s} protection from GD3 mediated apoptosis is overcome (Birks et al. 2011). To explore this, the JC-1 assay was used to determine if this threshold had been met by the increase in GD3 shown by flow cytometry when wild-type SIAE expression was induced (figure 3.23).

Upon induction of gene expression there was a significant increase in mitochondrial membrane depolarisation, indicative of early apoptosis with the wild-type SIAE (clone 1) expressing cell line ($p < 0.001$; figure 3.23). This change in depolarisation is a transient event and is reversible which may explain why this change is not seen in clone 2. This increase in membrane depolarisation is shown by an increase in the concentration of green monomers of JC-1 dye compared to red aggregates which accumulate in polarised mitochondria.

This significant change in depolarisation was not seen in cells with induced expression of SIAE clone 2 nor the catalytic mutant SIAE-S127A, nor the empty vector control EGFP ($p > 0.05$; figure 3.23).

Despite the significant increase in depolarisation with induction of SIAE expression in SIAE clone 1, the starting membrane polarisation of these cells appears very high (i.e. the samples are mostly depolarised at the start of the experiment). This means that this data cannot be relied on for an accurate conclusion on the effects of SIAE expression. The reasons for this will be discussed in chapter 4.

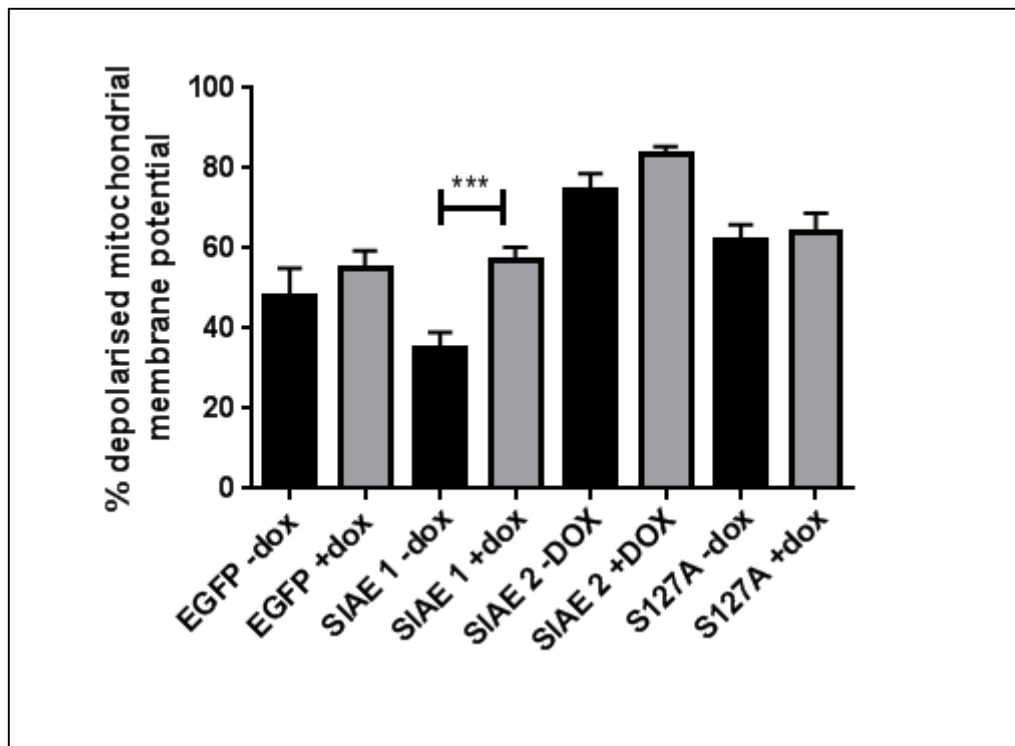


Figure 3.23 The mitochondrial membrane potential is depolarised by SIAE over-expression in RES256 cells. Polarisation of the mitochondrial membrane potential was determined using the JC-1 assay. Percentage change in membrane polarisation was determined between cells cultured in the presence and absence of doxycycline and presented as a percentage change. Expression of wild-type SIAE significantly depolarises the mitochondrial membrane potential in clone 11 RES256 cells and was significantly more depolarised than each of the other clones. Depolarisation did not occur in RES256 SIAE wild-type expressing clone 2. The EGFP and SIAE-S127A expressing clones did not have a significant reduction of the mitochondrial membrane potential. Data obtained using Nucleocounter 3000 and acquired using NucleoView software. Data analysed by unpaired two-tailed t-test using graph pad prism 6 software (* $p < 0.05$; ** $p < 0.01$), $n=3$ data presented as mean \pm SEM

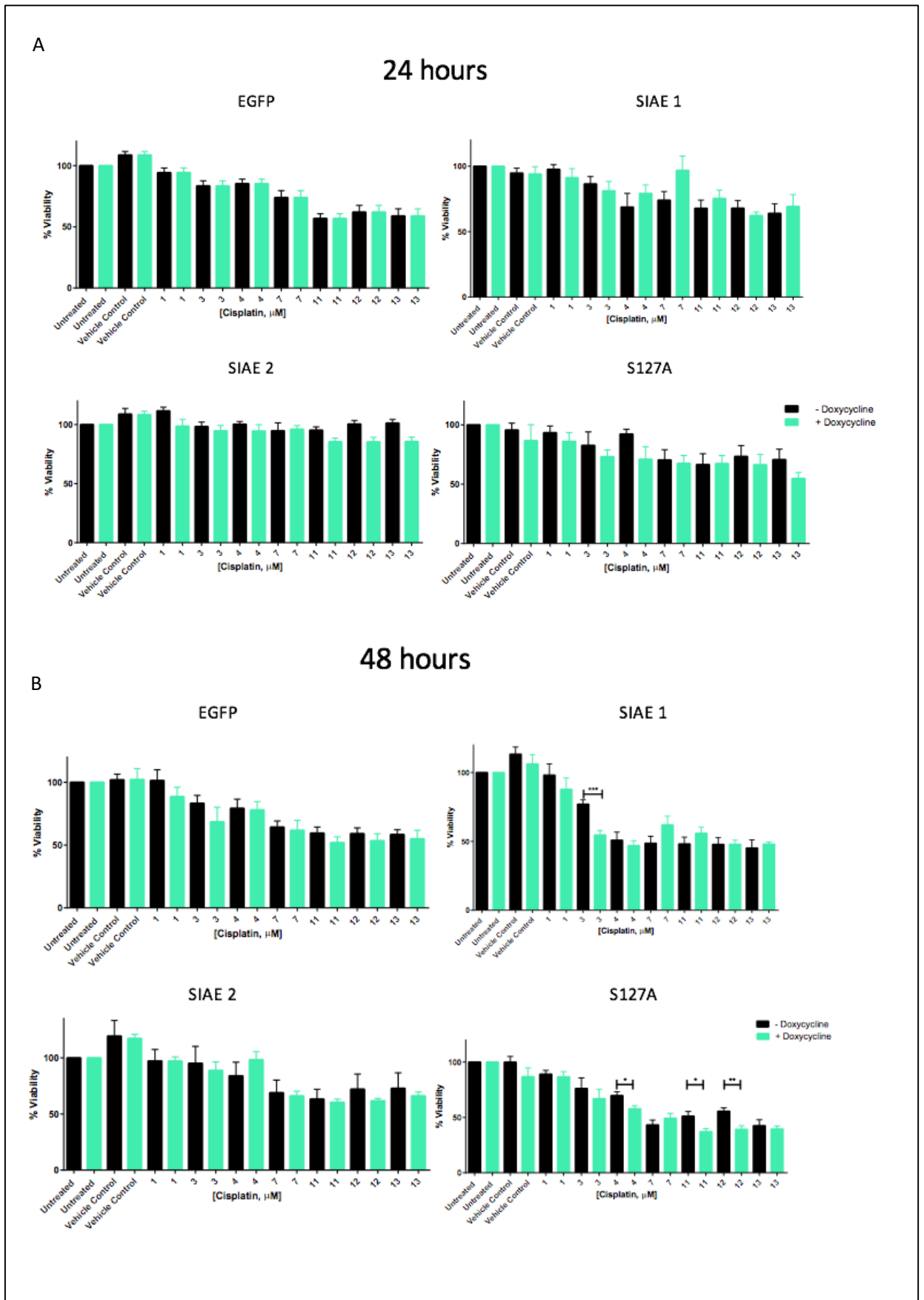
3.6.2 SIAE overexpression in conjunction with current chemotherapeutics

The effects of aggressive treatment of medulloblastoma on the developing brain often result in life-long treatment induced side effects such as neurocognitive deficits and endocrine disorders (Millard & De Braganca 2015). It may provide benefit to patients if the dose of chemotherapy could be lowered, without compromising survival. We therefore examined if SIAE overexpression could make RES256 cells more sensitive to chemotherapeutics in either a synergistic or additive way. Two drugs that are commonly used in medulloblastoma treatment regimens were chosen for testing, cisplatin and etoposide.

Etoposide is a drug that prevents transcription and DNA replication in a cell-cycle dependent manner. It works via inhibition of topoisomerase II. Topoisomerase II is an enzyme that unwinds DNA to allow transcription and DNA replication by causing transient double strand DNA breaks. These breaks relieve the tension on DNA generated by DNA polymerase. Etoposide prevents the re-ligation of the double strand DNA breaks by topoisomerase II. The double strand DNA breaks are maintained with drug binding and this causes apoptosis as transcription and replication of DNA cannot take place. The mechanism of action is described in more detail in chapter 2.

Cisplatin was also used to determine if SIAE overexpression sensitised RES256 cells to treatment. Cisplatin is a cell-cycle non-specific DNA alkylating drug that causes DNA adducts (mostly) between guanine residues. This causes apoptosis through direct DNA damage, as well as binding and recruiting proteins that generate kinks in the DNA helix. These kinks prevent any further transcription or replication of the DNA. The mechanism of action is further described in chapter 2.

In order to test our hypothesis that SIAE overexpression makes RES256 cells more susceptible to cell death when treated with etoposide or cisplatin, cells were treated with a range of concentrations of drug (or vehicle control) in the presence and absence of doxycycline. Cells were pre-treated for 48 hours with (or without) doxycycline to allow gene expression to be induced before the chemotherapeutic was added. Doxycycline was maintained in the media throughout the experiment where appropriate. MTS assays were then carried out after 24, 48 and 72 hours after treatment to determine if treatments caused a reduction in cell viability. Western blots were carried out in parallel to confirm SIAE and SIAE-S127A protein expression throughout the experiment. Data for each clone and time point is shown in figure 3.24 for cisplatin and 3.25 for etoposide.



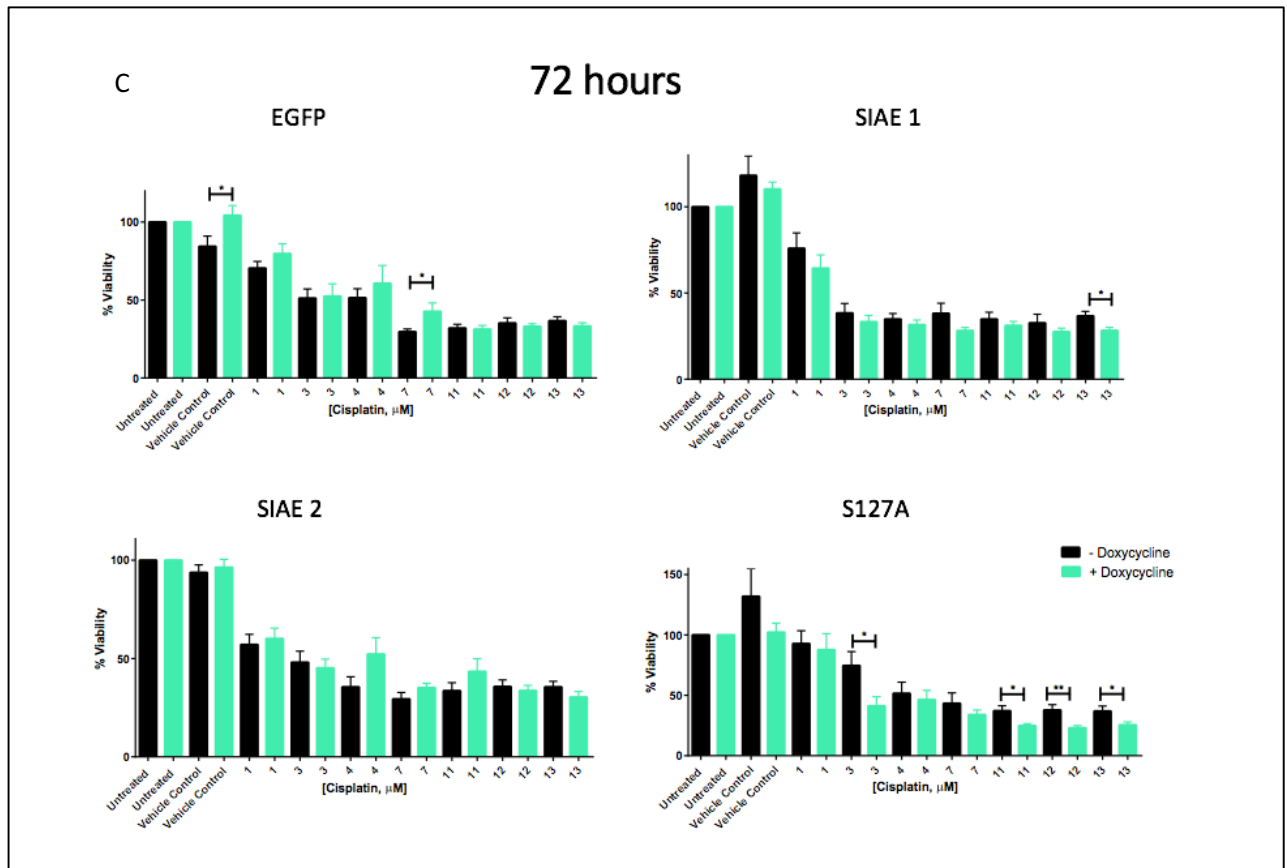
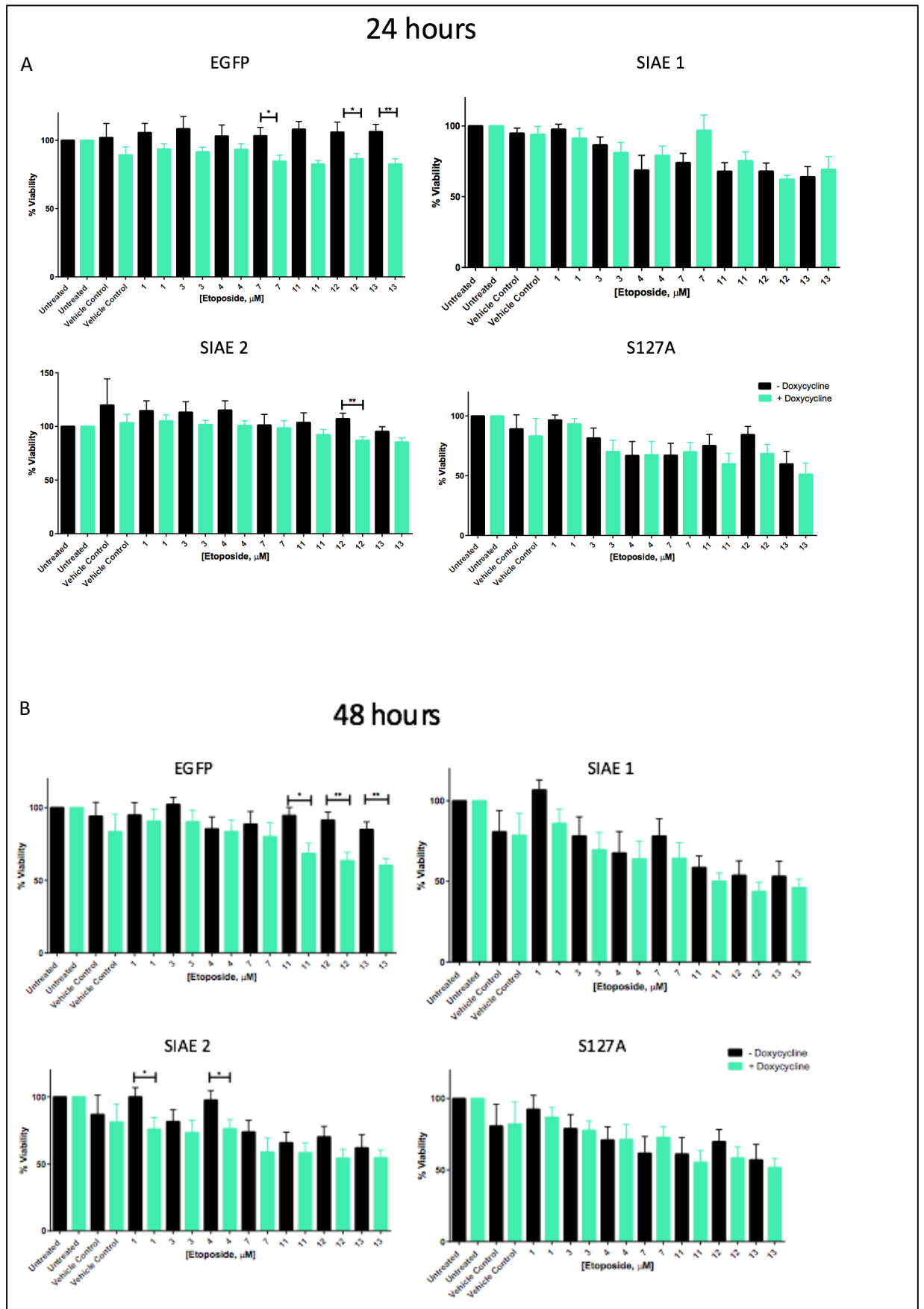


Figure 3.24 RES256 clones are treated with cisplatin after induction of gene expression using doxycycline. (A) 24 hour treatment with cisplatin shows that no change in viability is seen with induction of gene expression in any of the four clones. (B) 48 hour treatment with cisplatin shows no changes in viability with expression of EGFP. A significant decrease in viability was seen with 3 μ M cisplatin treatment in SIAE clone 1. This effect was not seen with increased concentrations of cisplatin, nor was it seen in SIAE clone 2. The catalytic mutant S127A interestingly showed a significant decrease in cell viability when treated with 4, 11 and 12 μ M cisplatin. (C) 72 hour treatment with cisplatin showed a significant increase in cell viability in vehicle control treated and 7 μ M treated cells EGFP expressing cells. The reason for this increase in cell viability is unknown. Wild-type SIAE expressing clone 1 showed only a significant reduction in cell viability with 13 μ M treatment with cisplatin but this effect was not seen in SIAE expressing clone 2. Once again the catalytic mutant S127A shows a significantly reduced cell viability with 3, 11, 12 and 13 μ M cisplatin treatment. (* $p < 0.05$; ** $p < 0.01$; *** $p < 0.001$) data presented as mean \pm SEM Data analysed by unpaired two-tailed t-test using GraphPad Prism 6 software $n = 3$



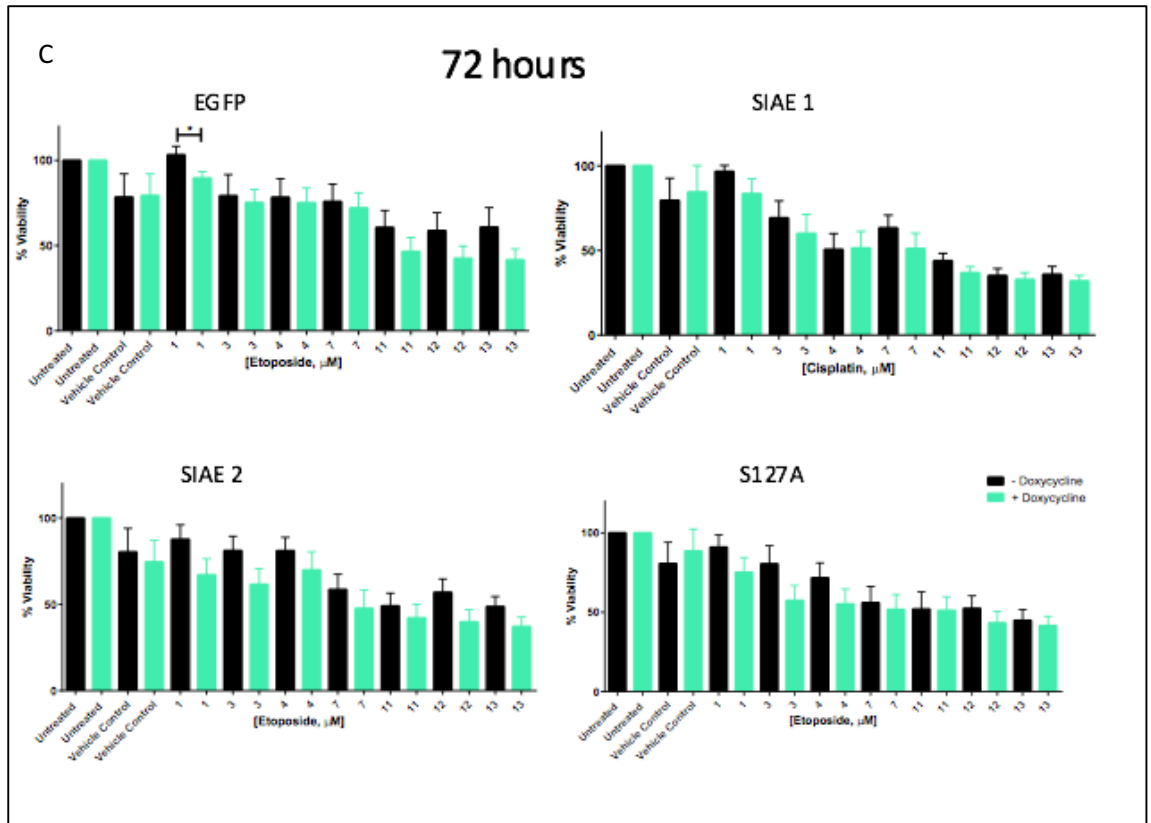


Figure 3.25 RES256 clones are treated with etoposide after induction of gene expression using doxycycline. (A) 24 hour treatment with etoposide shows no significant changes in cell viability in any of the four clones except EGFP expressing cells treated with 1 μ M etoposide, this effect however is not maintained with increasing concentrations of drug. (B) 48 hour treatment with etoposide shows significant decreases in viability in EGFP expressing clones treated with 11, 12 and 13 μ M etoposide. No significant decreases in viability was seen with induction of SIAE expression in clone 1. However, in clone 2 there were significant decreases in viability when cells were treated with 1 and 4 μ M etoposide. This effect was not maintained with increasing concentrations of etoposide. The catalytic mutant S127A showed no significant decreases in cell viability when treated with etoposide. (C) 72 hour treatment with etoposide showed no significant changes in cell viability in any of the four clones except EGFP expressing cells treated with 1 μ M etoposide, however this was not maintained with increased concentrations. (* $p < 0.05$; ** $p < 0.01$) data presented as mean \pm SEM Data analysed by unpaired two-tailed t-test using GraphPad Prism 6 software $n=3$

Cisplatin did not significantly reduce RES256 cell viability with induction of empty vector control expression, nor with SIAE wild-type or mutant expression at 24 hours (figure 3.24A). After 48 hours of cisplatin treatment there was a significant reduction in viability with 3 μM cisplatin in wild-type SIAE clone 1 ($p < 0.001$) but this effect was not concentration-dependent and was not maintained with higher doses (figure 3.24B). There was also a significant reduction in cell viability of S127A expressing cells with cisplatin treatment with 4 and 11 μM ($p < 0.05$; figure 3.24B) and with 12 μM cisplatin ($p < 0.01$; figure 3.24B). After 72 hours of cisplatin treatment there was a significant difference in EGFP viability with vehicle control ($p < 0.05$; figure 3.24C) and 7 μM cisplatin treatment ($p < 0.05$; figure 3.24C). There was also a significant reduction in viability with 13 μM cisplatin treatment in SIAE clone 1 ($p < 0.05$; figure 3.24C). There were also significant differences between 3, 11 and 13 μM cisplatin treatment ($p < 0.05$; figure 3.24C) and 12 μM cisplatin treatment ($p < 0.001$; figure 3.24C) in the SIAE-S127A expressing clone.

Etoposide significantly reduced RES256 cell viability with induction of empty vector control expression at 24 hours of treatment with 7 and 12 μM ($p < 0.05$; figure 3.25A) and with 13 μM treatment ($p < 0.01$; figure 3.25A). In SIAE wild-type expressing cells (clone 2) 12 μM etoposide treatment also had a significant difference with gene expression ($p < 0.01$; figure 3.25A). SIAE 2 and SIAE-S127A mutant expression at 24 hours however were not significantly different (figure 3.25A). After 48 hours of etoposide treatment there was a significant reduction in viability with 11 μM etoposide in EGFP expressing clones ($p < 0.005$; figure 3.25B) and with 13 μM treatment ($p < 0.01$; figure 3.25B). There was also a significant reduction in cell viability with etoposide treatment at 1 and 4 μM ($p < 0.05$; figure 3.25B).

After 72 hours of cisplatin treatment there was a significant difference 1 μ M etoposide treated cells ($p < 0.05$; figure 3.25C)

Together this suggests that SIAE expression may have an effect on cell survival when treated with cisplatin and etoposide, particularly with 48 and 72 hr treatments. This data will be analysed further in section 3.6.3 to see if there is a change in IC_{50} with treatment of cisplatin or etoposide and induction of gene expression, particularly as (although not always significant) there is a general trend for a reduction of viability with induction of gene expression at these time points.

3.6.3 Changes in IC_{50} with chemotherapy treatments

As chemotherapy treatments appeared to have significant effects on cell viability at 48 and 72 hours with induced gene expression (figures 3.24 and 3.25) we examined if there were significant changes in IC_{50} with treatment. We kept in mind that there was a general trend towards reduced cell viability with induction of gene expression and therefore hypothesised that the IC_{50} s may reduce with induction of expression. The IC_{50} is the concentration of (inhibitory) drug (or antagonist) required for a 50 % reduction in response. In this case the concentration of chemotherapeutic required for a 50 % reduction in cell viability. IC_{50} data for each time point and clone shown in figures 3.26 and 3.27 can be found in appendix 7.

Cisplatin IC_{50} s were determined at each time point and it was shown to only significantly affect the mutant SIAE-S127A clone at 48 hours of treatment, significantly reducing the IC_{50} from 4.1 (± 0.6) to 3.1 (± 0.5) μ M ($p < 0.05$; figure 3.26B). Data is normalised and constrained to a minimum and maximum response to cisplatin as defined by controls. This effect on IC_{50}

however was not present with 24 hr treatment (figure 3.26A) nor was it maintained with prolonged treatment (72 hr) (figure 3.26B).

When etoposide IC_{50} s were determined there was only a significant difference after 72 hr treatment. In SIAE clone 2 there was a reduction in the IC_{50} from 5.1 (± 1.3) to 1.9 (± 0.9) μM ($p < 0.001$; figure 3.27A) This difference in response however was not seen with induction of expression in SIAE clone 1, nor EGFP expression, nor the catalytic mutant. This effect on IC_{50} however was not present with 48 hr treatment (figure 3.27A; figure 3.27B). A summary of all IC_{50} data can be found in appendix 7.

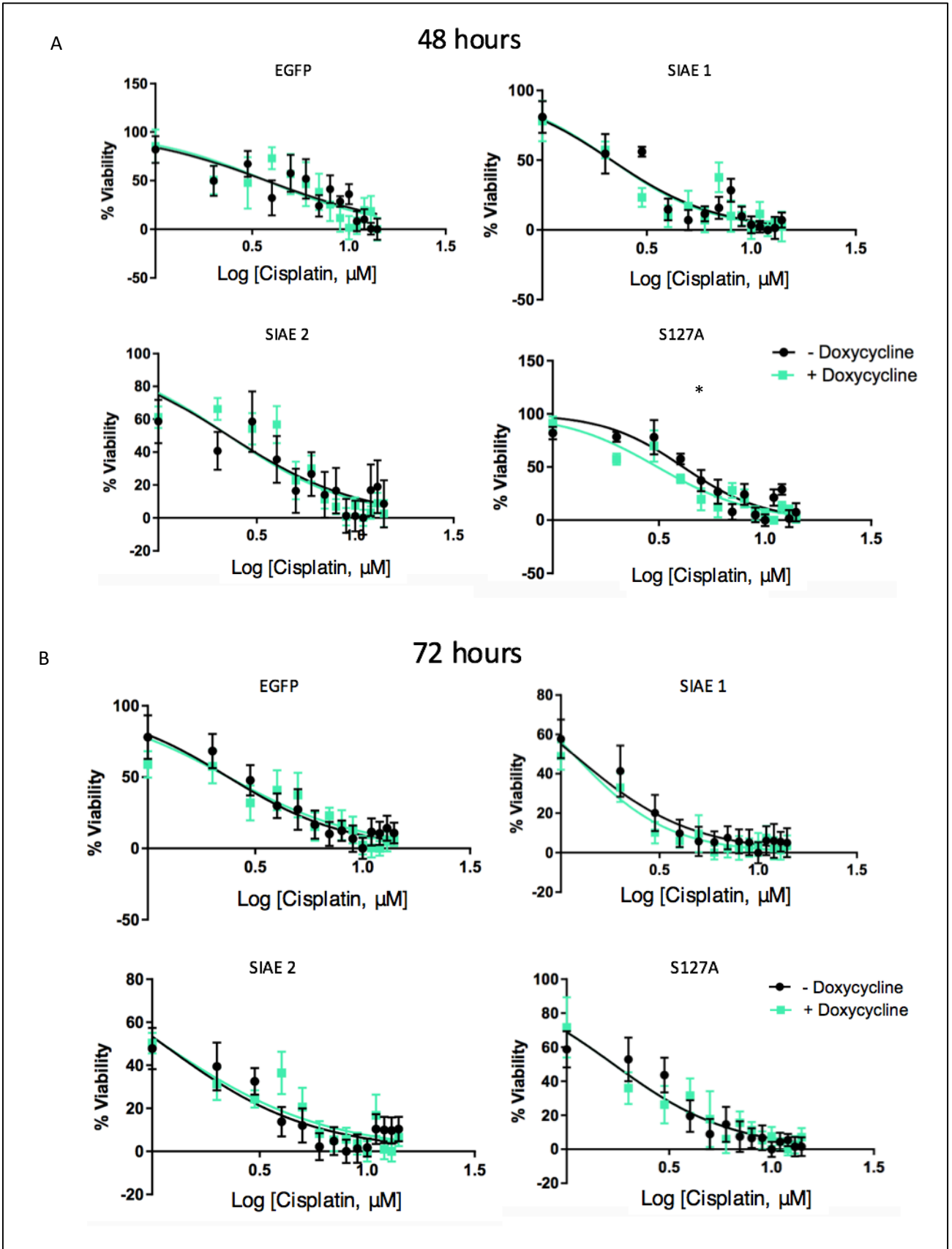
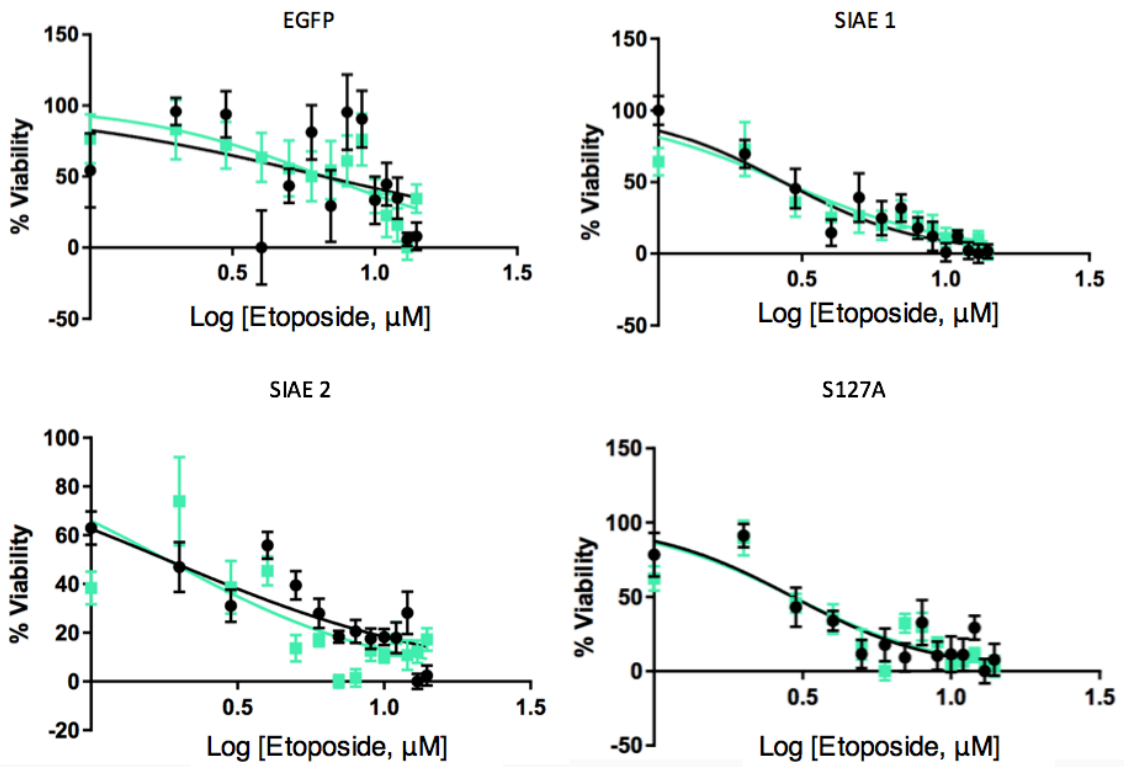


Figure 3.26 Dose-response of inducible RES256 clones to cisplatin treatment. (A) 48 hours after treatment of cisplatin IC₅₀s remain the same between each clone when gene expression is off (black) and when expression is induced with doxycycline treatment (green) except in the catalytic mutant S127A where expression of mutant protein reduces the IC₅₀ significantly. (B) 72 hours after treatment of cisplatin no significant differences are seen when protein expression is induced with doxycycline treatment. Data analysed using the sigmoidal dose-response EC50 comparison using constrained and normalised data by GraphPad Prism 6 software data presented as mean ±SEM (* p<0.05) n=3

A

48 hours



B

72 hours

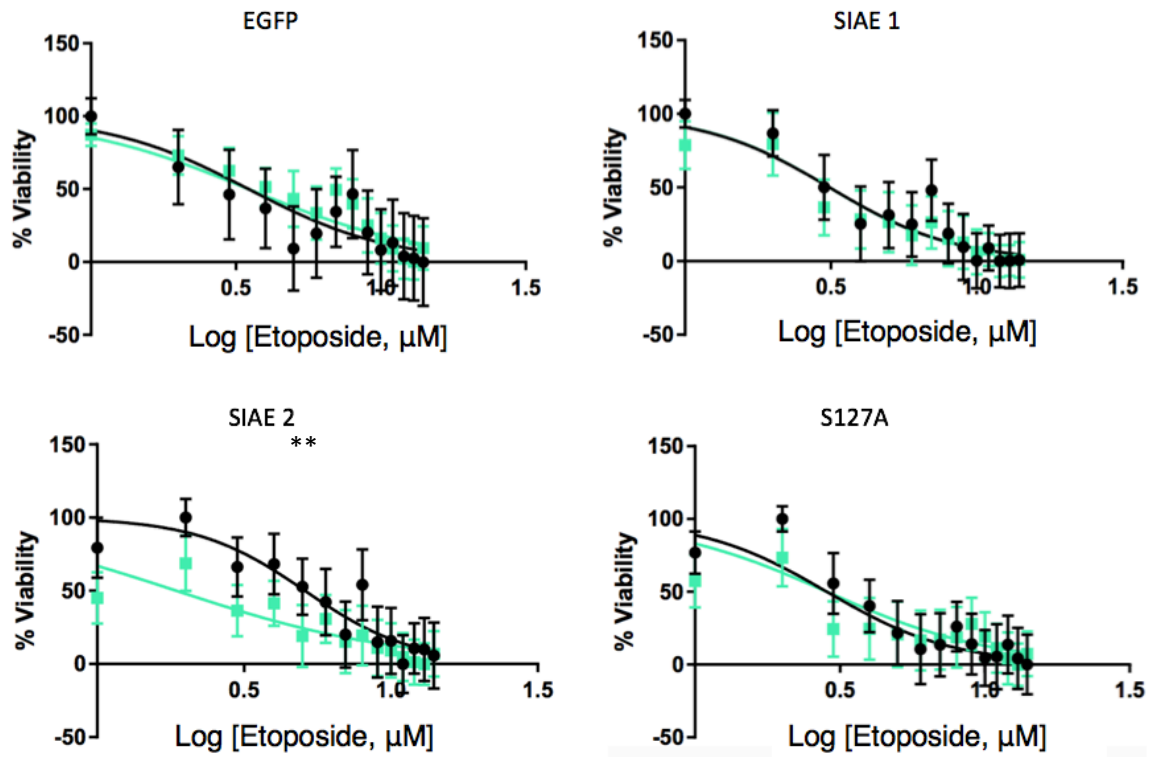


Figure 3.27 Dose-response of inducible RES256 clones to etoposide treatment. (A) 48 hours after treatment of etoposide IC₅₀s remain the same between each clone when gene expression is off (black) and when expression is induced with doxycycline treatment (green) (B) 72 hours after treatment of etoposide no significant differences are seen when protein expression is induced with doxycycline treatment in any of the clones except SIAE clone 2 where the IC₅₀ is significantly reduced with induction of protein expression (green). Data analysed using the sigmoidal dose-response EC50 comparison using constrained and normalised data by GraphPad Prism 6 software data presented at mean ±SEM (p<0.01) n=3**

4 Discussion

4.1 Introduction

The ganglioside acetylation pathway appears to be atypically expressed in medulloblastoma tissues and cell lines. The expression of the acetylation pathway appears to be in favour of the acetylated form of GD3, GD3^A. In medulloblastoma subgrouped tissue samples the expression of Cas1 and SIAE appear to be regulated in order to support our hypothesis that this balance is in favour of GD3^A. The expression of the acetylated ganglioside also appears to correlate with M stage as the highest levels of expression of the hypothesised acetylation enzyme Cas1 are seen in the highest M stage in this sample set (M₃). The expression of the human endogenous deacetylation enzyme SIAE was also shown to be lowest in the higher M stage subgroups which further indicates that the expression of GD3^A is likely to be highest in this subset of patients.

When explored in medulloblastoma cell lines, the expression of GD3 and GD3^A was seen at high levels. The expression of these two gangliosides is in favour of GD3^A. In SIAE over-expression studies the highest expresser of GD3^A, RES256 was transfected with inducible constructs. SIAE over-expression, but not expression of the catalytic mutant nor the empty vector control, led to the depolarisation of the mitochondrial membrane potential. The expression of SIAE also caused the RES256 cells to be more susceptible to treatment with etoposide but not cisplatin, chemotherapeutics commonly used to treat medulloblastoma. In light of this work, the GD3 acetylation pathway may have an important role in maintaining viability of RES256 cells. As a proof of principle study SIAE over-expression appears to influence the mitochondrial membrane potential, and response to the cell-cycle specific drug etoposide.

4.2 The GD3 acetylation pathway in neoplastic disease

The GD3 acetylation pathway has previously been described as a pathway necessary for the development of the brain (Mendez-Otero & Santiago 2003; Liang et al. 2011; Yu et al. 2004) and in malignancies such as high grade gliomas (Birks et al. 2011). Of particular interest to this project is GD3's role in the developing cerebellum. GD3 is expressed by the neuronal granule precursor cells of the developing cerebellum where it guides their migration (Goldman & Reynolds 1996). The granule neuron precursors are a known cell of origin of SHH, group 3 and group 4 medulloblastomas. Upon maturation of the brain, GD3 rapidly accumulates within the supernumary cells where it causes their mitochondrially-mediated apoptosis (Birks et al. 2011; Higgins et al. 2015). After birth, the expression of GD3 is virtually absent (Yu et al. 2012; Yu et al. 2004). In some cancers of neural crest origin, such as high grade gliomas (Birks et al. 2011), melanomas (Ohkawa et al. 2008), and as we show here, in medulloblastomas, GD3 becomes re-expressed. In acute lymphoblastic leukaemia (ALL), high levels of GD3 have been shown to protect from a pro-apoptotic phenotype, due to acetylation of GD3 (GD3^A). GD3^A can protect from GD3-mediated apoptosis and this balance of GD3 and GD3^A is thought to influence cell survival. The expression of GD3 in medulloblastoma has been previously described in little detail, with functional relevance absent (Gottfries et al. 1990).

In other cancers this pathway has proved to be important for cell survival (Mukherjee et al. 2008) (Parameswaran et al. 2013) and invasion (Hamamura et al. 2011; Shibuya et al. 2012; Ohkawa et al. 2015). In ALL, the expression of *O*-acetylated sialic acids such as GD3^A were shown have enhanced expression. This was also reported in melanoma (Ritter et al. 1990), Basalioma (Fahr & Schauer 2001) and breast cancer (Marquina et al. 1996). In a study on

ALL, the balance of activities of the sialic acid *O*-acetyl transferase (SOAT; a family of enzymes in which Cas1 resides), and SIAE were investigated and it was found that SOAT activity was enhanced whereas SIAE activity was reduced (Mandal et al. 2012). This balance of activity in favour of SOAT provides evidence for the preference for acetylation of GD3 by these cells. This acetylation is important as it has been shown to positively correlate with chemo-resistant disease and therefore impacts on patient survival (Giussani et al. 2014).

In glioblastoma multiforme (GBM), the most common and most aggressive neoplastic brain tumour of adulthood, a delicate balance exists between GD3 and GD3^A which influences cell survival. In a study by Birks *et. al*/ transfection of primary and established GBM cell lines with the GD3^A acetyl esterase enzyme haemagglutinin esterase (HE) demonstrated a reduction of viability when cleavage of GD3^A occurred (Birks et al. 2011). With cleavage of GD3^A this study also demonstrated a significant increase in GD3 expression (Birks et al. 2011) which leads to the translocation of GD3 to the mitochondrial membranes (Sorice et al. 2012) and ultimately to apoptosis (Malisan & Testi 2002a). One of the problems with using HE is its immunogenicity, something which could be overcome with the use of SIAE, the human endogenous deacetylation enzyme. When high levels of GD3 are expressed, cell viability is maintained by GD3^A expression. This has been shown to occur in several cell lines which can genetically switch on the acetyltransferase machinery, thought to be Cas1 (Chen et al. 2006). When GD3^A is present it has been shown that GD3^A cannot induce mitochondrially-mediated apoptosis and furthermore suppresses the ability of GD3 to induce apoptosis itself (Malisan et al. 2002). GD3^A expression has been shown to protect cells from chemotherapeutic insult, and also from endogenously added GD3, even at very low levels of expression (Kniep et al. 2006). High levels of GD3 are also associated with

increased invasive potential and enhanced malignant properties (Ohkawa et al. 2015). This effect may be due to the auto-acetylation of GD3 to GD3^A through the induction of its own acetylation machinery. As the study by Chen *et. al* exploring GD3 expression in correlation with invasive potential did not explore expression in a manner that was able to differentiate between the two gangliosides, this may be the effect of GD3 itself (Chen et al. 2006).

4.3 Synthesis and turnover of GD3 and GD3^A

The ganglioside synthesis pathways have been previously characterised and summarised (Yu et al. 2004) and the major players in the turnover of the gangliosides have been discovered in recent years. The enzyme that synthesises GD3 is ST8Sia1, the gene that encodes this enzyme is located on chromosome 12 at 12p12.1. In Yu *et. al's* study, it was stated that, assuming the concentration of the substrate of ST8Sia1 (GM3) is in constant supply, the outcome (GD3 expression) is dependent on the enzyme that catalyses its synthesis, and the enzyme that consumes the ganglioside intermediate (Yu et al. 2004). In other words, to increase the expression of the ganglioside GD3, the cell has to express the ganglioside (via ST8Sia1 expression or increased ST8Sia1 activity) but also decrease the expression (or activity) of the enzyme that uses it as a substrate (ST8Sia5).

Another enzyme that regulates this pathway is the human endogenous acetyl-transferase enzyme Cas1, whose encoding gene is located on chromosome 7 at 7q21.3. Cas1 is hypothesised to play a role in the acetylation of GD3 (Arming et al. 2011). There is little known about this enzyme and its roles *in vivo*, however a recent study by (Baumann et al. 2015), showed that knock-down of the Cas1 gene CASD1 using clustered regularly-interspaced short palindromic repeat/ crispr-associated protein (CRISPR/Cas) genome editing, abolished GD3 acetylation in HAP1, HEK293T and CHO cells when cells also

expressed ST8Sia1. This study provides evidence for the involvement of Cas1 in GD3 acetylation.

The final enzyme thought to play a role in the regulation of this pathway is the human endogenous deacetylation enzyme SIAE, whose gene is located on chromosome 11 at 11q24.2. SIAE is known to regulate the expression of GD3 and GD3^A and has been described in acute lymphoblastic leukaemia (ALL) (Mandal et al. 2012). SIAE has been shown to promote survival and drug resistance in ALL (Mukherjee et al. 2008) and in pre-B acute lymphoblastic leukaemia (Parameswaran et al. 2013). In the Parameswaran *et. al* study, the cell surface and intracellular 9-*O*-acetyl groups from sialic acids were de-acetylated using CHE-Fc esterase, sodium salicylate and a 9-*O*-acetyl esterase lentiviral vector described by (Malisan et al. 2002). They confirmed that GD3 deacetylation was occurring and showed that in pre-B acute lymphoblastic leukaemia cells this treatment proved to be lethal (Parameswaran et al. 2013).

4.4 GD3 synthesis enzymes are atypically expressed in medulloblastoma across subgroups and metastatic stages

From this study we show that the enzymes involved in regulation of this pathway are affected at the mRNA level in medulloblastoma tissue using a sub-grouped and M-stage classification approach.

When the mRNA expression of ST8Sia1 was investigated using a bioinformatics approach (figure 3.2A), the expression was found to be significantly down-regulated in comparison to non-neoplastic foetal and adult brain controls ($p < 0.0001$). Interestingly, the expression of ST8Sia1 is not significantly different between non-neoplastic foetal and adult brain. This

is interesting because it is widely reported that GD3 expression is tightly developmentally controlled and that GD3 expression is virtually absent in the adult brain (Yu et al. 2012). This can be explained as GD3 can be used as an intermediary ganglioside that is converted into the more complex gangliosides that are known to be expressed in the adult brain (Yu et al. 2004). When the samples were analysed according to molecular subgroup (figure 3.4A) there was a significantly lower expression of ST8Sia1 found in the best prognosis subgroup, WNT, compared to SHH and group 4 ($p < 0.0001$). This difference in expression may suggest that the WNT subgroup has the lowest GD3 expression. This has some relevance to a study carried out in glioblastoma multiforme cell lines which targeted co-expressed GD3^A and neuron-gial 2 (NG2) with an antibody conjugated toxin (Higgins et al. 2015) as co-expression of GD3^A and NG2 had previously been reported (Chekenya et al. 1999). In another study a relationship between GD3^A (which correlated with invasive potential) and NG2 (which correlated with high proliferation) was shown to be inversely correlated i.e. cells that expressed high levels of GD3^A expressed very low levels of NG2 and vice versa (Chekenya & Pilkington 2002). As GD3 is known to be correlated with invasive potential in gliomas (Ohkawa et al. 2015) and the WNT subgroup is very rarely metastatic (Taylor et al. 2012), this could provide further evidence to support the hypothesis that GD3 expression is low in this subgroup. In work done by Dr Taylor's group in Toronto, appendix 8, the mRNA expression of NG2 was found to be highest in the WNT subgroup which also supports this data, implying that GD3^A expression is likely to be lowest in this subgroup. On the contrary, the most metastatic subgroup, group 3, did not have the highest expression of ST8Sia1. Group 3 expression was found to be significantly lower than the rarely metastatic SHH subgroup ($p < 0.0001$), which had the highest expression of ST8Sia1. The expression of ST8Sia1 was similar in group 3 and group 4 samples.

When the expression of ST8Sia1 was examined at the metastatic stage (figure 3.7A), expression was low overall but highest expression was seen in the M₃ stage of disease. This correlates with GD3's role in invasion however this data was not significant, and as we found ST8Sia1 expression to be low at the mRNA level this led us to believe that ST8Sia1 may not be the only enzyme involved in the expression of GD3. As suggested by Yu (2004) the expression of the enzyme that uses GD3 as a substrate was also investigated.

In support of the hypothesis that GD3 expression is high, we would expect the expression of ST8Sia5 to be low as this would not further convert GD3 into the more complex gangliosides summarised in figure 1.5. The expression of ST8Sia5 was found to be higher in the WNT and SHH subgroups which are the least invasive (figure 3.4B), suggesting that the expression of GD3 in these subgroups may be converted into the GD2 or GT3 gangliosides (figure 3.3). The lowest expression of ST8Sia5 was seen in the more metastatic subgroups 3 and 4, suggesting that the expression of GD3 in these subgroups may be higher as it is less likely to be converted to GD2 or GT3 (figure 3.4B).

When the expression of this enzyme was explored at the M stage (figure 3.7B), the expression was expected to be lowest in the most metastatic subgroup M₃ as this would correlate with the highest expected GD3 expression level. ST8Sia5 was found to be significantly lower in M₃ compared to M₀ ($p < 0.05$) in support of the hypothesis.

4.4.1 Bioinformatics summary of the GD3 synthesis enzymes

Taken together the bioinformatics data for ST8Sia1 and ST8Sia5 suggest that the expression of GD3 is higher in the most metastatic subgroups, group 3 and group 4. The expression of ST8Sia5 suggests less of the expressed ganglioside could be converted to GD2 or GT3 despite the expression of ST8Sia1 being low in these subgroups. The expression of GD3 is

also suggested to be highest in the M₃ stage of disease; this is due to the lowest expression of ST8Sia5 suggesting a low level of GD3 would be converted into downstream gangliosides. The activity of the enzymes must also be considered however to fully determine this to be the case, but due to the fact that these samples are of limited size and that samples are not metabolically active this cannot be determined. The expression of the gangliosides cannot be determined directly using samples from the bioinformatics approach as this tissue was used for microarray and sample processing (paraffin embedding) is incompatible with ganglioside analysis (Debarbieux et al. 2009; Schwarz & Futerman 1997).

4.5 GD3 and GD3^A turnover enzymes are atypically expressed in medulloblastoma across subgroups and metastatic stages

If the expression of GD3 is considered to be present, then the two major enzymes that control the processing of GD3 to GD3^A are Cas1 and SIAE. The expression of Cas1 was found to be significantly up-regulated in medulloblastoma tissue compared to non-neoplastic foetal and adult brain controls ($p < 0.0001$) (figure 3.2B). The high expression of Cas1 suggests that there could be high expression of GD3^A in these tumours. When medulloblastoma tissue samples were subgrouped, the expression of Cas1 was shown to be lowest in WNT and SHH subgroups which are rarely metastatic, suggesting they may express less GD3^A (figure 3.6A). Cas1 expression was significantly lower in the WNT subgroup compared to group 3 ($p < 0.05$; figure 3.6A) and group 4 ($p < 0.001$; figure 3.6A) this also supports the hypothesis that the least metastatic subgroup expresses less GD3^A than the more metastatic subgroups. Expression was significantly lower in the SHH subgroup compared to group 4 ($p < 0.0001$; figure 3.6A) but not group 3. The highest levels of expression of Cas1 were seen in groups 3 and 4 suggesting that there may be the highest

levels of GD3^A in these subgroups, if Cas1 is the enzyme responsible for acetylation of GD3. Group 4 samples expressed the most Cas1 despite not being the most metastatic subgroup, but this may be promising as group 4 is the most common subgroup. If there is a high level of GD3^A expression in group 4, the most common subgroup, if deacetylation of GD3^A is a good therapeutic target, then this treatment could be relevant to a significant proportion of patients. While not being the most metastatic subgroup, a subset of group 4 patients do present with metastatic disease (Taylor et al. 2012).

When expression of Cas1 was characterised by metastatic stage, increasing expression correlated with increasing M stage (figure 3.8A). There was significantly higher expression of Cas1 in M₃ samples compared to M₀ (p<0.05) suggesting that if Cas1 is the enzyme responsible for GD3 acetylation, that GD3^A expression may be higher in the M₃ subgroup. This once again supports previous data in other cancers that GD3^A expression correlates with invasive potential (Hamamura et al. 2011; Shibuya et al. 2012).

Further characterisation of this pathway involved the human endogenous deacetylation enzyme SIAE. This enzyme was an important discovery to the regulation of this pathway and also its use as a therapeutic target. Previous studies involving deacetylation of GD3 have utilised enzymes that are not endogenous, such as the influenza enzyme haemagglutinin esterase used by Birks *et. al* for a study on glioblastoma multiforme (Birks et al. 2011). This enzyme proved to be highly immunogenic, since it was not human in origin, and therefore would not be able to be used in the clinic. This study, if successful, could overcome this problem, as the human endogenous enzyme would not be immunogenic.

The expression of SIAE was significantly down-regulated in medulloblastoma tissue compared to non-neoplastic foetal and adult brain controls ($p < 0.0001$) (figure 3.2C). This suggests that the expression of GD3^A would be lower in medulloblastoma compared to non-neoplastic brain. Interestingly there was also a significantly higher expression level of GD3^A in adult non-neoplastic brain compared to foetal non-neoplastic brain ($p < 0.05$; figure 3.2C), suggesting a higher level of GD3^A in the adult brain compared to foetal brain, despite reports of virtually absent GD3^A expression in the developed nervous system (Svennerholm et al. 1989). This data may show a limitation of this method, that mRNA does not correlate with protein expression, or that expression of the SIAE enzyme does not correlate with activity. Highest expression of SIAE was seen in the WNT subgroup, which expressed SIAE significantly more than SHH ($p < 0.0001$; figure 3.5B), group 3 ($p < 0.02$; figure 3.5B) and group 4 subgroups ($p < 0.0001$; figure 3.5B). As the WNT subgroup is the least metastatic this supports the hypothesis that GD3^A expression is lower in this subgroup along with the SHH subgroup. The lowest level of expression was seen in the SHH subgroup which expressed SIAE significantly less than group 3 ($p < 0.05$; figure 3.5B) and group 4 ($p < 0.01$; figure 3.5B). From this data, the expression of GD3^A could be expected to be highest in the SHH subgroup and lowest in the WNT subgroup.

When SIAE expression was characterised by metastatic stage (figure 3.8B), there was significantly higher expression in the M₀ and M₁ subgroups compared to M₃ ($p < 0.05$ and $p < 0.02$ respectively). From this data, it would suggest that there could be more GD3^A in the more metastatic subgroup M₃ compared to M₀ and M₁ as there is a lower expression of SIAE in these subgroups.

4.5.1 Bioinformatics summary of the GD3 and GD3^A turnover enzymes

In 2012, the current consensus of medulloblastoma molecular subgroups was published (Taylor et al. 2012), which linked together the molecular subgroups and genetic alterations. The genes encoding ST8Sia5 and Cas1 are located on 18q21.1 and 7q21.3 respectively. It is known that there are gains in both of these chromosomes in group 3 and group 4 subgroups which may suggest that expression of these enzymes are up-regulated in these subgroups. This is only supported by bioinformatics data for Cas1, which shows an increase of expression in these subgroups. The bioinformatics data for ST8Sia5 shows it is actually significantly down-regulated in these subgroups, suggesting a low level of expression.

Taken together this data suggests that the GD3 acetylation pathway is in favour of GD3^A in the most metastatic subgroups and in the worst prognosis subgroups group 3 and group 4 at the mRNA level.

4.6 GD3 and GD3^A are re-expressed by medulloblastoma cell lines

In the medulloblastoma cell lines used in this study (RES256, UW402 and CHLA-01-Med), there was a high level of both GD3^A and GD3 within the cells (figure 3.9). Flow cytometry data showed an average expression of GD3^A for each cell line to be 85.4, 74.4 and 79.4 % respectively and the expression of GD3 was 56.7, 61.3 and 45.1 % respectively. This supports the hypothesis that GD3^A is protecting the cells from GD3-mediated apoptosis. Despite reports that GD3^A can protect from GD3-mediated apoptosis at low levels (Kniep et al. 2006) we found similar levels of both gangliosides.

On the cell surface, expression of GD3^A by RES256, UW402 and CHLA-01-Med cell lines was 36.0, 17.5 and 0.6 % respectively, whereas GD3 expression was 55.0, 62.2 and 77.1 %

respectively. It has been shown that GD3^A can protect from GD3 mediated apoptosis (Malisan et al. 2002; Chen et al. 2006; Mukherjee et al. 2008). In this instance, if GD3 is not capable of collapsing the mitochondrial membrane potential, it can be utilised on the cell surface and co-localise with other factors such as Yes kinase and platelet-derived growth factor receptor alpha (PDGFR α) where it can increase the invasive potential of cells (Ohkawa et al. 2015). GD3 requires internalisation to become acetylated to GD3^A (Schauer 2004; Malisan & Testi 2002a), this may explain why so little GD3^A is expressed on the cell surface.

Only one of these cell lines has a published known subgroup, CHLA-01-Med is known to be a group 4 medulloblastoma (Erdreich-Epstein et al. 2014). It can be speculated that the RES256 cell line belongs to either the SHH or WNT subgroup as this cell line harbours a *TP53* mutation (Zhukova Thesis, 2012). *TP53* mutations are enriched in WNT patients (16%) and SHH patients (21%), and these mutations are virtually absent in group 3 and group 4 tumours ($p < 0.001$) (Zhukova et al. 2013). The absence of *TP53* mutations in groups 3 and 4 is because of the location of the *TP53* gene on the short arm of chromosome 17. Chromosome 17p is commonly lost in these subgroups, and there are gains in the long arm, as they harbour isochromosome 17q (i[17q]) (Taylor et al. 2012). The UW402 cell line is known to be *TP53* wild-type, and its subgroup is currently unknown (Zhukova Thesis, 2012). The high levels of expression support the hypothesis that the balance of these two gangliosides is in favour of GD3^A and is shown by flow cytometry. With regard to subgroup affiliation, there is no significant difference between GD3 and GD3^A expression between the cell lines despite the fact that RES256 and CHLA-01-Med probably belong to different

subgroups. The subgrouping of these cell lines is currently being determined by Dr. David Jones, Heidelberg.

The sub-cellular localisation of the two gangliosides is well characterised (Tempera et al. 2008), however the localisation of the gangliosides is very sensitive to fixation method (Debarbieux et al. 2009; Schwarz & Futerman 1997) and therefore no conclusions will be drawn from these data except that the antigens are found on both the cell surface and intracellularly and concur with flow cytometry data (figure 3.10).

Immunofluorescent studies of wild-type P5 and P60 mouse cerebellums demonstrated that there was a high level of GD3 and GD3^A expression in the internal granule layer (IGL) (figure 3.11A). Interestingly, group 4 disease is thought to arise from cells in the IGL in the >20 week foetal cerebellum (World Health Organisation 2007). The P5 cerebellum represents a 32-36 week brain and therefore this may provide evidence for group 4 tumours arising from GD3 and GD3^A positive cells (Semple et al. 2013). It has also been shown in other studies that GPCs express GD3^A in the external granule later (EGL) in the P1 mouse, representing a 23-32 week human brain, this provides further evidence for expression of both gangliosides in the areas of the cerebellum that give rise to group 4 disease at this time of development (Santiago et al. 2004). The P60 mouse cerebellum confirms that expression of these gangliosides is absent in the adult mouse brain (representing a 20+ year old human adult) (figure 3.10B) (Semple et al. 2013). The absence of GD3 and GD3^A expression in the P60 brain is in agreement with the literature stating that the expression of these gangliosides is virtually absent in the adult brain (Svennerholm et al. 1989). In order to provide further evidence studies with mice at each stage of development where each subgroup is thought to arise would be needed. Lineage of the positive cells should also be

carried out in further work. Another method to confirm the link between GD3 and GD3^A expression in cells of origin for this disease should utilise medulloblastoma mouse model tissue for staining with GD3 and GD3^A antibodies.

From an anatomical perspective it is quite difficult to determine likely subgroups arising from GD3 and GD3^A positive cells. For example, the WNT subgroup arises from the fourth ventricle and often infiltrates the brain stem and the SHH subgroup often arises in the cerebellar hemispheres (World Health Organisation 2007). From this study it was not possible to determine precise locations from the tissue available but would be an interesting avenue for further work. This study would require tissue from appropriate developmental stages of the brain in order to determine precise locations of GD3 and GD3^A positive staining, if any.

4.7 Over-expression of SIAE in RES256 cells

The next stage was to select a cell line for overexpression of SIAE, as the involvement of Cas1 is speculated, it was not deemed appropriate for knock-down studies. As there were similar levels of GD3^A in the three cell lines investigated, the cell line with the highest percentage of intracellular GD3^A expression, RES256 was chosen. Many attempts at stable cell lines using pEGFP-N3, pEGFP-N3-SIAE and pEGFP-N3-SIAE-His constructs were carried out, with only successful colony selection and expansion occurring in the empty vector control cell line RES256 pEGFP-N3. We therefore concluded that SIAE expression may be toxic to the cells and continued with transient expression of SIAE using the same constructs (appendix 1). This also proved inconclusive due to poor transfection efficiency (appendix 2), there was no change in either the expression of GD3 or GD3^A, and when the collapse of the mitochondrial membrane potential was explored, there was also no change in

polarisation (data not shown). It is important to note that two isoforms of SIAE exist, the lysosomal variant (variant 1), and the cytosolic variant (variant 2). It is generally accepted that the cleavage of 9-*O*-acetylated sialic acids are cleaved by the lysosomal isoform of SIAE which is transported into the cytoplasm (Mandal et al. 2012) and it has been demonstrated by (Orizio et al. 2015) that the cytosolic form of this enzyme has not been isolated in human tissue. Therefore, the lysosomal isoform of SIAE was used for overexpression studies.

4.8 An inducible system approach to SIAE over-expression reveals changes in GD3 expression

An inducible system approach was used to over-express SIAE that allowed cells to be cultured in the absence of expression from the construct, maintaining viability. In order to screen the initial expression of the construct pCMV-TetOn3G, a Tet-responsive luciferase assay was used and showed that this protein was capable of inducing expression of luciferase and therefore was suitable for induction of SIAE expression (appendix 4). The next round of screening involved the Tet-responsive constructs containing the genes of interest, EGFP and either SIAE or SIAE S127A. The SIAE S127A expressing cell line contains a gene with a mutation in the catalytic triad of the SIAE enzyme. This was discovered to have very little catalytic activity by (Surolia et al. 2010; Orizio et al. 2015; Chellappa et al. 2013) and was used as a control.

When cells were isolated and tested for expression, cells were treated with doxycycline, initiating expression of SIAE by the construct. Screening of these constructs was carried out by immunocytochemistry. This approach utilised the induction of EGFP expression (figure 3.16). This EGFP was not a fusion protein as the construct contained an internal ribosomal entry site, this was important to ensure no steric hindrance occurred when the enzyme

attempted to bind substrate (GD3^A). As the EGFP gene was cloned into multiple cloning site 2 of this plasmid the expression was poor and lost rapidly. This phenomenon is known in the literature (Mizuguchi et al. 2000; Bouabe et al. 2008) and allowed screening of constructs but no downstream interference with the spectra of antibodies or dyes used in subsequent assays.

SIAE expression was assessed by Western blot analysis and confirmed that gene expression was not leaky (figure 3.17). The appearance of two bands on each blot showed the fully glycosylated active form of SIAE at 62 kDa (Orizio et al. 2015), and a 32 kDa protein which possibly results from cleavage of SIAE.

When SIAE gene expression was induced with the addition of doxycycline, GD3^A expression did not significantly decrease as expected (figure 3.22A). This may be due to the time point assayed (48 hours as suggested by the manufacturer of the inducible system constructs). The turnover of GD3 autoacetylation is thought to be 6 hours (Chen et al. 2006). Further time points were assayed and SIAE over-expression confirmed (data not shown). The 48 hour time point was used for further experiments however as the mitochondrial membrane potential collapse was seen at this time. This assay had short-comings as we could not assess enzymatic activity of SIAE directly. Although the fully glycosylated 'active' form of protein was seen by Western blot analysis, we could not confirm that this enzyme was an active esterase. Despite this there was a concomitant significant increase in the expression of GD3 ($p < 0.05$; figure 3.22B), so one can assume that the esterase activity of SIAE is present (figure 3.22B). The lack of GD3^A cleavage can be explained by the auto-acetylation phenomenon of GD3 which has been demonstrated using exogenously added GD3 (Chen et al. 2006). If GD3 does induce its own acetylation machinery, the expression of Cas1 could

be explored in further studies to determine its involvement in this pathway.

When the GD3 and GD3^A expression was investigated in empty vector control cells (EGFP) there was a significant decrease in the expression of GD3^A despite there being no esterase cloned into the plasmid ($p < 0.05$; figure 3.22A). When the expression of GD3 was determined it was shown that there was no significant increase in expression, suggesting that GD3^A deacetylation that did occur should not affect the mitochondrial membrane potential.

In the catalytic mutant SIAE-S127A, there were no significant changes in the expression of either ganglioside, suggesting that there would be no changes in the mitochondrial membrane potential.

4.9 SIAE overexpression collapses the mitochondrial membrane potential in RES256 cells

As high levels of GD3 are known to collapse the mitochondrial membrane potential (Malisan & Testi 2002a), this was explored (figure 3.23). It is also known that these gangliosides exist in balance in order to protect cells from apoptosis (Birks et al. 2011) and therefore the collapse of the mitochondrial membrane potential would only occur if this threshold was reached. Upon induction of SIAE wild-type (clone 1) expression, the mitochondrial membrane significantly depolarised ($p < 0.05$; figure 3.23), demonstrated by the presence an increase of green monomers of JC-1 dye compared to red aggregates. This depolarisation did not occur with the catalytic mutant cell line SIAE-S127A nor did it occur in the empty vector control EGFP. Interestingly the collapse of the membrane potential did not occur in clone 2. However, this clone may reach significance with higher numbers of

replicates. It must also be noted that the collapse of the mitochondrial membrane potential is a transient event and therefore the lack of significant depolarisation seen with SIAE clone 2 may be due to an incorrect time point for this clone to be assayed. Another explanation for this difference in results between clones includes trafficking of GD3 and GD3^A to the cell membrane, a well-known phenomenon (Birks et al. 2011). This experiment also demonstrated flaws, the high levels of depolarisation of the mitochondrial membranes at the start seen in each clone demonstrate that cell-preparation may need to be optimised to get an accurate representation of membrane potentials. It is also clear that to determine cell death, be it by intrinsic or extrinsic apoptosis or autophagy, all of which have been described with regard to GD3's effects (Matarrese et al. 2014; Malisan & Testi 2002a), other means carried out in conjunction with JC-1 assays such as caspase release, cytochrome c translocation assays etc are required.

SIAE has been shown to be a secreted enzyme in its fully glycosylated form (Orizio et al. 2015), conditioned media studies were therefore carried out. Interestingly, the only clone that secreted active enzyme was the catalytic mutant SIAE-S127A cell line (figure 3.18). This is potentially because there was very little 62 kDa protein present when the lysates of SIAE-wild-type cells were analysed. There was however considerably more of the lower molecular weight 32 kDa band seen in the wild-type expressing cells. The 32 kDa cleavage product of SIAE may also have other roles other than acetyl esterase activity, this however would require further investigation to elucidate. To investigate possible identities of the 32 kDa product the human lysosomal SIAE sequence was run through peptide-cutter software to analyse the sequence for cleavage sites. When the sequence was analysed there was only one candidate for cleavage giving rise to these molecular weights that did not disturb

the antibody binding sequence, this candidate was caspase 1. This potential cleavage site is modelled in figure 3.21. Caspase 1 is an enzyme that has known involvement in neuronal cell-death following a diverse range of insults (Denes et al. 2012). As medulloblastoma is a cancer that arises from neural stem cells (particularly groups 3 and 4), which give rise to neurons (Marshall et al. 2014) this may be of particular interest due to caspase 1 being implicated in neuronal cell death.

Another role of caspase 1 is within the inflammasome, it has been suggested in medulloblastoma that ATP is released by apoptotic cells and recruits the NLRP3 inflammasome (Knight et al. 2013) via the purine receptor P2X₇ the mechanism of which has been described in dendritic cells and breast cancer (Ghiringhelli et al. 2009). This process involves caspase 1 activation. GD3 is also known to have a role in modulating the immune system when shed which perhaps helps to regulate the inflammatory response. While preliminary and in need of further investigation, this may have relevance and will be subject to further investigation beyond this project.

4.10 Chemotherapeutic response with SIAE overexpression

One of the purposes of a new therapeutic approach to medulloblastoma is to reduce the toxicity of existing chemotherapeutics. The current chemotherapeutic regime is aggressive and has significant effects on the developing nervous system and therefore the patient's quality of life (Kim et al. 2011). There is a need to either replace existing drugs or reduce the dose of existing treatments in order to reduce toxicity. Our approach for this is to overexpress SIAE to try and predispose medulloblastoma cells to existing treatments. The current treatment regime for medulloblastoma includes lomustine, cyclophosphamide, vincristine, methotrexate, cisplatin and etoposide (Mueller & S. Chang 2009; Gajjar et al.

1999; Michiels et al. 1996).

Following literature searches and searches of clinical trial data, cisplatin and etoposide were chosen as the two drugs we would test to see if SIAE overexpression significantly reduced viability of RES256 cells (figures 3.24, 3.25). These drugs were selected as the use of them remains in each of the treatment protocols researched.

Cisplatin is activated upon entering cells where the chloride atoms are replaced with water molecules by displacement. The hydrolysed product is a potent electrophile which can react with nucleophiles such as the sulfhydryl groups on proteins or nitrogen donor groups of nucleic acids (Dasari & Tchounwou 2014). The cytotoxic effect of cisplatin is primarily due to the interaction with the N7-sites of purine DNA bases to form DNA-protein and DNA-DNA interstrand and intrastrand crosslinks (Eastman et al. 1987). These cross-links cause DNA damage in cancer cells which block cell division and result in apoptosis. The intrastrand cross-links of purine bases are the most notable changes in DNA with cisplatin treatment. They include d(GpG) adducts (90 %) and d(ApG) adducts (10 %) (Dasari & Tchounwou 2014).

Cisplatin did not significantly reduce RES256 cell viability with induction of empty vector control expression, nor with SIAE wild-type or mutant expression at 24 hours (figure 3.24A). After 48 hours of cisplatin treatment there was a significant reduction in viability with 3 μ M cisplatin in wild-type SIAE clone 1 ($p < 0.001$) but this effect was not concentration-dependent and was not maintained with higher doses (figure 3.24B). There was also a significant reduction in cell viability of S127A expressing cells with cisplatin treatment with 4 and 11 μ M ($p < 0.05$; figure 3.24B) and with 12 μ M cisplatin ($p < 0.01$; figure 3.24B). After 72 hours of cisplatin treatment there was a significant difference in EGFP viability with

vehicle control ($p < 0.05$; figure 3.24C) and 7 μM cisplatin treatment ($p < 0.05$; figure 3.24C). There was also a significant reduction in viability with 13 μM cisplatin treatment in SIAE clone 1 ($p < 0.05$; figure 3.24C). There were also significant differences between 3, 11 and 13 μM cisplatin treatment ($p < 0.05$; figure 3.24C) and 12 μM cisplatin treatment ($p < 0.001$; figure 3.24C) in the SIAE-S127A expressing clone.

This suggests that cisplatin treatment has a greater effect on viability with induction of gene expression with time as the most significant data, particularly when the catalytic mutant expresser is seen at 72 hours. This data however does demonstrate some significance outside of clinically achievable concentrations (generally accepted to be up to 10 μM in the brain) (Stewart et al. 1995). When analysed as a dose-response, the catalytic mutant SIAE-S127A had a reduced IC_{50} with induction of gene expression ($p < 0.05$) demonstrating that the drug is having a greater effect when the mutant enzyme is expressed. As the catalytic mutant did not demonstrate any significant changes in GD3 or GD3^A expression, nor any significant depolarisation of the mitochondrial membrane potential, it may be that this effect does not involve the gangliosides.

As well as this, cells were still viable, even with high concentrations of cisplatin, mechanisms of resistance were investigated. (Siddik et al. 2003) suggests many mechanisms of resistance; two of these are relevant to the RES256 cell line. *TP53* mutation can contribute to resistance by inhibition of p53-dependent apoptotic programs. Another mechanism is overexpression of ERBB2 (Her2) which is known to correlate with poor prognosis in medulloblastoma. There are several pathways that ERBB2 overexpression can affect which contribute to cisplatin resistance, but the major mechanism in this case is inactivation of the pro-apoptotic protein Bad following its phosphorylation by protein

kinase b (Akt) (Siddik et al. 2003). Furthermore, the RES256 cell line was positive for ERBB2 expression with 67.9% of the population staining positive for the antigen (Zomerman et al. 2015).

Etoposide is a chemotherapeutic whose main target is topoisomerase II, an enzyme involved in inducing double strand transient breaks in DNA in order for a cell to replicate, and for tangles in DNA to be removed. The transient breaks in DNA are generated by a topoisomerase II / DNA complex (cleavage complex) which can be stabilised permanently by etoposide. This drug prevents re-ligation of the double-strand DNA break. These double-strand DNA breaks are lethal to the cell as there is failure in DNA damage repair mechanisms (Montecucco et al. 2015). The tumour suppressor p53 plays an important role in etoposide-induced apoptosis and is regulated by the drug (Dey et al. 2010). Another mechanism of action of etoposide has been described in isolated mitochondria from Jurkat cells (Robertson et al. 2000). In this study the mitochondrial membrane potential was shown to collapse with 50 μ M etoposide treatment. Although this study was carried out in a cell-free system, as we hypothesised that the mitochondrial membrane potential may collapse with SIAE overexpression (due to increased levels of GD3), the drug was chosen to determine if an additive or synergistic effect could be achieved with SIAE overexpression.

Etoposide significantly reduced RES256 cell viability with induction of empty vector control expression at 24 hours of treatment with 7 and 12 μ M ($p < 0.05$; figure 3.25A) and with 13 μ M treatment ($p < 0.01$; figure 3.25A). In SIAE wild-type expressing cells (clone 2) 12 μ M etoposide treatment also had a significant difference with gene expression ($p < 0.01$; figure 3.25A). SIAE 2 and SIAE-S127A mutant expression at 24 hours however were not significantly different (figure 3.25A). After 48 hours of etoposide treatment there was a

significant reduction in viability with 11 μM etoposide in EGFP expressing clones ($p < 0.005$; figure 3.25B) and with 13 μM treatment ($p < 0.01$; figure 3.25B). There was also a significant reduction in cell viability with etoposide treatment at 1 and 4 μM ($p < 0.05$; figure 3.25B). After 72 hours of cisplatin treatment there was a significant difference 1 μM etoposide treated cells ($p < 0.05$; figure 3.25C).

Clinically achievable levels of etoposide in the brain are not well reported in the literature. Publications on extraneural tumours such as neuroblastoma (Kiya et al. 1992) and leukaemia suggest levels in the plasma can reach up to 50 μM (Wen et al. 2000) this is very unlikely in the brain due to the blood-brain (or blood-tumour) barrier. It has also been shown that etoposide concentrations in the tumour core are higher than that of the rest of the brain (Stewart et al. 1984). Based on this it is difficult to suggest a clinically relevant range of etoposide concentrations. This may also mean that the study by Robertson (2000) used clinical unachievable levels of the drug which may mean that the mechanism of action proposed by this study does not take place at concentrations achievable *in vivo* (Robertson et al. 2000). In addition, the effects of etoposide are potentiated with time (Kiya et al. 1992). Despite early indications of etoposide seeming more effective using our initial analysis by dose (figure 3.25) particularly in the EGFP clone, when analysed as a dose-response (figure 3.27) only wild-type expressing clone 2 showed a significant reduction in IC_{50} compared to controls. Interestingly, SIAE clone 2 was the only clone to demonstrate a significant increase in GD3 expression with induction of SIAE expression.

These data suggest that SIAE expression may affect cell viability when cells are treated with etoposide, perhaps due to changes in the cell-cycle as etoposide is a cell-cycle dependent drug. High levels of GD3 have been shown (via overexpression of ST8Sia1) to increase

proliferation (Cazet et al. 2009). As GD3 has been shown to increase in SIAE clone 2 with induction of expression, this increase could then cause the cells to re-enter the cell cycle and proliferate, allowing etoposide to bind. This increase in GD3 was not seen in clone 1, but neither was a reduction in IC_{50} which may suggest that GD3 may play a role. There was some resistance seen with etoposide as the viability of cells remained at around 40 % with treatment. It has been demonstrated that RES256 cells have mutant *TP53* status (Zhukova Thesis, 2012), and that the mechanism of cell death by etoposide is reliant on p53. It has also been shown that medulloblastoma cells with mutations in *TP53* are resistant (or less sensitive) to etoposide treatment (Meley et al. 2010).

The reported IC_{50} data obtained from MTS experiments shown in figures 3.26 and 3.27 should not be considered final. MTS experiments report the metabolic state of cells and it is clear that there is a difference in the starting viability in SIAE clone 2 expressing cells treated for 72 hours with etoposide. This reduction in IC_{50} therefore may not be an accurate representation of the effect of etoposide, but rather an altered metabolic state as a result of this experimental condition. In order to determine accurate and reliable IC_{50} data the experiments carried out using MTS assays must also be carried out as colony formation assays to determine drug responses. The IC_{50} data shown in figures 3.26 and 3.27 must also be repeated across a narrower range of drug concentrations. In order to determine accurate IC_{50} data there should be at least 5 data points reported before a 50 % response is seen. Limitations in the experimental methods are recognised and in further work should be further optimised and repeated.

4.11 Conclusions

One of the aims of this work was to demonstrate that GD3 and GD3^A were re-expressed by

medulloblastoma cells and that a balance between them existed. We have shown that the expression of these two gangliosides is high, and that the balance of GD3 to GD3^A is in favour of GD3^A within these cells, as hypothesised. We demonstrate that the expression of GD3^A is low on the cell-surface, which is supportive of work by Chen (H. Y. Chen et al. 2006) stating that GD3 requires internalisation to be acetylated. We investigated the role of these two gangliosides in medulloblastoma cell viability by over-expressing the human endogenous deacetylation enzyme SIAE. Over-expression of SIAE significantly increased the expression of GD3 in these cells, but not in catalytic mutant cells or empty vector controls. Further to this we demonstrated in preliminary work that the mitochondrial membrane potential could be depolarised with induction of SIAE over-expression (in clone 1 only), but experimental limitations make conclusions difficult to draw, other methods such as caspase 3/7 activation, cytochrome *c* release or studies of *bcl-2* or *bax* are necessary to draw conclusion on this topic. We also demonstrated that with treatment of these cell lines with cisplatin and etoposide, the IC₅₀ with etoposide treatment is significantly reduced in wild-type SIAE expressing clone 2 with 72 hour treatment. We did not demonstrate any changes in susceptibility to cisplatin-mediated reductions in cell viability possibly in wild-type expressing clones suggesting that SIAE over-expression causes changes in the cell cycle which does not affect the response to cisplatin. We did however demonstrate a significant reduction in cell viability in the mutant expressing cell line after 48 hours of treatment with cisplatin.

It could be investigated in further work if the increase in GD3 expression of viable cells could increase invasive potential, something that, if true, could affect the potential success of this therapeutic approach. If the invasive potential is increased then cell survival may

increase, something not desirable in a therapy. If, however trafficking of GD3 to the mitochondria is sufficient to cause a reduction in cell viability this increase in invasive potential would be unlikely. In support of this, studies on this pathway in glioblastoma multiforme showed that invasive potential was not increased upon cleavage of GD3^A (Birks et al. 2011).

We also demonstrate that SIAE can be secreted and that there is a greater amount of secretion in the catalytically mutated clone. This may be due to caspase 1 involvement, but will be subject to further work to support or reject this hypothesis and further dissect mechanisms of reduced viability in these cells. Caspase 1 involvement will also be investigated with down-stream apoptosis assays, such as executioner caspase 3 assays in order to determine if cell death occurs and by which mechanisms if it does.

4.12 Further work

In this study we have demonstrated as a proof of principle that this pathway could be utilised as a therapeutic target. In further work more cell lines should be used in order to further demonstrate this principle. Gene delivery should also be a focus of further study, in work done by (Birks et al. 2011) the baculovirus has shown promise for this application. This approach could be utilised as a method of targeting cells left behind after surgical resection to either cause their mitochondrially-mediated apoptosis, or sensitise them to lower doses of chemotherapy. It would obviously be important if this were to reach the clinic to ensure that lower doses of chemotherapy did not risk under-treatment of disease and that the doses used are clinically achievable.

The limitations of the JC-1 assay and chemotherapy experiments described above require

further optimisation before conclusions can be drawn, it would therefore be important for these experiments to be carried out in further work. Other considerations should be combinations of chemotherapy to determine if any synergism occurs with SIAE over-expression and current therapeutic regimes. Of particular interest would be mitochondrially-targeted agents such as clomipramine, a tricyclic antidepressant drug which has shown promise in the treatment of glioma. Another agent of interest for that targets mitochondria that has shown promise in SHH medulloblastoma is dichloroacetate, a drug that targets pyruvate kinase (Di Magno et al. 2014) . This could help to determine optimum time for delivery of this gene if it were to reach the clinic.

References

- Ahmad, Z., Lukasz, J., Gil, V., Howell, L., Hallsworth, A., Petrie, K., ... Chesler, L., 2015. Molecular and in vivo characterization of cancer-propagating cells derived from MYCN-dependent medulloblastoma. J. S. Castresana, ed. *PLoS ONE*, 10(3), p.e0119834.
- Alcántara, S., Ruiz, M., De Castro, F., Soriano, E., Sotelo, C., 2000. Netrin 1 acts as an attractive or as a repulsive cue for distinct migrating neurons during the development of the cerebellar system. *Development (Cambridge, England)*, 127(7), pp.1359–1372.
- Alder, J., Cho, NK. & Hatten, ME., 1996. Embryonic precursor cells from the rhombic lip are specified to a cerebellar granule neuron identity. *Neuron*, 17(3), pp.389–399.
- American Cancer Society, 2014. Signs and Symptoms of brain and spinal cord tumours in children. *Cancer.org*. Available at: <http://www.cancer.org/cancer/braincnstumorsinchildren/detailedguide/brain-and-spinal-cord-tumors-in-children-signs-and-symptoms> [Accessed November 12, 2015].
- An, Q., Fillmore, HL., Vouri, M., Pilkington, GJ., 2014. Brain tumor cell line authentication, an efficient alternative to capillary electrophoresis by using a microfluidics-based system. *Neuro-oncology*, 16(2), pp.265–273.
- Arming, S., Wipfler, D., Mayr, J., Merling, A., Vilas, U., Schauer, R., ... Vlasak, R., 2011. The human Cas1 protein: a sialic acid-specific O-acetyltransferase? *Glycobiology*, 21(5), pp.553–564.
- Bandopadhyay, P., Bergthold, G., Nguyen, B., Schubert, S., Gholamin, S., Tang, ..., Cho, YE., 2014. BET bromodomain inhibition of MYC-amplified medulloblastoma. *Clinical cancer research : an official journal of the American Association for Cancer Research*, 20(4), pp.912–925.
- Basu, S., Ma, R., Moskal, JR., Basu, M., 2012. Ganglioside biosynthesis in developing brains and apoptotic cancer cells: X. regulation of glyco-genes involved in GD3 and Sialyl-Lex/a syntheses. *Neurochemical research*, 37(6), pp.1245–1255.
- Baumann, AMT., Bakkers, MJG., Buettner, FFR., Hartmann, M., Grove, M., Langeris, MA., de Groot, RJ., Mühlhoff, M., 2015. 9-O-Acetylation of sialic acids is catalysed by CASD1 via a covalent acetyl-enzyme intermediate. *Nature communications*, 6, p.7673.
- Bihannic, L. & Ayrault, O., 2016. Insights into cerebellar development and medulloblastoma. *Bulletin du cancer*, 103(1), pp.30–40.
- Birklé, S., Xeng, G., Gao, L., Yu, RK., Aubry, J., 2003. Role of tumor-associated gangliosides in cancer progression. *Biochimie*, 85(3-4), pp.455–463.
- Birks, S.M., Danquah, JO., King, L., Vlasak, R., Gorecki, DC., Pilkington, GJ., 2011. Targeting the GD3 acetylation pathway selectively induces apoptosis in glioblastoma. *Neuro-oncology*, 13(9), pp.950–960.

- Borowska, A. & Jóźwiak, J., 2016. Medulloblastoma: molecular pathways and histopathological classification. *Archives of medical science : AMS*, 12(3), pp.659–666.
- Bouabe, H., Fässler, R. & Heesemann, J., 2008. Improvement of reporter activity by IRES-mediated polycistronic reporter system. *Nucleic acids research*, 36(5), pp.e28–e28.
- Brain Tumour Research, 2015. Statistics. *Brain Tumour Research*. Available at: <http://www.braintumourresearch.org/statistics> [Accessed January 13, 2016].
- Brezicka, P.F.K.H.T., 2015. Gangliosides as Therapeutic Targets for Cancer. *BioDrugs: clinical immunotherapy* 17(3) pp.155–167.
- Buckles, GR. Thorpe, CJ., Ramel, MC., Lekven, AC., 2004. Combinatorial Wnt control of zebrafish midbrain-hindbrain boundary formation. *Mechanisms of development*, 121(5), pp.437–447.
- Butts, T., Green, M.J. & Wingate, R.J.T., 2014. Development of the cerebellum: simple steps to make a 'little brain'. *Development (Cambridge, England)*, 141(21), pp.4031–4041.
- Campbell, F., Appleton, MA., Fuller, CE., Greeff, MP., Hallgrimsson, J., Katoh, R., ... Williams, ED., 1994. Racial variation in the O-acetylation phenotype of human colonic mucosa. *The Journal of pathology*, 174(3), pp.169–174.
- Cancer Research UK, 2015. Brain tumour risks and causes. p.Brain tumour risks and causes. Available at: <http://www.cancerresearchuk.org/about-cancer/type/brain-tumour/about/brain-tumour-risks-and-causes>.
- Cazet, A., Groux-Degroote, S., Teylaert, B., Kwon, KM., Lehoux, S., Slomianny, C., ... Delannoy, P., 2009. GD3 synthase overexpression enhances proliferation and migration of MDA-MB-231 breast cancer cells. *Biological chemistry*, 390(7), pp.601–609.
- Chang, CH., Housepian, E.M. & Herbert, C., 1969. An operative staging system and a megavoltage radiotherapeutic technic for cerebellar medulloblastomas. *Radiology*, 93(6), pp.1351–1359.
- Chekenya, M. & Pilkington, G.J., 2002. NG2 precursor cells in neoplasia: functional, histogenesis and therapeutic implications for malignant brain tumours. *Journal of neurocytology*, 31(6-7), pp.507–521.
- Chekenya, M., Pilkington, G.J., 1999. The NG2 chondroitin sulfate proteoglycan: role in malignant progression of human brain tumours. *International journal of developmental neuroscience : the official journal of the International Society for Developmental Neuroscience*, 17(5-6), pp.421–435.
- Chellappa, V., Taylor, KN., Pedrick, K., Donado, C., Netravali, IA., Haider, K., ..., Pillai, S., 2013. M89V Sialic acid Acetyl Esterase (SIAE) and all other non-synonymous common variants of this gene are catalytically normal. G. P. Bansal, ed. *PLoS ONE*, 8(1),

p.e53453.

- Chen, HY., Challa, AK. & Varki, A., 2006. 9-O-acetylation of exogenously added ganglioside GD3. The GD3 molecule induces its own O-acetylation machinery. *Journal of Biological Chemistry*, 281(12), pp.7825–7833.
- Cheresh, DA. Pytela, R., Pierschbacher, MD., Klier, FG., Ruoslahti, E., Reisfeld, RA., 1987. An Arg-Gly-Asp-directed receptor on the surface of human melanoma cells exists in an divalent cation-dependent functional complex with the disialoganglioside GD2. *The Journal of cell biology*, 105(3), pp.1163–1173.
- Cheresh, DA. Pierschbacher, MD., Herzig, MA., Mujoo, K., 1986. Disialogangliosides GD2 and GD3 are involved in the attachment of human melanoma and neuroblastoma cells to extracellular matrix proteins. *The Journal of cell biology*, 102(3), pp.688–696.
- Children's Oncology Group, 2013. Study ACNS0331. *Children's Oncology Group*. Available at: <https://childrensoncologygroup.org/index.php/acns0331> [Accessed February 28, 2016].
- Ciani, L. & Salinas, P.C., 2005. WNTs in the vertebrate nervous system: from patterning to neuronal connectivity. *Nature reviews. Neuroscience*, 6(5), pp.351–362.
- Colell, A., García-Ruiz, C., Roman, J., Ballesta, A., Fernández-Checa, JC., 2001. Ganglioside GD3 enhances apoptosis by suppressing the nuclear factor-kappa B-dependent survival pathway. *FASEB journal : official publication of the Federation of American Societies for Experimental Biology*, 15(6), pp.1068–1070.
- Dahmane, N. & Ruiz i Altaba, A., 1999. Sonic hedgehog regulates the growth and patterning of the cerebellum. *Development (Cambridge, England)*, 126(14), pp.3089–3100.
- Dahmen, RP., Koch, A., Denkhaus, D., Tonn, JC., Sörensen, N., Bertohold, F., ... Pietsch, T., 2001. Deletions of AXIN1, a component of the WNT/wingless pathway, in sporadic medulloblastomas. *Cancer research*, 61(19), pp.7039–7043.
- Dasari, S. & Tchounwou, P.B., 2014. Cisplatin in cancer therapy: molecular mechanisms of action. *European journal of pharmacology*, 740, pp.364–378.
- de Bont, JM., Packer, RJ., Michils, EM., den Boer, ML., Pieters, R., 2008. Biological background of pediatric medulloblastoma and ependymoma: a review from a translational research perspective. *Neuro-oncology*, 10(6), pp.1040–1060.
- de Haas, T., Oussoren, E., Grajkowska, W., Perek-Polnik, M., Popovik, M., Zdravec-Zaletel, L., ... Kool, M., 2006. OTX1 and OTX2 expression correlates with the clinicopathologic classification of medulloblastomas. *Journal of neuropathology and experimental neurology*, 65(2), pp.176–186.
- De Maria, R., Rippo, MR., Schuchman, EH., Testi, R., 1998. Acidic sphingomyelinase (ASM) is necessary for fas-induced GD3 ganglioside accumulation and efficient apoptosis of

- lymphoid cells. *The Journal of experimental medicine*, 187(6), pp.897–902.
- Debarbieux, S., Popa, I., Thomas, L., Kanitakis, J., Pirot, F., Portoukalian, J., Haftek, M., 2009. Detection of GD3 ganglioside in primary melanomas depends on histopathologic procedures used for tumor preservation. *Acta dermatovenerologica Croatica : ADC*, 17(3), pp.209–216.
- Denes, A., Lopez-Castejon, G. & Brough, D., 2012. Caspase-1: is IL-1 just the tip of the ICEberg? *Cell death & disease*, 3(7), p.e338.
- Dey, A., Lane, DP. & Verma, CS., 2010. Modulating the p53 pathway. *Seminars in cancer biology*, 20(1), pp.3–9.
- Di Magno, L., Manzi, D., D'Amico, D., Coni, S., Macone, A., Infante, P.,... Canettieri, G., 2014. Druggable glycolytic requirement for Hedgehog-dependent neuronal and medulloblastoma growth. *Cell cycle (Georgetown, Tex.)*, 13(21), pp.3404–3413.
- Diaz, S., Higa, HH. & Varki, A., 1989. Glycoprotein sialate 7(9)-O-acetyltransferase from rat liver Golgi vesicles. *Methods in enzymology*, 179, pp.416–422.
- Dolo, V., Li, R., Dillinger, M., Flati, S., Mnela, J., Taylor, BJ., Pavan, A., Ladisch, S., 2000. Enrichment and localization of ganglioside G(D3) and caveolin-1 in shed tumor cell membrane vesicles. *Biochimica et biophysica acta*, 1486(2-3), pp.265–274.
- Dufour, C., Beaugrand, A., Pizer, B., Micheli, J., Aubelle, MS., Fourcade, A., ... C., Grill, J., 2012. Metastatic Medulloblastoma in Childhood: Chang's Classification Revisited. *International Journal of Surgical Oncology*, 2012(6), pp.1–6.
- Dyatlovitskaya, EV. & Bergelson, LD., 1987. Glycosphingolipids and antitumor immunity. *Biochimica et biophysica acta*, 907(2), pp.125–143.
- Eastman, A., 1987. The formation, isolation and characterization of DNA adducts produced by anticancer platinum complexes. *Pharmacology & therapeutics*, 34(2), pp.155–166.
- Eberhart, CG., 2012. Three down and one to go: modeling medulloblastoma subgroups. *Cancer cell*, 21(2), pp.137–138.
- Eberhart, CG., Tihan, T. & Burger, PC., 2000. Nuclear localization and mutation of beta-catenin in medulloblastomas. *Journal of neuropathology and experimental neurology*, 59(4), pp.333–337.
- Ellison, DW., Dalton, J., Kocak, M., Nicholson, SL., Fraga, C., Neale., ... Gilbertson, RJ., 2011. Medulloblastoma: clinicopathological correlates of SHH, WNT, and non-SHH/WNT molecular subgroups. *Acta neuropathologica*, 121(3), pp.381–396.
- Ellison, DW., Clifford, SC., Gajjar, A., Gilbertson, RJ., 2003. What's new in neuro-oncology? Recent advances in medulloblastoma. *European journal of paediatric neurology : EJPN : official journal of the European Paediatric Neurology Society*, 7(2), pp.53–66.

- Erdreich-Epstein, A., Robison, N., Ren, X., Zhou, H., Xu, J., Davidson, TB., ... Asgharaxadeh, S., 2014. PID1 (NYGGF4), a new growth-inhibitory gene in embryonal brain tumors and gliomas. *Clinical cancer research : an official journal of the American Association for Cancer Research*, 20(4), pp.827–836.
- Fahr, C. & Schauer, R., 2001. Detection of sialic acids and gangliosides with special reference to 9-O-acetylated species in basaliomas and normal human skin. *The Journal of investigative dermatology*, 116(2), pp.254–260.
- Ferri, KF. & Kroemer, G., 2000. Control of apoptotic DNA degradation. *Nature cell biology*, 2(4), pp.E63–4.
- Fujii, K. & Miyashita, T., 2014. Gorlin syndrome (nevroid basal cell carcinoma syndrome): update and literature review. *Pediatrics international : official journal of the Japan Pediatric Society*, 56(5), pp.667–674.
- Fukumoto, S., Mutoh, T., Hasegawa, T., Miyazaki, H., Okada, M., Goto, G., ... Urano, T., 2000. GD3 synthase gene expression in PC12 cells results in the continuous activation of TrkA and ERK1/2 and enhanced proliferation. *Journal of Biological Chemistry*, 275(8), pp.5832–5838.
- Gajjar, A., Kühl, J., Epelman, S., Bailey, C., Allen, J., 1999. Chemotherapy of medulloblastoma. *Child's nervous system : ChNS : official journal of the International Society for Pediatric Neurosurgery*, 15(10), pp.554–562.
- Gajjar, A., Hernan, R., Kocak, M., Fuller, C., Lee, Y., McKinnon, PJ., ... Gilbertson, RJ., 2004. Clinical, histopathologic, and molecular markers of prognosis: toward a new disease risk stratification system for medulloblastoma. *Journal of clinical oncology : official journal of the American Society of Clinical Oncology*, 22(6), pp.984–993.
- Gajjar, A., Chintagumpala, M., Ashley, D., Kellie, S., Kun, LE., Merchant, TE., ... Gilbertson, RJ., 2006. Risk-adapted craniospinal radiotherapy followed by high-dose chemotherapy and stem-cell rescue in children with newly diagnosed medulloblastoma (St Jude Medulloblastoma-96): long-term results from a prospective, multicentre trial. *The Lancet. Oncology*, 7(10), pp.813–820.
- Gajjar, AJ. & Robinson, GW., 2014. Medulloblastoma-translating discoveries from the bench to the bedside. *Nature reviews. Clinical oncology*, 11(12), pp.714–722.
- Garcia-Ruiz, C., Morales, A. & Fernández-Checa, J.C., 2015. Glycosphingolipids and cell death: one aim, many ways. *Apoptosis : an international journal on programmed cell death*, 20(5), pp.607–620.
- Garzia, L., Kijima, N., Morrissey, A., Donovan, L., Wu, X., Luu, B., Ramaswamy, V., ... Taylor, MD., 2015. Hematogenous dissemination of medulloblastoma metastasis to the leptomeninges. *Society for Neuro-oncology*.
- Gendoo, DMA., Smirnov, P., Lipien, M., Haibe-Kains, B., 2015. Personalized diagnosis of medulloblastoma subtypes across patients and model systems. *Genomics*, 106(2),

pp.96–106.

- Ghiringhelli, F., Apetoh, L., Tesniere, A., Aymeric, L., Ma, Y., Ortix, C., ..., Zitvogel, L., 2009. Activation of the NLRP3 inflammasome in dendritic cells induces IL-1beta-dependent adaptive immunity against tumors. *Nature medicine*, 15(10), pp.1170–1178.
- Gibson, P., Tong, Y., Robinson, G., Thompson, MC., Currle, DS., Eden, C., ... Gilbertson, RJ., 2010. Subtypes of medulloblastoma have distinct developmental origins. *Nature*, 468(7327), pp.1095–1099.
- Gilbertson, R., Wickramasinghe, C., Hernan, R., Balaji, V., Hunt, D., Jones-Wallace, D., ... Ellison, D., 2001. Clinical and molecular stratification of disease risk in medulloblastoma. *British journal of cancer*, 85(5), pp.705–712.
- Gilbertson, RJ., 2004. Medulloblastoma: signalling a change in treatment. *The Lancet. Oncology*, 5(4), pp.209–218.
- Gilbertson, RJ. & Clifford, SC., 2003. PDGFRB is overexpressed in metastatic medulloblastoma. *Nature genetics*, 35(3), pp.197–198.
- Gilbertson, RJ., Clifford, SC., MacMeekin, W., Meekin, W., Wright, C., Perry, RH., ... Lunec, J., 1998. Expression of the ErbB-neuregulin signaling network during human cerebellar development: implications for the biology of medulloblastoma. *Cancer research*, 58(17), pp.3932–3941.
- Gilbertson, RJ., Perry, RH., Kelly, PJ., Pearson, AD., lunec, J., 1997. Prognostic significance of HER2 and HER4 coexpression in childhood medulloblastoma. *Cancer research*, 57(15), pp.3272–3280.
- Giussani, P., Tringali, C., Riboni, L., Viana, P., Venerando, B., 2014. Sphingolipids: key regulators of apoptosis and pivotal players in cancer drug resistance. *International journal of molecular sciences*, 15(3), pp.4356–4392.
- Goldman, JE. & Reynolds, R., 1996. A reappraisal of ganglioside GD3 expression in the CNS. *Glia*, 16(4), pp.291–295.
- Goschzik, T., Zur, Mühlen, A., Kristiansen, G., Haberler, C., Stefantitis, H., ... Pietsch, T., 2015. Molecular stratification of medulloblastoma: comparison of histological and genetic methods to detect Wnt activated tumours. *Neuropathology and applied neurobiology*, 41(2), pp.135–144.
- Gottfries, J., Fredman, P., Månsson, JE., Collins, VP., von Holst, H., Armstrong, DD., P... Svennerholm, L., 1990. Determination of Gangliosides in Six Human Primary Medulloblastomas. *Journal of Neurochemistry*, 55(4), pp.1322–1326.
- Gratsa, A., Rooprai, HK., Rogers, JP., Martin, KK., Pilkington, GJ., 1997. Correlation of expression of NCAM and GD3 ganglioside to motile behaviour in neoplastic glia. *Anticancer research*, 17(6B), pp.4111–4117.
- Grayson, G. & Ladisch, S., 1992. Immunosuppression by human gangliosides. II.

- Carbohydrate structure and inhibition of human NK activity. *Cellular immunology*, 139(1), pp.18–29.
- Gupta, S., Takebe, N. & Lorusso, P., 2010. Targeting the Hedgehog pathway in cancer. *Therapeutic advances in medical oncology*, 2(4), pp.237–250.
- Hamamura, K., Tsuji, M., Hotta, H., Ohkawa, Y., Takahashi, M., Shibuya, H., ... Furukawa, K., 2011. Functional Activation of Src Family Kinase Yes Protein Is Essential for the Enhanced Malignant Properties of Human Melanoma Cells Expressing Ganglioside GD3. *Journal of Biological Chemistry*, 286(21), pp.18526–18537.
- Hatten, ME. & Roussel, MF., 2011. Development and cancer of the cerebellum. *Trends in neurosciences*, 34(3), pp.134–142.
- HeadSmart, 2011. HeadSmart Be Brain Tumour Aware. *HeadSmart Be Brain Tumour Aware*. Available at: <http://www.headsmart.org.uk> [Accessed January 13, 2016].
- Hedberg, KM., Dellheden, B., Wikstrand, CJ., Freman, P., 2000. Monoclonal anti-GD3 antibodies selectively inhibit the proliferation of human malignant glioma cells in vitro. *Glycoconjugate journal*, 17(10), pp.717–726.
- Henssen, A., Thor, T., Odersky, A., Heukamp, L., El-Hindy, N., Beckers, A., ...A., Schulte, JH., 2013. BET bromodomain protein inhibition is a therapeutic option for medulloblastoma. *Oncotarget*, 4(11), pp.2080–2095.
- Hernan, R., Fasheh, R., Calabrese, C., Frank, AJ., Maclean, KH., Allard, ..., R., Gilbertson, RJ., 2003. ERBB2 up-regulates S100A4 and several other prometastatic genes in medulloblastoma. *Cancer research*, 63(1), pp.140–148.
- Hersey, P., 1991. Ganglioside antigens in tissue sections of skin, naevi, and melanoma--implications for treatment of melanoma. *Cancer treatment and research*, 54, pp.137–151.
- Higa, HH., Diaz, S. & Varki, A., 1987. Biochemical and genetic evidence for distinct membrane-bound and cytosolic sialic acid O-acetyl-esterases: serine-active-site enzymes. *Biochemical and Biophysical Research Communications*, 144(3), pp.1099–1108.
- Higgins, SC., Fillmore, HL., Keyoumars, A., Butt, AM., Pilkington, GJ., 2015. Dual targeting NG2 and GD3A using Mab-Zap immunotoxin results in reduced glioma cell viability in vitro. *Anticancer research*, 35(1), pp.77–84.
- Hooper, CM., Hawes, SM., Kees, UR., Gottardo, NG., Dallas, PB., 2014. Gene expression analyses of the spatio-temporal relationships of human medulloblastoma subgroups during early human neurogenesis. B. Alsina, ed. *PLoS ONE*, 9(11), p.e112909.
- Huang, H., Mahler-Araujo, BM., Sankila, A., Chimelli, L., Yonekawa, Y., Kleihues, P., Ohgaki, H., 2000. APC mutations in sporadic medulloblastomas. *The American journal of pathology*, 156(2), pp.433–437.

- Hwang, J., Lee, S., Lee, J.T., Kwon, T.K., Kim, D.R., Kim, H., ... Suk, K., 2010. Gangliosides induce autophagic cell death in astrocytes. *British journal of pharmacology*, 159(3), pp.586–603.
- Jacob, D.A., Mercer, S.I., Osheroff, N., Deweese, J.E., 2011. Etoposide quinone is a redox-dependent topoisomerase II poison. *Biochemistry*, 50(25), pp.5660–5667.
- Jakacki, R.I., Hamilton, M., Gilbertson, R.J., Blaney, S.M., Tersak, J., Krailo, M.D., ...Adamson, P.C., 2008. Pediatric phase I and pharmacokinetic study of erlotinib followed by the combination of erlotinib and temozolomide: a Children's Oncology Group Phase I Consortium Study. *Journal of clinical oncology : official journal of the American Society of Clinical Oncology*, 26(30), pp.4921–4927.
- Jones, D.T.W., Jäger, N., Kool, M., Zichner, T., Hutter, B., Sultan, M., ... Lichter, P., 2012. Dissecting the genomic complexity underlying medulloblastoma. *Nature*, 488(7409), pp.100–105.
- Kalderon, D., 2002. Similarities between the Hedgehog and Wnt signaling pathways. *Trends in cell biology*, 12(11), pp.523–531.
- Kang, D.E., Soriano, S., Xia, X., Eberhart, C.G., De Strooper, B., Xheng, H., Koo, E.H., 2002. Presenilin couples the paired phosphorylation of beta-catenin independent of axin: implications for beta-catenin activation in tumorigenesis. *Cell*, 110(6), pp.751–762.
- Kasahara, K., Watanabe, Y., Yamamoto, T., Sanai, Y., 1997. Association of Src family tyrosine kinase Lyn with ganglioside GD3 in rat brain. Possible regulation of Lyn by glycosphingolipid in caveolae-like domains. *Journal of Biological Chemistry*, 272(47), pp.29947–29953.
- Kasahara, K., Watanaba, K., Takeuchi, K., Kaneko, H., Oohira, A., Yamamoto, T., Sanai, Y., 2000. Involvement of gangliosides in glycosylphosphatidylinositol-anchored neuronal cell adhesion molecule TAG-1 signaling in lipid rafts. *Journal of Biological Chemistry*, 275(44), pp.34701–34709.
- Kawai, H., Sango, K., Mullin, K.A., Proia, R.L., 1998. Embryonic stem cells with a disrupted GD3 synthase gene undergo neuronal differentiation in the absence of b-series gangliosides. *Journal of Biological Chemistry*, 273(31), pp.19634–19638.
- Kawai, K., Kuroda, S., Watarai, S., Takahashi, H., Ikuta, F., 1994. Occurrence of GD3 ganglioside in reactive astrocytes--an immunocytochemical study in the rat brain. *Neuroscience letters*, 174(2), pp.225–227.
- Kennea, N.L. & Mehmet, H., 2002. Neural stem cells. *The Journal of pathology*, 197(4), pp.536–550.
- Kim, W., Choy, W., Dye, J., Nagasawa, D., Safaee, M., Fong, B., Yang, I., 2011. The tumor biology and molecular characteristics of medulloblastoma identifying prognostic factors associated with survival outcomes and prognosis. *Journal of clinical neuroscience : official journal of the Neurosurgical Society of Australasia*, 18(7),

pp.886–890.

- Kiya, K, Uozumi, T., Ogasawara, H., Sugiyama, K., Hotta, T., Mikami, T., Kurisu, K., 1992. Penetration of etoposide into human malignant brain tumors after intravenous and oral administration. *Cancer chemotherapy and pharmacology*, 29(5), pp.339–342.
- Kniep, B., Kniep, E., Ozkucur, N., Barz, S., Bachmann, M., Maisan, F, ... Rieber, EP., 2006. 9-O-acetyl GD3 protects tumor cells from apoptosis. *International Journal of Cancer*, 119(1), pp.67–73.
- Knight, ERW.2013. PhD Thesis: Immune molecules regulate medulloblastoma and neuronal apoptosis. Chapel Hill. Available at:
<https://cdr.lib.unc.edu/indexablecontent/uuid:03d3964d-b3da-4170-b7b2-Odbaf6f90>.
- Knott, JC., Edwards, AJ., Gullan RW., Clarke. TM., Pilkington, GJ.,1990. A human glioma cell line retaining expression of GFAP and gangliosides, recognized by A2B5 and LB1 antibodies, after prolonged passage. *Neuropathology and applied neurobiology*, 16(6), pp.489–500.
- Kong, Y., Li, R. & Ladisch, S., 1998. Natural forms of shed tumor gangliosides. *Biochimica et biophysica acta*, 1394(1), pp.43–56.
- Koochekpour, S. & Pilkington, G.J., 1996. Vascular and perivascular GD3 expression in human glioma. *Cancer letters*, 104(1), pp.97–102.
- Koochekpour, S., Merzak, A. & Pilkington, G.J., 1995. Growth factors and gangliosides stimulate laminin production by human glioma cells in vitro. *Neuroscience letters*, 186(1), pp.53–56.
- Kortmann, RD., Kühl, J., Timmermann, B., Mittler, U., Urban, C., Budach, V., ... Bamberg, M., 2000. Postoperative neoadjuvant chemotherapy before radiotherapy as compared to immediate radiotherapy followed by maintenance chemotherapy in the treatment of medulloblastoma in childhood: results of the German prospective randomized trial HIT '91. *International journal of radiation oncology, biology, physics*, 46(2), pp.269–279.
- Kotani, M., Terashima, T. & Tai, T., 1995. Developmental changes of ganglioside expressions in postnatal rat cerebellar cortex. *Brain research*, 700(1-2), pp.40–58.
- Krengel, U. & Bousquet, PA., 2014. Molecular recognition of gangliosides and their potential for cancer immunotherapies. *Frontiers in immunology*, 5, p.325.
- Laughton, SJ., Merchant, TE., Sklar, CA., Kun, LE., Fouladi, M., Broniser, A., ... Gajjar, A., 2008. Endocrine outcomes for children with embryonal brain tumors after risk-adapted craniospinal and conformal primary-site irradiation and high-dose chemotherapy with stem-cell rescue on the SJMB-96 trial. *Journal of clinical oncology : official journal of the American Society of Clinical Oncology*, 26(7), pp.1112–1118.

- Li, Y. & Chen, X., 2012. Sialic acid metabolism and sialyltransferases: natural functions and applications. *Applied Microbiology and Biotechnology*, 94(4), pp.887–905.
- Liang, YJ., Yang, BC., Chen, JM., Lin, YH., Huang, CL., Cheng, YY., ... Yu, J., 2011. Changes in glycosphingolipid composition during differentiation of human embryonic stem cells to ectodermal or endodermal lineages. *Stem cells (Dayton, Ohio)*, 29(12), pp.1995–2004.
- Louis, DN., Perry, A., Reifenberger, G., von Deimling, A., Figarella-Branger, D., Cabeneo, WK., ... Ellison, DW., 2016. The 2016 World Health Organization Classification of Tumors of the Central Nervous System: a summary. *Acta neuropathologica*, 131(6), pp.803–820.
- Lrhorfi, LA., Srinivasan, GV. & Schauer, R., 2007. Properties and partial purification of sialate-O-acetyltransferase from bovine submandibular glands. *Biological chemistry*, 388(3), pp.297–306.
- MacDonald, TJ., Brown, KM., LaFleur, B., Peterson, K., Lawlor, C., Chen, Y., P... Stephan, DA., 2001. Expression profiling of medulloblastoma: PDGFRA and the RAS/MAPK pathway as therapeutic targets for metastatic disease. *Nature genetics*, 29(2), pp.143–152.
- Macmillan, 2014. Signs and Symptoms of a Brain Tumour. *Macmillan.org.uk*. Available at: <https://www.macmillan.org.uk/information-and-support/brain-tumours/diagnosing/how-cancers-are-diagnosed/signs-and-symptoms/signs-and-symptoms-of-a-brain-tumour.html#tcm:9-155683> [Accessed January 13, 2016].
- Mahajan, VS. & Pillai, S., 2016. Sialic acids and autoimmune disease. *Immunological reviews*, 269(1), pp.145–161.
- Maidment, SL., Merzak, A., Koochekpour, S., Rooprai, HK., Rucklidge, GJ., Pilkington, GJ., 1996. The effect of exogenous gangliosides on matrix metalloproteinase secretion by human glioma cells in vitro. *European journal of cancer (Oxford, England : 1990)*, 32A(5), pp.868–871.
- Malisan, F. & Testi, R., 2002a. GD3 ganglioside and apoptosis. *Biochimica et biophysica acta*, 1585(2-3), pp.179–187.
- Malisan, F. & Testi, R., 2002b. GD3 in cellular ageing and apoptosis. *Experimental gerontology*, 37(10-11), pp.1273–1282.
- Malisan, F., Franchi, L., Tomassini, B., Ventura, N., Condó, I., Rippo, MR., ... Testi, R., 2002. Acetylation suppresses the proapoptotic activity of GD3 ganglioside. *The Journal of experimental medicine*, 196(12), pp.1535–1541.
- Mandal, C., Madnal, C., Chandra, S., Schauer, R., Mandal, C., 2012. Regulation of O-acetylation of sialic acids by sialate-O-acetyltransferase and sialate-O-acetyltransferase activities in childhood acute lymphoblastic leukemia. *Glycobiology*, 22(1), pp.70–83.

- Marquina, G., Waki, H., Fernandez, LE., Kon, K., Carr, A., Valiente, O., ... Ando, S., 1996. Gangliosides expressed in human breast cancer. *Cancer research*, 56(22), pp.5165–5171.
- Marshall, GM., Carter, DR., Cheung, BB., Lui, T., Mateos, MK., Meyerowitz, JG., Weiss, WA., 2014. The prenatal origins of cancer. *Nature reviews. Cancer*, 14(4), pp.277–289.
- Matarrese, P., Garofalo, T., Manganelli, V., Gambardella, L., Marconi, M., Grasson, M., ... Sorice, M., 2014. Evidence for the involvement of GD3 ganglioside in autophagosome formation and maturation. *Autophagy*, 10(5), pp.750–765.
- Meley, D., Spiller, DG., White, MRH., McDowell, H., Pizer, B., Sée, V., 2010. p53-mediated delayed NF-κB activity enhances etoposide-induced cell death in medulloblastoma. *Cell death & disease*, 1(5), p.e41.
- Mendez-Otero, R. & Santiago, MF., 2003. Functional role of a specific ganglioside in neuronal migration and neurite outgrowth., 36(8), pp.1003–1013.
- Mendez-Otero, R., Schlosshauer, B., Barnstable, CJ., Constantine-Paton, M., 1988. A developmentally regulated antigen associated with neural cell and process migration. *The Journal of neuroscienc : the official journal of the Society for Neuroscience*, 8(2), pp.564–579.
- Merzak, A., Koochekpour, S. & Pilkington, GJ., 1995. Adhesion of human glioma cell lines to fibronectin, laminin, vitronectin and collagen I is modulated by gangliosides in vitro. *Cell adhesion and communication*, 3(1), pp.27–43.
- Merzak, A., Koochekpour, S. & Pilkington, GJ., 1994. Cell surface gangliosides are involved in the control of human glioma cell invasion in vitro. *Neuroscience letters*, 177(1-2), pp.44–46.
- Merzak, A., Koochekpour, S., McCrea, S., Roxanis, Y., Pilkington, GJ., 1995. Gangliosides modulate proliferation, migration, and invasiveness of human brain tumor cells in vitro. *Molecular and chemical neuropathology / sponsored by the International Society for Neurochemistry and the World Federation of Neurology and research groups on neurochemistry and cerebrospinal fluid*, 24(2-3), pp.121–135.
- Michiels, EM., Schouten-Van Meeteren, AYN., Doz, F., van Dalen, EC., 1996. *Chemotherapy for children with medulloblastoma* E. M. Michiels, ed., Chichester, UK: John Wiley & Sons, Ltd.
- Millard, NE. & De Braganca, KC., 2015. Medulloblastoma. *Journal of child neurology*, p.0883073815600866.
- Miyakoshi, LM., Mendez-Otero, R. & Hedin-Pereira, C., 2001. The 9-O-acetyl GD3 gangliosides are expressed by migrating chains of subventricular zone neurons in vitro. *Brazilian journal of medical and biological research*, 34(5), pp.669–673.
- Mizuguchi, H., Xu, Z., Ishii-Watabe, A., Uchida, E., Hayakawa, T., 2000. IRES-dependent

second gene expression is significantly lower than cap-dependent first gene expression in a bicistronic vector. *Molecular therapy : the journal of the American Society of Gene Therapy*, 1(4), pp.376–382.

Molander, M., Berthold, CH., Persson, H., Fredman, P., 2000. Immunostaining of ganglioside GD1b, GD3 and GM1 in rat cerebellum: cellular layer and cell type specific associations. *Journal of neuroscience research*, 60(4), pp.531–542.

Montecucco, A., Zanetta, F. & Biamonti, G., 2015. Molecular mechanisms of etoposide. *EXCLI journal*, 14, pp.95–108.

Morfoouace, M., Shelat, A., Jacus, M., Freeman, BB., Turner, D., Robinson, S., ... Roussel, MF., 2014. Pemetrexed and gemcitabine as combination therapy for the treatment of Group3 medulloblastoma. *Cancer cell*, 25(4), pp.516–529.

Mueller, S. & Chang, S., 2009. Pediatric brain tumors: current treatment strategies and future therapeutic approaches. *Neurotherapeutics : the journal of the American Society for Experimental NeuroTherapeutics*, 6(3), pp.570–586.

Mukherjee, K., Chava, AK., Mandal, C., Dey, SN., Kniep, B., Chandra, S., Mandal, C., 2008. O-acetylation of GD3 prevents its apoptotic effect and promotes survival of lymphoblasts in childhood acute lymphoblastic leukaemia. *Journal of cellular biochemistry*, 105(3), pp.724–734.

Muthuswamy, SK., Gilman, M. & Brugge, JS., 1999. Controlled dimerization of ErbB receptors provides evidence for differential signaling by homo- and heterodimers. *Molecular and cellular biology*, 19(10), pp.6845–6857.

National cancer institute, 2015. Childhood Central Nervous System Embryonal Tumors Available at www.cancer.gov/types/brain/hp/child-cns-embryonal-treatment-pdq#section/_3 [Accessed January 16, 2016]

Ngamukote, S., Yanagisawa, M., Ariga, T., Ando, S., Yu, RK., 2007. Developmental changes of glycosphingolipids and expression of glycogenes in mouse brains. *Journal of Neurochemistry*, 103(6), pp.2327–2341.

Northcott, PA., Korshunov, A., Witt, H., Hielscher, T., Eberhart, CG., Mack, S., ... Taylor MD., ., 2011. Medulloblastoma comprises four distinct molecular variants. *Journal of clinical oncology : official journal of the American Society of Clinical Oncology*, 29(11), pp.1408–1414.

Northcott, PA., Dubuc, AM., Pfister, S., Taylor MD., 2015. Molecular subgroups of medulloblastoma. *Expert review of neurotherapeutics*, 12(7), pp.871–884.

Northcott, PA., Jones, DTW., Kool, M., Robinson, GW., Gilbertson, RJ., Cho, YJ., ... Pfister SM., 2012. Medulloblastomics: the end of the beginning. *Nature reviews. Cancer*, 12(12), pp.818–834.

Northcott, PA., Korshunov, A., Pfister, SM., Taylor, MD., 2012. The clinical implications of

- medulloblastoma subgroups. *Nature reviews. Neurology*, 8(6), pp.340–351.
- Northcott, PA., Shih, DJH., Peacock, J., Garzia, L., Morrissy, AS., Zichner, T., ... Taylor, MD., 2012. Subgroup-specific structural variation across 1,000 medulloblastoma genomes. *Nature*, 488(7409), pp.49–56.
- Office for National Statistics, 2013. Brain cancer rates have risen by a quarter over the past three decades. *Brain Cancer Rates Have Risen by a Quarter Over the Past Three Decades*.
- Offner, H., Thieme, T. & Vandenbark, AA., 1987. Gangliosides induce selective modulation of CD4 from helper T lymphocytes. *Journal of immunology (Baltimore, Md. : 1950)*, 139(10), pp.3295–3305.
- Ogiso, M., Ohta, M., Harada, Y., Kubo, H., Hirano, S., 1991. Developmental change in ganglioside expression in primary culture of rat neurons. *Neuroscience*, 41(1), pp.167–176.
- Ohkawa, Y., Miyazaki, S., Miyata, M., Hamamura, K., Furukawa, K., Furukawa, K., 2008. Essential roles of integrin-mediated signaling for the enhancement of malignant properties of melanomas based on the expression of GD3. *Biochemical and Biophysical Research Communications*, 373(1), pp.14–19.
- Ohkawa, Y., Miyazaki, S., Hamamura, K., Kambe, M., Miyata, M., Tajima, O., ... Furukawa, K., 2010. Ganglioside GD3 enhances adhesion signals and augments malignant properties of melanoma cells by recruiting integrins to glycolipid-enriched microdomains. *The Journal of biological chemistry*, 285(35), pp.27213–27223.
- Ohkawa, Y., Momota, H., Kato, A., Hashimoto, N., Tsunda, Y., Kotani, N., ... Furukawa, K., 2015. Ganglioside GD3 Enhances Invasiveness of Gliomas by Forming a Complex with Platelet-derived Growth Factor Receptor α and Yes Kinase. *The Journal of biological chemistry*, 290(26), pp.16043–16058.
- Olshefski, R. & Ladisch, S., 1996. Intercellular transfer of shed tumor cell gangliosides. *FEBS Letters*, 386(1), pp.11–14.
- Orizio, F., Damiati, E., Giacomuzzi, E., Benaglia, G., Pianta, S., Schauer, R., ... Monti, E., 2015. Human sialic acid acetyl esterase: Towards a better understanding of a puzzling enzyme. *Glycobiology*, p.cwv034.
- Packer, RJ., Sutton, LN., Elterman, R., Lange, B., Goldwein, J., Nicholson, HS., ... Wechsler-Jentzsch, K., 1994. Outcome for children with medulloblastoma treated with radiation and cisplatin, CCNU, and vincristine chemotherapy. *Journal of neurosurgery*, 81(5), pp.690–698.
- Packer, RJ., Goldwein, J., Nicholson, HS., Vezina, LG., Allen, JC., Ris, MD., ... Boyett, JM., 1999. Treatment of children with medulloblastomas with reduced-dose craniospinal radiation therapy and adjuvant chemotherapy: A Children's Cancer Group Study. *Journal of clinical oncology : official journal of the American Society of Clinical*

- Oncology*, 17(7), pp.2127–2136.
- Packer, R.J., Rood, B.R. & MacDonald, T.J., 2003. Medulloblastoma: present concepts of stratification into risk groups. *Pediatric neurosurgery*, 39(2), pp.60–67.
- Padhy, L.C., Shih, C., Cowing, D., Finkelstein, R., Weinberg, R.A., 1982. Identification of a phosphoprotein specifically induced by the transforming DNA of rat neuroblastomas. *Cell*, 28(4), pp.865–871.
- Parameswaran, R., Lim, M., Arutyunyan, Y., Abdel-Azim, H., Hurtz, C., Lau, K., ... Groffen, J., 2013. O-acetylated N-acetylneuraminic acid as a novel target for therapy in human pre-B acute lymphoblastic leukemia. *The Journal of experimental medicine*, 210(4), pp.805–819.
- Parker, K. & Pilkington, G.J., 2005. Morphological, immunocytochemical and flow cytometric in vitro characterisation of a surface-adherent medulloblastoma. *Anticancer research*, 25(6B), pp.3855–3863.
- Patel, S.K., Mullins, W.A., O'Neil, S.H., Wilson, K., 2011. Neuropsychological differences between survivors of supratentorial and infratentorial brain tumours. *Journal of intellectual disability research : JIDR*, 55(1), pp.30–40.
- Perry, S.W., Norman, J.P., Barbieri, J., Brown, E.B., Gelbard, H.A., 2011. Mitochondrial membrane potential probes and the proton gradient: a practical usage guide. *BioTechniques*, 50(2), pp.98–115.
- Phi, J.H., Lee, J., Wang, K.C., Cho, B.Y., Kim, I.O., Park, C.K., ... Kim, S.K., 2011. Cerebrospinal fluid M staging for medulloblastoma: reappraisal of Chang's M staging based on the CSF flow. *Neuro-oncology*, 13(3), pp.334–344.
- Phoenix, T.N., Patmore, D., Boop, S., Boulos, N., Jacus, M.O., Patel, Y.T., ... Gilbertson, R.J., 2016. Medulloblastoma Genotype Dictates Blood Brain Barrier Phenotype. *Cancer cell*, 29(4), pp.508–522.
- Pilkington, G.J., 1992. Glioma heterogeneity in vitro: the significance of growth factors and gangliosides. *Neuropathology and applied neurobiology*, 18(5), pp.434–442.
- Pilkington, G.J., Dunan, J.R., Rogers, J.P., Clarke, T.M., Knott, J.C., 1993. Growth factor modulation of surface ganglioside expression in cloned neoplastic glia. *Neuroscience letters*, 149(1), pp.1–5.
- Polkinghorn, W.R. & Tarbell, N.J., 2007. Medulloblastoma: tumorigenesis, current clinical paradigm, and efforts to improve risk stratification. *Nature clinical practice. Oncology*, 4(5), pp.295–304.
- Potapenko, M., Shurin, G.V. & de León, J., 2007. Gangliosides as immunomodulators. *Advances in experimental medicine and biology*, 601, pp.195–203.
- Pöschl, J., Stark, S., Neumann, P., Gröbner, S., Kawauchi, D., Jones, D.T.W., ... Ulrich, S., 2014. Genomic and transcriptomic analyses match medulloblastoma mouse models

- to their human counterparts. *Acta neuropathologica*, 128(1), pp.123–136.
- Prinetti, A., Prioni, S., Chigorno, V., Karagogeous, D., Tettamanti, G., Sonnno, S., 2001. Immunoseparation of sphingolipid-enriched membrane domains enriched in Src family protein tyrosine kinases and in the neuronal adhesion molecule TAG-1 by anti-GD3 ganglioside monoclonal antibody. *Journal of Neurochemistry*, 78(5), pp.1162–1167.
- Proia, RL., 2004. Gangliosides help stabilize the brain. *Nature genetics*, 36(11), pp.1147–1148.
- Pugh, TJ., Weeraratne, SD., Archer, TC., Pomeranz Krummel, DA., Auclair, D., Bochicchio, J., ... Cho, YJ., 2012. Medulloblastoma exome sequencing uncovers subtype-specific somatic mutations. *Nature*, 488(7409), pp.106–110.
- Pukel, CS., Vilcaes, AA., Torres Demichelis, V., Ruggiero, FM., Rodireguez-Walker, M., 1982. GD3, a prominent ganglioside of human melanoma. Detection and characterisation by mouse monoclonal antibody. *The Journal of experimental medicine*, 155(4), pp.1133–1147.
- Ramaswamy, V., Remke, M., Adamski, J., Bartels, U., Tabori, U., Wang, X., ... Bouffet, E., 2015. Medulloblastoma subgroup-specific outcomes in irradiated children: who are the true high-risk patients? *Neuro-oncology*, p.nou357.
- Ramaswamy, V., Remke, M., Bouffet, E., Faria, CC., Perreault, S., Cho, YJ., ... Taylor, MD., 2013. Recurrence patterns across medulloblastoma subgroups: an integrated clinical and molecular analysis. *The Lancet. Oncology*, 14(12), pp.1200–1207.
- Raybaud, C., Ramaswamy, V., Taylor, MD., Laughlin, S., 2015. Posterior fossa tumors in children: developmental anatomy and diagnostic imaging. *Child's nervous system : ChNS : official journal of the International Society for Pediatric Neurosurgery*, 31(10), pp.1661–1676.
- Regina Todeschini, A. & Hakomori, SI., 2008. Functional role of glycosphingolipids and gangliosides in control of cell adhesion, motility, and growth, through glycosynaptic microdomains. *Biochimica et biophysica acta*, 1780(3), pp.421–433.
- Reynolds, R. & Wilkin, GP., 1988. Expression of GD3 ganglioside by developing rat cerebellar Purkinje cells in situ. *Journal of neuroscience research*, 20(3), pp.311–319.
- Rippo, MR., Malisan, F., Ravagnan, L., Tomassini, B., Condo, I., Costantini, P., ... Testi, R., 2000. GD3 ganglioside directly targets mitochondria in a bcl-2-controlled fashion. *FASEB journal : official publication of the Federation of American Societies for Experimental Biology*, 14(13), pp.2047–2054.
- Ris, MD., Packer, R., Goldwein, J., Jones-Wallace, D., Boyette, JM., 2001. Intellectual outcome after reduced-dose radiation therapy plus adjuvant chemotherapy for medulloblastoma: a Children's Cancer Group study. *Journal of clinical oncology : official journal of the American Society of Clinical Oncology*, 19(15), pp.3470–3476.

- Ritter, G., Boosfeld, E., Markstein, E., Yu, RK., Ren, SL., Stallcup, WB., ... Livingston, PO., 1990. Biochemical and serological characteristics of natural 9-O-acetyl GD3 from human melanoma and bovine buttermilk and chemically O-acetylated GD3. *Cancer research*, 50(5), pp.1403–1410.
- Robertson, JD., Gogvadze, V., Zhivotovsky, B., Orrenius, S., 2000. Distinct pathways for stimulation of cytochrome c release by etoposide. *Journal of Biological Chemistry*, 275(42), pp.32438–32443.
- Robinson, G., Parker, M., Kranenburg, TA., Lu, C., Chen, X., Ding, L., ...Gilbertson, RJ., 2012. Novel mutations target distinct subgroups of medulloblastoma. *Nature*, 488(7409), pp.43–48.
- Roussel, MF. & Robinson, GW., 2013. Role of MYC in Medulloblastoma. *Cold Spring Harbor perspectives in medicine*, 3(11), pp.a014308–a014308.
- Rubin, LL. & de Sauvage, FJ., 2006. Targeting the Hedgehog pathway in cancer. *Nature reviews. Drug discovery*, 5(12), pp.1026–1033.
- Ruiz i Altaba, A., 1997. Catching a Gli-mpse of Hedgehog. *Cell*, 90(2), pp.193–196.
- Ryan, JM., Rice, GE. & Mitchell, MD., 2013. The role of gangliosides in brain development and the potential benefits of perinatal supplementation. *Nutrition research (New York, N.Y.)*, 33(11), pp.877–887.
- Salaroli, R., Ronchi, A., Buttarelli, FR., Cortesi, F., Marchese, V., Della, Bella, E., ... Cenacchi, G., 2015. Wnt activation affects proliferation, invasiveness and radiosensitivity in medulloblastoma. *Journal of Neuro-Oncology*, 121(1), pp.119–127.
- Samkari, A., White, J. & Packer, R., 2015. SHH inhibitors for the treatment of medulloblastoma. *Expert review of neurotherapeutics*, 15(7), pp.763–770.
- Sandhoff, K. & Harzer, K., 2013. Gangliosides and gangliosidoses: principles of molecular and metabolic pathogenesis. *The Journal of neuroscience : the official journal of the Society for Neuroscience*, 33(25), pp.10195–10208.
- Santiago, MF., Berredo-Pinho, M., Costa, MR., Gandra, M., Cavalcante, LA Mendez-Otero, R., 2001. Expression and function of ganglioside 9-O-acetyl GD3 in postmitotic granule cell development. *Molecular and cellular neurosciences*, 17(3), pp.488–499.
- Santiago, MF., Costa, MR. & Mendez-Otero, R., 2004. Immunoblockage of 9-O-acetyl GD3 ganglioside arrests the in vivo migration of cerebellar granule neurons. *The Journal of neuroscience : the official journal of the Society for Neuroscience*, 24(2), pp.474–478.
- Sato, C., Matsuda, T. & Kitajima, K., 2002. Neuronal differentiation-dependent expression of the disialic acid epitope on CD166 and its involvement in neurite formation in Neuro2A cells. *Journal of Biological Chemistry*, 277(47), pp.45299–45305.
- Schauer, R., 2004. Sialic acids: fascinating sugars in higher animals and man. *Zoology (Jena, Germany)*, 107(1), pp.49–64.

- Schengrund, CL., 2015. Gangliosides: glycosphingolipids essential for normal neural development and function. *Trends in biochemical sciences*, 40(7), pp.397–406.
- Schroeder, K. & Gururangan, S., 2014. Molecular variants and mutations in medulloblastoma. *Pharmacogenomics and personalized medicine*, 7, pp.43–51.
- Schuler, D., Hauser, P. & Garami, M., 2014. Chemotherapy of Medulloblastoma in Children A. L. Abujamra, ed. *In Tech*, pp.1–15.
- Schwarz, A. & Futerman, A.H., 1997. Determination of the localization of gangliosides using anti-ganglioside antibodies: comparison of fixation methods. *The journal of histochemistry and cytochemistry : official journal of the Histochemistry Society*, 45(4), pp.611–618.
- Segal, RA., Goumnerova, LC., Kwon, YK., Stiles, CD., Pomeroy, SL., 1994. Expression of the neurotrophin receptor TrkC is linked to a favorable outcome in medulloblastoma. *Proceedings of the National Academy of Sciences of the United States of America*, 91(26), pp.12867–12871.
- Segatto, O., King, CR., Pierce, JH., Di Fiore, PP., Aaronson, SA., 1988. Different structural alterations upregulate in vitro tyrosine kinase activity and transforming potency of the erbB-2 gene. *Molecular and cellular biology*, 8(12), pp.5570–5574.
- Semple, BD., Blomgren, K., Gimlin, K., Ferriero, DM., Noble-Haesslein, LJ., 2013. Brain development in rodents and humans: Identifying benchmarks of maturation and vulnerability to injury across species. *Progress in neurobiology*, 106-107, pp.1–16.
- Seyfried, TN. & Mukherjee, P., 2010. Ganglioside GM3 Is Antiangiogenic in Malignant Brain Cancer. *Journal of oncology*, 2010(1), pp.961243–8.
- Shi, WX., Chammas, R. & Varki, A., 1996. Linkage-specific action of endogenous sialic acid O-acetyltransferase in Chinese hamster ovary cells. *Journal of Biological Chemistry*, 271(25), pp.15130–15138.
- Shibuya, H., Hamamura, K., Hotta, H., Matsumoto, Y., Nishida, Y., Hattori, H., ... Koichi, F., 2012. Enhancement of malignant properties of human osteosarcoma cells with disialyl gangliosides GD2/GD3. *Cancer Science*, 103(9), pp.1656–1664.
- Siddik, ZH., 2003. Cisplatin: mode of cytotoxic action and molecular basis of resistance. *Oncogene*, 22(47), pp.7265–7279.
- Smeyne, RJ., Chu, T., Lewin, A., Bian, F., Sanlioglu, S., S-Crisman, S., ... Oberdick, J., 1995. Local control of granule cell generation by cerebellar Purkinje cells. *Molecular and cellular neurosciences*, 6(3), pp.230–251.
- Smith, MJ., Beetz, C., Williams, SG., Bhaskar, SS., O'Sullivan, J., Anderson, B., ... Evans, DGR., 2014. Germline mutations in SUFU cause Gorlin syndrome-associated childhood medulloblastoma and redefine the risk associated with PTCH1 mutations. *Journal of clinical oncology : official journal of the American Society of Clinical*

- Oncology*, 32(36), pp.4155–4161.
- Sorice, M., Garofalo, T., Misasi, R., Manganelli, V., Vona, R., Malorni, W., 2012. Ganglioside GD3 as a raft component in cell death regulation. *Anti-cancer agents in medicinal chemistry*, 12(4), pp.376–382.
- Srinivasan, GV. & Schauer, R., 2009. Assays of sialate-O-acetyltransferases and sialate-O-acetylerases. *Glycoconjugate journal*, 26(8), pp.935–944.
- Staal, JA., Lau, LS., Zhang, H., Ingram, WJ., Hallahan, AR., Northcott, PA., ... Rood, BR., 2015. Proteomic profiling of high risk medulloblastoma reveals functional biology. *Oncotarget*, 6(16), pp.14584–14595.
- Stewart, DJ., Molepo, JM., Green, RM., Montpetit, VA., Hugenholtz, H., Lamothe, A., ... Goel, R., 1995. Factors affecting platinum concentrations in human surgical tumour specimens after cisplatin. *British journal of cancer*, 71(3), pp.598–604.
- Stewart, DJ., Richard, MT., Hugenholtz, H., Dennery, JM., Belanger, R., Gerin-Lajoie, J., ... Hopkins, HS., 1984. Penetration of VP-16 (etoposide) into human intracerebral and extracerebral tumors. *Journal of Neuro-Oncology*, 2(2), pp.133–139.
- Strother, D., Ashley, D., Kellie, SJ., Patel, A., Jones-Wallace, D., Thompson, S., ... Gajjar, A., 2001. Feasibility of four consecutive high-dose chemotherapy cycles with stem-cell rescue for patients with newly diagnosed medulloblastoma or supratentorial primitive neuroectodermal tumor after craniospinal radiotherapy: results of a collaborative study. *Journal of clinical oncology : official journal of the American Society of Clinical Oncology*, 19(10), pp.2696–2704.
- Surolia, I., Pirnie, SP., Chellappa, V., Taylor, KN., Cariappa, A., Moya, J., ... Pillai, S., 2010. Functionally defective germline variants of sialic acid acetylerase in autoimmunity. *Nature*, 466(7303), pp.243–247.
- Susin, SA., Lorenzo, HK., Zamzami, N., Marzo, I., Snow, BE., Brothers, GM., ... Kroemer, G., 1999. Molecular characterization of mitochondrial apoptosis-inducing factor. *Nature*, 397(6718), pp.441–446.
- Svennerholm, L., 1963. The gangliosides. *Journal of lipid research*, pp.145–155.
- Svennerholm, L., Rynmark, BM., Vilbergsson, G., Fredman, P., Gottfries, J., Månsson, JE., Percy, A., 1991. Gangliosides in human fetal brain. *Journal of Neurochemistry*, 56(5), pp.1763–1768.
- Svennerholm, L., Boström, K., Fredman, P., Månsson, JE., Rosengren, B., Rynmark, BM., 1989. Human brain gangliosides: developmental changes from early fetal stage to advanced age. *Biochimica et biophysica acta*, 1005(2), pp.109–117.
- Swartling, FJ., Hede, SM. & Weiss, WA., 2013. What underlies the diversity of brain tumors? *Cancer metastasis reviews*, 32(1-2), pp.5–24.
- Taipale, J., Copper, MK., Maiti, T., Beachy, PA., 2002. Patched acts catalytically to suppress

- the activity of Smoothed. *Nature*, 418(6900), pp.892–897.
- Takematsu, H., Diaz, S., Stoddart, A., Zhang, Y., Varki, A., 1999. Lysosomal and cytosolic sialic acid 9-O-acetyltransferase activities can be encoded by one gene via differential usage of a signal peptide-encoding exon at the N terminus. *Journal of Biological Chemistry*, 274(36), pp.25623–25631.
- Tanaka, S., Diaz, S., Stoddart, A., Zhang, Y., Varki, A., 2009. The Gs-linked receptor GPR3 inhibits the proliferation of cerebellar granule cells during postnatal development. L. Mei, ed. *PLoS ONE*, 4(6), p.e5922.
- Tarbell, NJ., Friedman, H., Polkinghorn, WR., Tock, T., Zhou, T., Chen, Z., ... Larry, K., 2013. High-risk medulloblastoma: a pediatric oncology group randomized trial of chemotherapy before or after radiation therapy (POG 9031). *Journal of clinical oncology : official journal of the American Society of Clinical Oncology*, 31(23), pp.2936–2941.
- Taylor, MD., Northcott, PA., Korshunov, A., Remke, M., Cho, YJ., Clifford, SC., ... Pfister, SM., 2012. Molecular subgroups of medulloblastoma: the current consensus., 123(4), pp.465–472.
- Taylor, MD., Liu, L., Raffel, C., Hui, CC., Mainprize, TG., Zhang, X., ... Hogg, D., 2002. Mutations in SUFU predispose to medulloblastoma. *Nature genetics*, 31(3), pp.306–310.
- Taylor, RE., Bailey, CC., Robinson, K., Weston, CL., Ellison, D., Ironside, J., ... Lashford, LS., 2003. Results of a randomized study of preradiation chemotherapy versus radiotherapy alone for nonmetastatic medulloblastoma: The International Society of Paediatric Oncology/United Kingdom Children's Cancer Study Group PNET-3 Study. *Journal of clinical oncology : official journal of the American Society of Clinical Oncology*, 21(8), pp.1581–1591.
- Tempera, I., Buchetti, B., Lococo, E., Gradini, R., Mastronardi, A., Mascellino, MT., ... Lenti, L., GD3 nuclear localization after apoptosis induction in HUT-78 cells. *Biochemical and Biophysical Research Communications*, 368(3), pp.495–500.
- Thomas, PR., Deutsch, M., Kepner, JL., Boyett, JM., Krischer, J., Aronin, P., ... Kin, LE., Low-stage medulloblastoma: final analysis of trial comparing standard-dose with reduced-dose neuraxis irradiation. *Journal of clinical oncology : official journal of the American Society of Clinical Oncology*, 18(16), pp.3004–3011.
- Tichy, J., Zinke, J., Bunz, B., Meyerann, R., Harter, PN., Mittelbronn, M., 2015. Expression Profile of Sonic Hedgehog Pathway Members in the Developing Human Fetal Brain. *BioMed research international*, 2015(4), pp.494269–15.
- Vandamme-Feldhaus, V. & Schauer, R., 1998. Characterization of the enzymatic 7-O-acetylation of sialic acids and evidence for enzymatic O-acetyl migration from C-7 to C-9 in bovine submandibular gland. *Journal of biochemistry*, 124(1), pp.111–121.

- Varki, A., Muchmore, E. & Diaz, S., 1986. A sialic acid-specific O-acetyl esterase in human erythrocytes: possible identity with esterase D, the genetic marker of retinoblastomas and Wilson disease. *Proceedings of the National Academy of Sciences of the United States of America*, 83(4), pp.882–886.
- Vlasak, R., Krystal, M., Nacht, M., Palese, P., 1987. The influenza C virus glycoprotein (HE) exhibits receptor-binding (hemagglutinin) and receptor-destroying (esterase) activities. *Virology*, 160(2), pp.419–425.
- Wallace, VA., 1999. Purkinje-cell-derived Sonic hedgehog regulates granule neuron precursor cell proliferation in the developing mouse cerebellum. *Current biology : CB*, 9(8), pp.445–448.
- Wang, X., Sun, P., Al-Qamari, A., Tai, T., Kawashima, I., Paller, AS., 2001. Carbohydrate-carbohydrate binding of ganglioside to integrin alpha(5) modulates alpha(5)beta(1) function. *Journal of Biological Chemistry*, 276(11), pp.8436–8444.
- Wechsler-Reya, R. & Scott, MP., 2001a. The developmental biology of brain tumors. In *Annual Review of Neuroscience*. Annual Reviews 4139 El Camino Way, P.O. Box 10139, Palo Alto, CA 94303-0139, USA, pp. 385–428.
- Wechsler-Reya, R. & Scott, MP., 2001b. The developmental biology of brain tumours. *annual review of neuroscience*, 24(1), pp.385–428.
- Wechsler-Reya, RJ., 2003. Analysis of gene expression in the normal and malignant cerebellum. *Recent progress in hormone research*, 58, pp.227–248.
- Wechsler-Reya, RJ. & Scott, MP., 1999. Control of neuronal precursor proliferation in the cerebellum by Sonic Hedgehog. *Neuron*, 22(1), pp.103–114.
- Weiner, DB., Lui, J., Cohen, JA., Williams, WV., Greene, MI., 1989. A point mutation in the neu oncogene mimics ligand induction of receptor aggregation. *Nature*, 339(6221), pp.230–231.
- Weiner, HL., Bakst, R., Hurlbert, MS., Ruggiero, J., Ahn, E., Lee, WS., ... Turnbull, DH., 2002. Induction of medulloblastomas in mice by sonic hedgehog, independent of Gli1. *Cancer research*, 62(22), pp.6385–6389.
- Welte, K., Miller, G., Chapman, PB., Yuasa, H., Naoli, E., Kunicka, JE., ... Houghton, AN., 1987. Stimulation of T lymphocyte proliferation by monoclonal antibodies against GD3 ganglioside. *Journal of immunology (Baltimore, Md. : 1950)*, 139(6), pp.1763–1771.
- Wen, J., Ramadevi, N., Nguyen, D., Perkins, C., Worthington, E., Bhalla, K., 2000. Antileukemic drugs increase death receptor 5 levels and enhance Apo-2L-induced apoptosis of human acute leukemia cells. *Blood*, 96(12), pp.3900–3906.
- Wingate, RJ., 2001. The rhombic lip and early cerebellar development. *Current opinion in neurobiology*, 11(1), pp.82–88.

- Wipfler, D., Srinivasan GV., Sadick, H., Kniep, B., Arming, S., Willhauch-Fleckenstein, M., ... Schwartz-Albiez, R., 2011. Differentially regulated expression of 9-O-acetyl GD3 (CD60b) and 7-O-acetyl-GD3 (CD60c) during differentiation and maturation of human T and B lymphocytes. *Glycobiology*, 21(9), pp.1161–1172.
- Wolswijk, G., 1995. Strongly GD3+ cells in the developing and adult rat cerebellum belong to the microglial lineage rather than to the oligodendrocyte lineage. *Glia*, 13(1), pp.13–26.
- World Health Organisation, 2007. World Health Organization Classification of Tumours WHO Classification of Tumours of the Central Nervous System 4th Edition. pp.1–20.
- Yanagisawa, M., Yoshimura, S. & Yu, RK., 2011. Expression of GD2 and GD3 gangliosides in human embryonic neural stem cells. *ASN neuro*, 3(2), pp.69–74.
- Yarden, Y. & Sliwkowski, MX., 2001. Untangling the ErbB signalling network. *Nature reviews. Molecular cell biology*, 2(2), pp.127–137.
- Yu, RK., Bieberich, E., Xia, T., Zeng, G., 2004. Regulation of ganglioside biosynthesis in the nervous system. *Journal of lipid research*, 45(5), pp.783–793.
- Yu, RK., Tsai, YT. & Ariga, T., 2012. Functional Roles of Gangliosides in Neurodevelopment: An Overview of Recent Advances. *Neurochemical research*, 37(6), pp.1230–1244.
- Zamzami, N. & Kroemer, G., 2001. The mitochondrion in apoptosis: how Pandora's box opens. *Nature reviews. Molecular cell biology*, 2(1), pp.67–71.
- Zeng, G., Gao, L., Birklé, S., Yu, RK., 2000. Suppression of ganglioside GD3 expression in a rat F-11 tumor cell line reduces tumor growth, angiogenesis, and vascular endothelial growth factor production. *Cancer research*, 60(23), pp.6670–6676.
- Zhu, H., Chan, HC., Zhou, Z., Li, J., Zhu, H., Yin, L., ... Sha, J., 2004. A Gene Encoding Sialic-Acid-Specific 9-O-Acetyltransferase Found in Human Adult Testis. *Journal of biomedicine & biotechnology*, 2004(3), pp.130–136.
- Zhukova, N., Ramaswamy, V., Remke, M., Pfaff, E., Shh, DJH., Martin, DC., ... Tabori, U., 2013. Subgroup-specific prognostic implications of TP53 mutation in medulloblastoma. *Journal of clinical oncology : official journal of the American Society of Clinical Oncology*, 31(23), pp.2927–2935.
- Zomerman, WW., Plaschaert, SLA., Diks, SH., Lourens, HJ., Meeuwsende Boer, T., Hoving, EW., ... de Bont, ESJM., 2015. Exogenous HGF Bypasses the Effects of ErbB Inhibition on Tumor Cell Viability in Medulloblastoma Cell Lines. J. W. Lee, ed. *PLoS ONE*, 10(10), p.e0141381.
- Zurawel, RH., Chiappa, SA., Allen, C., Raffel, C., 1998. Sporadic medulloblastomas contain oncogenic beta-catenin mutations. *Cancer research*, 58(5), pp.896–899.

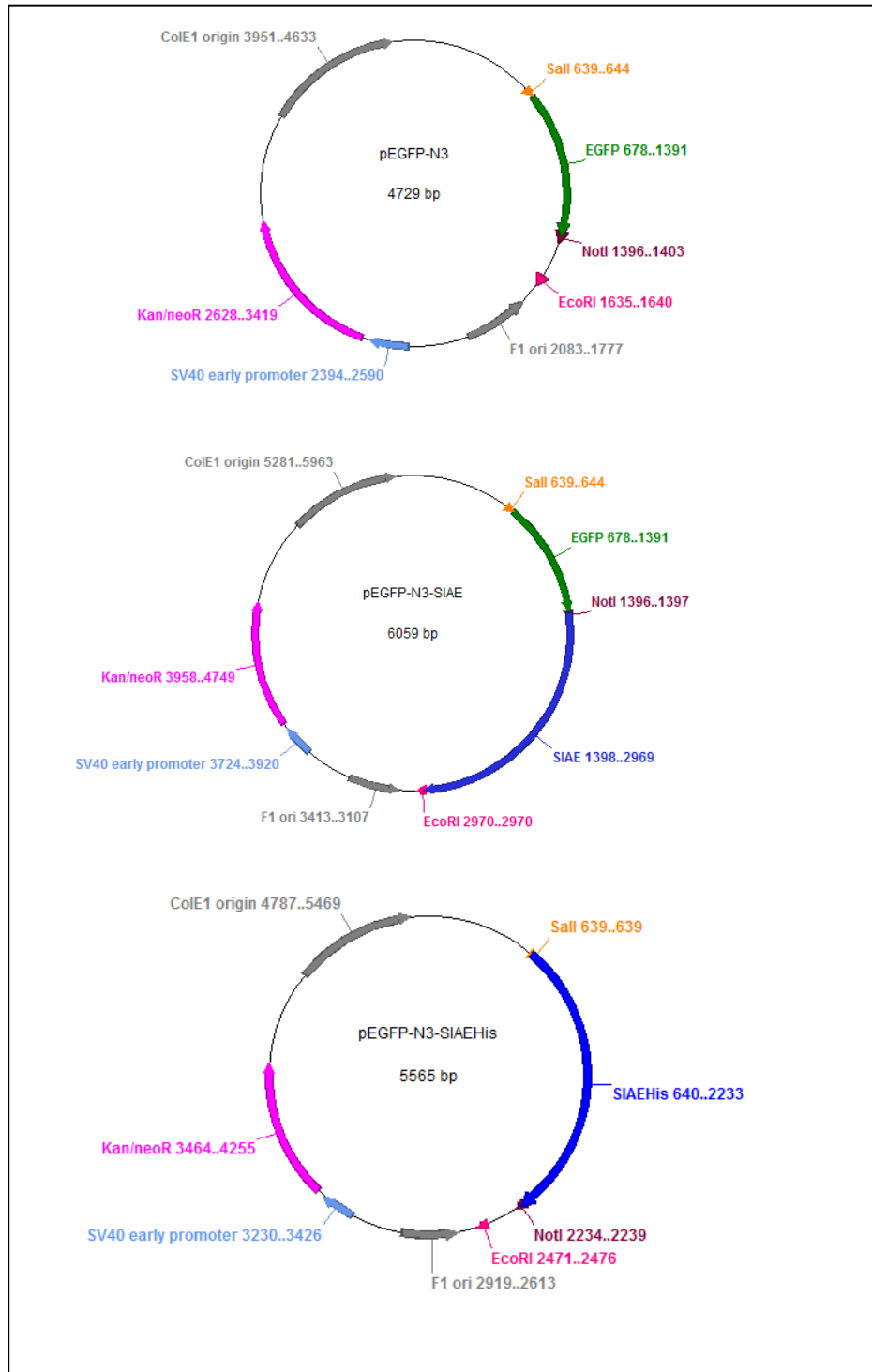
Appendices

Appendix 1 – Plasmid maps and sequence homology of pEGFP-N3, pEGFP-N3-SIAE and pEGFP-N3-SIAEHis

Dr. Reinhard Vlasak, our collaborator at the University of Salzburg, Austria, provided SIAE constructs for overexpression studies (appendix 1.1). The pEGFP-N3 construct encodes a red-shifted variant of wild-type green fluorescent protein (GFP), which has been optimised for brighter expression and a higher level of expression in mammalian cells. This enhanced green fluorescent protein (EGFP) has amino acid substitutions of F64L and S65T that generate a brighter fluorophore than wild-type GFP. The coding sequence of EGFP contains 190 silent base changes that optimise the sequence for human codon usage preferences. The constructs provided were pEGFP-N3 (empty vector control); pEGFP-N3-SIAE (wild-type enzyme) and pEGFP-N3-SIAE-His (wild-type enzyme containing a His-tag).

The multiple cloning site (MCS) in pEGFP-N3 is between the immediate early promoter of cytomegalovirus (CMV) and the EGFP gene. Genes that are cloned into the multiple cloning site are expressed as *N*-terminal fusion proteins with EGFP. SV40 polyadenylation signals downstream of the EGFP gene direct proper processing of the 3' end of the EGFP mRNA. The vector backbone also contains an SV40 origin of replication in mammalian cells expressing the SV40 T-antigen. A neomycin resistance gene (Neo^r) consisting of the SV40 early promoter, the neomycin/kanamycin resistance gene of Tn5, and polyadenylation signals from the herpes simplex virus thymidine kinase (HSV TK) gene, allows the selection of stably transfected cell lines with G-418. A bacterial promoter located upstream of this gene expresses kanamycin resistance in *E.coli*. In *E.coli* this construct also provides a pUC origin of replication and an f1 origin for single stranded DNA production.

The constructs were sequenced (appendix 1.2) to ensure that gene inserts had been incorporated correctly, standard pCMV primers and a downstream sequencing primer due to transcript length (Eurofins Genomics).



Appendix 1.1 Plasmid maps of pEGFP-N3, pEGFP-N3-SIAE and pEGFP-N3-SIAEHis provided by Dr. Reinhard Vlasak.

<p>REFERENCE_SIAE_ISOFORM_1 SIAE_PLASMID SIAEHIS_PLASMID</p>	<p>1 10 20 30 40 50 60</p>	<p>ATGGTCGGCCGGGGCTTGTACTCGGGCTGGTGTGCCATTAATCCTGTGGGCCGACAGA ATGGTCGGCCGGGGCTTGTACTCGGGCTGGTGTGCCATTAATCCTGTGGGCCGACAGA ATGGTCGGCCGGGGCTTGTACTCGGGCTGGTGTGCCATTAATCCTGTGGGCCGACAGA</p>
<p>REFERENCE_SIAE_ISOFORM_1 SIAE_PLASMID SIAEHIS_PLASMID</p>	<p>70 80 90 100 110 120</p>	<p>AGTGCAGGTATTGGTTTTCGCTTTCGCTTCATACATCAATAATGATATGGTGTGCTGCAGAAG AGTGCAGGTATTGGTTTTCGCTTTCGCTTCATACATCAATAATGATATGGTGTGCTGCAGAAG AGTGCAGGTATTGGTTTTCGCTTTCGCTTCATACATCAATAATGATATGGTGTGCTGCAGAAG</p>
<p>REFERENCE_SIAE_ISOFORM_1 SIAE_PLASMID SIAEHIS_PLASMID</p>	<p>130 140 150 160 170 180</p>	<p>GAGCCTGCTGGGGCAGTGATATGGGGCTTCGGTACACCTGGAGCCACAGTGACCCTGACC GAGCCTGCTGGGGCAGTGATATGGGGCTTCGGTACACCTGGAGCCACAGTGACCCTGACC GAGCCTGCTGGGGCAGTGATATGGGGCTTCGGTACACCTGGAGCCACAGTGACCCTGACC</p>
<p>REFERENCE_SIAE_ISOFORM_1 SIAE_PLASMID SIAEHIS_PLASMID</p>	<p>190 200 210 220 230 240</p>	<p>CTGCGCCAAGGTCAGGAAACCATCATGAAGAAAGTGACCAGTGTGAAAGCTCACTCTGAT CTGCGCCAAGGTCAGGAAACCATCATGAAGAAAGTGACCAGTGTGAAAGCTCACTCTGAT CTGCGCCAAGGTCAGGAAACCATCATGAAGAAAGTGACCAGTGTGAAAGCTCACTCTGAT</p>
<p>REFERENCE_SIAE_ISOFORM_1 SIAE_PLASMID SIAEHIS_PLASMID</p>	<p>250 260 270 280 290 300</p>	<p>ACGTGGATGGTGGTACTGGATCCTATGAAGCCTGGAGGACCTTTCGAAAGTGTGGCACA ACGTGGATGGTGGTACTGGATCCTATGAAGCCTGGAGGACCTTTCGAAAGTGTGGCACA ACGTGGATGGTGGTACTGGATCCTATGAAGCCTGGAGGACCTTTCGAAAGTGTGGCACA</p>
<p>REFERENCE_SIAE_ISOFORM_1 SIAE_PLASMID SIAEHIS_PLASMID</p>	<p>310 320 330 340 350 360</p>	<p>CAGACTTTGGAGAAAATAAACTTCACCTGAGAGTTCATGACGTCCTGTTGGAGATGTC CAGACTTTGGAGAAAATAAACTTCACCTGAGAGTTCATGACGTCCTGTTGGAGATGTC CAGACTTTGGAGAAAATAAACTTCACCTGAGAGTTCATGACGTCCTGTTGGAGATGTC</p>
<p>REFERENCE_SIAE_ISOFORM_1 SIAE_PLASMID SIAEHIS_PLASMID</p>	<p>370 380 390 400 410 420</p>	<p>TGGCTCTGTAGTGGGCAGAGTAACATGCAGATGACTGTGTTACAGATATTTAATGCTACA TGGCTCTGTAGTGGGCAGAGTAACATGCAGATGACTGTGTTACAGATATTTAATGCTACA TGGCTCTGTAGTGGGCAGAGTAACATGCAGATGACTGTGTTACAGATATTTAATGCTACA</p>
<p>REFERENCE_SIAE_ISOFORM_1 SIAE_PLASMID SIAEHIS_PLASMID</p>	<p>430 440 450 460 470 480</p>	<p>AGGGAGTTGTCTAACACTGCGGCATATCAGTCTGTCCGCATCCTCTCTGCTCTCCCAT AGGGAGTTGTCTAACACTGCGGCATATCAGTCTGTCCGCATCCTCTCTGCTCTCCCAT AGGGAGTTGTCTAACACTGCGGCATATCAGTCTGTCCGCATCCTCTCTGCTCTCCCAT</p>
<p>REFERENCE_SIAE_ISOFORM_1 SIAE_PLASMID SIAEHIS_PLASMID</p>	<p>490 500 510 520 530 540</p>	<p>CAAGCAGAGCAGGAGCTGGAGGACCTTGTGCGGTTGACTTGCAGTGGTCTAAGCCACC CAAGCAGAGCAGGAGCTGGAGGACCTTGTGCGGTTGACTTGCAGTGGTCTAAGCCACC CAAGCAGAGCAGGAGCTGGAGGACCTTGTGCGGTTGACTTGCAGTGGTCTAAGCCACC</p>
<p>REFERENCE_SIAE_ISOFORM_1 SIAE_PLASMID SIAEHIS_PLASMID</p>	<p>550 560 570 580 590 600</p>	<p>TCAGAAAACCTTAGGCCATGGATATTTCAAGTACATGTCAGCAGTGTGCTGGCTCTTTGGA TCAGAAAACCTTAGGCCATGGATATTTCAAGTACATGTCAGCAGTGTGCTGGCTCTTTGGA TCAGAAAACCTTAGGCCATGGATATTTCAAGTACATGTCAGCAGTGTGCTGGCTCTTTGGA</p>
<p>REFERENCE_SIAE_ISOFORM_1 SIAE_PLASMID SIAEHIS_PLASMID</p>	<p>610 620 630 640 650 660</p>	<p>CGTCACCTTTATGACACTCTGCAGTATCCCATCGGGCTGATCGCCTCCAGCTGGGGCGGG CGTCACCTTTATGACACTCTGCAGTATCCCATCGGGCTGATCGCCTCCAGCTGGGGCGGG CGTCACCTTTATGACACTCTGCAGTATCCCATCGGGCTGATCGCCTCCAGCTGGGGCGGG</p>

670 680 690 700 710 720
REFERENCE_SIAE_ISOFORM_1 ACACCCATTGAAGCCTGGTCATCTGGACGGTCACTGAAAGCCTGTGGGGTCCCTAAACAA
SIAE_PLASMID ACACCCATTGAAGCCTGGTCATCTGGACGGTCACTGAAAGCCTGTGGGGTCCCTAAACAA
SIAEHIS_PLASMID ACACCCATTGAAGCCTGGTCATCTGGACGGTCACTGAAAGCCTGTGGGGTCCCTAAACAA

730 740 750 760 770 780
REFERENCE_SIAE_ISOFORM_1 GGGTCCATTCCATACGATTCTGTAAGTGGTCCCAGTAAGCACTCTGTTCTCTGGAATGCC
SIAE_PLASMID GGGTCCATTCCATACGATTCTGTAAGTGGTCCCAGTAAGCACTCTGTTCTCTGGAATGCC
SIAEHIS_PLASMID GGGTCCATTCCATACGATTCTGTAAGTGGTCCCAGTAAGCACTCTGTTCTCTGGAATGCC

790 800 810 820 830 840
REFERENCE_SIAE_ISOFORM_1 ATGATCCATCCACTGTGCAATATGACTCTGAAAGGGGTAGTATGGTACCAGGGGGAGTCC
SIAE_PLASMID ATGATCCATCCACTGTGCAATATGACTCTGAAAGGGGTAGTATGGTACCAGGGGGAGTCC
SIAEHIS_PLASMID ATGATCCATCCACTGTGCAATATGACTCTGAAAGGGGTAGTATGGTACCAGGGGGAGTCC

850 860 870 880 890 900
REFERENCE_SIAE_ISOFORM_1 AATATAAATTATAACACGGATCTGTACAATTGCACATTCCTTGCACATCATCGAAGACTGG
SIAE_PLASMID AATATAAATTATAACACGGATCTGTACAATTGCACATTCCTTGCACATCATCGAAGACTGG
SIAEHIS_PLASMID AATATAAATTATAACACGGATCTGTACAATTGCACATTCCTTGCACATCATCGAAGACTGG

910 920 930 940 950 960
REFERENCE_SIAE_ISOFORM_1 CGTGAAACCTTCCACCGTGGTTCCAGGGGCAGACGGAGCGTTTCTTCCCATTGGACTT
SIAE_PLASMID CGTGAAACCTTCCACCGTGGTTCCAGGGGCAGACGGAGCGTTTCTTCCCATTGGACTT
SIAEHIS_PLASMID CGTGAAACCTTCCACCGTGGTTCCAGGGGCAGACGGAGCGTTTCTTCCCATTGGACTT

970 980 990 1000 1010 1020
REFERENCE_SIAE_ISOFORM_1 GTCCAGTTATCTTCAGATTTGTCTAAGAAGAGCTCAGACGATGGATTTCCCAGATCCGT
SIAE_PLASMID GTCCAGTTATCTTCAGATTTGTCTAAGAAGAGCTCAGACGATGGATTTCCCAGATCCGT
SIAEHIS_PLASMID GTCCAGTTATCTTCAGATTTGTCTAAGAAGAGCTCAGACGATGGATTTCCCAGATCCGT

1030 1040 1050 1060 1070 1080
REFERENCE_SIAE_ISOFORM_1 TGGCATCAAACAGCAGACTTCGGCTATGTCCCAACCCAAAGATGCCCAATACCTTTCATG
SIAE_PLASMID TGGCATCAAACAGCAGACTTCGGCTATGTCCCAACCCAAAGATGCCCAATACCTTTCATG
SIAEHIS_PLASMID TGGCATCAAACAGCAGACTTCGGCTATGTCCCAACCCAAAGATGCCCAATACCTTTCATG

1090 1100 1110 1120 1130 1140
REFERENCE_SIAE_ISOFORM_1 GCTGTAGCTATGGATCTCTGTGATAGAGACTCGCCCTTTTGGCAGCATCCACCCCTCGAGAT
SIAE_PLASMID GCTGTAGCTATGGATCTCTGTGATAGAGACTCGCCCTTTTGGCAGCATCCACCCCTCGAGAT
SIAEHIS_PLASMID GCTGTAGCTATGGATCTCTGTGATAGAGACTCGCCCTTTTGGCAGCATCCACCCCTCGAGAT

1150 1160 1170 1180 1190 1200
REFERENCE_SIAE_ISOFORM_1 AAACAGACTGTGGCTTATCGGGCTGCATTTGGGGGCCCGTCTCTGGCTTATGGTGAGAAG
SIAE_PLASMID AAACAGACTGTGGCTTATCGGGCTGCATTTGGGGGCCCGTCTCTGGCTTATGGTGAGAAG
SIAEHIS_PLASMID AAACAGACTGTGGCTTATCGGGCTGCATTTGGGGGCCCGTCTCTGGCTTATGGTGAGAAG

1210 1220 1230 1240 1250 1260
REFERENCE_SIAE_ISOFORM_1 AATTTGACCTTTGAAGGACCACTGCCTGAGAAGATAGAAGTCTTTGGCTCACAAGGGGCTG
SIAE_PLASMID AATTTGACCTTTGAAGGACCACTGCCTGAGAAGATAGAAGTCTTTGGCTCACAAGGGGCTG
SIAEHIS_PLASMID AATTTGACCTTTGAAGGACCACTGCCTGAGAAGATAGAAGTCTTTGGCTCACAAGGGGCTG

1270 1280 1290 1300 1310 1320
REFERENCE_SIAE_ISOFORM_1 CTC AATCTCACATATTACCAGCAAATCCAGGTGCAGAAAAAGGACAACAAGATATTTGAG
SIAE_PLASMID CTC AATCTCACATATTACCAGCAAATCCAGGTGCAGAAAAAGGACAACAAGATATTTGAG
SIAEHIS_PLASMID CTC AATCTCACATATTACCAGCAAATCCAGGTGCAGAAAAAGGACAACAAGATATTTGAG


```

1330      1340      1350      1360      1370      1380
REFERENCE_SIAE_ISOFORM_1 ATCTCCTGTTGCAGTGACCATCGATGCAAGTGGCTTCCAGCTTCTATGAACACCGTCTCC
SIAE_PLASMID           ATCTCCTGTTGCAGTGACCATCGATGCAAGTGGCTTCCAGCTTCTATGAACACCGTCTCC
SIAEHIS_PLASMID       ATCTCCTGTTGCAGTGACCATCGATGCAAGTGGCTTCCAGCTTCTATGAACACCGTCTCC

1390      1400      1410      1420      1430      1440
REFERENCE_SIAE_ISOFORM_1 ACCCAGTCCCTGACCCTGGCGATCGATTCTTGTCATGGCACTGTGGTTGCTCTCCGCTAT
SIAE_PLASMID           ACCCAGTCCCTGACCCTGGCGATCGATTCTTGTCATGGCACTGTGGTTGCTCTCCGCTAT
SIAEHIS_PLASMID       ACCCAGTCCCTGACCCTGGCGATCGATTCTTGTCATGGCACTGTGGTTGCTCTCCGCTAT

1450      1460      1470      1480      1490      1500
REFERENCE_SIAE_ISOFORM_1 GCTTGGACCACGTGGCCTTGTGAATATAAGCAGTGTCCCTATAACCACCCAGTAGTGCC
SIAE_PLASMID           GCTTGGACCACGTGGCCTTGTGAATATAAGCAGTGTCCCTATAACCACCCAGTAGTGCC
SIAEHIS_PLASMID       GCTTGGACCACGTGGCCTTGTGAATATAAGCAGTGTCCCTATAACCACCCAGTAGTGCC

1510      1520      1530      1540      1550      1560
REFERENCE_SIAE_ISOFORM_1 CTGCCAGCCCCTCCCTTCATTGCTTTCATTACAGACCAGGGTCCTGGACATCAGAGCAAT
SIAE_PLASMID           CTGCCAGCCCCTCCATTTCATTGCTTTCATTACAGACCAGGGTCCTGGACATCAGAGCAAT
SIAEHIS_PLASMID       CTGCCAGCCCCTCCATTTCATTGCTTTCATTACAGACCAGGGTCCTGGACATCAGAGCAAT

1570
REFERENCE_SIAE_ISOFORM_1 GTTGCTAAATGA.....
SIAE_PLASMID           GTTGCTAAATGA.....
SIAEHIS_PLASMID       GTTGCTAAATGGCATCACCATCACCATCACTGA

```

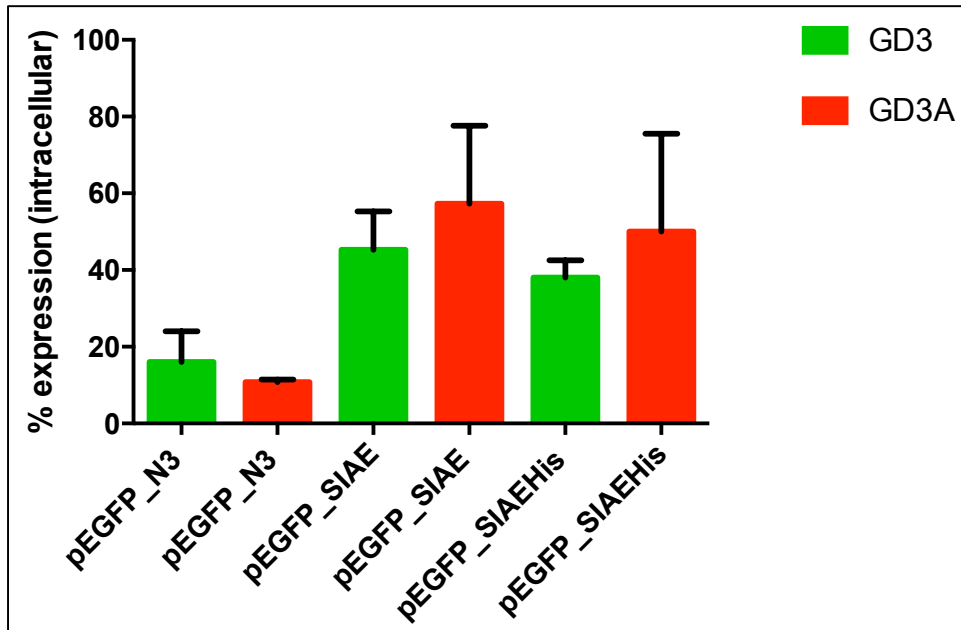
Appendix 1.2 Homology of SIAE sequences cloned into plasmids shown in appendix 1.1. The sequences contained within pEGFP-N3 and pEGFP-SIAEHIS were homologous to reference SIAE isoform 1 sequences from the Ensembl genome browser (<http://www.ensembl.org>). One base pair change was seen at 1515 however this codes for the same amino acid. The SIAEHIS sequence contains a C-terminal His tag (6 histidine residues).

Appendix 2 – Transfection efficiency and GD3/GD3^A changes in cells transfected with pEGFP-N3, pEGFP-N3-SIAE and pEGFP-N3-SIAEHis

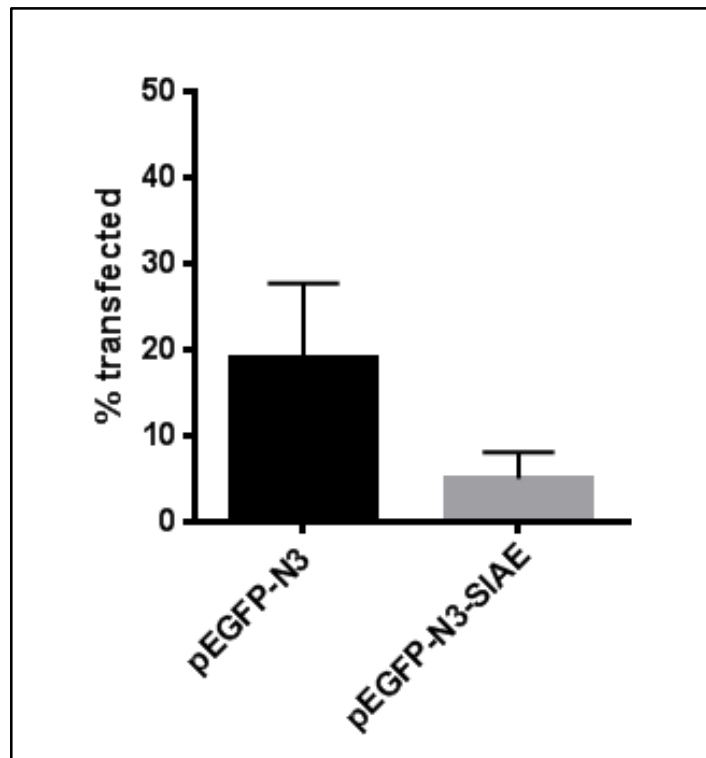
pEGFP-N3, pEGFP-N3-SIAE and pEGFP-N3-SIAE-His constructs were cloned into RES256 cells. After two weeks in selection media that had been replenished every 4 days, colonies had not formed for selection (data not shown).

In order to determine if SIAE overexpression had an effect on GD3^A deacetylation in RES256 cells, transient transfections with the same constructs were carried out. Cells were transfected as previously described. After the incubation period of 24 hours, the cells were instead harvested for analysis of GD3 and GD3^A (Appendix 2.1), and transfection efficiency (Appendix 2.2).

The transfection efficiency of the transiently transfected cell lines was examined by EGFP assay and was poor (7.5 % for SIAE expressing cells; appendix 2.2). Transfection of pEGFP-N3-SIAEHis was determined by anti-His Western blot. Protein expression was not detected using this method suggesting poor transfection efficiency (data not shown). Changes in the GD3 and GD3^A content was not significant as determined by flow cytometry (appendix 2.1), which may be due to such poor transfection efficiency. JC-1 assays were also carried out to determine if the balance of GD3 and GD3^A had been altered, and reduced viability of the transfected cells, this data demonstrated no loss in cell viability and no changes in the mitochondrial membrane polarisation (data not shown).



Appendix 2.1 Transient expression of SIAE does not affect GD3 and GD3^A expression in RES256 cells. Cells transfected with SIAE did not express significantly different levels of GD3 or GD3^A compared to empty vector controls (pEGFP-N3). ($p > 0.05$). Data analysed by One-Way analysis of Variance and Tukey's multiple comparison post-hoc test using Graph Pad Prism 6 software $n = 3 \pm \text{SEM}$



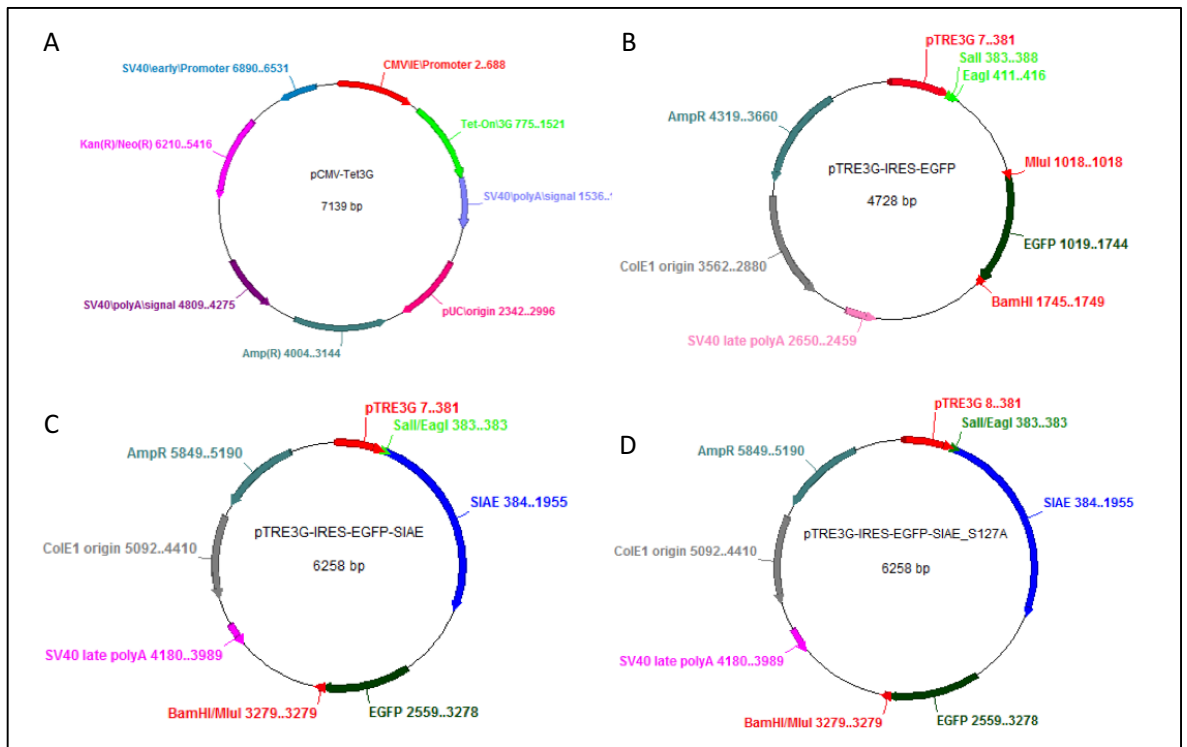
Appendix 2.2 Transfection efficiency is low in transiently transfected cell lines. Transfection efficiency assay based on EGFP expression showed on average pEGFP-N3 was transfected into 33.6 % of cells and pEGFP-N3-SIAE into 7.5 % of cells. N=3 \pm SEM

Appendix 3 – Plasmid maps and sequence homology of pCMV-TetOn3G, pTRE3G-IRES-EGFP, pTRE3G-IRES-EGFP-SIAE and pTRE3G-IRES-EGFP-SIAE-S127A

Inducible system SIAE constructs for overexpression studies were purchased from Clontech and EGFP, SIAE and SIAE-S127A genes cloned into the backbone as previously described. The pCMV-TetOn3G construct encodes a doxycycline responsive protein which undergoes a conformational change with doxycycline binding allowing the binding of the protein to P_{TRE3G} , driving gene transcription. The Tet-On 3G transactivator protein was developed by Clontech and displays high sensitivity to doxycycline. The pTRE3G-IRES-EGFP, pTRE3G-IRES-EGFP-SIAE and pTRE3G-IRES-EGFP-SIAE-S127A constructs are shown in appendix 3.1.

The inducible promoter (P_{TRE3G}) allows very low basal expression and high maximal expression with doxycycline induction. There are 7 repeats of a 19 bp *tet* operator sequence which is located upstream of the CMV promoter. When doxycycline is present the Tet-On 3G protein binds specifically to the P_{TRE3G} and activates the transcription of EGFP and SIAE (or SIAE-S127A). The P_{TRE3G} promoter lacks binding sites for endogenous mammalian transcription factors so is virtually silent in the absence of doxycycline.

The constructs were sequenced (appendix 3.2) to ensure that gene inserts had been incorporated correctly (Eurofins Genomics).



Appendix 3.3 Plasmid maps for inducible system studies. (A) All cells were transfected first with pCMV-TetOn3G. (B) Empty vector control pTRE3G-IRES-EGFP. (C-D) Cells were transfected with either (C) or (D).

	1	10	20	30	40	50	60
SIAE_Reference_Sequence	ATGGTCGCGCCGGGGCTGTACTCGGGCTGGTGCTGCCATTAATCCTGTGGGCCGACAGA						
SIAE_Plasmid	ATGGTCGCGCCGGGGCTGTACTCGGGCTGGTGCTGCCATTAATCCTGTGGGCCGACAGA						
SIAE-S127A_Plasmid	ATGGTCGCGCCGGGGCTGTACTCGGGCTGGTGCTGCCATTAATCCTGTGGGCCGACAGA						
	70	80	90	100	110	120	
SIAE_Reference_Sequence	AGTGCAGGTATGGTTTTCGCTTTCGCTTCATACATCAATAATGATATGGTGCTGCAGAAG						
SIAE_Plasmid	AGTGCAGGTATGGTTTTCGCTTTCGCTTTCATACATCAATAATGATATGGTGCTGCAGAAG						
SIAE-S127A_Plasmid	AGTGCAGGTATGGTTTTCGCTTTCGCTTTCATACATCAATAATGATATGGTGCTGCAGAAG						
	130	140	150	160	170	180	
SIAE_Reference_Sequence	GAGCCTGCTGGGGCAGTGATATGGGGCTTCGGTACACCTGGAGCCACAGTGACCGTGACC						
SIAE_Plasmid	GAGCCTGCTGGGGCAGTGATATGGGGCTTCGGTACACCTGGAGCCACAGTGACCGTGACC						
SIAE-S127A_Plasmid	GAGCCTGCTGGGGCAGTGATATGGGGCTTCGGTACACCTGGAGCCACAGTGACCGTGACC						
	190	200	210	220	230	240	
SIAE_Reference_Sequence	CTGGCCAAAGTTCAGGAAACCATCATGAAGAAAGTGACCAGTGTGAAAGCTCAGCTCTGAT						
SIAE_Plasmid	CTGGCCAAAGTTCAGGAAACCATCATGAAGAAAGTGACCAGTGTGAAAGCTCAGCTCTGAT						
SIAE-S127A_Plasmid	CTGGCCAAAGTTCAGGAAACCATCATGAAGAAAGTGACCAGTGTGAAAGCTCAGCTCTGAT						
	250	260	270	280	290	300	
SIAE_Reference_Sequence	ACGTGGATGGTGGTACTGGATCCTATGAAGCCTGGAGGACCTTTCGAAGTGTGGCCACAA						
SIAE_Plasmid	ACGTGGATGGTGGTACTGGATCCTATGAAGCCTGGAGGACCTTTCGAAGTGTGGCCACAA						
SIAE-S127A_Plasmid	ACGTGGATGGTGGTACTGGATCCTATGAAGCCTGGAGGACCTTTCGAAGTGTGGCCACAA						
	310	320	330	340	350	360	
SIAE_Reference_Sequence	CAGACTTTGGAGAAAATAAACTTCACCCTGAGAGTTCATGACGTCCTGTTGGAGATGTC						
SIAE_Plasmid	CAGACTTTGGAGAAAATAAACTTCACCCTGAGAGTTCATGACGTCCTGTTGGAGATGTC						
SIAE-S127A_Plasmid	CAGACTTTGGAGAAAATAAACTTCACCCTGAGAGTTCATGACGTCCTGTTGGAGATGTC						
	370	380	390	400	410	420	
SIAE_Reference_Sequence	TGGCTCTGTAGTGGGCAGAGFAACATGCAGATGACTGTGTTACAGATATTTAATGCTACA						
SIAE_Plasmid	TGGCTCTGTAGTGGGCAGAGFAACATGCAGATGACTGTGTTACAGATATTTAATGCTACA						
SIAE-S127A_Plasmid	TGGCTCTGTAGTGGGCAGAGFAACATGCAGATGACTGTGTTACAGATATTTAATGCTACA						
	430	440	450	460	470	480	
SIAE_Reference_Sequence	AGGGAGTTGTCTAACACTGCGGCATATCAGTCTGTCCGCATCCTCTCFGTCTCTCCCATF						
SIAE_Plasmid	AGGGAGTTGTCTAACACTGCGGCATATCAGTCTGTCCGCATCCTCTCFGTCTCTCCCATF						
SIAE-S127A_Plasmid	AGGGAGTTGTCTAACACTGCGGCATATCAGTCTGTCCGCATCCTCTCFGTCTCTCCCATF						
	490	500	510	520	530	540	
SIAE_Reference_Sequence	CAAGCAGAGCAGGAGCTGGAGGACCTTGTTCGGTTGACTTGCAAGTGGTCTAAGCCCACC						
SIAE_Plasmid	CAAGCAGAGCAGGAGCTGGAGGACCTTGTTCGGTTGACTTGCAAGTGGTCTAAGCCCACC						
SIAE-S127A_Plasmid	CAAGCAGAGCAGGAGCTGGAGGACCTTGTTCGGTTGACTTGCAAGTGGTCTAAGCCCACC						
	550	560	570	580	590	600	
SIAE_Reference_Sequence	TCAGAAAACCTTAGGCCATGGATATTTCAAGTACATGTCAGCAGTGTGCTGGCTCTTTGGA						
SIAE_Plasmid	TCAGAAAACCTTAGGCCATGGATATTTCAAGTACATGTCAGCAGTGTGCTGGCTCTTTGGA						
SIAE-S127A_Plasmid	TCAGAAAACCTTAGGCCATGGATATTTCAAGTACATGTCAGCAGTGTGCTGGCTCTTTGGA						
	610	620	630	640	650	660	
SIAE_Reference_Sequence	CGTCACCTTTATGACACTCTGCAGTATCCCATCGGGCTGATCGCCTCCAGCTGGGGCGGG						
SIAE_Plasmid	CGTCACCTTTATGACACTCTGCAGTATCCCATCGGGCTGATCGCCTCCAGCTGGGGCGGG						
SIAE-S127A_Plasmid	CGTCACCTTTATGACACTCTGCAGTATCCCATCGGGCTGATCGCCTCCAGCTGGGGCGGG						

670 680 690 700 710 720
SIAE_Reference_Sequence ACACCCATTGAAGCCTGGTCATCTGGACGGTCACTGAAAGCCTGTGGGGTCCCTAAACAA
SIAE_Plasmid ACACCCATTGAAGCCTGGTCATCTGGACGGTCACTGAAAGCCTGTGGGGTCCCTAAACAA
SIAE-S127A_Plasmid ACACCCATTGAAGCCTGGTCATCTGGACGGTCACTGAAAGCCTGTGGGGTCCCTAAACAA

730 740 750 760 770 780
SIAE_Reference_Sequence GGGTCCATTCCATACGATTCTGTAAGTGGTCCCAGTAAGCACTCTGTTCCTCTGGAATGCC
SIAE_Plasmid GGGTCCATTCCATACGATTCTGTAAGTGGTCCCAGTAAGCACTCTGTTCCTCTGGAATGCC
SIAE-S127A_Plasmid GGGTCCATTCCATACGATTCTGTAAGTGGTCCCAGTAAGCACTCTGTTCCTCTGGAATGCC

790 800 810 820 830 840
SIAE_Reference_Sequence ATGATCCATCCACTGTGCAATATGACTCTGAAAGGGGTAGTATGGTACCAGGGGGAGTCC
SIAE_Plasmid ATGATCCATCCACTGTGCAATATGACTCTGAAAGGGGTAGTATGGTACCAGGGGGAGTCC
SIAE-S127A_Plasmid ATGATCCATCCACTGTGCAATATGACTCTGAAAGGGGTAGTATGGTACCAGGGGGAGTCC

850 860 870 880 890 900
SIAE_Reference_Sequence AATATAAATTATAACACGGATCTGTACAAATGCACATTCCTGCCTCATCGAAGACTGG
SIAE_Plasmid AATATAAATTATAACACGGATCTGTACAAATGCACATTCCTGCCTCATCGAAGACTGG
SIAE-S127A_Plasmid AATATAAATTATAACACGGATCTGTACAAATGCACATTCCTGCCTCATCGAAGACTGG

910 920 930 940 950 960
SIAE_Reference_Sequence CGTGAAACCTTCCACCGTGGTCCCAGGGGCAGACGGAGCGTTTCTTCCCATTTGGACTT
SIAE_Plasmid CGTGAAACCTTCCACCGTGGTCCCAGGGGCAGACGGAGCGTTTCTTCCCATTTGGACTT
SIAE-S127A_Plasmid CGTGAAACCTTCCACCGTGGTCCCAGGGGCAGACGGAGCGTTTCTTCCCATTTGGACTT

970 980 990 1000 1010 1020
SIAE_Reference_Sequence GTCCAGTTATCTTCAGATTTGCTAAGAAGAGCTCAGACGATGGATTTCCCAGATCCGT
SIAE_Plasmid GTCCAGTTATCTTCAGATTTGCTAAGAAGAGCTCAGACGATGGATTTCCCAGATCCGT
SIAE-S127A_Plasmid GTCCAGTTATCTTCAGATTTGCTAAGAAGAGCTCAGACGATGGATTTCCCAGATCCGT

1030 1040 1050 1060 1070 1080
SIAE_Reference_Sequence TGGCATCAAACAGCAGACTTCGGCTATGTCCCCAACCCAAAGATGCCCAATACCTTCATG
SIAE_Plasmid TGGCATCAAACAGCAGACTTCGGCTATGTCCCCAACCCAAAGATGCCCAATACCTTCATG
SIAE-S127A_Plasmid TGGCATCAAACAGCAGACTTCGGCTATGTCCCCAACCCAAAGATGCCCAATACCTTCATG

1090 1100 1110 1120 1130 1140
SIAE_Reference_Sequence GCTGTAGCTATGGATCTCTGTGATAGAGACTCGCCTTTTGGCAGCATCCACCCTCGAGAT
SIAE_Plasmid GCTGTAGCTATGGATCTCTGTGATAGAGACTCGCCTTTTGGCAGCATCCACCCTCGAGAT
SIAE-S127A_Plasmid GCTGTAGCTATGGATCTCTGTGATAGAGACTCGCCTTTTGGCAGCATCCACCCTCGAGAT

1150 1160 1170 1180 1190 1200
SIAE_Reference_Sequence AAACAGACTGTGGCTTATCGGCTGCATTTGGGGGCCCGTGTCTCTGGCTTATGGTGAGAAG
SIAE_Plasmid AAACAGACTGTGGCTTATCGGCTGCATTTGGGGGCCCGTGTCTCTGGCTTATGGTGAGAAG
SIAE-S127A_Plasmid AAACAGACTGTGGCTTATCGGCTGCATTTGGGGGCCCGTGTCTCTGGCTTATGGTGAGAAG

1210 1220 1230 1240 1250 1260
SIAE_Reference_Sequence AATTTGACCTTTGAAGGACCCTGCCTGAGAAGATAGAAGTCTTGGCTCACAAAGGGGCTG
SIAE_Plasmid AATTTGACCTTTGAAGGACCCTGCCTGAGAAGATAGAAGTCTTGGCTCACAAAGGGGCTG
SIAE-S127A_Plasmid AATTTGACCTTTGAAGGACCCTGCCTGAGAAGATAGAAGTCTTGGCTCACAAAGGGGCTG

1270 1280 1290 1300 1310 1320
SIAE_Reference_Sequence CTCAAATCTCACATATTACCAGCAAAATCCAGGTGCAGAAAAAGGACAACAAGATATTTGAG
SIAE_Plasmid CTCAAATCTCACATATTACCAGCAAAATCCAGGTGCAGAAAAAGGACAACAAGATATTTGAG
SIAE-S127A_Plasmid CTCAAATCTCACATATTACCAGCAAAATCCAGGTGCAGAAAAAGGACAACAAGATATTTGAG


```

1330      1340      1350      1360      1370      1380
SIAE_Reference_Sequence ATCTCCTGTTGCAGTGACCATCGATGCAAGTGGCTTCCAGCTTCTATGAACACCGTCTCC
SIAE_Plasmid           ATCTCCTGTTGCAGTGACCATCGATGCAAGTGGCTTCCAGCTTCTATGAACACCGTCTCC
SIAE-S127A_Plasmid    ATCTCCTGTTGCAGTGACCATCGATGCAAGTGGCTTCCAGCTTCTATGAACACCGTCTCC

1390      1400      1410      1420      1430      1440
SIAE_Reference_Sequence ACCCAGTCCCTGACCCCTGGCGATCGATTCCTTGTCATGGCACTGTGGTTGCTCTCCGCTAT
SIAE_Plasmid           ACCCAGTCCCTGACCCCTGGCGATCGATTCCTTGTCATGGCACTGTGGTTGCTCTCCGCTAT
SIAE-S127A_Plasmid    ACCCAGTCCCTGACCCCTGGCGATCGATTCCTTGTCATGGCACTGTGGTTGCTCTCCGCTAT

1450      1460      1470      1480      1490      1500
SIAE_Reference_Sequence GCTTGGACCACGTGGCCCTTGTAATATAAGCAGTGTCCCTATACCACCCAGTAGTGCC
SIAE_Plasmid           GCTTGGACCACGTGGCCCTTGTAATATAAGCAGTGTCCCTATACCACCCAGTAGTGCC
SIAE-S127A_Plasmid    GCTTGGACCACGTGGCCCTTGTAATATAAGCAGTGTCCCTATACCACCCAGTAGTGCC

1510      1520      1530      1540      1550      1560
SIAE_Reference_Sequence CTGCCAGCCCTGCCCTTCATTGCTTTTCATTACAGACCAGGGTCTGGACATCAGAGCAAT
SIAE_Plasmid           CTGCCAGCCCTGCCCTTCATTGCTTTTCATTACAGACCAGGGTCTGGACATCAGAGCAAT
SIAE-S127A_Plasmid    CTGCCAGCCCTGCCCTTCATTGCTTTTCATTACAGACCAGGGTCTGGACATCAGAGCAAT

1570
SIAE_Reference_Sequence GTTGCTAAATGA
SIAE_Plasmid           GTTGCTAAATGA
SIAE-S127A_Plasmid    GTTGCTAAATGA

```

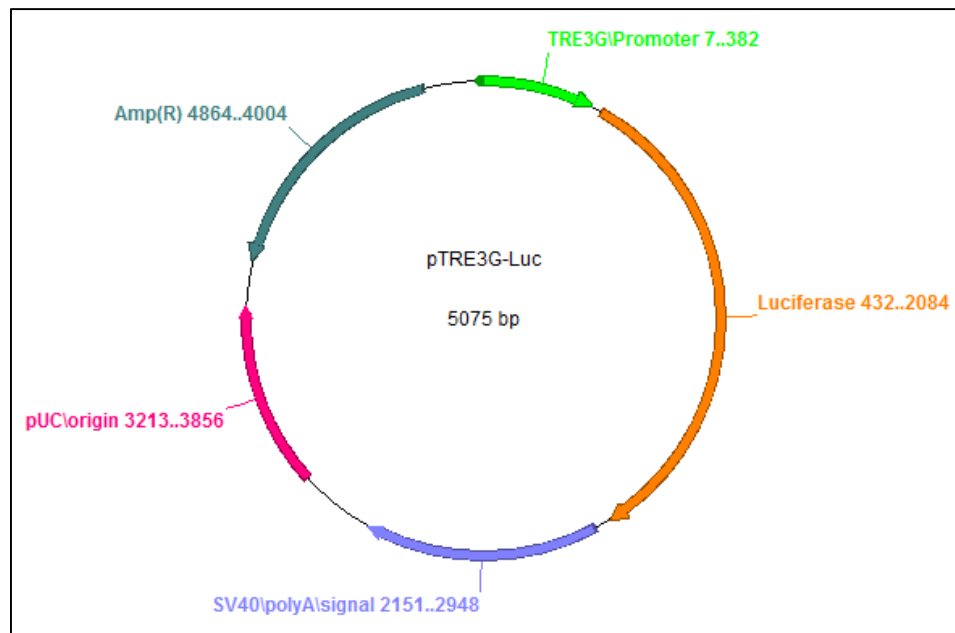
Appendix 3.2 Homology of SIAE sequences cloned into plasmids shown in appendix 3.1. The sequences contained within pTRE3G-IRES-SIAE and pTRE3G-IRES-SIAE-S127A were homologous to reference SIAE isoform 1 sequences from the Ensembl genome browser (<http://www.ensembl.org>). The S127A mutation is confirmed at bases 379-390 which encodes an amino acid substitution from a serine to an alanine residue.

Appendix 4 – Induction testing of pCMV-TetOn3G clones

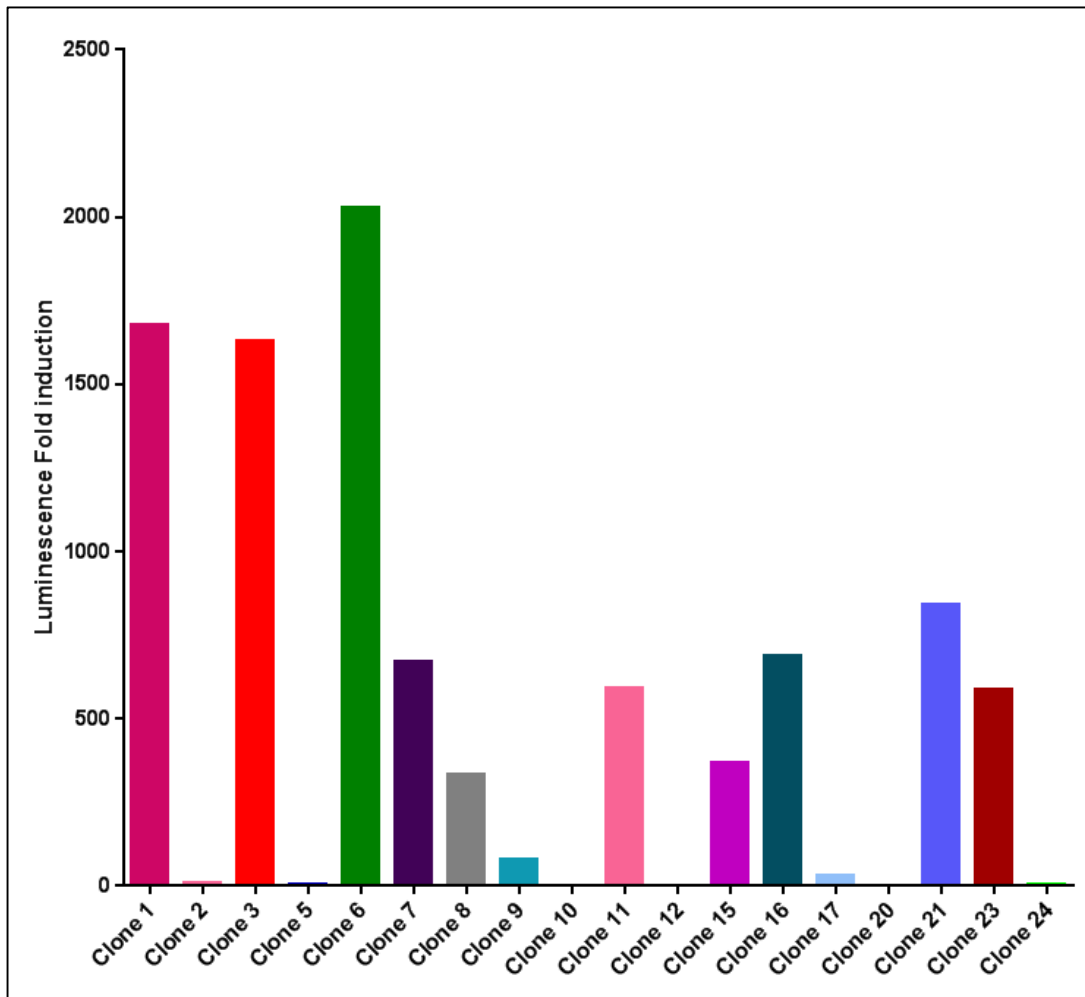
In order to generate double-stable inducible system cell lines, cells were first transfected with pCMV-TetOn3G constructs (appendix 3.1). To determine the clones that best expressed the Tet-On 3G protein, and were therefore capable of inducing expression of tet-responsive constructs, transient transfections using a tet-responsive luciferase construct was carried out.

pTRE3G-Luc is a construct whose expression is driven by Tet On 3G protein. In order for the Tet On 3G protein to bind to the promoter of the pTRE3G-Luc construct doxycycline must be present. Doxycycline induces a conformational change in the Tet On 3G protein which allows binding to the promoter. The binding of the protein to the promoter drives expression of luciferase which is then quantified using a dual luciferase assay described in chapter 2 (appendix 4.2).

Fold-induction of the luciferase protein was defined as the fold-change between cells in the presence and absence of doxycycline. This was used as a measure of induction of each clone. Clones 1, 3 and 6 were determined as the clones best able to induce gene expression and were used to generate inducible system cell lines. Clone 1 was the clone that produced cultures expressing each of the proteins and was used for down-stream analysis.



Appendix 4.1 pTRE3G-Luc. Doxycycline-responsive luciferase construct used to determine the capability of clones to induce protein expression.



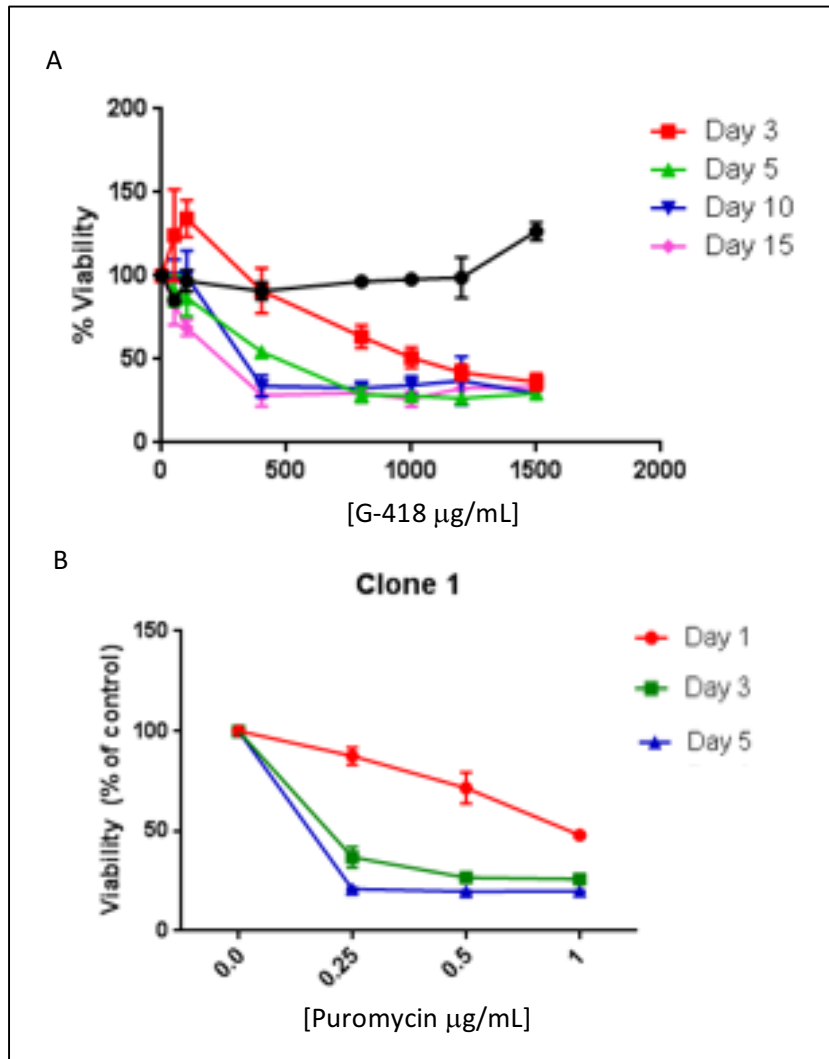
Appendix 4.2 RES256 clones express functional tet-responsive protein. 25 RES256 clones were tested to confirm expression of doxycycline-responsive protein. Clones 1,3 and 6 were the best inducers of gene expression as shown by the highest fold-induction of luciferase expression.

Appendix 5 – RES256 Antibiotic selection of clones

For stable transfection, the concentration of G-418 and puromycin required to remove cells that have not integrated plasmid DNA was determined. pCMV-TetOn3G constructs contain a G-418 resistance cassette and pTRE3G-IRES constructs were co-transfected with a linear puromycin resistance gene at a ratio that makes it unlikely for this DNA to be integrated without plasmid DNA.

G-418 concentrations that resulted in reduced viability of cells without resistance genes were determined by MTS assay as previously described. The concentration that caused a greater than 50% reduction in cell viability after 5 days of treatment, and no viable cells after 15 days of treatment was deemed 1 mg/mL for RES256 cells (appendix 5.1A).

The concentration of puromycin required for no viable cells to remain after 6 days was determined as previously described. The concentration used to remove viable RES256 cells that did not integrate a resistance gene into the genome was 1.5 µg/mL (appendix 5.1B).

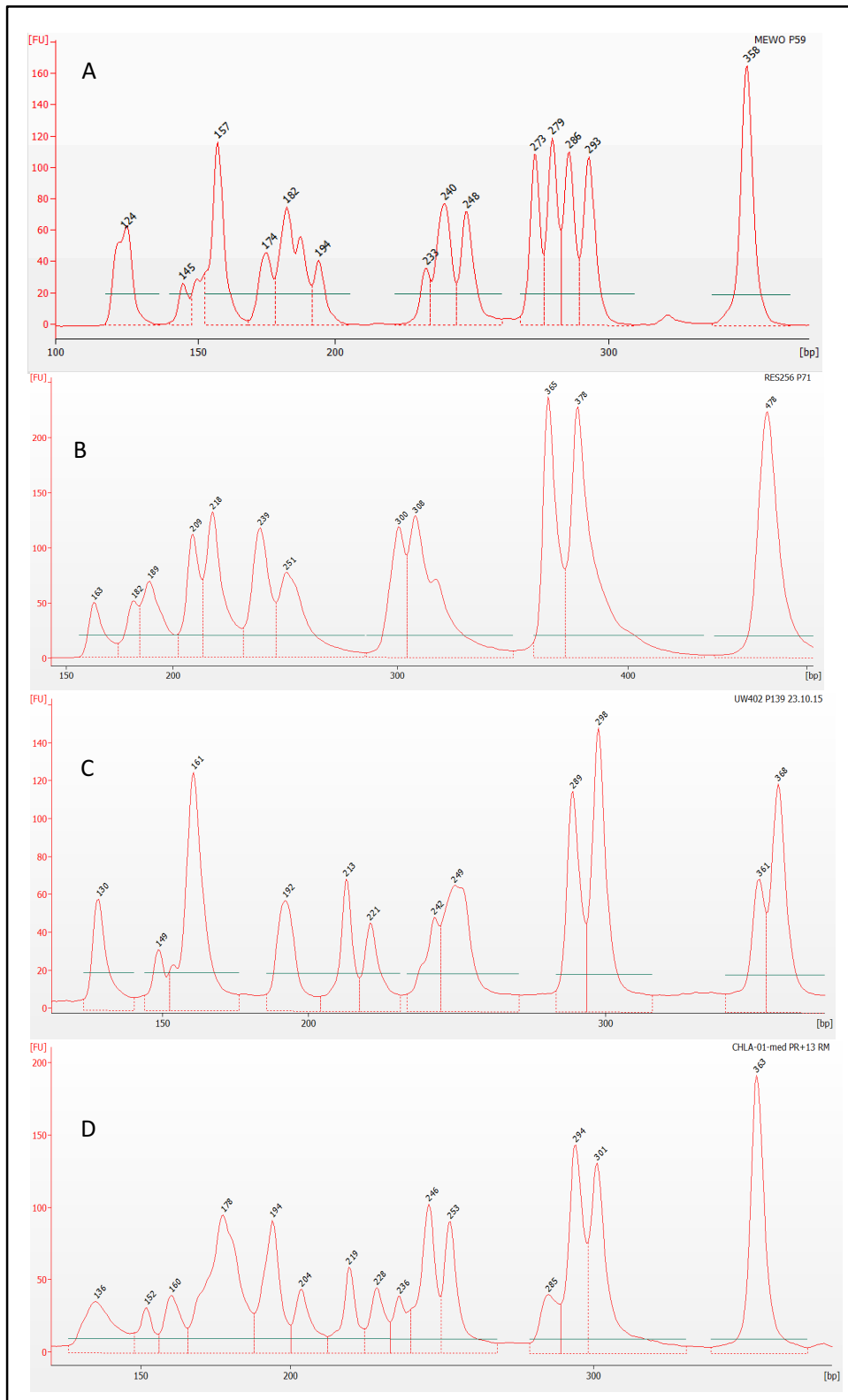


Appendix 5.1 RES256 kill curves. (A) G-418 dose-response for 15 days shows a decrease in viability with increasing dose and time. A dose of 1000 µg/mL caused a significant reduction in viability after 5 days (green) and by 15 days (pink) viability had plateaued. (B) Puromycin dose-response for 5 days shows a decrease in viability after 3 and 5 days (green and blue) with 0.5 µg puromycin making this the concentration used to select transfected clones.. N=3 ± SEM

Appendix 6 – Cell line authentication

The cell lines used in this project were authenticated to ensure there was no contamination with other cell lines and microbes. The cell lines used throughout this project were the medulloblastoma cell lines RES256, CHLA-01-Med and UW402, and also the metastatic melanoma cell line MeWo.

The authenticity of cell lines used in the following experiments were confirmed by DNA fingerprint analysis carried out by Mrs. Katie Loveson (Appendix 6.1). This genotyping confirms the expression of several short tandem repeat sequences of DNA that are unique to the cell line. This data was compared to published genotypes where available. This PCR based technique described previously was carried out to ensure quality of data.



Cell Line	Amelogenin	D5S818	vWA	TH01	D13S317	D21S11	D7S820	TPOX	D16S539	CSF1PO
Res256	X	11, 12	16, 18	9.3, 9.3	11, 11	29, 29	10, 12	8, 8	12, 12	11, 12
CHLA-01-Med	X, Y	11, 13	16, 17	6, 9.3	8, 14		10, 10	9, 12	9, 11	11, 11
UW402	X	11, 12	14, 14	9.3, 9.3	13, 13	28, 31	10, 11	11, 11	11, 11	11, 12
MeWo	X, Y	12, 13	15, 15	7, 9	9, 9	30, 32.2	10, 12	8, 10	10, 12	12, 12

Appendix 6.0.1 DNA fingerprint analysis of the cell lines used in this project. (A) MeWo, (B) RES256, (C) UW402 and (D) CHLA-01-Med medulloblastoma cell lines. These fingerprints are unique to each cell line and are used to ensure no contamination of cultures occurred throughout this project. The data is also represented in tabular form with data from each gene amplified shown.

Morphology

The morphology of each cell line was examined throughout the study using phase contrast microscopy. By inspecting cultures regularly, it was ensured that contaminations could be identified quickly as well as any morphological changes that may occur following any treatments could be investigated.

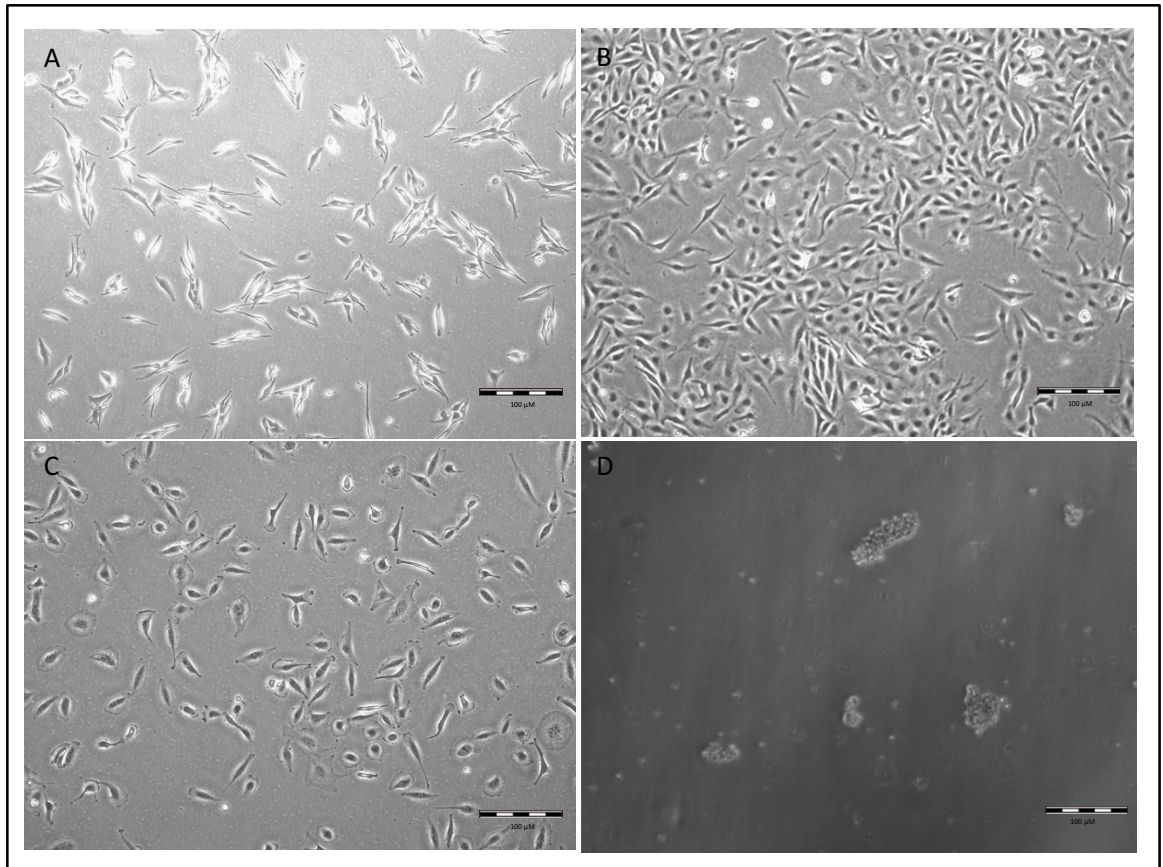
MeWo is a commercially available metastatic melanoma derived from a lymph node. These cells are elongated, homogenous and are of high passage. (Appendix 6.2A)

RES256 and UW402 are high passage cell lines and therefore homogenous (appendix 6.2B-C). These cell lines have small rounded cells that have few processes.

CHLA-01-Med is a commercially available medulloblastoma cell line which grows in suspension culture. These cells grow as large spheres and some as single cell suspension, but are morphologically similar. This cell line is also high passage (appendix 6.2D).

Only one of the medulloblastoma cell lines has a published known subgroup, CHLA-01-Med is, a group 4 medulloblastoma described by (Erdreich-Epstein et al. 2014). It can be speculated that the RES256 cell line belongs to either the SHH or WNT subgroup as this cell line harbours a *TP53* mutation described by (Zhukova Thesis, 2012). *TP53* mutations are enriched in WNT patients (16 %) and SHH patients (21 %), and these mutations are virtually absent in group 3 and group 4 tumours shown by (Zhukova et al. 2013). The absence of *TP53* mutations in groups 3 and 4 is because of the location of the *TP53* gene on the short arm of chromosome 17. Chromosome 17p is commonly lost in these subgroups, and there are gains in the long arm, as they harbour isochromosome 17q (i[17q]). The UW402 cell line

is known to be *TP53* wild-type, shown by (Zhukova Thesis, 2012) and its subgroup is currently unknown. by flow cytometry.



Appendix 6.2 Morphology of cell lines used in this project was monitored for changes to determine contamination and morphological changes with treatment. (A) MeWo, a surface adherent melanoma cell line known to express GD3 and GD3^A, Passage 85; (B) RES256 a surface adherent medulloblastoma cell line Passage 86; (C) UW402, a surface adherent medulloblastoma cell line Passage 106; (D) CHLA-01-Med a group 4 medulloblastoma cell line that grows as clusters and as single cells in suspension Passage (from receipt) 10. Cells imaged using an Olympus IX71 inverted-phase contrast microscope using a 4 X objective

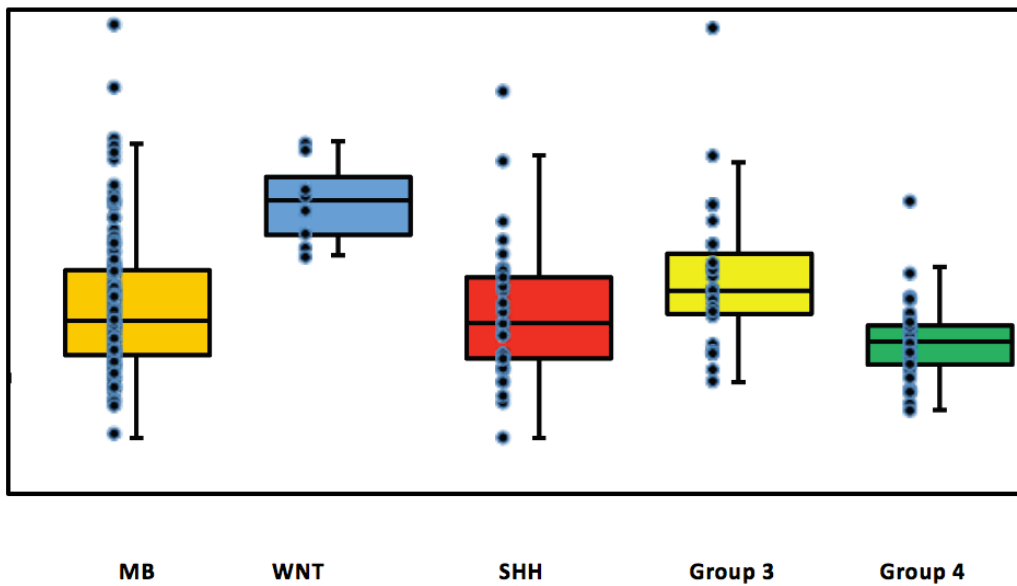
Appendix 7- IC₅₀ data after treatments with cisplatin and etoposide

The IC₅₀ is the concentration of (inhibitory) drug (or antagonist) required for a 50 % reduction in response. In this case the concentration of chemotherapeutic required for a 50 % reduction in cell viability. IC₅₀ data for each time point and clone is shown below. Significant changes in IC₅₀s are shown in green.

Appendix 7.1- IC₅₀s for each clone after treatment with cisplatin or etoposide. Significant data shown in green. Data analysed by GraphPad Prism 6 software using non-linear regression analysis of logIC₅₀. n=3.

Clone	Drug	IC ₅₀ - Dox (μM) ± 95 % CI	IC ₅₀ + Dox (μM) ± 95 % CI	Time Point (Hours)	p value	Statistically significant?
EGFP	Cisplatin	4.3 ± 1.2	4.2 ± 0.9	24	0.9303	No
SIAE 1	Cisplatin	3.7 ± 1.4	n.d	24	0.4091	No
SIAE 2	Cisplatin	3.4 ± 1.3	2.4 ± 1.1	24	0.4091	No
S127A	Cisplatin	3.1 ± 1.3	2.7 ± 0.8	24	0.6675	No
EGFP	Etoposide	4.6 ± 3.8	n.d	24	0.8028	No
SIAE 1	Etoposide	2.4 ± 1.1	3.0 ± 2.2	24	0.7065	No
SIAE 2	Etoposide	4.1 ± 1.9	1.2 ± 0.9	24	0.0744	No
S127A	Etoposide	n.d	4.5 ± 2.0	24	0.1691	No
EGFP	Cisplatin	3.6 ± 2.9	3.8 ± 1.2	48	0.8485	No
SIAE 1	Cisplatin	2.3 ± 0.4	2.0 ± 0.4	48	0.2769	No
SIAE 2	Cisplatin	1.8 ± 0.7	2.8 ± 0.5	48	0.1058	No
S127A	Cisplatin	4.1 ± 0.6	3.1 ± 0.5	48	0.0165	Yes
EGFP	Etoposide	6.7 ± 2.9	6.6 ± 1.8	48	0.9785	No
SIAE 1	Etoposide	3.0 ± 0.6	2.3 ± 0.6	48	0.1547	No
SIAE 2	Etoposide	2.1 ± 0.5	1.6 ± 0.5	48	0.3322	No
S127A	Etoposide	3.0 ± 0.6	2.8 ± 0.5	48	0.6991	No
EGFP	Cisplatin	2.7 ± 0.6	2.0 ± 0.6	72	0.1727	No
SIAE 1	Cisplatin	1.3 ± 0.3	1.0 ± 0.2	72	0.2153	No
SIAE 2	Cisplatin	1.1 ± 0.3	1.1 ± 0.3	72	0.9892	No
S127A	Cisplatin	1.8 ± 0.4	1.7 ± 0.4	72	0.7893	No
EGFP	Etoposide	3.0 ± 1.4	4.2 ± 1.1	72	0.3198	No
SIAE 1	Etoposide	3.5 ± 0.3	2.8 ± 0.2	72	0.3899	No
SIAE 2	Etoposide	5.1 ± 1.3	1.9 ± 0.9	72	0.0034	Yes
S127A	Etoposide	3.5 ± 1.0	1.9 ± 0.9	72	0.0718	No

Appendix 8- High NG2 mRNA expression is associated with the WNT subgroup



Appendix 8.1 NG2 mRNA expression in Medulloblastoma subgroups. NG2 expression is highest in WNT group of Medulloblastomas providing supportive evidence that GD3^A expression is lowest in this subgroup as also supported by data in chapter 3 and published work which demonstrates an inverse correlation between NG2 and GD3^A expression in glioma. Similar expression of NG2 is seen in SHH group 3 and group 4 samples. (Data from Taylor group, Toronto).

Appendix 9 – UPR16 Form and ethical approval letter



FORM UPR16

Research Ethics Review Checklist

Please include this completed form as an appendix to your thesis (see the Postgraduate Research Student Handbook for more information)

Postgraduate Research Student (PGRS) Information		Student ID:	460066
PGRS Name:	Rebecca Louise Mather		
Department:	School of Pharmacy and Biomedical Sciences	First Supervisor:	Prof. Geoff Pilkington
Start Date: (or progression date for Prof Doc students)	Oct 2012		
Study Mode and Route:	Part-time <input type="checkbox"/>	MPhil <input type="checkbox"/>	MD <input type="checkbox"/>
	Full-time <input checked="" type="checkbox"/>	PhD <input checked="" type="checkbox"/>	Professional Doctorate <input type="checkbox"/>
Title of Thesis:	Deacetylation of GD3A as a potential therapeutic target for paediatric medulloblastoma		
Thesis Word Count: (excluding ancillary data)	56,664 words		
<p>If you are unsure about any of the following, please contact the local representative on your Faculty Ethics Committee for advice. Please note that it is your responsibility to follow the University's Ethics Policy and any relevant University, academic or professional guidelines in the conduct of your study</p> <p>Although the Ethics Committee may have given your study a favourable opinion, the final responsibility for the ethical conduct of this work lies with the researcher(s).</p>			
UKRIO Finished Research Checklist:			
(If you would like to know more about the checklist, please see your Faculty or Departmental Ethics Committee rep or see the online version of the full checklist at: http://www.ukrio.org/what-we-do/code-of-practice-for-research/)			
a) Have all of your research and findings been reported accurately, honestly and within a reasonable time frame?	YES	<input checked="" type="checkbox"/>	
	NO	<input type="checkbox"/>	
b) Have all contributions to knowledge been acknowledged?	YES	<input checked="" type="checkbox"/>	
	NO	<input type="checkbox"/>	
c) Have you complied with all agreements relating to intellectual property, publication and authorship?	YES	<input checked="" type="checkbox"/>	
	NO	<input type="checkbox"/>	
d) Has your research data been retained in a secure and accessible form and will it remain so for the required duration?	YES	<input checked="" type="checkbox"/>	
	NO	<input type="checkbox"/>	
e) Does your research comply with all legal, ethical, and contractual requirements?	YES	<input checked="" type="checkbox"/>	
	NO	<input type="checkbox"/>	
Candidate Statement:			
I have considered the ethical dimensions of the above named research project, and have successfully obtained the necessary ethical approval(s)			
Ethical review number(s) from Faculty Ethics Committee (or from NRES/SCREC):		NRES reference number 11/SC/0048	
If you have <i>not</i> submitted your work for ethical review, and/or you have answered 'No' to one or more of questions a) to e), please explain below why this is so:			

UPR16 – August 2015

Signed (PGRS):	 <i>R. Mather</i>	Date: 10/06/16



Health Research Authority

NRES Committee South Central - Hampshire A

Level 3, Block B
Whitefriars
Lewins Mead
Bristol
BS1 2NT

Tel: 0117 342 1381

16 July 2014

Professor Geoffrey J Pilkington
Professor of Cellular and Molecular Neuro-oncology
University of Portsmouth
School of Pharmacy and BMS
St Michael's Building
Portsmouth
PO1 2DT

Dear Professor Pilkington

Study title: The Cellular and Molecular Biology of Brain Tumours: Migration, apoptosis, malignancy and therapeutic applications.
REC reference: 11/SC/0048
Amendment number: Substantial Amendment 1
Amendment date: 26 June 2014
IRAS project ID: 67028

The above amendment was reviewed by the Sub-Committee in correspondence.

Ethical opinion

The members of the Committee taking part in the review gave a favourable ethical opinion of the amendment on the basis described in the notice of amendment form and supporting documentation.

Approved documents

The documents reviewed and approved at the meeting were:

<i>Document</i>	<i>Version</i>	<i>Date</i>
Notice of Substantial Amendment (non-CTIMP)	Substantial Amendment 1	26 June 2014
Participant consent form [BT Patient Assent Form: Noncompetent Minor Assent Form]	1.1	09 June 2014
Participant consent form [Epileptic patient Noncompetent Minor Assent Form]	1	09 June 2014
Participant consent form [Informed Consent form for Epileptic Patients:Adult/Competent Minor]	1	09 June 2014

Participant consent form [Informed Consent form for Epileptic Patients: Parents/Guardians Consent Form]	1	09 June 2014
Participant consent form [BT Parents/guardians Informed Consent Form]	2	09 June 2014
Participant consent form [BT Informed Consent Form: Adult Competent Minor]	2	09 June 2014
Participant information sheet (PIS) [BT Patient Information Sheet for noncompetent minor to aid consent]	2	09 June 2014
Participant information sheet (PIS) [Patient Information Sheet for Epileptic Patients: Noncompetent minor to aid consent]	1	09 June 2014
Participant information sheet (PIS) [Patient Information Sheet for Epileptic Patients: Standard Adult/Competent Minor]	1	09 June 2014
Participant information sheet (PIS) [Patient Information Sheet for Epileptic Patients: Parents/Guardians]	1	09 June 2014
Participant information sheet (PIS) [BT Patient Information Sheet for non competent consenting minors]	2	09 June 2014
Participant information sheet (PIS) [BT Patient Information Sheet for adult/competent minor]	2	09 June 2014
Research protocol or project proposal	3	19 June 2014

Membership of the Committee

The members of the Committee who took part in the review are listed on the attached sheet.

R&D approval

All investigators and research collaborators in the NHS should notify the R&D office for the relevant NHS care organisation of this amendment and check whether it affects R&D approval of the research.

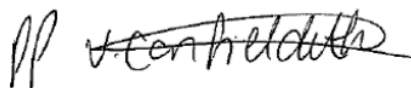
Statement of compliance

The Committee is constituted in accordance with the Governance Arrangements for Research Ethics Committees and complies fully with the Standard Operating Procedures for Research Ethics Committees in the UK.

We are pleased to welcome researchers and R & D staff at our NRES committee members' training days – see details at <http://www.hra.nhs.uk/hra-training/>

11/SC/0048:	Please quote this number on all correspondence
--------------------	---

Yours sincerely



Dr Ronja Bahadori
Alternate Vice-Chair

E-mail: nrescommittee.southcentral-hampshirea@nhs.net

Enclosures: List of names and professions of members who took part in the review